NASA CR-108570
R-8224

FINAL REPORT

NONCIRCULAR ORIFICE HOLES AND ADVANCED FABRICATION TECHNIQUES FOR LIQUID ROCKET INJECTORS

PHASE I: ANALYTICAL AND EXPERIMENTAL STUDY OF NONCIRCULAR INJECTOR ORIFICES, AND ELEMENTS FOR LIQUID/LIQUID INJECTORS

NAS9-9528

By

W. H. Nurick
R. M. McHale

Rocketdyne
A Division of North American Rockwell Corporation

prepared for

NASA MANNED SPACECRAFT CENTER

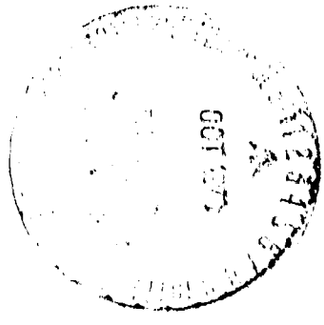

NASA CR-108570

R-8224

FINAL REPORT

NONCIRCULAR ORIFICE HOLES AND ADVANCED FABRICATION TECHNIQUES FOR LIQUID ROCKET INJECTORS

PHASE I: ANALYTICAL AND EXPERIMENTAL STUDY OF NONCIRCULAR INJECTOR ORIFICES, AND ELEMENTS FOR LIQUID/LIQUID INJECTORS

NAS9-9528

By

W. H. Nurick
R. M. McHale

Rocketdyne
A Division of North American Rockwell Corporation

prepared for

NASA MANNED SPACECRAFT CENTER

FOREWORD

This report was prepared for NASA Manned Spacecraft Center, Houston, Texas by Rocketdyne, a Division of North American Rockwell Corporation. The study was conducted in accordance with Contract NAS9-9528, G.O. 09206.

Mr. M. F. Lausten of the Manned Spacecraft Center served as NASA Technical Manager. The Rocketdyne Program Manager was Mr. S. D. Clapp.

ABSTRACT

The Phase I results to investigate the use of advanced fabrication techniques for liquid rocket injectors which allow for fabrication of non-circular orifices, and to determine if noncircular orifices can provide greater flexibility and/or a significant improvement in injector element designs are presented. The study consists of an analytical study of various injector patterns and elements that utilize noncircular orifices, and experimental evaluations of promising element configurations. Cold-flow characterization and theoretical combustion modeling combined with single element hot-firing experiments are employed to predict the relative merits of liquid rocket engine injector elements incorporating orifices of noncircular shape as compared to circular shapes. The frozen wax technique is used to determine dropsize; water/trichloroethylene spray collection through a tube matrix is used to determine mixing efficiency. Unlike-doublet elements incorporating circular, triangular, rectangular, and self-atomizing orifices are compared on the basis of overall c* efficiency. Results indicate that at optimum design conditions for equal thrust per element designs, mixing levels are higher for noncircular shapes while circular orifices produce smaller dropsizes.

CONTENTS

ILLUSTRATIONS

TABLES

1.0 INTRODUCTION

The most commonly used rocket engine injector designs in existence today employ circular orifices. Historically, circular holes have been employed because of manufacturing limitations. With the advent of new fabrication techniques, circular orifices can now be made by means other than twist drilling. Noncircular orifices can also be produced with relative ease. Because of these fabrication advances, it is appropriate to re-evaluate injector design practices to determine whether noncircular orifice designs can offer superior qualities either in terms of greater flexibility, lower costs, and better reproducibility, or in terms of equivalent or improved performance and injector-thrust chamber design compatibility.

Potential advantages of noncircular orifices can be seen from an examination of current problem areas associated with circular orifices. Circular orifice design is particularly sensitive to tolerances and machining practices which control such parameters as: impingement point, orifice diameter, entrance conditions, and free-stream L/D. Minor misimpingement of two circular streams (in terms of a few thousandths of an inch for a 0.030-inch-diameter orifice) causes gross distortion of fan shape and distribution. In spite of the specification of very close tolerances, engine-to-engine performance and thrust chamber wall erosion variations occur which can be traced, in part, to slight misimpingement. The flowrate through a circular orifice is proportional to the diameter squared, and thus local flowrates are particularly sensitive to drill diameter. In addition, the diameter ratio used in the design of circular orifice unlike-impinging-stream patterns, is dictated by consideration of the propellant momentum and diameter ratio required to maximize mixing. Almost without exception, unequal sizes result. Although this condition may produce the best mixing, it is highly probable that atomization is impared (the fan shape is also influenced).

Many of these disadvantages can be overcome utilizing noncircular orifice shapes. For instance, tolerance control relaxation can be exercised on rectangular orifices on the small side (which is more difficult to control) because flow variation is less sensitive to this single dimension. In addition, the use of noncircular orifices certainly lends itself to the possibility of equalizing contact dimension (impingement of a square on the smaller side of a rectangle, for instance).

To assess the possible advantages of noncircular orifices, an applied research program was conducted containing analysis, design, and experiment to determine if noncircular orifices can provide greater flexibility and/or a significant improvement in injector designs as opposed to the conventional circular orifices. The overall program is divided into two phases: Phase I, analytical and experimental study of noncircular orifices and elements-liquid/liquid propellants, and Phase II, analytical and experimental study of noncircular orifices and elements-gas/liquid propellants. To meet program objectives, the program is structured such that, initially, orifice and element designs are conceived with no restraints other than those imposed by specific propellant combinations, engine size, and operating conditions. The orifice and element geometry concepts are then evaluated by a rating technique which includes orifice flow and element spray characteristics as well as fabrication considerations. The preliminary evaluation is made using only analytical and existing empirical estimations. Following this, data are obtained with single orifice and element cold-flow and hot-fire characterization experiments using selected geometries. These data are then fed back into the established rating system. The results of Phase I of this program are presented herein.

2.0 SUMMARY

This report contains the results of Phase I of an applied research program of analysis, design, and experiment to evaluate and characterize potential liquid rocket engine injector element designs that utilize the flexibility of advanced fabrication techniques and noncircular orifices utilizing liquid/liquid and gas/liquid propellants. The overall program objective is to determine if noncircular orifices can provide greater flexibility and/or a significant improvement in injector element designs, as opposed to the conventional circular orifices.

Phase I consists of an analytical study of various injector patterns and elements that utilize noncircular orifices and experimental evaluation of promising element configurations. The most promising orifices are cold-flow tested with propellant simulants to characterize them as well as verify analytical predictions. The orifices are configured into promising element configurations and analytical predictions made with regard to their combustion and operating characteristics. These elements are then cold flowed and hot fired in a small test engine (designed as a part of this program) to further characterize them as well as to verify the analytical predictions.

Phase I is organized in three sections; (1) Preliminary Evaluation of Orifices and Elements, (2) Experimental Evaluation of Orifices and Elements, and (3) Final Evaluation of Orifices and Elements.

The Preliminary Evaluation included selection of program guidelines and criteria which were then used to judge the relative merit of circular and noncircular configurations. As a result of this evaluation, nine orifices [circle, square, retangle (aspect ratio = 2 and 8), triangle (isosceles and equilateral), diamond, and spray nozzle] were selected for cold-flow study. The unlike-doublet injector element type was selected as a standard for comparison with the various orifice shapes (circle, rectangles, triangles, and spray nozzles).

Experimental evaluation encompassed cold-flow characterization of single orifices, cold-flow characterization of elements with regard to both mixing and atomization, and hot-fire evaluation of elements. Data obtained with single orifices indicates that all shapes produce similar discharge coefficients and flow characteristics. Noncircular shapes were, in general, less sensitive to operating conditions than circular orifices.

Cold-flow evaluation of single elements showed that at equivalent design conditions noncircular elements produce more uniformly mixed sprays but larger spray dropsizes.

Final evaluation of elements showed that noncircular and circular orifices have advantages and disadvantages and that selection would depend upon the specific application.

3.0 PRELIMINARY EVALUATION

The objective of the preliminary evaluation is to investigate the relative merits of noncircular orifices and injector elements with respect to circular orifices and elements. Because there are an infinite number of possible orifice shapes and element types, the first task of the preliminary evaluation is to conduct a preliminary analysis to define the design of typical element types applicable to liquid/liquid and gas/liquid propellant rocket engines. The preliminary evaluation was then used to define the shapes and elements most promising for application to an NTO/A-50 rocket engine. The evaluation is based upon the most pertinent existing experimental data and analytical techniques available. Where data are not available, extrapolations are made based upon some rational analytical approach. The preliminary evaluation then shows where additional technology are required, and therefore, defines the scope of the Experimental Evaluation. Described in a later section of this report, the experimental results were subsequently used to check the initial assumptions and a re-evaluation is made.

The preliminary evaluation criteria for evaluation of orifice shapes are subdivided into two major categories: (1) functional, and (2) fabrication. Functional considerations are those which describe the fluid flow characteristics of an orifice. Fabrication considerations describe the degree of difficulty and cost of fabricating the orifice.

Eight criteria were selected for functional evaluation:

1. ΔP, Pressure drop
2. C_D, Orifice coefficient
3. Free-stream stability
4. Sensitivity to propellant temperature

5. Sensitivity to propellant backpressure

6. Sensitivity to cross velocity at the orifice entrance

7. Sensitivity to ΔP fluctuations

8. Sensitivity to contamination.

The basic factors considered for each of the criterion along with those characteristics which would be considered desirable under each criterion are listed in Table 1.

Criteria selected for the evaluation of orifice shapes from a fabrication standpoint are:

1. Tolerance Obtainable

2. Design Flexibility

3. Fabrication Time

4. Fabrication Cost

5. Inspection

6. Tooling Structural Limits

The factors considered for each criterion along with desirable features for each are listed in Table 2.

Six manufacturing techniques are selected for evaluation of orifice shapes for the various fabrication criterion. These techniques are:

1. Cast

2. Electrical-Discharge Machining (EDM)

3. Electrochemical Machining (ECM)

TABLE 1

BASIC CONSIDERATIONS FOR FUNCTIONAL CRITERION

Criterion	Consideration	Desirable Features
Pressure Drop	Flowrate vs ΔP characteristics over a range of pressure drop	Predictable characteristics; C_D relatively constant over ΔP range.
Orifice Coefficient	Value of orifice coefficient at a given operating level (i.e., Reynolds No. or ΔP).	High values of C_D
Free-Stream Stability	Stability of liquid jet	Stable jet; predictable direction
Sensitivity to Propellant Temperature	Effect of propellant temperature on the value of C_D	C_D insensitive to propellant temperature
Sensitivity to Propellant Pressure	Effect of operating pressure level (i.e., P_c) on hydraulic flip characteristics	C_D unaffected by operating pressure level
Sensitivity to Cross Velocity	The degree to which C_D and jet stability are effected by cross velocity	C_D and jet uneffected by cross velocity
Sensitivity to ΔP Fluctuations	The degree to which ΔP oscillations produce flowrate oscillations	$\frac{d\dot{w}}{d\Delta P}$ small
Sensitivity to Contamination	The likelihood of a given size particle lodging in an orifice	Orifice which will pass normal size contaminants

TABLE 2

BASIC CONSIDERATIONS FOR FABRICATION CRITERIA

Criterion	Consideration	Desirable Features
Tolerance Obtainable	Defines the ability to obtain both close and repeatable tolerance on size, shape, and location	Good tolerance obtained with relative ease
Design Flexibility	The ability to incorporate minor revisions in size and/or shape with relatively minor changes in setup or tooling	Shapes and fabrication methods which do not require complete retooling for minor changes of dimensions
Fabrication Time	Time required to produce a hole of given area at a given depth	Short time
Fabrication Cost	Dollars required to produce a given hole	Low cost
Inspection	Ability to perform in-process and after fabrication inspections	Easily inspected
Tooling Structural Limits	Susceptibility to breakage and/or wear of tooling	Tooling with long projected life

4. Photoetch

5. Powder Metallurgy (P/M)

6. Electroforming (E/F)

For circular orifices, the additional technique of twist drilling is considered. All manufacturing techniques for all shapes are evaluated using the circular-shaped orifice manufactured by twist drilling as a standard of comparison. Each fabrication technique is considered under each evaluation criterion.

The results of the preliminary evaluation were reviewed by three independent research teams, each performing a separate evaluation. Each team assigned numerical values to the various evaluation criteria which reflected the opinion of that particular team. The final preliminary evaluation values were obtained by numerically averaging the evaluations of the three teams. An identical technique was used to perform the final evaluation.

All criteria in the preliminary evaluation were given equal weight. This was done so as to make the evaluation as general as possible. Weighting factors are strongly affected by the specific application of a given injector element. For specific application, one may choose his own weighting factors, and using the values shown in the preliminary evaluation, perform a weighted evaluation.

3.1 PRELIMINARY ANALYSIS

There is an infinity of orifice shapes and injector element types which could be envisioned for application to rocket engine injector design. In addition, there are many propellant configurations and engine operating level requirements which could be considered for each injector type. Consequently, it is mandatory to first define the engine operating conditions which are most representative of current engine requirements, and element types which could be envisioned for practical designs. For the purposes of the Preliminary Analysis, five propellant combinations were selected. These combinations, along with specific operating conditions for each, are listed in Table 3.

The results of an analytical study of the applicability of various injector element types to the propellant combinations and engine operating conditions listed in Table 3 are presented. This evaluation is based upon present circular orifice technology concerning mixing and atomization.

The element types considered include:

1. Unlike doublet
2. Two-on-one (triplet)
3. Four-on-one
4. Like doublet

For the triplet and the four-on-one, analysis is performed for elements with the oxidizer in the center orifice and with the oxidizer in the outer orifices for the liquid/liquid combinations. For gas/liquid propellants, only elements with the gas species in the center orifice are considered.

TABLE 3

ENGINE OPERATING CONDITIONS

Propellant Combinations	Chamber Pressure, psia	Thrust, pounds	Injector Orifice ΔP, psia	Mixture Ratio, o/f
N_2O_4 (50/50)				
Pressure-Fed	100	20,000	20 to 50	1.4 to 1.8
F_2/H_2				
Pressure-Fed	100 to 300	3,000 to 20,000	10 to 50	8 to 16
Pump-Fed	300 to 800	3,000 to 20,000	50 to 200	8 to 16
FLOX/CH_4				
Pressure-Fed	100 to 300	3,000 to 20,000	10 to 50	4 to 8
Pump-Fed	300 to 800	3,000 to 20,000	50 to 200	4 to 8
OF_2/B_2H_6				
Pressure-Fed	100 to 300	3,000 to 20,000	10 to 50	2.5 to 5
H_2/O_2				
Pressure-Fed	100 to 300	3,000 to 20,000	10 to 50	4 to 6
Pump-Fed	300 to 1,300	3,000 to 20,000	50 to 200	4 to 6

A calculation procedure for the design of an injector element is shown in Fig. 1. A primary consideration in the indicated procedure is attainment of optimum propellant mixing. The input, or independent, conditions are:

1. mixture ratio
2. thrust per element
3. oxidizer orifice ΔP

At the outset of each design for a given propellant combination, the oxidizer orifice pressure drop, thrust per element (sea level optimum), overall mixture ratio, chamber pressure, and propellant temperatures are specified. The area ratios for each unlike impinging element are then computed using empirical (cold-flow) mixing criteria. In the case of the like doublets, mixing is not a function of area ratio, but rather geometric orientation. Consequently, the area ratio was set equal to 1.0 (for the gas-liquid like-doublet elements, the ΔP ratio was set equal to 1.0). Area ratios are defined in two different ways. Area ratio is obtained by dividing the area of one oxidizer orifice by the area of one fuel orifice. Total area ratio is computed by dividing total element oxidizer area by total element fuel area.

Once the area ratios have been computed, the velocity, momentum and ΔP ratios are computed, based on the overall mixture ratio, the density ratio, and the area ratio. The total element flowrate is determined

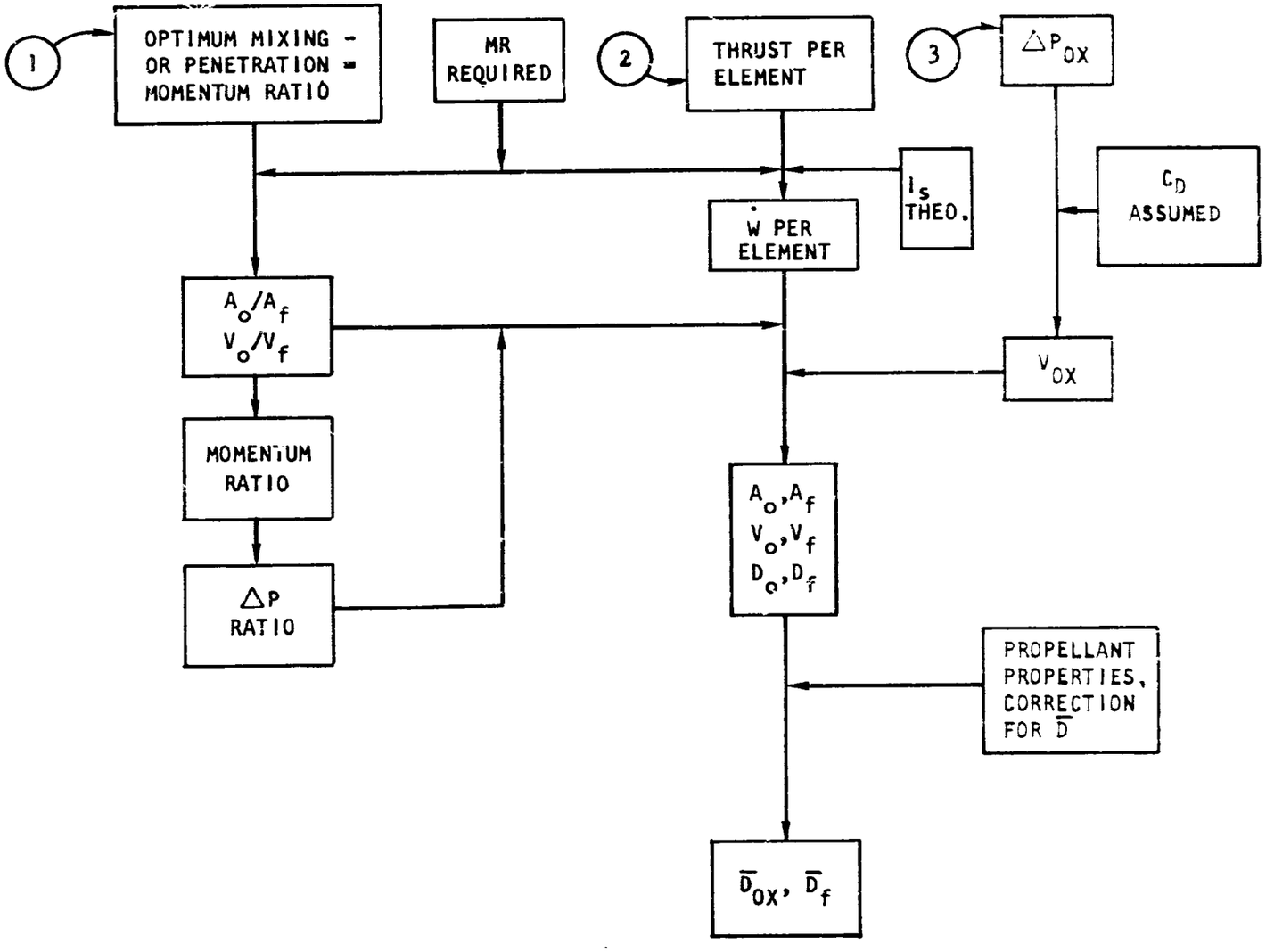

Figure 1. Element Analysis Procedures

next from the theoretical, thermochemical value of specific impulse and the assumed value of thrust per element. The oxidizer velocity is computed from the given value of oxidizer ΔP and an assumed value of C_D. The fuel velocity is computed from the velocity ratio, and, based on an assumed fuel side C_D, the fuel ΔP is calculated. Actual fuel and oxidizer areas are then computed from the continuity equation. Finally, mean dropsize ratios are computed to compare the atomization capabilities of the components of the various elements to the oxidizer size of the unlike-doublet element (used as a standard of comparison).

The details of mixing and atomization calculations are presented in the following sections.

3.1.1 DESIGN CRITERIA FOR MIXING

For liquid-liquid propellant combinations, optimum mixing design conditions were computed using equations developed by Elverum and Morey (Ref. 1) and Rupe (Ref. 2).

Rupe's equation (Ref. 2), for circular orifices, expresses the relationship between propellant properties and element geometry for optimum mixing for unlike doublets. The equation appears below:

$$\frac{D_2}{D_1} = \left(\frac{\dot{w}_2}{\dot{w}_1}\right)^{2/3} \left(\frac{\rho_1}{\rho_2}\right)^{1/3} \qquad (1)$$

where

D = orifice diameter

ρ = propellant density

$\dot{w}$ = propellant flowrate

This relationship, given a propellant density ratio and mixture ratio, defines a specific area ratio for the orifices in the element.

For the gas-liquid propellant combinations, the design criterion (i.e., for optimum mixing with triplet and four-on-one injector elements) is that the liquid jet should penetrate half way through the central gas jet. However, for the unlike doublet, the penetration should be 100 percent of jet diameter. The terminology is illustrated in Fig. 2 . Thus, for triplet and four-on-one elements, optimum penetration is defined as $X_p = 0.5\ D_G$ or $X_p/D_G = 0.5$. The design equation for penetration is taken from a study accomplished at Rocketdyne by Dickerson (Ref. 3).

$$\frac{A_L}{A_G} = K \frac{\dot{w}_L^2}{\dot{w}_G^2} \left(\frac{N_G}{N_L}\right)^2 \frac{\rho_G}{\rho_L} \qquad (2)$$

where

A = Area of one orifice

K = 1.56 for unlike doublet

w = Flowrate

N = Number of orifices of given type in element

ρ = Density

subscripts

L = Liquid

G = Gas

Again an optimum area ratio will be specified upon selection of mixture ratio and the ratio of propellant densities.

3.1.2 ATOMIZATION ANALYSIS

The final step in the element evaluation is the computation of dropsize. The equations of Dickerson (Ref. 4) were used to calculate dropsizes for liquid-liquid systems while Ingebo's equation (Ref. 5) was used to calculate dropsize for the gas-liquid systems.

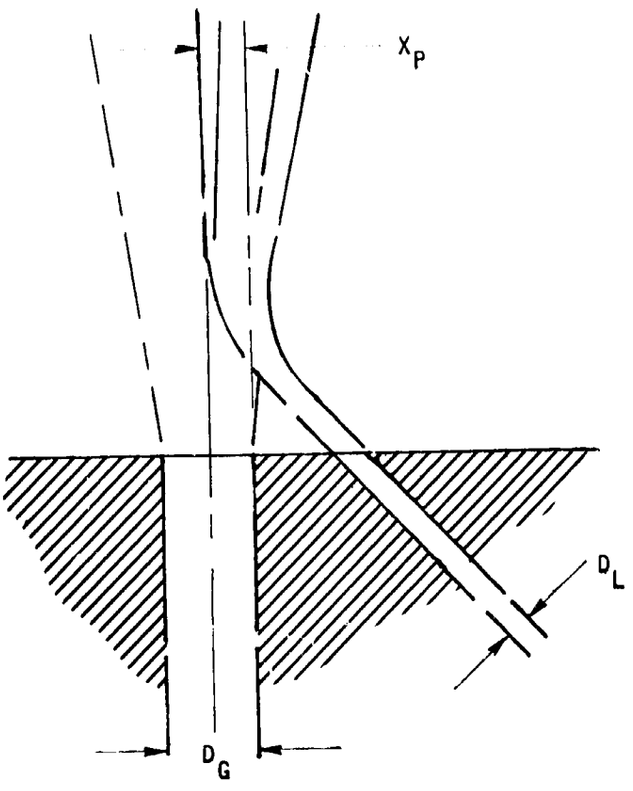

Figure 2. Penetration Terminology

3.1.3 RESULTS OF PRELIMINARY ANALYSIS

The results of the preliminary analysis are presented in Tables 4 through 12. The propellant combinations and operating conditions considered were listed in Table 3. Primary considerations for the selection of an injector element are: (1) mixing, (2) atomization, and (3) pressure drop. Further, the consideration of relative area is important for elements with circular orifices. If the circular orifices in a given element have greatly different areas, their diameters will be different and result in nonimpingement of some of the fluid from the larger orifices. This produces degradation of mixing and atomization.

The element concepts analyzed were each based upon criteria of optimum mixing. It is important to note that optimum mixing for each type of element does not imply any comparison of mixing level from one type of element to another. For example, an optimum four-on-one may produce more uniform mixing than an optimum unlike doublet.

The results of the element analyses for the two liquid/liquid propellant combinations are presented in Tables 4 for N_2O_4 (50-50) and 12 for OF_2/B_2H_6. In general, all of the element types are applicable to these two propellant combinations. The selection of the specific element would depend upon the particular propellant combination selected. For example, certain of the elements do represent rather poor designs from an overall system point of view. For example, in Table 4 for N_2O_4 (50-50), the four-on-one element requires a great deal of difference between the fuel and oxidizer ΔP's. The reason that the four-on-one with oxidizer in the center produces small propellant droplets relative to the other elements is that the fuel ΔP is large. For OF_2/B_2H_6, on the other hand (Table 12), the four-on-one with a fuel center has a reasonable relationship between fuel and oxidizer ΔP's. For the OF_2/B_2H_6, the four-on-one with oxidizer in the center is totally unrealistic with respect to ΔP fuel.

TABLE 4. N_2O_4/N_2H_4-UDMH (50-50) ELEMENT ANALYSIS

			Oxidizer	Fuel
Mixture Ratio	1.6	Density, lbm/ft^3	89	55
Chamber Pressure, psia	100	Viscosity, lbm/ft-sec		
Thrust Range, lbf*	20,000	Surface Tension, lbf/ft		
Injector ΔP_{ox}, psid	30	Critical Pressure/Temperature		

T_{inj} fuel, R 70
I_s opt (sea level), seconds 186.4
Thrust Per Element, lbf 30

	Element Type**				
	Unlike Doublet ○ ●	Triplet Two-on-One ● ○ ●	○ ● ○	Four-on-One		Like Doublet ○ ○ / ● ●
Momentum Ratio, o/f	1.165	1.56	0.946	0.47	2.57	1.0
Dropsize, o/f $\bar{D}$ + $\bar{D}_{ox}$ unlike doublet	1.0/1.2514	0.674/1.518	0.8307/0.9269	0.2008/0.4000	0.9776/1.0187	0.7714/1.1425
Diameter Ratio, o/f	1.165	1.425	0.915	3.67	0.392	1.0
Area Ratio, o/f	1.358	2.03	0.837	13.48	0.1538	1.0
Total Area Ratio, o/f	1.358	1.015	1.673	3.37	0.615	1.0
D_{ox}/D_{fuel}, inches	0.0675/0.0579	0.0675/0.0474	0.0477/0.0523	0.0675/0.0184	0.0337/0.0860	0.0477/0.0477
ΔP_{fuel} (C_D = 1)	34.9	19.9	51.5	217.0	7.2	18.5
ΔP Ratio, o/f	0.86	1.507	0.582	0.1385	4.16	1.62
$\Delta P_{ox}/P_c$	0.3	0.3	0.3	0.3	0.3	0.3
$\Delta P_{fuel}/P_c$ (C_D = 1)	0.35	0.20	0.52	2.17	0.072	0.185
Fuel Mach No. Velocity Ratio (V_O/V_F)	0.726	1.0	0.59	0.293	1.61	1.0
Injection Velocity (oxidizer/fuel), ft/sec	44.8/61.6	44.8/44.6	44.8/76.0	44.8/153	44.8/27.8	44.8/44.8

*Optimum (sea level)
**○ Oxidizer Orifice
● Fuel Orifice

TABLE 5. H_2/O_2 ELEMENT ANALYSIS (P_c = 300, T_{H_2} = 200)

			Oxidizer	Fuel
Mixture Ratio	5.0	Density, lbm/ft^3	71.2	0.280
Chamber Pressure, psia	300	Viscosity, lbm/ft-sec	8.06 x 10^{-6}	3.33 x 10^{-6}
Thrust Range, lbf*	3,000 to 20,000	Surface Tension, lbf/ft	9.0 x 10^{-4}	
Injector ΔP_{ox}, psid	40	Critical Pressure/Temperature		

T_{inj} fuel, R 200
I_s opt (sea level), seconds 344.7
Thrust Per Element, lbf 30

	Element Type**			
	Unlike Doublet	Triplet Two-on-One	Four-on-One	Like Doublet
	O ●	● O ● O ● O X 2	● ● O O ● O O X 4	O O ● ●
Momentum Ratio, o/f	0.64	0.320	0.640	1.00
Dropsize, o/f $\bar{D} \div \bar{D}_{ox}$ unlike doublet	1.0	0.399	0.708	
Diameter Ratio, o/f	0.391	0.392	0.196	0.630
Area Ratio, o/f	0.153	0.1535	0.0384	0.397
Total Area Ratio, o/f	0.153	0.307	0.1535	0.397
D_{ox}/D_{fuel}, inches	0.0568/0.145	0.0401/0.1025	0.0284/0.145	0.0401/0.0636
ΔP_{fuel} (C_D = 1)	7	23	5	40.0
ΔP Ratio, o/f	5.72	1.74	8.0	1.00
$\Delta P_{ox}/P_c$	0.133	0.133	0.133	0.133
$\Delta P_{fuel}/P_c$ (C_D = 1)	0.023	0.0767	0.0167	0.133
Fuel Mach No.	0.171	0.325	0.1625	0.425
Velocity Ratio (V_O/V_F)	0.1284	0.064	0.128	0.491
Injection Velocity (oxidizer/fuel), ft/sec	57.7/450	57.7/901	57.7/450	57.7/1176

*Optimum (sea level)
**O Oxidizer Orifice
● Fuel Orifice

TABLE 6. H_2/O_2 ELEMENT ANALYSIS (P_c = 750, T_{H_2} = 200)

			Oxidizer	Fuel
Mixture Ratio	5.0	Density, lbm/ft^3	71.7	0.690
Chamber Pressure, psia	750	Viscosity, lbm/ft-sec	13.88 x 10^{-6}	3.33 x 10^{-6}
Thrust Range, lbf*	3,000 to 20,000	Surface Tension, lbf/ft	9.0 x 10^{-4}	
Injector ΔP_{ox}, psid	120	Critical Pressure/Temperature		

T_{inj} fuel, R 200

I_s opt (sea level), seconds 382.1

Thrust Per Element, lbf 30

	Element Type**			
	Unlike Doublet ○ ●	Triplet Two-on-One ● ○ ● ○ ● ○	Four-on-One ● ○ ● ○ ○ ● ○ ○	Like Doublet ○ ○ ● ●
Momentum Ratio, o/f	0.64	0.321	0.642	1.00
Dropsize, o/f $\bar{D} : \bar{D}_{ox}$ unlike doublet	1.0	0.399	0.709	
Diameter Ratio, o/f	0.611	0.613	0.307	0.796
Area Ratio, o/f	0.376	0.375	0.094	0.629
Total Area Ratio, o/f	0.376	0.751	0.375	0.629
D_{ox}/D_{fuel}, inches	0.041/0.067	0.0291/0.0473	0.0205/0.0668	0.0291/0.0366
ΔP_{fuel} (C_D = 1)	46	179	43	120
ΔP Ratio, o/f	2.61	0.671	2.79	1.00
$\Delta P_{ox}/P_c$	0.16	0.16	0.16	0.16
$\Delta P_{fuel}/P_c$ (C_D = 1)	0.061	2.59	0.574	0.16
Fuel Mach No.	0.295	0.562	0.281	0.465
Velocity Ratio (V_0/V_F)	0.128	0.0641	0.128	0.0774
Injection Velocity (oxidizer/fuel), ft/sec	99.7/780	99.7/1557	99.7/777	99.7/1290

*Optimum (sea level)

** ○ Oxidizer Orifice

● Fuel Orifice

TABLE 7. H_2/O_2 ELEMENT ANALYSIS (P_c = 750, T_{H_2} = 600)

			Oxidizer	Fuel
Mixture Ratio	5.0	Density, lbm/ft^3	71.7	0.23
Chamber Pressure, psia	750	Viscosity, lbm/ft-sec	13.5 x 10^{-6}	
Thrust Range, lbf*	3,000 to 20,000	Surface Tension, lbf/ft	9.3 x 10^{-4}	
Injector ΔP_{ox}, psid	120	Critical Pressure Temperature		

T_{inj} fuel, R 600
I_s opt (sea level), seconds 382.1
Thrust Per Element, lbf 30

	Element Type**			
	Unlike Doublet ○ ●	Triplet Two-on-One ● ○ ● ○ ● ○	Four-on-One ● ● ○ ● ○ ○ ● ○ ○	Like Doublet ○ ○ ● ●
Momentum Ratio, o/f	0.64	0.32	0.64	1.00
Dropsize, o/f $\bar{D} = \bar{D}_{ox}$ unlike doublet	1.0	0.599	0.709	
Diameter Ratio, o/f	0.354	0.354	0.177	0.590
Area Ratio, o/f	0.1252	0.1252	0.0313	0.348
Total Area Ratio, o/f	0.1252	0.2504	0.1252	0.348
D_{ox}/D_{fuel}, inches	0.041/0.1158	0.0291/0.0821	0.0205/0.1158	0.0291/0.0493
ΔP_{fuel} (C_D = 1)	13	61	15	120
ΔP Ratio, o/f	9.24	1.97	9.24	1.00
$\Delta P_{ox}/P_c$	0.16	0.16	0.16	0.16
$\Delta P_{fuel}/P_c$ (C_D = 1)	0.0174	0.080	0.0174	0.16
Fuel Mach No.	0.166	0.332	0.166	0.465
Velocity Ratio (V_O/V_F)	0.128	0.064	0.128	0.0461
Injection Velocity (oxidizer/fuel), ft/sec	99.7/780	99.7/1560	99.7/780	99.7/2163

*Optimum (sea level)
○ Oxidizer Orifice
● Fuel Orifice

TABLE 8. 80-20 FLOX/CH_4 ELEMENT ANALYSIS (P_c = 200)

			Oxidizer	Fuel
Mixture Ratio	5.7	Density, lbm/ft^3	89.1	0.249
Chamber Pressure, psia	200	Viscosity, lbm ft-sec	138 x 10^{-6}	8.42 x 10^{-6}
Thrust Range, lbf*	3,000 to 20,000	Surface Tension, lbf ft	102 x 10^{-5}	
Injector ΔP_{ox}, psid	30	Critical Pressure Temperature	815 239 R	673 344 R

T_{inj} fuel, R 1,200 I_s opt (sea level), seconds 314.2 Thrust Per Element, lbf 30	Element Type**			
	Unlike Doublet	Triplet Two-on-One	Four-on-One	Like Doublet
Momentum Ratio, o/f	0.64	0.319	0.638	1.00
Dropsize, o/f $\bar{D} \div \bar{D}_{ox}$ unlike doublet	1.0	0.400	0.663	
Diameter Ratio, o/f	0.376	0.377	0.188	0.603
Area Ratio, o/f	0.146	0.142	0.0354	0.367
Total Area Ratio, o/f	0.146	0.284	0.142	0.367
D_{ox}/D_{fuel}, inches	0.061/0.162	0.043/0.114	0.027/0.143	0.043/0.0712
ΔP_{fuel} (C_D = 1)	5	18	5	30
ΔP Ratio, o/f	6.0	1.68	6.00	1.00
$\Delta P_{ox}/P_c$	0.15	0.15	0.15	0.15
$\Delta P_{fuel}/P_c$ (C_D = 1)	0.025	0.091	0.025	0.15
Fuel Mach No.	0.181	0.377	0.187	0.480
Velocity Ratio (V_0/V_F)	0.1124	0.0560	0.112	0.0438
Injection Velocity (oxidizer/fuel), ft/sec	44.8/398	44.8/798	44.8/399	44.8/1020

*Optimum (sea level)

** ○ Oxidizer Orifice

● Fuel Orifice

TABLE 9. 80-20 FLOX/CH_4 ELEMENT ANALYSIS (P_c = 500)

			Oxidizer	Fuel
Mixture Ratio	5.7	Density, lbm/ft^3	89.7	0.622
Chamber Pressure, psia	500	Viscosity, lbm ft-sec	1.38 x 10^{-5}	8.65 x 10^{-5}
Thrust Range, lbf*	3,000 to 20,000	Surface Tension, lbf/ft	1.81 x 10^{-3}	
Injector ΔP_{ox}, psid	100	Critical Pressure Temperature		

T_{inj} fuel, R 1200
I_s opt (sea level), seconds 334.2
Thrust Per Element, lbf 30

	Element Type**			
	Unlike Doublet ○ ●	Triplet Two-on-One ● ○ ● ○ ● ○	Four-on-One	Like Doublet ○ ○ ● ●
Momentum Ratio, o/f	0.64	0.320	0.659	1.00
Dropsize, o/f $\bar{D} = \bar{D}_{ox}$ unlike doublet	1.0	0.585	0.714	
Diameter Ratio, o/f	0.595	0.608	0.297	0.764
Area Ratio, o/f	0.353	0.370	0.088	0.583
Total Area Ratio, o/f	0.353	0.740	0.352	0.583
D_{ox}/D_{fuel}, inches	0.043/0.072	0.031/0.051	0.022/0.074	0.031/0.041
ΔP_{fuel} (C_D = 1)	36	180	37	100
ΔP Ratio, o/f	2.78	0.556	2.70	1.00
$\Delta P_{ox}/P_c$	0.20	0.20	0.20	0.20
$\Delta P_{fuel}/P_c$ (C_D = 1)	0.072	0.36	0.074	0.20
Fuel Mach No.	0.329	0.72	0.34	0.55
Velocity Ratio (V_0/V_F)	0.1124	0.0555	0.112	0.070
Injection Velocity (oxidizer/fuel), ft/sec	81.3/725	81.3/1527	81.3/727	81.3/1165

*Optimum (sea level)
**○ Oxidizer Orifice
● Fuel Orifice

TABLE 10. F_2/H_2 ELEMENT ANALYSIS (P_c = 200)

			Oxidizer	Fuel
Mixture Ratio	14	Density, lbm/ft^3	90	0.025
Chamber Pressure, psia	200	Viscosity, lbm/ft-sec	8.5 x 10^{-6}	11.5 x 10^{-6}
Thrust Range, lbf*	3,000 to 20,000	Surface Tension, lbf/ft	1.0 x 10^{-3}	
Injector ΔP_{ox}, psid	30	Critical Pressure Temperature		

T_{inj} fuel, R 1460
I_s opt (sea level), seconds 337.15
Thrust Per Element, lbf 30

	Element Type**			
	Unlike Doublet ○ ●	Triplet Two-on-One ● ○ ● ○ ● ○	Four-on-One ● ○ ● ○ ○ ● ○ ○	Like Doublet ○ ○ ● ●
Momentum Ratio, o/f	0.64	0.32	0.64	1.00
Dropsize, o/f $\bar{D} \div \bar{D}_{ox}$ unlike doublet	1.0	0.45	0.700	
Diameter Ratio, o/f	0.291	0.292	0.146	0.58
Area Ratio, o/f	0.085	0.0852	0.0213	0.337
Total Area Ratio, o/f	0.085	0.170	0.0852	0.337
D_{ox}/D_{fuel}, inches	0.0618/0.212	0.0437/0.15	0.0309/0.212	0.0437/0.0753
ΔP_{fuel} (C_D = 1)	3	11	3	30
ΔP Ratio, o/f	10.0	2.73	10	1.0
$\Delta P_{ox}/P_c$	0.15	0.15	0.15	0.15
$\Delta P_{fuel}/P_c$ (C_D = 1)	0.15	0.055	0.015	0.15
Fuel Mach No.	0.136	0.271	0.1375	0.535
Velocity Ratio (V_O/V_F)	0.04568	0.0229	0.0457	0.01162
Injection Velocity (oxidizer/fuel), ft/sec	44.4/970	44.4/1935	44.4/980	44.4/3820

*Optimum (sea level)
** ○ Oxidizer Orifice
● Fuel Orifice

TABLE 11. F_2/H_2 ELEMENT ANALYSIS (P_c = 500)

			Oxidizer	Fuel
Mixture Ratio	14	Density, lbm/ft^3	90	0.063
Chamber Pressure, psia	500	Viscosity, lbm/ft-sec	6.5×10^{-6}	11.5×10^{-6}
Thrust Range, lbf*	3,000 to 20,000	Surface Tension, lbf/ft	2.0×10^{-3}	
Injector ΔP_{ox}, psid	100	Critical Pressure/Temperature		

T_{inj} fuel, R 1460
I_s opt (sea level), seconds 384.96
Thrust Per Element, lbf 30

	Element Type**			
	Unlike Doublet O ●	Triplet Two-on-One ● O ● O O ●	Four-on-One ● ● O ● O O O	Like Doublet O O ● ●
Momentum Ratio, o/f	0.64	0.32	0.64	1.00
Dropsize, o/f $\bar{D} \div \bar{D}_{ox}$ unlike doublet	1.0	0.416	0.709	
Diameter Ratio, o/f	0.463	0.463	0.232	0.666
Area Ratio, o/f	0.214	0.214	0.0536	0.444
Total Area Ratio, o/f	0.214	0.428	0.214	0.444
D_{ox}/D_{fuel}, inches	0.0427/0.0922	0.0302/0.0653	0.0213/0.092	0.0302/0.0454
ΔP_{fuel} (C_D = 1)	22	92	22	100
ΔP Ratio, o/f	4.55	1.087	4.55	1.0
$\Delta P_{ox}/P_c$	0.20	0.2	0.2	0.2
$\Delta P_{fuel}/P_c$ (C_D = 1)	0.044	0.184	0.044	0.2
Fuel Mach No.	0.248	0.497	0.250	0.515
Velocity Ratio (V_0/V_F)	0.04568	0.0229	0.0457	
Injection Velocity (oxidizer/fuel), ft/sec	81.2/1775	81.2/3550	81.2/1780	81.2/3670

*Optimum (sea level)
**O Oxidizer Orifice
● Fuel Orifice

TABLE 12. OF_2/B_2H_6 ELEMENT ANALYSIS

			Oxidizer	Fuel
Mixture Ratio	4.0	Density, lbm/ft^3	32.5	21.47
Chamber Pressure, psia	150	Viscosity, lbm/ft-sec	3.2526×10^{-5}	0.0462×10^{-5}
Thrust Range, lbf*	3,000 to 20,000	Surface Tension, lbf/ft	0.42×10^{-5}	3.384×10^{-5}
Injector ΔP_{ox}, psid	30	Critical Pressure/Temperature		

T_{inj} fuel, R 70
I_s opt (sea level), seconds
Thrust Per Element, lbf 30

	Element Type**				
	Unlike Doublet	Triplet Two-on-One		Four-on-One	Like Doublet
Momentum Ratio, o/f	19.72	2.350	1.447	0.568	3.125	1.0
Dropsize, o/f $\bar{D} \div \bar{D}_{ox}$ unlike doublet	1.0/0.4446	0.6334/0.9214	1.017/0.9146	0.1577/0.2025	1.089/0.974	1.173/1.2127
Diameter Ratio, o/f	2.17	1.883	1.20	5.42	0.578	1.0
Area Ratio, o/f	4.72	3.54	1.44	29.4	0.334	1.0
Total Area Ratio, o/f	4.72	1.775	2.88	7.36	1.336	1.0
D_{ox}/D_{fuel}, inches	0.0559/0.0395	0.0559/0.0297	0.0395/0.0329	0.0559/0.0103	0.02794/0.0463	0.0395/0.0395
ΔP_{fuel} (C_D = 1)	65.1	22.9	59.2	389	12.86	11.96
ΔP Ratio, o/f	0.461	0.763	0.507	0.0772	2.333	2.56
$\Delta P_{ox}/P_c$	0.20	0.20	0.20	0.20	0.20	0.20
$\Delta P_{fuel}/P_c$ (C_D = 1)	0.434	0.152	0.395	2.59	0.0858	0.0796
Fuel Mach No. Velocity Ratio (V_0/V_F)	0.221	0.588	0.363	0.142	0.782	1.040
Injection Velocity (oxidizer/fuel), ft/sec	59.8/271	59.8/101.8	59.8/165	59.8/421	59.8/76.5	59.8/57.5

*Optimum (sea level)
** ○ Oxidizer Orifice
● Fuel Orifice

3.2 PRELIMINARY EVALUATION

The preliminary evaluation is made for orifices and elements for use with the N_2O_4 (50-50) propellant combination. Therefore, the evaluation of injector element types will be based on the data presented in Table 4 only.

3.2.1 ORIFICE SHAPE EVALUATION

Functional

Based simply on the very general guidelines for analysis (i.e., propellant combinations and engine operating conditions), it is difficult, a priori, to eliminate any particular orifice shapes or configurations from evaluation.

However, to limit the number of orifices which will be considered for incorporation into element design, a selection of orifice shapes must be made. Nine shapes were, therefore, chosen which appeared to be most amenable to injector element design. These shapes are listed below:

1. Circle
2. Square
3. Rectangle
4. Equilateral Triangle
5. Isosceles Triangle
6. Diamond
7. Ellipse
8. Star
9. Self-Atomizing Nozzle

A basis for evaluation for each orifice is presented. Quantitative techniques are employed where data or theory are available; otherwise, analysis is based upon qualitative reasoning. Results of the orifice shape preliminary functional evaluation are presented in Table 13. Note that for each parameter an arbitrary ranking of 10 is given to the circle. Parameters ranked greater than 10 have operational characteristics better than the circular orifice standard.

For the comparison of various shapes, the length-to-diameter ratio and cross-sectional area of all shapes will be equal. The diameter, or characteristic length, of an orifice shape is assumed to be the hydraulic diameter. The hydraulic diameter is defined as four times the cross-sectional area divided by the wetted perimeter;

$$D_H = \frac{4A}{P}$$

The terminology used in describing orifices is explained in the sketch shown below.

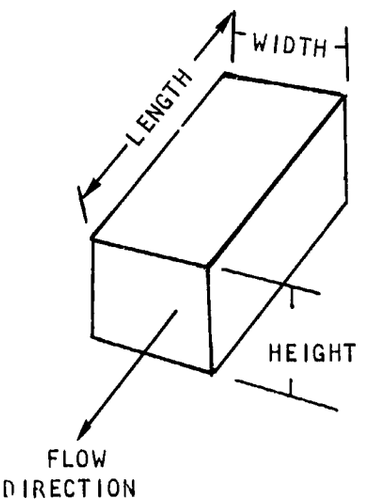

The basis for each ranking is given below.

TABLE 13

SINGLE ORIFICE RATING CHART, FUNCTIONAL RATING PARAMETERS

Orifice Configuration	Operating Sensitivity								Functional Totals
	C_D		Free Stream Stability	Propellant Temperature	Propellant Pressure	Cross Velocity	ΔP Variations	Contamination Sensitivity (Plugging)	
	VAR	Level							
 Circular (Base Point)	10	10	10	10	10	10	10	10	80
 Square	8	12	9	9	9	9	8	10	74
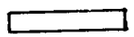 Rectangle AR = 8	3	15	3	12	12	6	5	4	59
 Equilateral Triangle	7	13	8	8	8	8	-	9	68
 Isosceles Triangle AR = 4	6	14	5	8	8	6	6	3	56
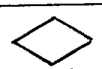 Diamond AR = 4	4	13	4	8	8	6	-	4	54
 Elipse AR = 4	4	12	6	9	10	7	4	6	58
 Star	3	11	4	7	4	5	9	3	46
 Nozzle	8	8	11	13	12	12	8	8	80

C_D Variation. Pressure drop defines the consistency of operation of an orifice shape over a range of flowrate and pressure drop. A desirable feature for an orifice would be a discharge coefficient, C_D, which remains constant over a large ΔP range. An undesirable feature would be a significant discontinuity of flow coefficient at one or more ΔP levels, making predictions of flowrate versus pressure drop difficult.

It would be expected that the perimeter of a shape at the entrance to an orifice would have the controlling influence on the major pressure drop characteristics of the orifice. The greater the perimeter and the more irregularities in the shape of that perimeter, the more sensitive the orifice should be to ΔP level.

Because no analytical data were available before initiation of this program, the evaluation of shapes is based upon wetted perimeter. The shapes with the greatest length of perimeter are ranked lowest. Since perimeter and aspect ratio are related, shapes with the high aspect ratio receive low ranking in Table 13.

C_D Level. Flow coefficient evaluation was based on limited data available for noncircular-orifice orifices with short length to hydraulic diameter (L/D_H). Data taken by Calleghan and Bowden in 1949 (Ref. 6) indicates that the higher the perimeter for a given area, the higher the flow coefficient. The authors showed that a short circular orifice would yield a value of C_D lower than any other shape. This result they rationalized on the basis of the number of degrees into which momentum is converted from radial to axial momentum at the entrance to an orifice. For a circle, momentum is converted in all 360 degrees at the entrance, while for a slot of infinite width, momentum is converted from only two directions.

Orifices are evaluated on the basis that a large C_D is desirable from minimum orifice pressure drop considerations. Based on Calleghan and Bowden's work, those shapes which deviate most from a circle will have the highest C_D's. This criterion is used in Table 13 to rank all of the shapes except for the spray nozzle. The nozzle has unique pressure drop characteristics that must be estimated qualitatively.

Free-Stream Stability. The stability of a liquid jet penetrating a gaseous environment is affected by the shape of the orifice which produces the jet and the condition of the fluid upstream of the orifice. For a flow with a given volume flux, the most stable jet will be produced by an orifice with a minimum wetted perimeter for a given cross-sectional area. The orifice shape which satisfies this criterion is, of course, the circle.

The factors which affect free jet mechanics are (1) the tendency of surface tension forces to minimize the surface area of a jet, (2) the drag of the environment over the surface of the jet, and (3) the level of turbulence in the fluid upon injection. Premature jet breakup is undesirable for impinging type injector elements. Jets which have undergone substantial breakup prior to impingement (i.e., incoherent) produce sprays which are poorly mixed and atomized. Incoherent jets can also lead to impingement which in turn leads to poor mixing and atomization.

Rating of the various shapes in Table 13 follows basically their deviation from circular configurations. The lowest ratings are given to shapes with large perimeters and large deviation from circular shape.

Propellant Temperature. Propellant temperature can influence the flow characteristics of an orifice in several ways. One way is the change of viscosity with temperature. Because the Reynolds number is inversely proportional to temperature, the Reynolds number varies directly with temperature.

Another effect of fluid temperature on orifice performance is produced by changes in the vapor pressure of the fluid and the level of solubility of gases in the fluid. Both vapor pressure and dissolved gas affect the operational level at which an orifice will undergo hydraulic flip. As the temperature of a fluid is increased, its vapor pressure is increased which, in turn, increases the likelihood of cavitation. On the other hand, as the temperature increases, the solubility of foreign gases decreases, decreasing the sensitivity from sudden decompression. (If a fluid in which there is a great deal of dissolved gas is suddenly decompressed, the gas will come out of solution and form bubbles. This can happen as a fluid proceeds from a reservoir to the exit of an orifice.) These two effects tend to offset one another. However, the degree to which they do is not well-known. The evaluation shown in Table 13 is based on estimated sensitivity to cavitation, separation, and hydraulic flip.

Propellant Pressure. Many of the comments made concerning propellant temperature apply equally well to propellant pressure. The pressure level of a system affects the hydraulic flip characteristics. The higher the pressure, the higher the ΔP must be to produce hydraulic flip. Propellant pressure evaluation is shown in Table 13.

Cross Velocity. Sensitivity to cross velocity will depend not only on orifice shape but also on the directional orientation of the cross velocity to the shape. For the purpose of the rating, it is assumed that the cross velocity vector is parallel to the longest axis or side of a given shape. With this velocity orientation, the lower ratings in Table 13 are given to the shapes with the higher aspect ratios. This rating is, by nature, qualitative. No data exists to relate shape to cross velocity sensitivity.

ΔP Variations. It is assumed that all shapes operate at a fixed average ΔP such that all are in their "unflipped" regime. Sensitivity to ΔP

variations is defined as the amount of flowrate variation exhibited for a given ΔP variation or $d\dot{W}/d\Delta P$. The higher this ratio, the more sensitive. To obtain a crude estimate of the ratio $d\dot{W}/d\Delta P$, the orifice flow equation is differentiated (Eq. 3).

$$\frac{d\dot{W}}{d\Delta P} = 1/2 \frac{C_D A \sqrt{2 g \rho}}{\sqrt{\Delta P}} \qquad (3)$$

From Eq. 3 it is evident that the flow sensitivity is indirectly proportional to the square root of the average ΔP level and directly proportional to C_D. Therefore, an efficient orifice is a sensitive orifice.

Contamination Sensitivity. Evaluation under this category is fairly obvious. As shown by the relative rankings given in Table 13, those shapes with narrow passages are more likely to be contaminated and received a lower ranking value than those with fairly open cross sections.

Overall Functional Rating of Orifice Shapes. From a functional point of view, the circle, spray nozzle, square, and equilateral triangle received the highest ratings. The poorest rating was received by the star shape.

Fabrication

Results of the fabrication evaluation are presented in Table 14. This evaluation is based upon the criteria shown in Table 14. Evaluation within each criterion was made for each of the six manufacturing techniques which are listed in Table 14, under fabrication methods. Rankings greater than 10 are better than the twist drill standard.

In the fabrication evaluation, both the shape and the fabrication technique employed to make that shape were considered. As shown in "Fabrication Totals" (Table 14), the electrical discharge machining (EDM) process received the highest rating among all the fabrication techniques, regardless of the shape of the orifice upon which it was employed.

TABLE 14. SINGLE ORIFICE RATING CHART, FABRICATION RATING EVALUATION

Orifice Configuration	Fabrication Methods	Tolerance Obtainable	Design Flexibility	Fabrication Time	Fabrication Cost	Inspection	Tooling Structural Limits	Fabrication Totals
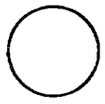 Circular (Base Point)	Drill	10	10	10	10	10	10	60
	Cast	6	5	13	14	6	8	52
	EDM	12	9	11	15	10	13	70
	ECM	8	9	7	8	9	13	54
	P/M	8	7	9	10	9	12	55
	E/F	7	7	9	8	7	8	46
 Square	Cast	4	4	13	10	6	8	45
	EDM	11	8	11	14	8	13	65
	ECM	7	7	7	8	7	13	49
	P/M	7	6	9	8	8	8	46
	E/F	6	7	9	9	7	8	46
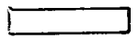 Rectangle	Cast	3	3	11	10	4	8	39
	EDM	10	7	9	13	7	10	56
	ECM	7	6	6	7	7	10	43
	P/M	6	5	8	7	8	7	39
	E/F	8	6	8	11	8	8	47
 Equilateral Triangle	Cast	5	4	11	10	8	8	44
	EDM	11	7	9	14	8	13	61
	ECM	7	7	6	8	8	13	49
	P/M	6	6	8	8	7	8	43
	E/F	7	6	8	9	7	8	45
 Isosceles Triangle	Cast	3	3	11	10	4	6	37
	EDM	9	6	9	13	7	11	55
	ECM	7	6	6	7	7	11	44
	P/M	5	5	8	7	6	6	39
	E/F	6	5	8	11	6	7	43
 Diamond	Cast	3	4	8	9	4	7	35
	EDM	10	7	9	12	7	11	56
	ECM	7	7	7	7	7	11	46
	P/M	6	6	6	7	6	6	37
	E/F	7	6	6	10	6	7	42

EDM = Electrical Discharge Machining
ECM = Electrical Chemical Machining
P/M = Powder Metallurgy
E/F = Electroforming

TABLE 14

(Concluded)

Orifice Configuration	Fabrication Methods	Tolerance Obtainable	Design Flexibility	Fabrication Time	Fabrication Cost	Inspection	Tooling Structural Limits	Fabrication Totals
 Ellipse	Cast	5	4	13	[illegible]	[illegible]	[illegible]	45
	EDM	10	7	11	[illegible]	[illegible]	12	62
	ECM	8	6	9	[illegible]	[illegible]	12	55
	P/M	7	5	[illegible]	[illegible]	[illegible]	[illegible]	41
	E/F	7	6	[illegible]	[illegible]	[illegible]	[illegible]	44
 Star	Cast	2	3	8	[illegible]	[illegible]	3	25
	EDM	8	5	9	[illegible]	[illegible]	[illegible]	43
	ECM	6	4	[illegible]	[illegible]	[illegible]	6	35
	P/M	4	3	[illegible]	[illegible]	[illegible]	3	29
	E/F	5	4	6	[illegible]	[illegible]	4	31
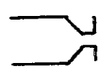 Nozzle Compound	Cast	3	4	11	[illegible]	[illegible]	[illegible]	33
	EDM	9	7	9	[illegible]	[illegible]	[illegible]	45
	ECM	6	7	6	[illegible]	[illegible]	[illegible]	37
	P/M	6	6	[illegible]	[illegible]	[illegible]	[illegible]	35
	E/F	7	6	[illegible]	[illegible]	[illegible]	[illegible]	42

EDM = Electrical Discharge Machining
ECM = Electrical Chemical Machining
P/M = Powder Metallurgy
E/F = Electroforming

If it is assumed that all shapes are manufactured by the EDM process, then the circle, square, triangle, and ellipse rank highest among the shapes from a fabrication point of view.

3.2.2 SUMMARY OF RESULTS

A composite evaluation of all orifice shapes is presented in Table 15. An overall average rating number is presented which includes both the functional and fabrication rating numbers.

Based upon the EDM process, the circle, square, equilateral triangle and the spray nozzle receive the highest ratings.

3.2.3 ELEMENT CONFIGURATION EVALUATION

Results of the element configuration evaluation are presented in Table 16. This evaluation is based on the preliminary analysis data from Table 4. The various elements are evaluated for the N_2O_4 (50-50) propellant combination at 30 lb_f thrust per element, mixture ratio 1.6, chamber pressure 100 psia, and oxidizer orifice ΔP = 30 psid.

Tolerance Considerations

Tolerance sensitivity ratings were based on qualitative estimates made by design specialists as to the relative degree of difficulty of producing elements of each type. Also considered was the degree of difficulty of manufacture.

Performance Considerations

It has been shown in the past with circular orifices that the level of mixing is quite similar for the different element types shown in Table 16. when each has been designed for optimum mixing. During preliminary evaluation, it was assumed that this would also be true for noncircular

TABLE 15

SINGLE ORIFICE RATING CHART, COMPOSITE
EVALUATION OF ALL ORIFICE SHAPES

Orifice Configuration	Fabrication Methods	Functional and Fabrication Totals	Overall Average
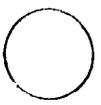 Circular (Base Point)	Drill	140	10
	Cast	132	9.43
	EDM	150	10.71
	ECM	134	9.57
	P/M	135	9.64
	E/F	126	9.0
 Square	Cast	119	8.50
	EDM	139	9.93
	ECM	123	8.79
	P/M	120	8.57
	E/F	114	8.14
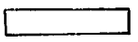 Rectangle	Cast	98	7.0
	EDM	115	8.21
	ECM	102	7.29
	P/M	98	7.0
	E/F	106	7.57
 Equilateral Triangle	Cast	112	8.00
	EDM	129	9.21
	ECM	117	8.36
	P/M	111	7.93
	E/F	113	8.07
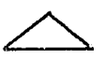 Isosceles Triangle	Cast	93	6.64
	EDM	111	7.92
	ECM	100	7.14
	P/M	95	6.79
	E/F	99	7.07
 Diamond	Cast	89	6.36
	EDM	110	7.86
	ECM	100	7.14
	P/M	91	6.50
	E/F	96	6.86
 Ellipse	Cast	103	7.36
	EDM	120	8.57
	ECM	111	7.93
	P/M	99	7.07
	E/F	102	7.29
 Star	Cast	71	5.07
	EDM	89	6.36
	ECM	79	5.64
	P/M	75	5.36
	E/F	77	5.5
 Nozzle Compound	Cast	113	8.07
	EDM	126	9.0
	ECM	117	8.36
	P/M	116	8.29
	E/F	122	8.71

TABLE 16. ELEMENT CONFIGURATION EVALUATION

Ranking Parameter / Element Configuration	Tolerance Sensitivity (Fabrication and Operation) Difficulty in Manufacture	Performance				Combustion Stability	Total	Average	Remarks
		Mixing	Atomization	ΔP	Average				
○ ● Unlike Doublet	10	10	10	10	10	10	30	10.0	Standard of comparison - comparison based upon N_2O_4 (50-50)
○ ● ○ Triplet	9	10	11.4	6.7	9.4	10	28.4	9.45	
● ○ ● Triplet	9	10	10.2	8.8	9.6	10	28.6	9.53	
○ ○ ● ○ ○ Four-on-One	6	10	10	6	8.7	10	24.7	8.23	Four-on-one elements are difficult to manufacture and to manifold. These considerations have been considered.
● ● ○ ● ● Four-on-One	6	10	23.8	2	11.9	10	27.2	9.06	
○ ● Like Doublet ○ ●	8	10	10.9	8.4	9.8	10	27.8	9.26	

*Shaded orifices indicate fuel
Open orifices indicate oxidizer

orifices. As shown in Table 16, all elements have been given an equivalent rating with respect to mixing.

Since mixing has been optimized, the performance considerations which are left for comparison are:

1. Pressure drop (fuel)
2. Atomization

It is interesting first to note the pressure drop considerations. The oxidizer pressure drop has been fixed at 30 psid. The dependent variable is, therefore the fuel ΔP. Relative magnitude of the fuel ΔP versus oxidizer ΔP is obtained from the row labeled ΔP ratio in Table 16. These ratios were obtained by dividing the oxidizer by the fuel ΔP. The ratios for the unlike doublet, triplet, and like doublet are reasonable. That is, for a pressure-fed mission, the two propellant ΔP's should be fairly close to one another from an overall system design standpoint. However, for the four-on-one element, the ΔP ratio is 0.1385 with the oxidizer in the center and 4.16 with the fuel in the center. This makes the fuel ΔP's respectively 217 and 7.2 psid. These are not reasonable values.

Rating for the ΔP consideration is shown in Table 16. Highest ratings are given to elements with the fuel and oxidizer ΔP's closest in value.

Results of the atomization equations are shown along the row labeled "Dropsize" in Table 16. The values were computed by dividing the mass mean dropsize of a given propellant by the dropsize of the oxidizer produced in the unlike doublet. The term o/f indicates that the oxidizer dropsize is given first followed by that of the fuel. It appears from the data that the four-on-one oxidizer center stream element possesses significant advantages for atomization. However, the small relative dropsizes are merely a reflection of the high fuel velocity caused by the high fuel ΔP. That is, an advantage is produced as a byproduct of a disadvantage. Aside from this element, the dropsizes produced by the other elements are

all fairly close in magnitude. The largest drops are produced by the fuel side of the triplet with oxidizer center stream. Large drops are undesirable from a performance standpoint because of the time required to complete vaporization. Rating in Table 16 is such that small drops yield high ratings.

Stability Considerations

Rating with respect to combustion stability is based on a preliminary analysis. This analysis indicated that the stability characteristics of all the elements should be quite similar. Therefore, all were given the same rating (see Table 16).

3.2.4 SELECTION OF MOST PROMISING ORIFICES AND ELEMENTS

The ratings for performance, stability, and machineability were added together and averaged. These results are shown in Table 16.

The conclusion which must be drawn from element rating of N_2O_4/N_2H_4-UDMH (50-50) is that the unlike doublet is the superior element. In addition, the triplet and the like doublet are good candidate elements. A four-on-one element does not appear to offer any significant advantages. It must be remembered that these evaluations were made based on analysis techniques and data which were developed for, and with, circular orifices. Noncircular orifices may greatly effect the rating and evaluation.

Only one element type, the unlike doublet, was selected for further evaluation in the experimental portion of this program. This selection was based upon the evaluation shown in Table 16 as well as the fact that it is the most basic of all injector element types. The unlike doublet is easy to manifold and simple to fabricate.

Seven orifice shapes were selected for cold-flow experimental evaluation. The shapes are:

1. Circle
2. Square
3. Rectangle
4. Slot (rectangle with large aspect ratio)
5. Equilateral triangle
6. Isosceles triangle
7. Diamond

The self-atomizing spray orifice was also selected. However, it was not classified as an independent noncircular orifice shape. It was used in element testing and is discussed in the subsequent text.

It will be noted that the list of orifices includes all those shown in Table 15, with the exception of the elliptical and star shapes. The star was eliminated because of its poor rating in the evaluation. The ellipse was eliminated because of its complex contour. It is difficult to generate an accurate elliptical contour on the small scale required for these orifices.

4.0 EXPERIMENTAL DEFINITION OF ORIFICE FLOW AND ELEMENT SPRAY CHARACTERISTICS

Cold-flow and hot-fire experimentation were conducted to determine the hydraulic characteristics for single orifices, and the spray mixing, atomization characteristics and operating characteristics for single element injectors. The scope of the experimental program was defined from the analysis of the preliminary evaluation, which served to illustrate where additional technology were required. A total of 9 orifice shapes were studied which included circular, triangular, rectangular, and diamond shapes. These shapes were then configured into several unlike-doublet types (triangle-on-triangle, rectangle-on-rectangle, triangle-on-rectangle, and circle-on-circle). In addition, several types of self-atomizing nozzles were also studied. The overal study required 409 orifice tests and 154 cold-flow element spray tests. Orifice C_D, and flip characteristics as a function of orifice L/D, entrance condition, cross velocity, and backpressure were determined for the various shapes. Also, 11 tests using NTO and A-50 propellants were conducted using single orifices. Mixing and atomization characteristics were determined for the elements. The overall cold-flow results were then used to predict hydraulic and performance characteristics. Hot-fire tests were then conducted to determine operating characteristics. A complete summary of the orifice and element cold-flow and element hot-fire tests is contained in Appendix A. The results of these experiments and a description of the experimental hardware are described below.

4.1 EXPERIMENTAL APPARATUS*

4.1.1 SINGLE ORIFICE DESIGNS

As a result of the preliminary evaluation, seven orifice shapes were selected for evaluation. The seven orifice shapes included four basic geometric configurations: circle, rectangle, diamond, and triangle. Perturbations in aspect ratio for the rectangle and triangle provided the additional three shapes.

The basic orifice shapes are shown in Fig. 3. Nominal dimensions and aspect ratios for these shapes are also given. All orifices have the same area, 0.0028 $in.^2$, which is the area of a circle 0.060 inches in diameter. Certain of the shapes are not only aspect ratio variations but are considered separate shapes on their own merit. For example, the rectangle is a basic shape as well as an aspect ratio variation of a square. The hydraulic diameters, aspect ratios, and orifice lengths for the various L/D_H's as fabricated are shown in Table 17.

The orifices were fabricated from aluminum primarily to minimize material and fabrication costs. The electrical discharge machining (EDM) process was used to fabricate the orifices. The EDM process functions by discharging a capacitor bank across a narrow gap (0.001 inch) formed between the work (anode) and the tool (cathode) to remove a minute piece of anode. The tool and work are immersed in a dielectric fluid that provides continuous flushing of the part. Generally, the process is applicable to all electrically conductive materials.

The initial seven orifice plates fabricated using the EDM process are shown in Fig. 4 and 5, 25X magnified. Inspection under both 50 and

*To maintain continuity of thought, the descriptions of the cold-flow and hot-firing facilities as well as the experimental procedures are presented in Appendix D rather than with the orifice and injector designs.

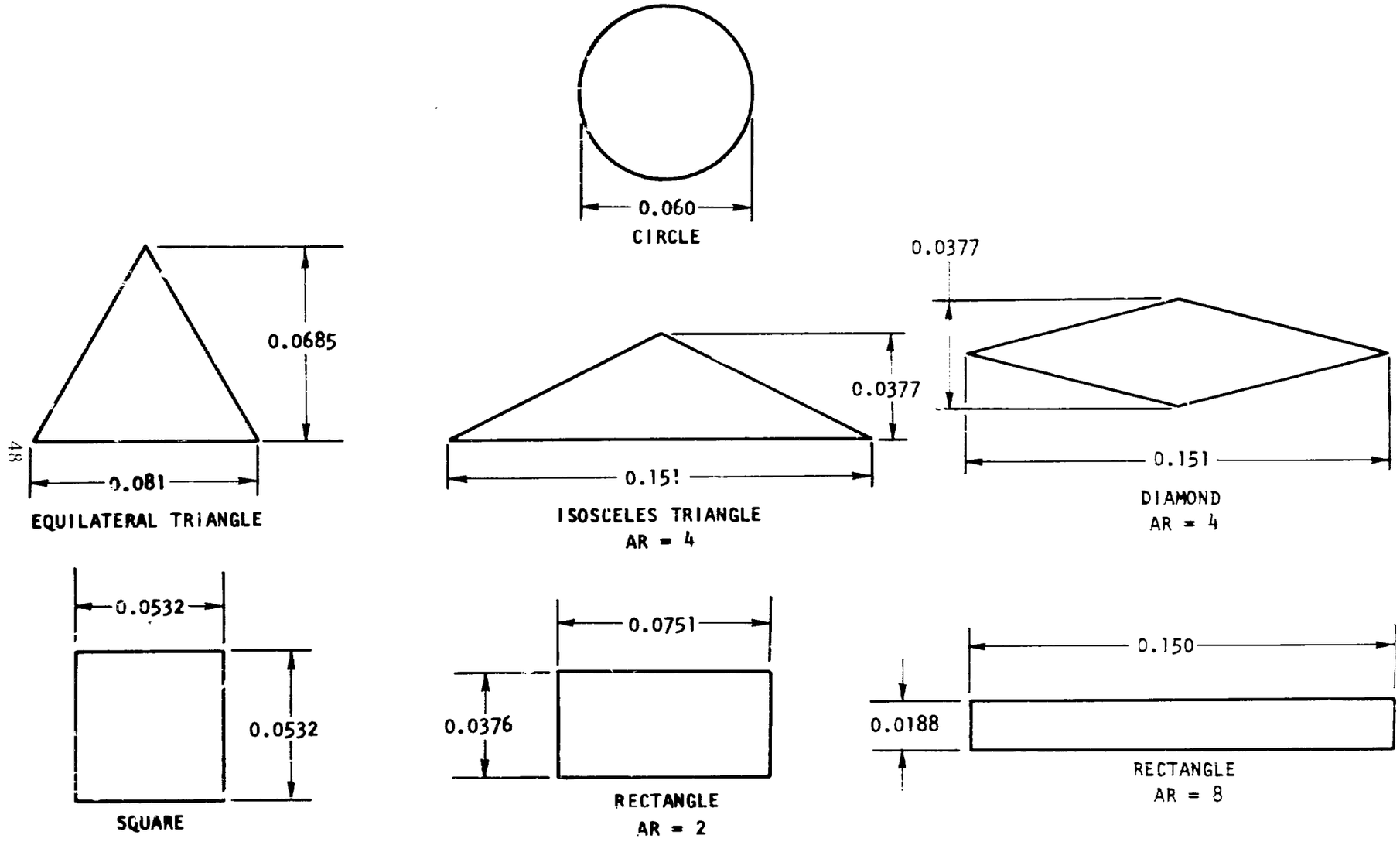

Figure 3. Orifices Selected for Single Orifice Cold-Flow Evaluation

TABLE 17

ORIFICE TEST HARDWARE DATA

Shape	Nominal L/D	Actual L/D	Area, $in.^2$	Length, inch	Hydraulic Diameter, inch
Circle	*6(1)	1.97	0.00289	0.120	0.061
	4	3.93	0.00285	0.240	0.061
	*6(1)	5.90	0.00278	0.360	0.061
	6(2)	5.89	0.00317	0.359	0.061
	20	20.73	0.00271	1.20	0.0579
Square	2	1.89	0.00309	0.106	0.0561
	4	3.83	0.00296	0.212	0.0554
	6(1)	5.91	0.00272	0.319	0.0540
	6(2)	6.06	0.00310	0.321	0.0539
	20	20.64	0.00281	1.063	0.0515
Rectangle	2	1.93	0.00286	0.099	0.0512
	4	3.84	0.00286	0.199	0.0518
	6(1)	5.64	0.00286	0.298	0.0528
	6(2)	5.91	0.00352	0.318	0.0538
	20	19.84	0.00289	0.994	0.0501
Slot	2	1.22	0.00382	0.0535	0.0438
	4	2.84	0.00372	0.1205	0.0425
	6(1)	4.69	0.00334	0.1865	0.0398
	6(2)	5.49	0.00445	0.251	0.0457
	20	18-92	0.00313	0.664	0.0351
Equilateral Triangle	2	1.84	0.00334	0.092	0.050
	4	3.60	0.00328	0.185	0.0514
	6(1)	5.22	0.00306	0.277	0.0531
	6(2)	5.99	0.00330	0.278	0.0464
	20	20.26	0.00304	0.924	0.0456
Isosceles Triangle	6(1)	4.88	0.00329	0.210	0.043
Diamond	6(1)	5.14	0.00322	0.216	0.042

*L/D's of 2 and 4 were made from 6(1), 6(2) was made from 20. L/D = 6(2) was rounded.

500 power magnification showed that the first three orifice shapes (Fig. 4) were within tolerance (±0.001 of the specified dimensions) on the exit side of the orifice with approximately 0.001 enlarging taper on the entry side. Small irregularities of approximately 0.002 maximum on the side walls and 0.002 corner radii were observed. Rounding of the hole edge was prevalent on the exit side. Sectioning of a typical machined hole showed an overall surface finish of 80 to 90 RMS.

Several electrode materials and two designs were evaluated. Electrodes made of copper tungsten, silver tungsten, tellurium copper, and free machining brass were used. Also, a stepped electrode to minimize hole taper was investigated. In summary, orifice plates machined with nonstepped brass electrodes were found to be adequate. The four shapes numbered -3, -5, -7, and -9 in Fig. 4 and 5 were produced using this type of electrode.

The photo of Fig. 4 shows the electrical discharge machine (EDM) setup during the machining of the No. 9 high aspect ratio rectangular shape. A voltage-sensitive stepping motor servo located at the top of the arbor support is used for tool positioning. The low-voltage EDM machine used during this program has a dielectric tank containing Shell 140 fluid and is positioned on an adjustable crossfeed slide table.

4.1.2 SINGLE ELEMENT DESIGNS

Two major categories of element hardware were utilized: (1) spray nozzles, and (2) impinging elements.

Spray Nozzles

The spray nozzle type injector elements utilized were available from a commercial vendor. The nozzles were purchased from Spray Systems Incorporated. The nozzles represent off-the-shelf items and affected a considerable cost savings over in-house-fabricated parts. The three basic

a. Electrical Discharge Machining (EDM)

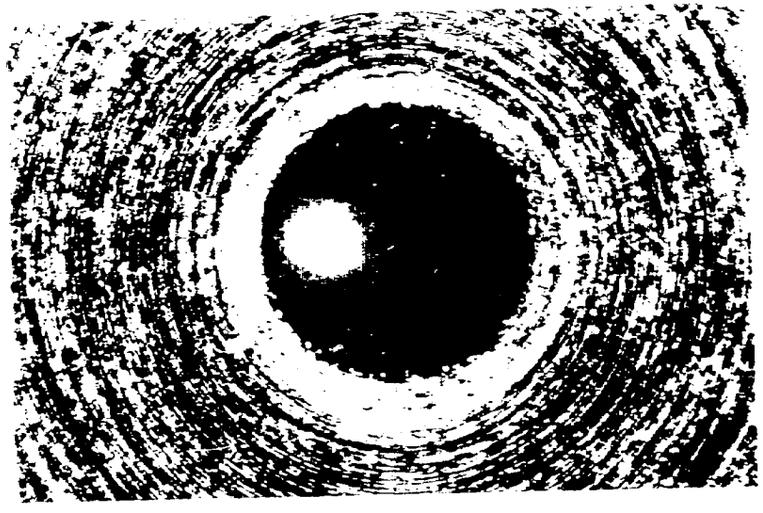

b. No. 3 Circle Area = [illegible] in.^{2}

25X Magnification

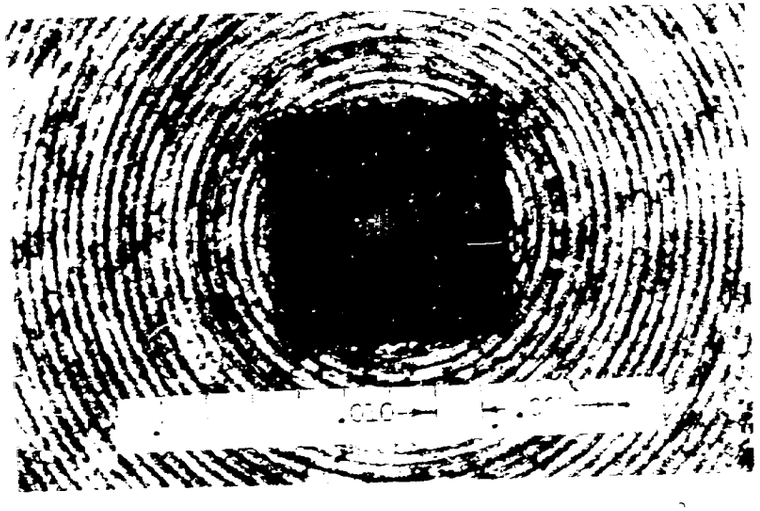

c. No. 5 Square Area = 0.00286 in.^{2}

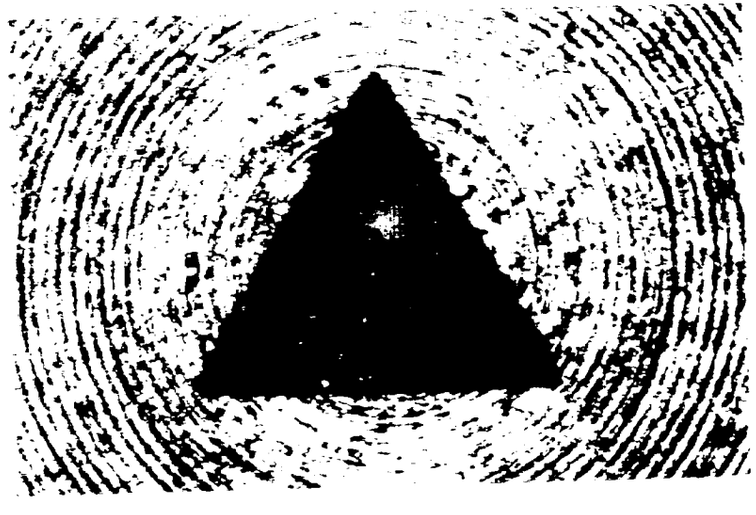

d. No. 6 Equilateral Triangle Area = [illegible] in.^{2}

Figure 4. Single Orifice Basic Shapes

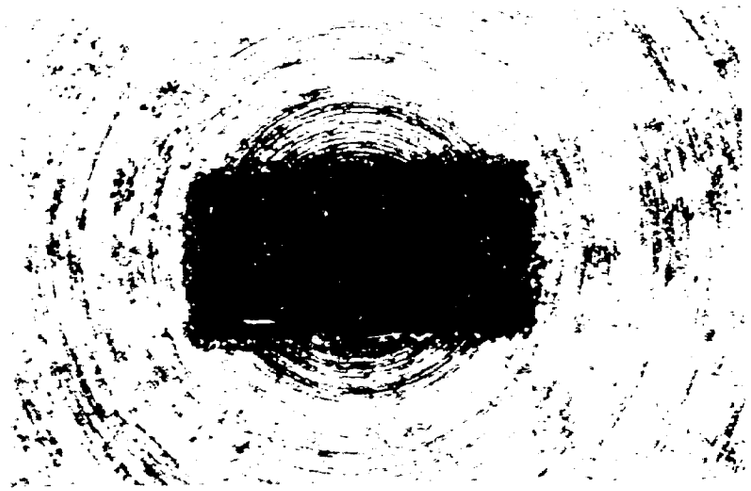

a. No. 7 Rectangle (AR = 2) Area = 0.00300 in.^{2}

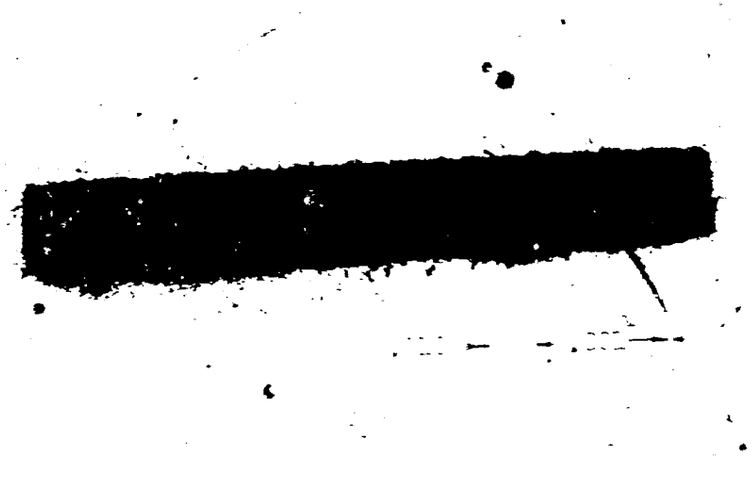

b. No. 9 Rectangle (AR = 8) AREA = 0.00348 in.^{2}

25X Magnification

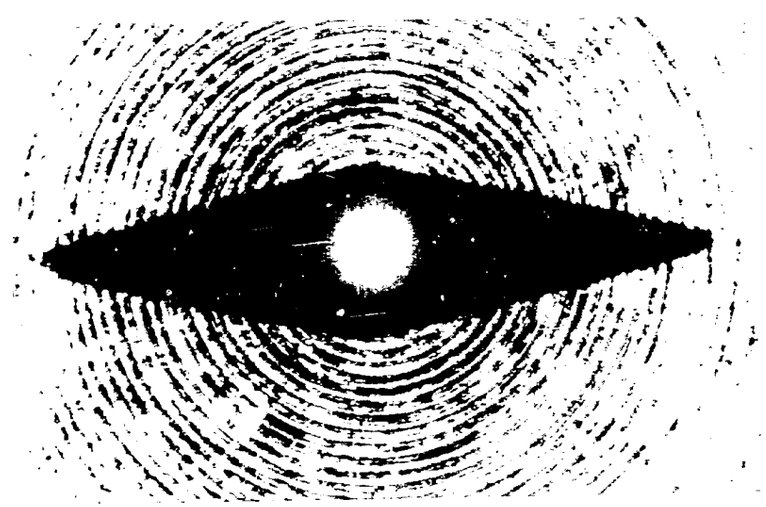

c. No. 19 Diamond (AR = 4) Area = 0.00336 in.^{2}

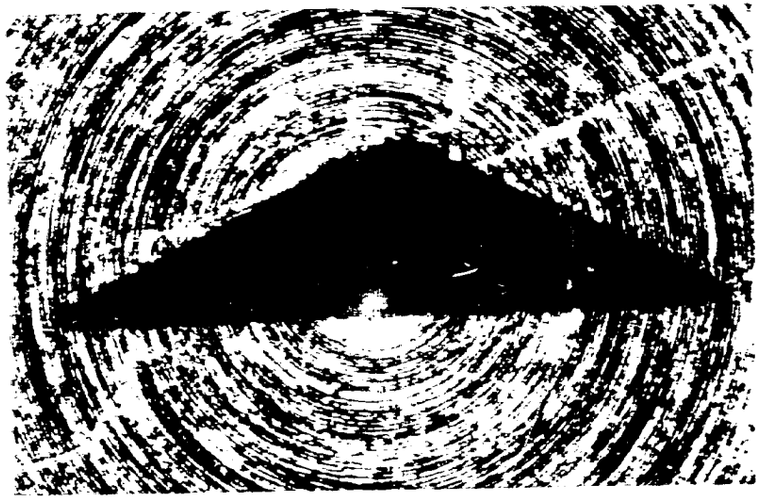

d. No. 17 Isosceles Triangle (AR = 4)
Area = 0.00345 in.^{2}

Figure 3. Single Orifice Shapes With Variations in Aspect Ratio

types of spray nozzles shown in Fig. 6 were evaluated. As shown, two designs provided a swirling hollow-cone injection pattern while the other produced a flat spray fan. One of the swirl designs (hydraulic) consisted of a swirl chamber into which the liquid entered through a tangential port and is then injected from the swirl chamber through a central orifice. The liquid swirls within the swirl chamber around an air core. This results in the fluid being injected into the engine combustion chamber in the form of a hollow conical sheet which is easily disintegrated into droplets. The other swirl type (mechanical) contains a center body with machined helical passages that impart a swirling flow pattern prior to fluid injection through the central orifice. Because the injection orifices of the swirl-type nozzle are not full-flowing, low discharge coefficients (C_D = 0.2 to 0.3) result.

The third design, the spray fan nozzles, contain circular orifices drilled from the back side of the injector face which intersect slots machined into the faces. The intersections form eliptical-shaped holes. The injected liquid expands within the slots and produces a narrow fan-shaped sheet prior to droplet breakup. Higher discharge coefficients (C_D = 0.7 to 0.8) are achievable with this design.

A total of one mechanical and four hydraulic swirl nozzles as well as five self-atomizing spray fan nozzles were utilized. A complete summary of all nozzles and pertinent parameters are listed in Table 18. Note that a range in size from an equivalent orifice diameter of from 0.062 to 0.124 inch for the swirl nozzles and from 0.018 to 0.072 inch for the fan nozzles was considered in the overall study.

A fixture was designed to hold the spray nozzles for the mass and mixture ratio distrubition studies. This fixture (Fig. 7) allows the nozzles to be positioned with respect to each other with variable spacing and impingement angle. The main body (No. AP-69-273) is a universal fixture which holds various orifices at a fixed spacing with a 60-degree included impingement angle.

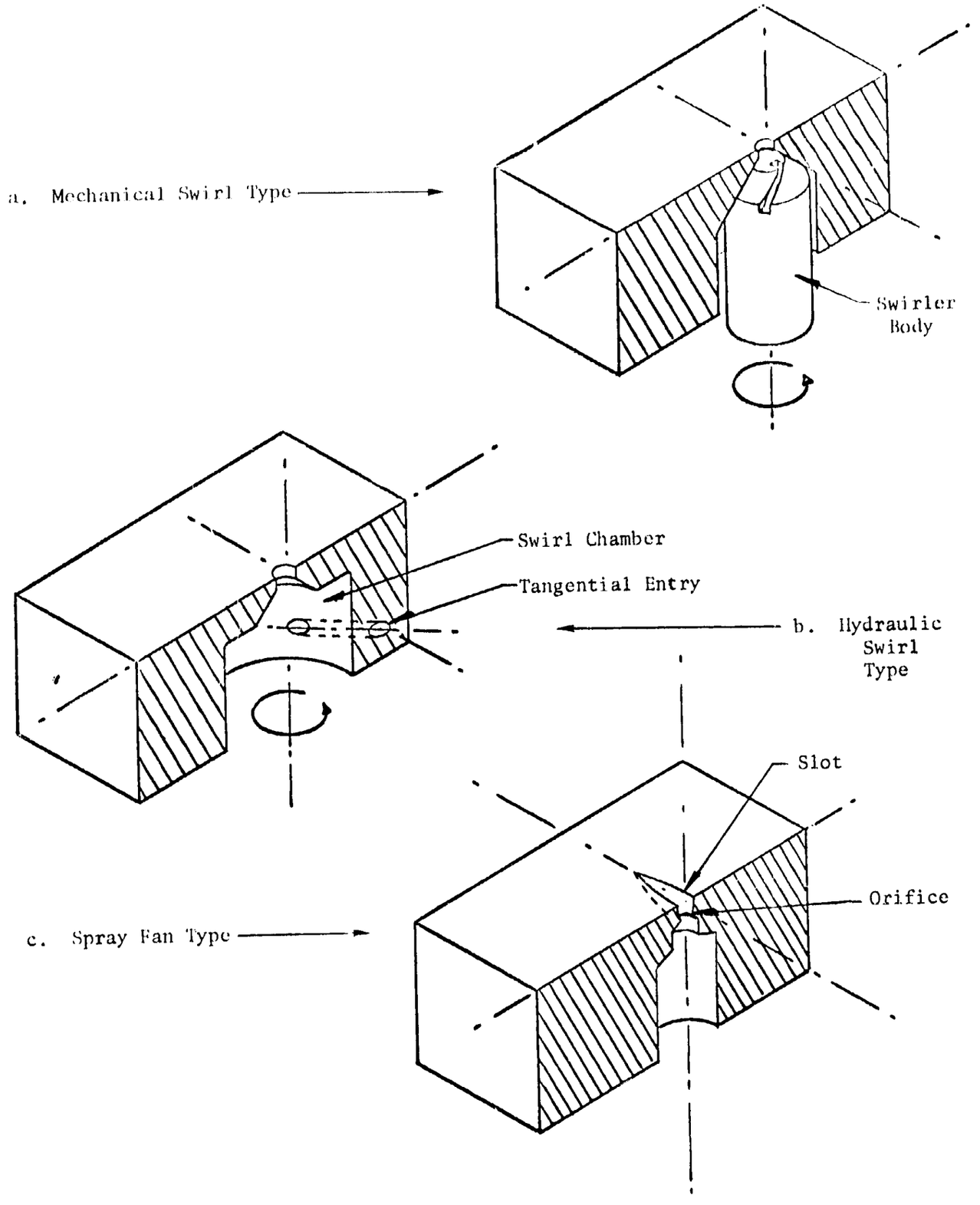

Figure 6. Model Injector Nozzle Configurations

TABLE 18

SUMMARY OF SELF-ATOMIZING INJECTOR NOZZLES AND ELEMENT CONFIGURATIONS

A - Nozzles

Nozzle Type	Manufacturer* Part No.	Equivalent Orifice Diameter, inch	Spray Angle, degrees
Vee Jet-VV (Spray Fan)	800050	0.018	80
	8001	0.026	80
	8002	0.036	80
	8006	0.062	80
	8008	0.072	80
Hydraulic Swirl	1/8 B-1	0.062	80
	1/8 B-2	0.078	80
	1/8 B-3	0.094	80
	1/8 B-05	0.047	80
Mechanical Swirl	1/4 M-26	0.086	80

B - Elements

Element Type	Manufacturer Part No.		Equivalent Orifice Diameter, inch		Spacing Between Elements, inch
	Oxidizer	Fuel	Oxidizer	Fuel	
Vee Jet-VV (Fan)	8006	8006	0.062	0.062	0.5
	8006	8006	0.062	0.062	1.0
	8008	8006	0.072	0.062	0.5
Hydraulic Swirl	1/8 B-3	1/8 B-2	0.094	0.078	0.5

*Spraying Systems Inc.

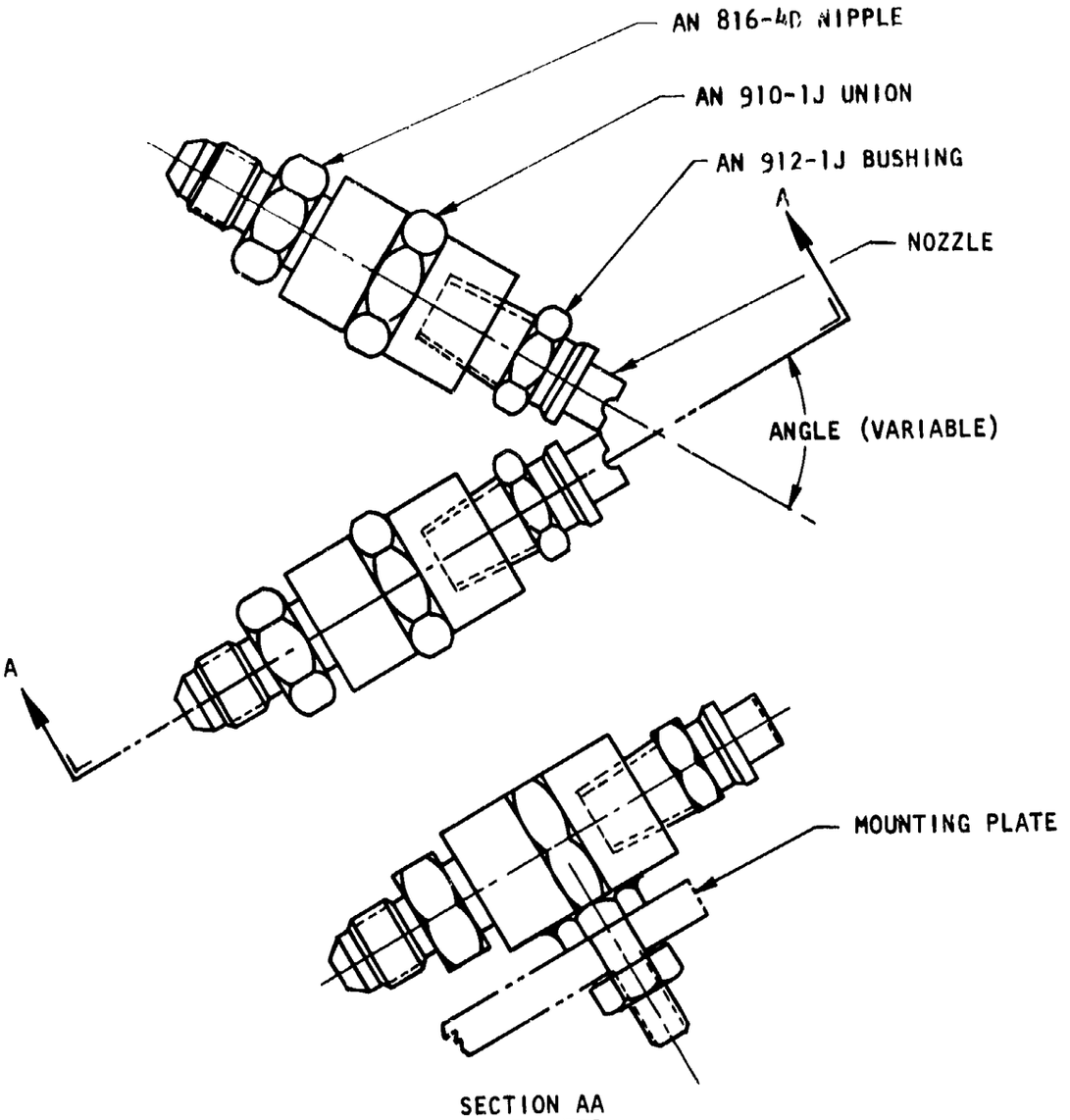

Figure 7. Nozzle Test Fixture

Unlike Doublets

Orifices for three basic doublet-type elements were fabricated. The configurations include (1) rectangle-on-rectangle, (2) triangle-on-triangle, and (3) rectangle-on-triangle. In addition, a circular orifice unlike doublet was also fabricated. The various combinations cold-flow evaluated are shown schematically in Table 19, and a summary of pertinent dimensions for each configuration is shown in Table 20. Note that the configurations include three aspect ratio perturbations for each of the three noncircular doublet types. The elements are designed for 30-pounds-force thrust per element level.

All orifices for the unlike-doublet elements are fabricated using the EDM process. During the initial phase of the single orifice characterization phase of the program, considerable difficulty was experienced in the machining of the very thin EDM electrodes. Improved techniques in fabricating the tooling for the single element hardware subsequently produced electrodes with tolerances held within 0.0002 inch. A time-pulsed vacuum flushing technqiue was used during the electrical discharge machining of the element orifice holes. The combination of machining the electrodes to very close tolerances, grinding the entrance and exit sides of the orifice blanks, and the time-pulsed vacuum flushing technique provided orifices with very little taper, closely controlled dimensions, smooth finishes, and sharp orifice entrance and exit conditions.

Typical photographs of EDM fabricated ports for four noncircular orifices are shown in Fig. 8 . The individual orifice inserts form an unlike-doublet pair when installed in the cold-flow fixture shown in Fig. 9 . This apparatus was used for both the mixing and atomization cold-flow studies of the noncircular single orifice elements.

TABLE 19

SUMMARY OF UNLIKE-DOUBLET ELEMENT DESIGNS

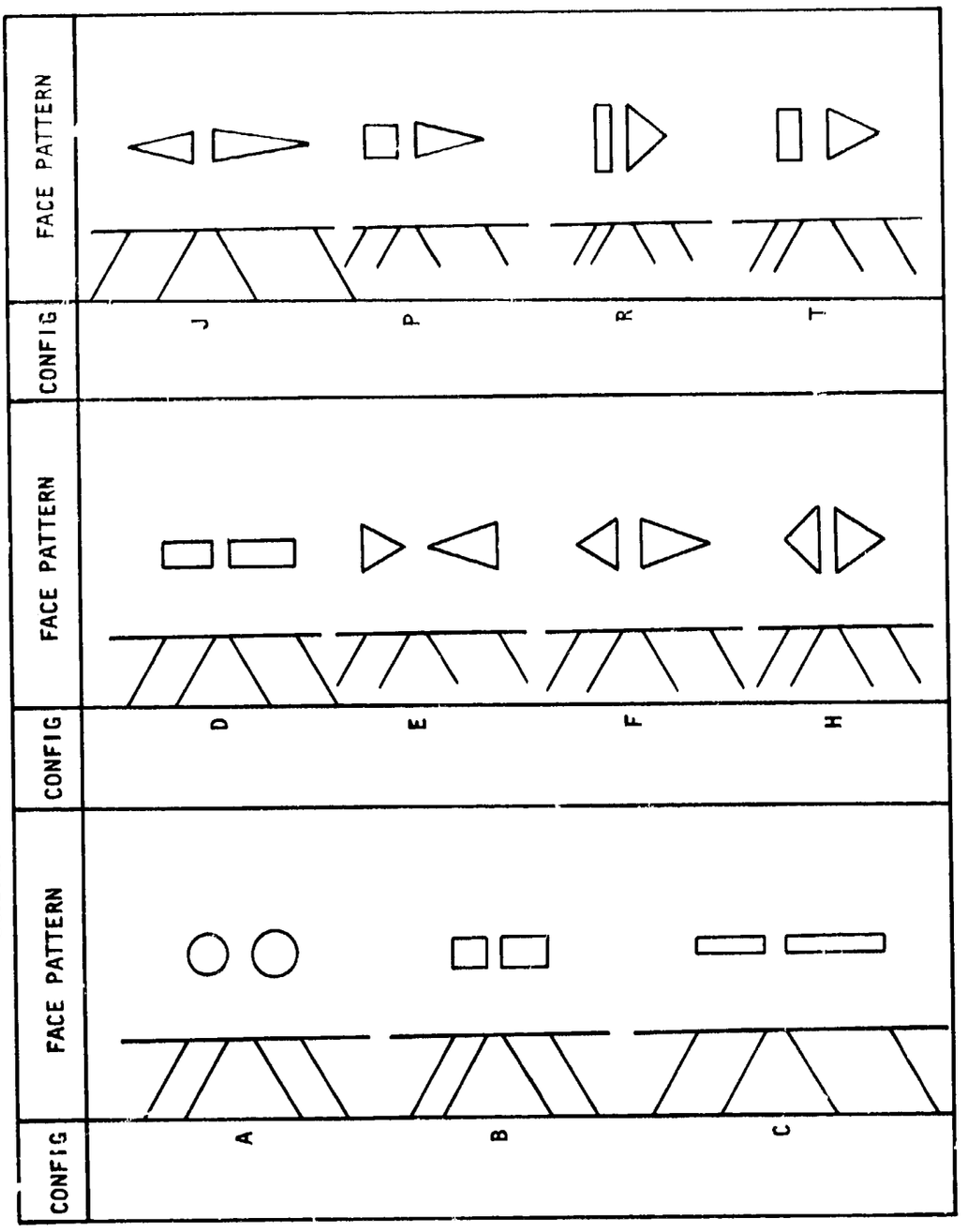

TABLE 20

SUMMARY OF UNLIKE-DOUBLET ELEMENT DESIGNS

Configuration Designation		Aspect Ratio		Hydraulic Diameter, inch		Orifice Areas, $in.^2$	
		Oxidizer	Fuel	Oxidizer	Fuel	Oxidizer	Fuel
○ ○	A	--	--	0.0718	0.0631	0.00343	0.00257
□	B	1.52	1.0	0.0631	0.0562	0.00326	0.00263
▯	C	5.42	4.0	0.0528	0.0471	0.00374	0.00255
	D	2.72	2.0	0.0579	0.0512	0.00339	0.00237
▽ △	E	1.17	0.9	0.0543	0.0465	0.00354	0.00252
△	F	1.17	0.9	0.0543	0.0465	0.00354	0.00252
▽	H	0.68	0.54	0.0496	0.0436	0.00348	0.00272
	J	2.71	1.97	0.0436	0.0438	0.00361	0.00296
△	P	1.97	1.0	0.0438	0.0562	0.00296	0.00263
□	R	0.54	4.0	0.0436	0.0471	0.00272	0.00255
	T	0.90	2.0	0.0465	0.0512	0.00252	0.00237

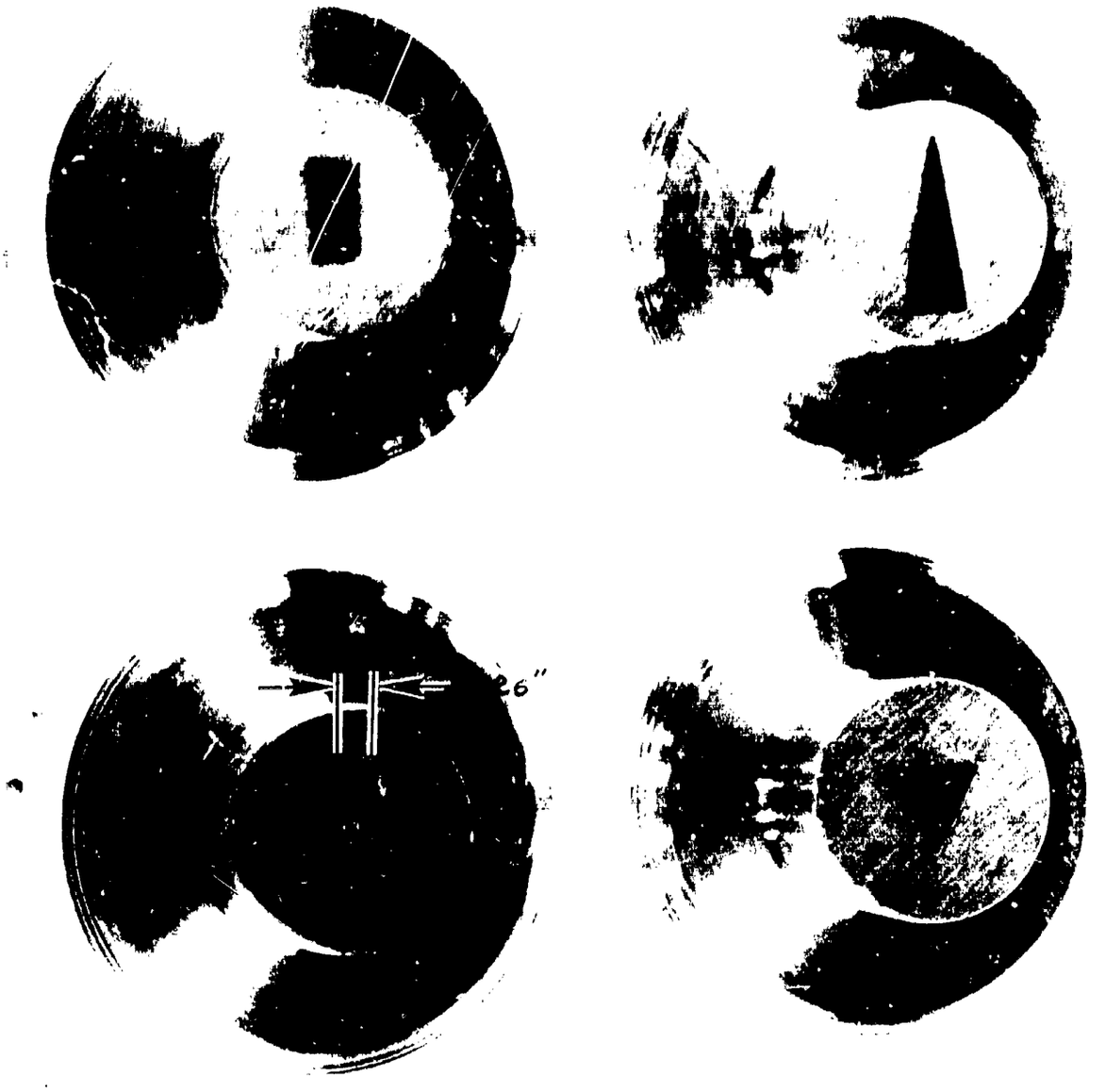

Figure 8. Orifice Elements Fabricated by EDM Techniques

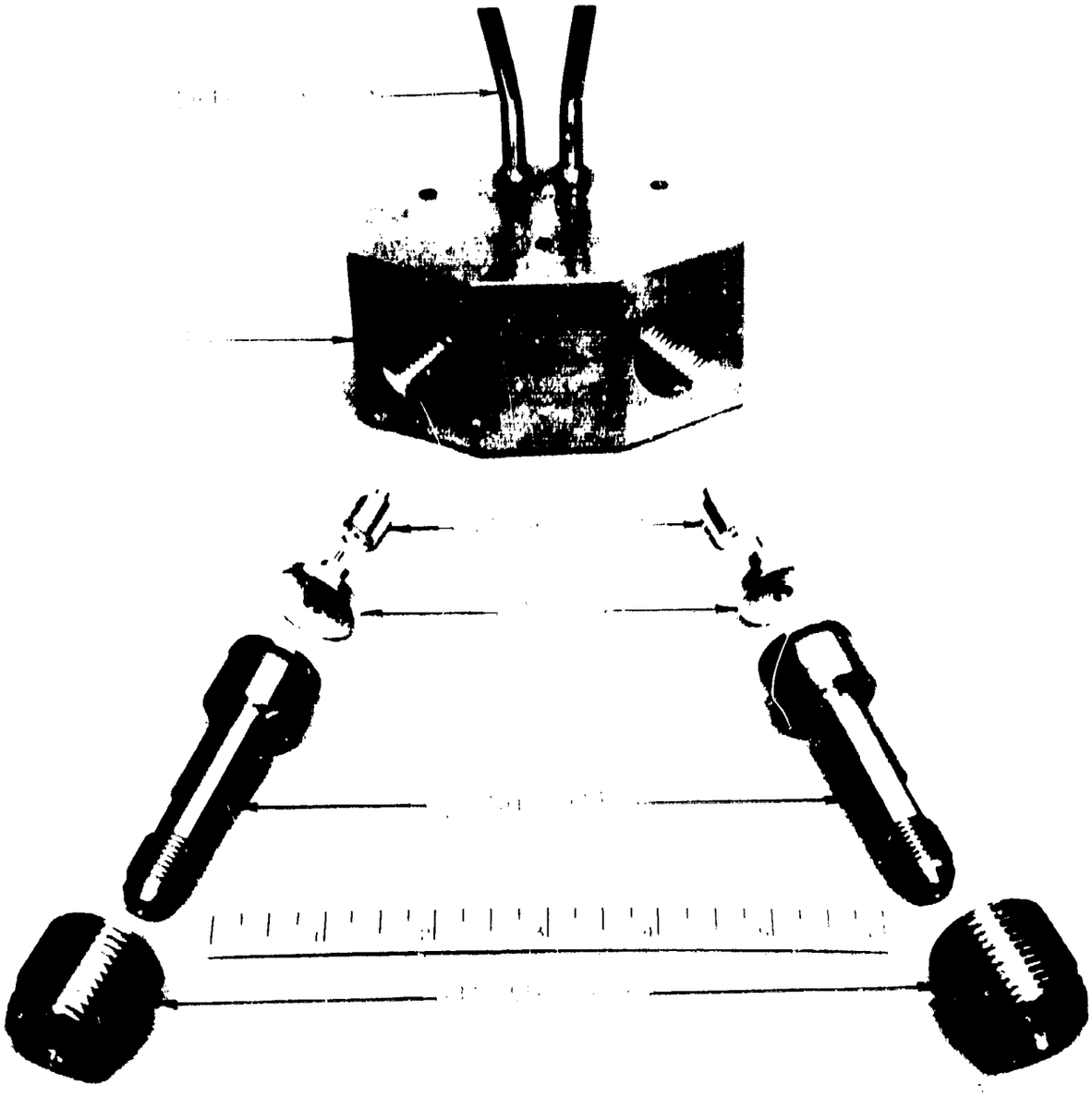

Figure 9. Model Injector Cold-Flow Apparatus

4.1.3 THRUST CHAMBER AND INJECTOR DESIGN

A schematic of the Phase I chamber and injector design is shown in Fig. 10. The engine is designed for 100-psia chamber pressure and 30 pounds of thrust. As noted, the chamber is uncooled and fabricated from copper. Chamber sections were also fabricated to provide L* variations of 30 and 60 inches (the design shown is for an l* of 15 inches). In addition, pressure taps are provided near the beginning of convergence for measurement of the chamber static pressure. The injector was also designed such that an injector face pressure was obtained.

Four hot-fire injectors were designed and fabricated for evaluation. The injectors included three unlike doublets: circular, rectangular, triangular, and a self-atomizing fan nozzle. The specific configurations choosen were determined from the cold-flow element study. The injector configurations were:

Shape	Configuration	Impingement Angle, degrees	Fan Angle, degrees	$(D_O/D_F)_{HYD}$
Circular	A	60	N.A.	1.138
Triangular	F	60	N.A.	1.169
Rectangular	D	60	N.A.	1.130
Fan*	0.5 spacing	N.A.	60	N.A.

An exploded view of the total assembly is shown in the upper photograph of Fig. 11. The longest chamber extension spool is 7.9 inches in length. The small tubes protruding from the nozzle section are thermocouples (one is near the throat and the other two are upstream of the throat). Also shown in Fig. 11 is a photograph of an injector. For size reference, the inner circular portion is 1.14 inches in diameter.

*$D_F = 0.062"$, $D_O = 0.072"$

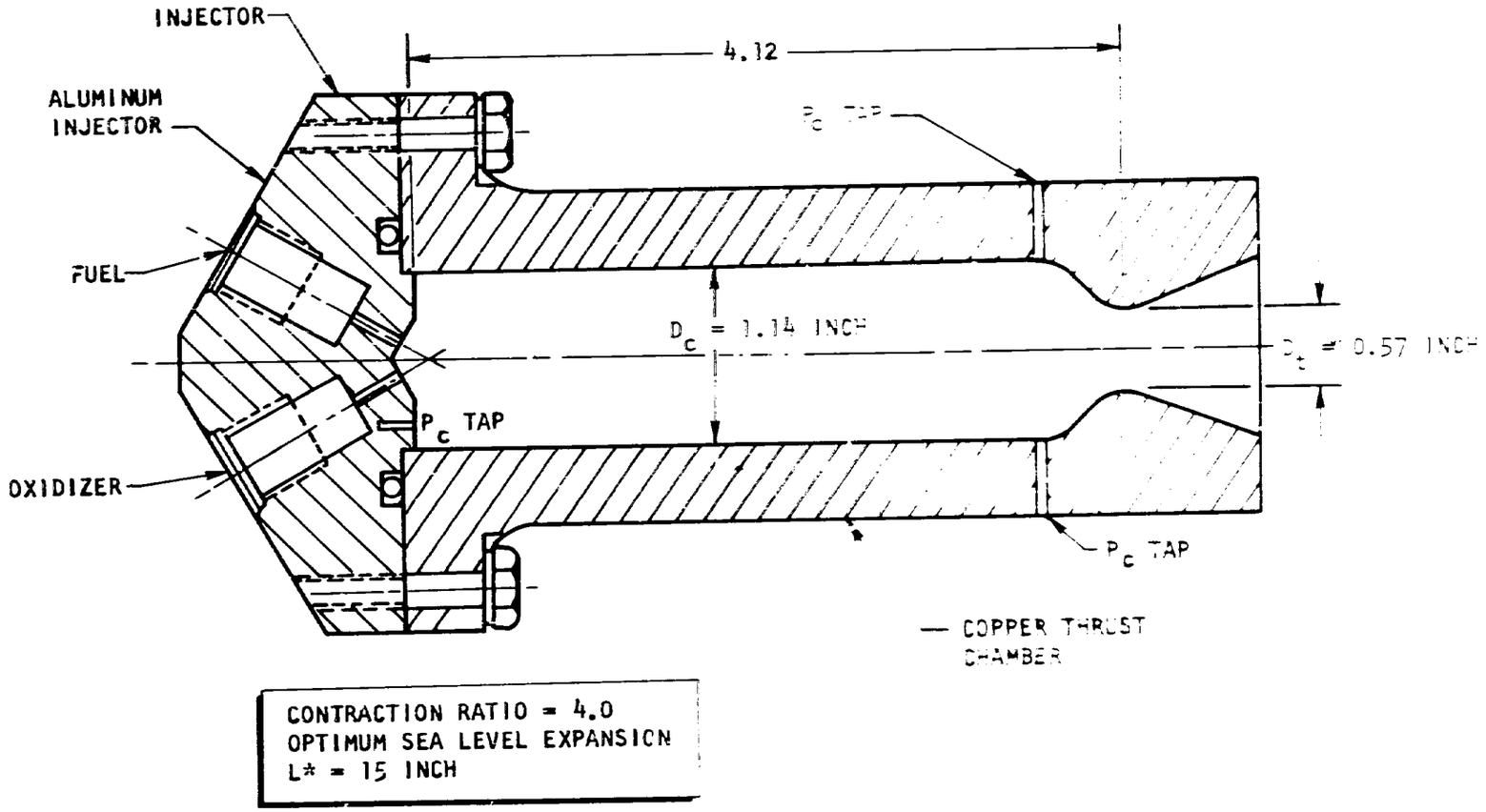

Figure 10. Single Element Injector Thrust Chamber Assembly

Model Injector Thrust Chamber Assembly

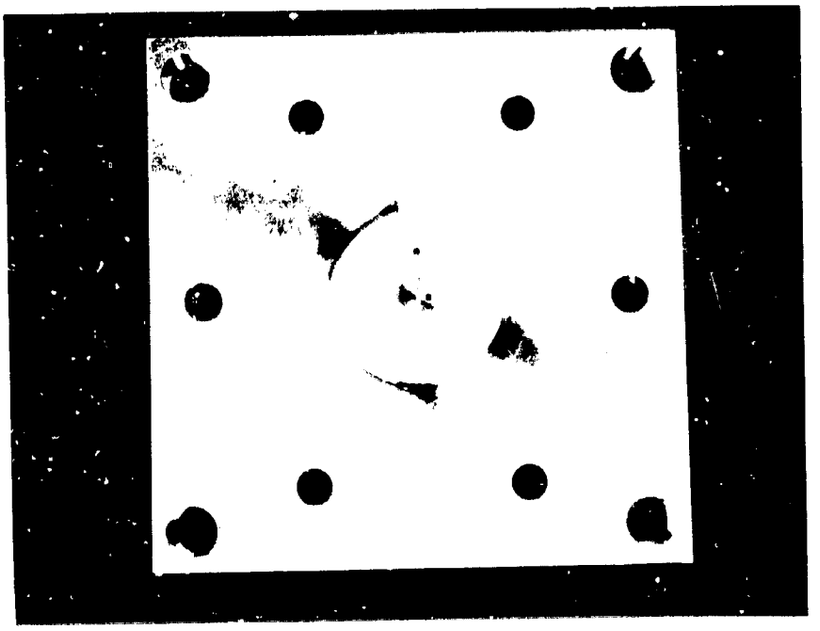

Single Element Circular Unlike Doublet

Figure 11. Model Injector Hardware

4.2 COLD-FLOW EVALUATION

4.2.1 SINGLE ORIFICE STUDY

The objective of the single orifice study was to obtain experimental data required to improve on the evaluation criteria and techniques used for the preliminary evaluation of orifice shapes. To accomplish this objective, both cold-flow and hot-fire data were generated with small orifices of various shapes. These data, in terms of the "discharge coefficient", were correlated with the physical parameters of orifice design and operation. During the process of correlating these data, improved techniques for predicting the discharge coefficient and evaluating potential orifice-to-orifice differences were discovered.

A simplified matrix showing the orifice and operational variables tested during cold-flow experimentation is presented in Table 21. A total of seven orifice shapes were investigated: (1) circle, (2) square, (3) rectangle, (4) equilateral triangle, (5) slot, (6) diamond, and (7) isosceles triangle. All shapes were designed to have an area equal to that of an 0.06-inch-diameter circle.

The test program is shown in schematic form in Fig. 12. Note that the testing was conducted in three steps: (1) Initial Characterization and Screening, (2) Design and Operational Sensitivity, and (3) Fluid Properties Study.

For Step 1, seven shapes were fabricated with an L/D_H nominally equal to 6.0. These orifices had sharp entrances. Each orifice was evaluated at 0, 50, and 100 psig backpressure over a pressure drop range from 15 to 60 psid. Gaseous nitrogen was used as a pressurant for most of the testing; however, two of the shapes were tested with helium. Manifold cross velocity was set at zero and the water temperature was ambient.

TABLE 21

TEST MATRIX

Shape	L/D_H 2 4 6 20	P_b, psig 0 50 100	V_c, ft/sec 0 5 10 20	Helium	GN_2	ΔP, psid 15- 20 60	Temperature Ambient --	Low -65	High 130	Sharp	Rou-
Circle	X	X	X X X X		X	X	X			X	
	X	X	X X X X		X	X	X			X	
	X	X X X	X X X X	X	X	X	X	X	X	X	X
	X	X	X X X X		X	X	X			X	
Square	X	X	X X X X		X	X	X			X	
	X	X	X X X X		X	X	X			X	
	X	X X X	X X X X	X	X	X	X	X	X	X	X
	X	X	X X X X		X	X	X			X	
Rectangle	X	X	X X X X		X	X	X			X	
	X	X	X X X X		X	X	X			X	
	X	X X X	X X X X		X	X	X			X	X
	X	X	X X X X		X	X	X			X	
Equilateral Triangle	X	X	X X X X		X	X	X			X	
	X	X	X X X X		X	X	X			X	
	X	X X X	X X X X		X	X	X	X	X	X	X
	X	X	X X X X		X	X	X			X	
Slot	X	X	X X X X		X	X	X			X	
	X	X	X X X X		X	X	X			X	
	X	X X X	X X X X		X	X	X				X
	X	X	X X X X		X	X	X			X	
Diamond	X	X X X	X X X X		X	X	X			X	
Isosceles Triangle	X	X X X	X X X X		X	X	X			X	

L/D_H = orifice length to hydraulic diameter ratio
V_c = manifold cross velocity
P_b = chamber back pressure
ΔP = orifice pressure drop

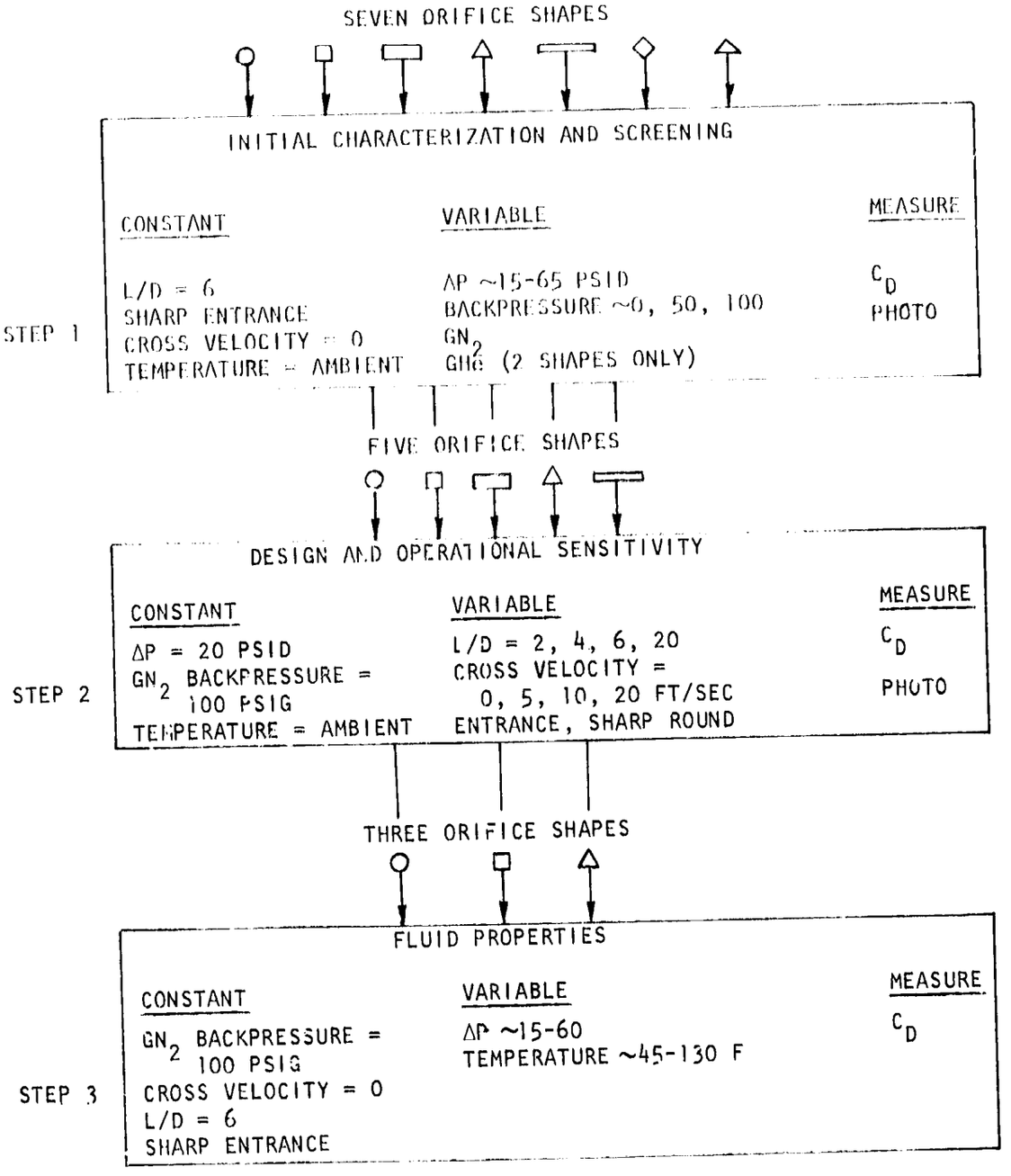

Figure 12. Single Orifice Cold-Flow Characterization Program

Following Step 1, two of the shapes, the isosceles triangle and the diamond, were eliminated from further study. This left five orifice shapes for testing in Step 2. In Step 2, the orifice pressure drop was fixed at 20 psid, the backpressure fixed at 100 psig (GN_2), and ambient temperature water employed. Each orifice shape was tested at L/D's of 2, 4, 6, and 20 (sharp entrance) with cross velocities of 0, 5, 10, and 20 ft/sec. The L/D = 6 configurations were also tested with rounded entrances* at cross velocities of 0, 5, 10, and 20 ft/sec. To test the effect of water temperature on orifice coefficient, three of the shapes were selected for additional testing in Step 3 with water temperatures varied from 45 to 130 F. The orifices were run over a pressure drop range from 15 to 60 psid.

The data and a detailed matrix of test conditions for each run appear in Appendix A. A discussion of the precision of the data is presented in Appendix B.

The results are presented in graphical form, with appropriate discussion, in sections which group tests together having common effects. These sections are (1) effect of pressure drop and backpressure, (2) effect of cross velocity, (3) effect of entrance condition, and (4) effect of water temperature. The effect of orifice L/D is not treated explicitly until the section on reevaluation of orifice criteria. However, the data for various L/D's are presented as functions of cross velocity. (The effect of L/D requires cross plots.)

Effect of Pressure Drop and Backpressure with Gaseous Nitrogen Pressurant

For this study, the length-to-diameter ratio for all orifices was six. All orifices had sharp entrances and were tested with ambient temperature water and zero manifold cross velocity. The experimental results for all seven shapes are presented in Fig. 13.

*The radius of the rounded entrance was made equal to the orifice diameter for the circular-orifice and equal to the orifice height for the noncircular shapes.

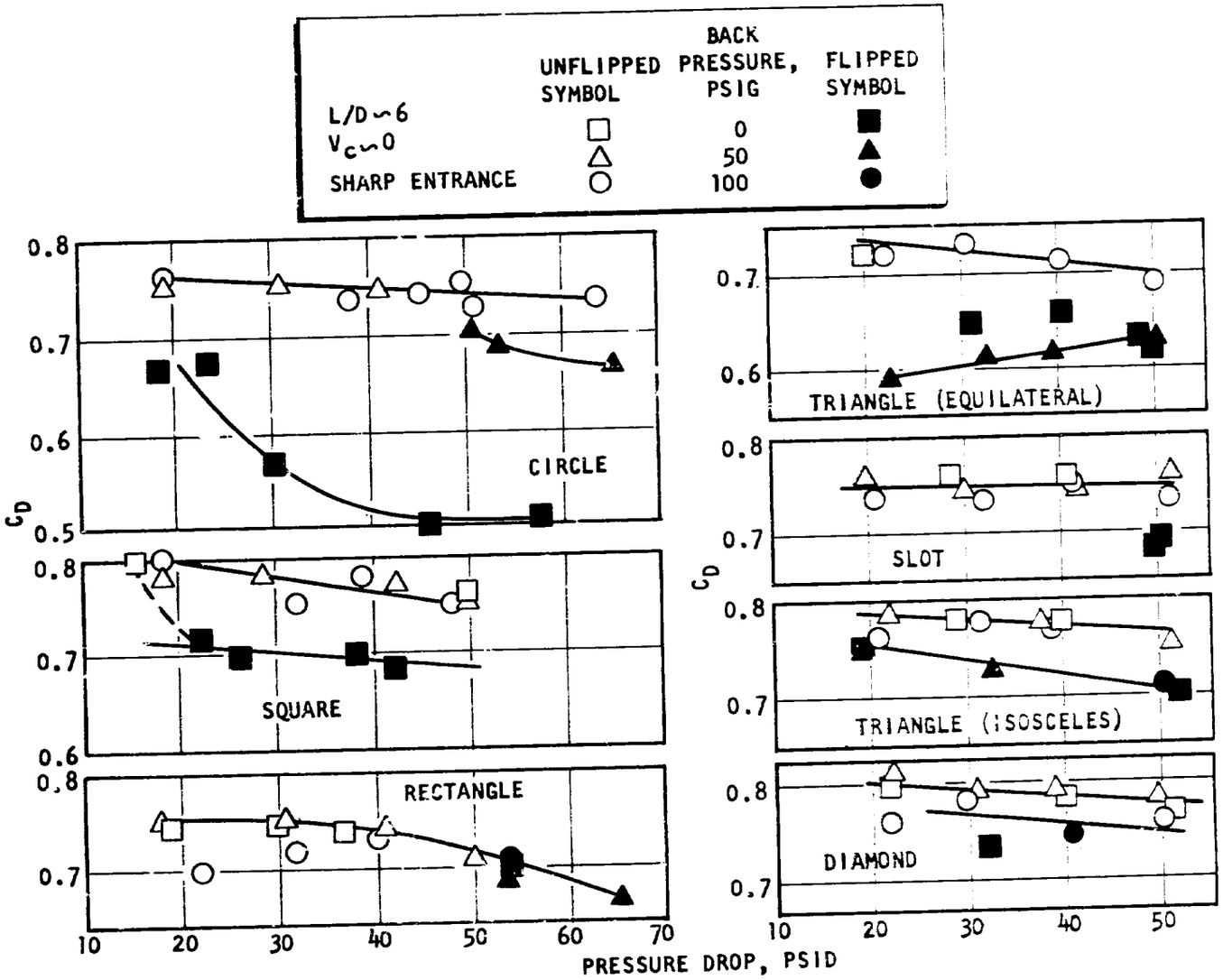

Figure 13. Effect of Pressure Drop and Backpressure

In Fig. 13, orifice coefficient, C_D, is plotted as a function of pressure drop across the orifice, ΔP, for backpressures of 0, 50, and 100 psia. The data were taken with GN_2 as the backpressurant. The data for each shape are presented in two groups, open and closed symbols. Open symbols are used to denote points which are assumed to be "unflipped". This distinction is not a clear one, and in many instances it is quite difficult to choose points which are definitely "flipped".

It is well known that the tendency for an orifice to flip is affected by the backpressure into which the orifice is flowing. As the backpressure is increased, the pressure drop at which hydraulic flip is first experienced increases. Thus, the higher the backpressure, the less likely an orifice is to flip at a given pressure drop.

It is evident from the data in Fig. 13 that the circle was most affected by hydraulic flip (or backpressure). The circle shows the greatest difference in values of C_D for flipped and unflipped conditions. For the other shapes, the appearance of flip is not clear. For example, it is doubtful whether or not hydraulic flip occurred for the diamond at all over the range of variables tested. Similarly, the slot and the rectangle produced results which are difficult to interpret.

Only two of the shapes represented in Fig. 13 show evidence of true separated flow. They are the circle and the equilateral triangle. The other shapes do produce what appears to be different levels of operation. However, the values of the discharge coefficient at these "other" levels are not indicative of separated flow. It may be that the shapes which did not experience separation could be forced to separate at other operating conditions than those tested under this program (for example, different Reynolds No. or L/D). However, over the range of variables tested, orifices other than the circle and equilateral triangle did resist separation.

It is interesting that an orifice may "flip" from one operating level to another and not experience simple flow separation or reattachment. This is quite significant for injector orifice design, for the change of operating level is still accompanied by changes in the free-jet characteristics. This could produce changes in mixing and atomization characteristics of injector elements incorporating these orifices.

Effect of Cross Velocity, Sharp Entrances

Cross velocity was imposed on the orifices by a 0.34 by 0.34 in. sq passage behind the orifice. Orifices were oriented so that the cross velocity vector was parallel to the largest axis of the orifice.

Five shapes were tested with cross velocity: (1) circle, (2) square, (3) rectangle, (4) equilateral triangle, and (5) slot.

Data for sharp entrance orifices is presented in Fig. 14 in which discharge coefficient is plotted against cross velocity for each of the length to diameter ratios studied. The values of L/D quoted are nominal. All tests were conducted at a nominal pressure drop of 20 psid.

Two conclusions may be drawn from the cross velocity results: (1) discharge coefficient decreases with cross velocity for all shapes, and (2) cross velocity causes some of the orifices with small L/D's to both flip and unflip.

Unstable flow (flip and unflip) is found with the circle at L/D ≈ 2, the triangle L/D = 4, the rectangle L/D = 2, and the square L/D = 2. The slot did not show evidence of instability.

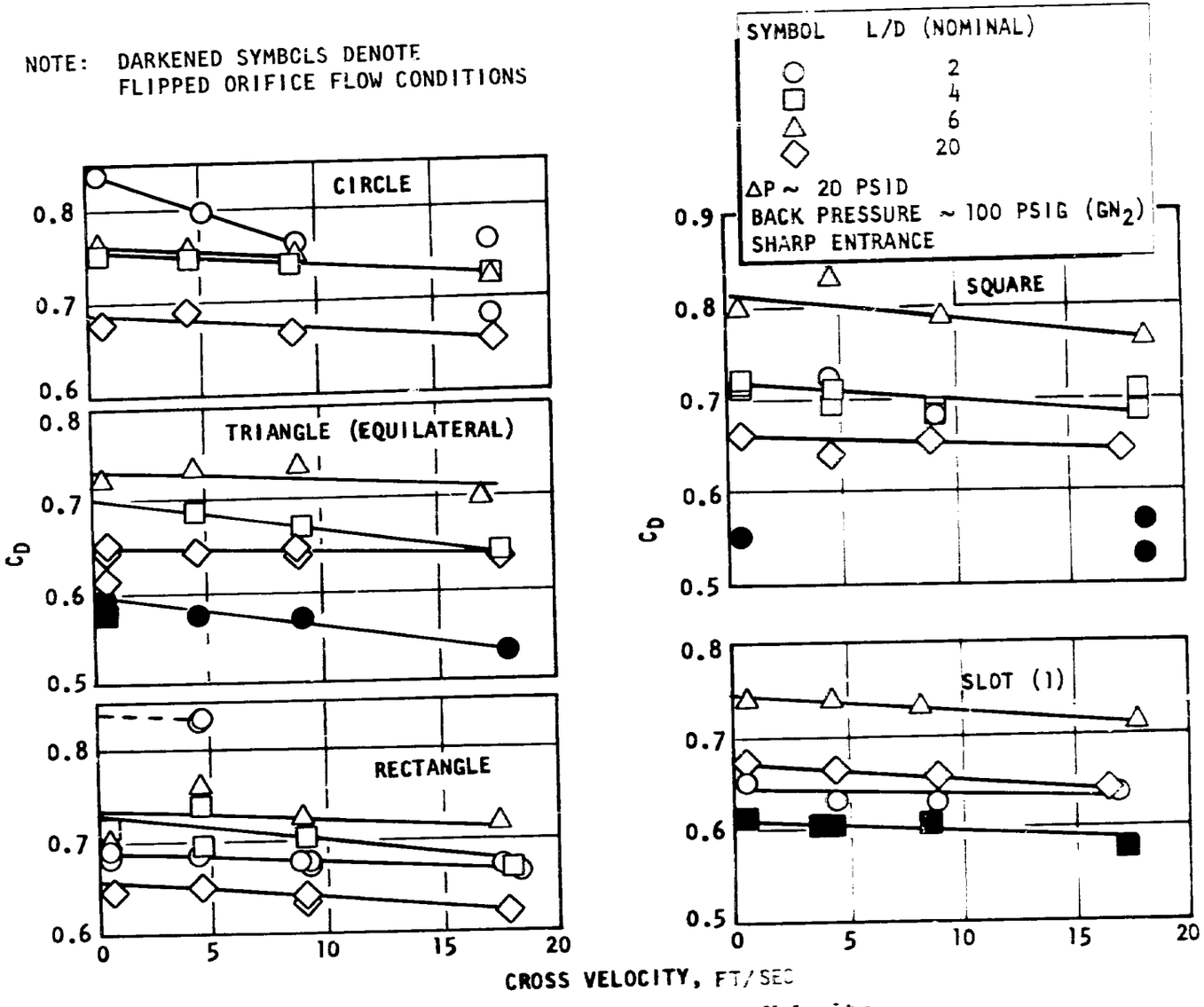

Figure 14. Effect of Cross Velocity

Effect of Cross Velocity, Rounded Entrances

Orifices with L/D = 6.0 were tested with well-rounded entrances as well as with sharp entrances. These orifices were tested at 20-psid pressure drop with variable cross velocity. The results of this test series are shown in Fig. 15a. Solid lines labeled "sharp" are included for each shape to show the average level of the results for orifices of L/D = 6 with sharp entrances. In contrast to the sharp entranced orifices, the C_D values for the rounded entrances increased with cross velocity. (Discussion of these effects are included below.)

Effect of Fluid Temperature

To determine the effect of fluid temperature on C_D, the circular, triangular, and square orifices (sharp entrances, L/D = 6) were tested over a significant pressure drop range with water temperatures of 45, 75, and 135 F and backpressure = 100 psig (GN_2). These data are presented in Fig. 15b. Within the precision of the experiment, no effect due to temperature could be isolated. No attempt was made to determine the effect of temperature on orifice hydraulic flip characteristics.

Effect of Various Parameters on Jet Appearance

One distinct trend in jet appearance was noted during the program. Increased agitation and early jet breakup were noted as L/D was decreased as well as when cross velocities were imposed on the orifices. The most disturbed jets were observed from short orifices with high cross velocities. Agitation was much reduced at a given set of operating conditions by rounding the entrance of an orifice.

To aid in interpretation of data, photographs at selected operating conditions were taken of the jets. The results of the photographic coverage of the single orifice flow studies are presented in Fig. 16 through 19. Each photograph shows the free liquid jet for a distance of approximately 3 inches downstream or a free jet L/D of 50 for the circular orifices.

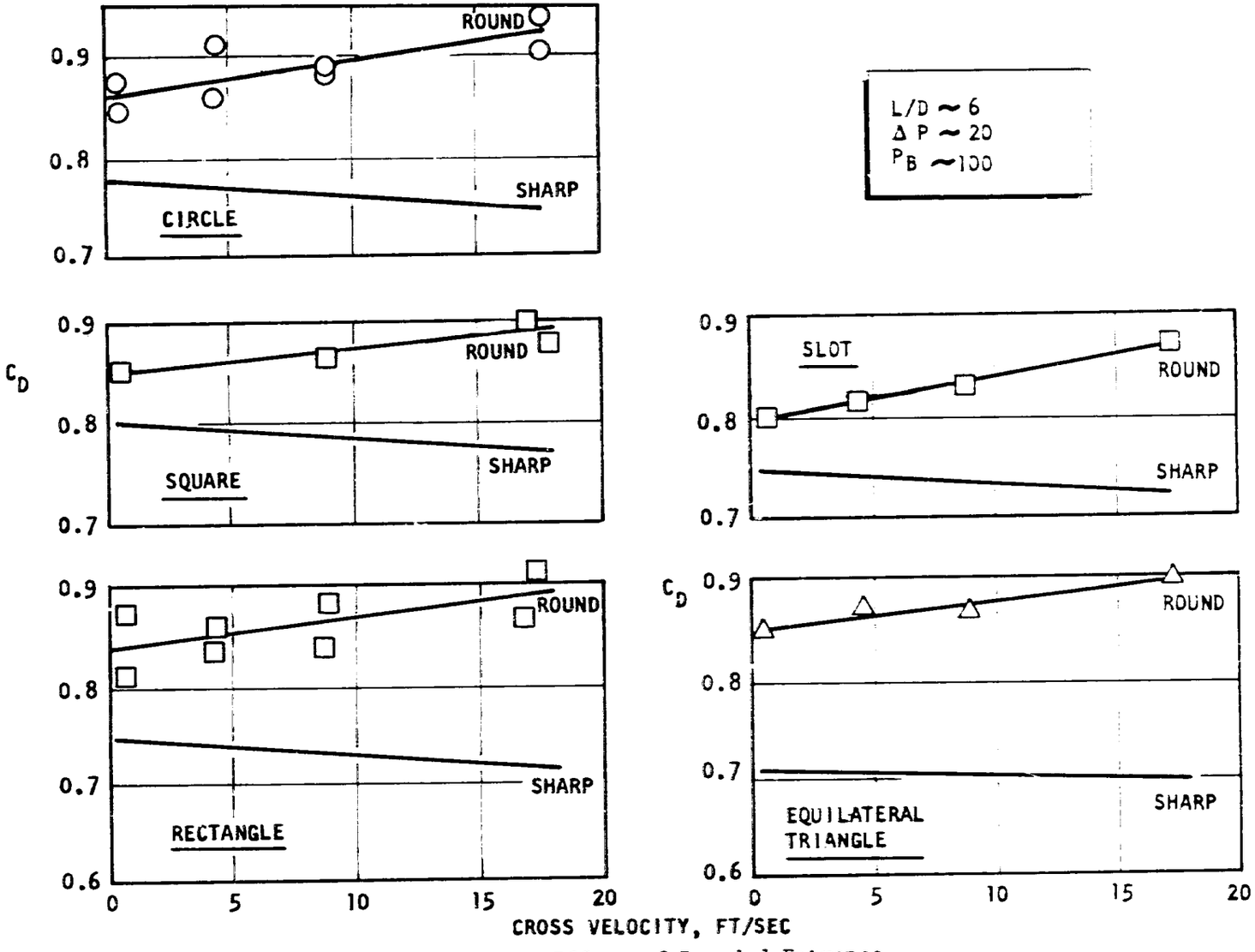

Figure 15a. Effect of Rounded Entrance

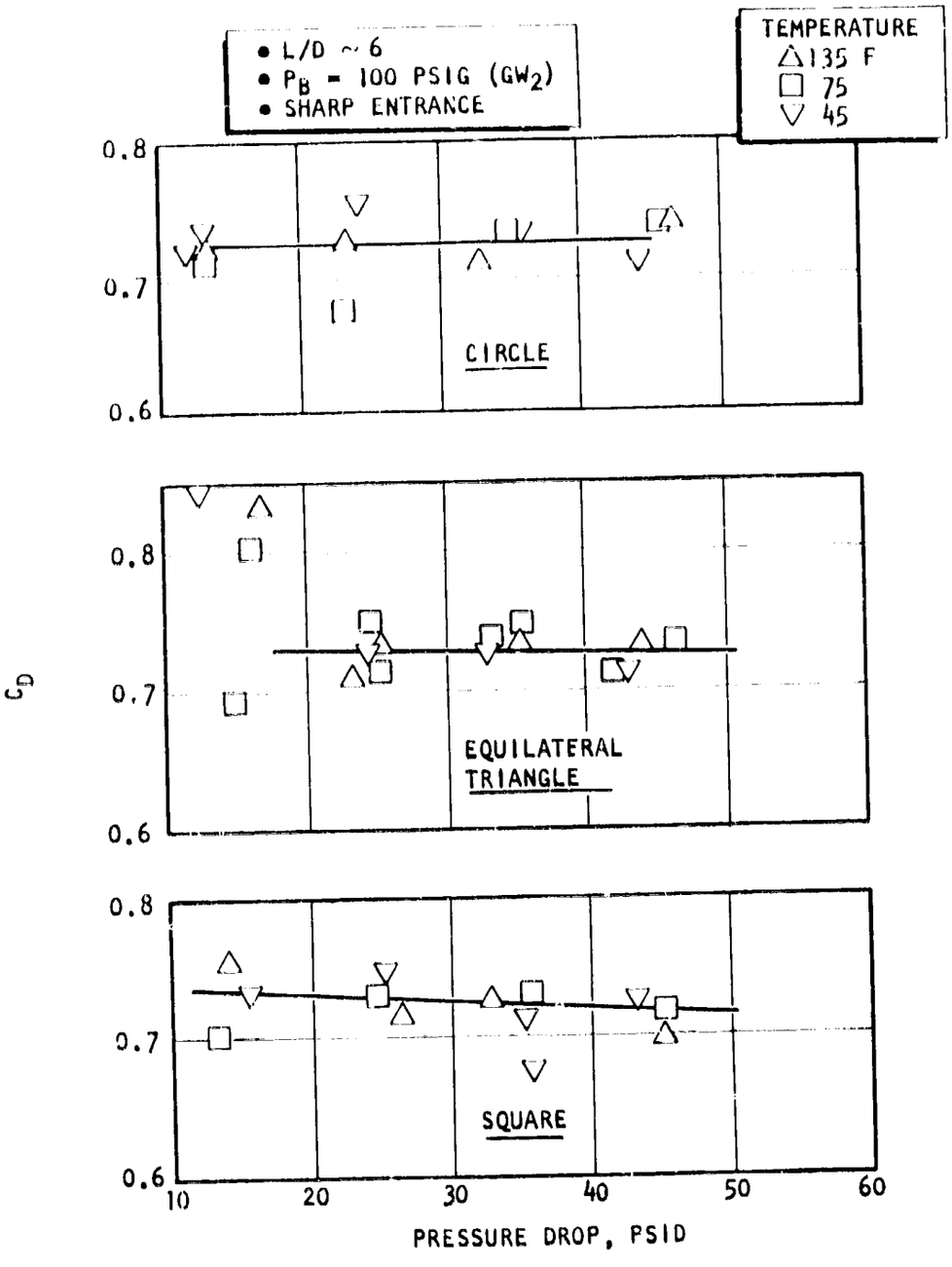

Figure 15b. Temperature Effects

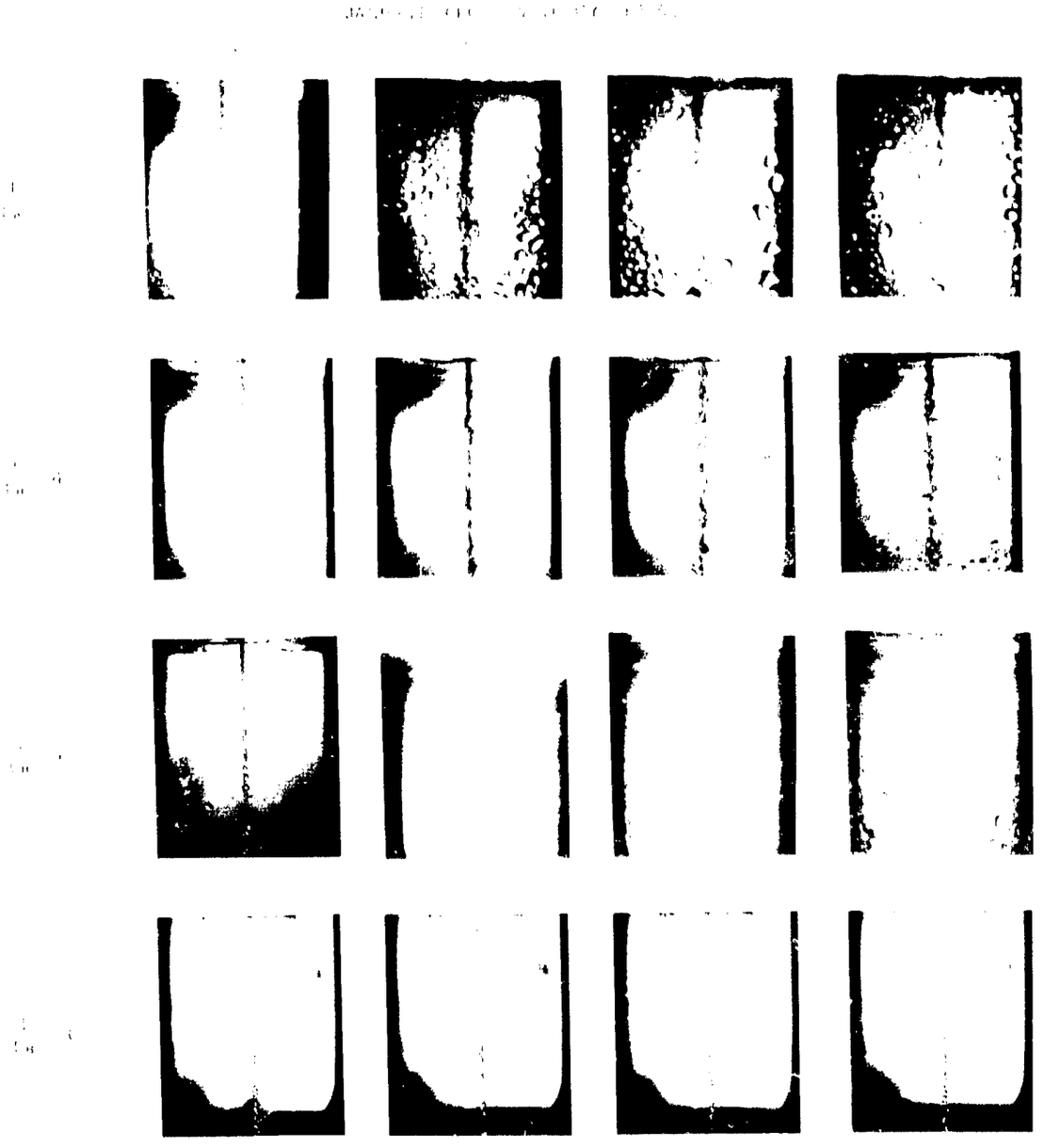

Figure 16. Flow Characteristic of Noncircular Orifices With Variable L/D_H and Cross Velocity--Circle

Figure 17. Flow Characteristic of Noncircular Orifices With Variable L/D_H and Cross Velocity--Equilateral Triangle

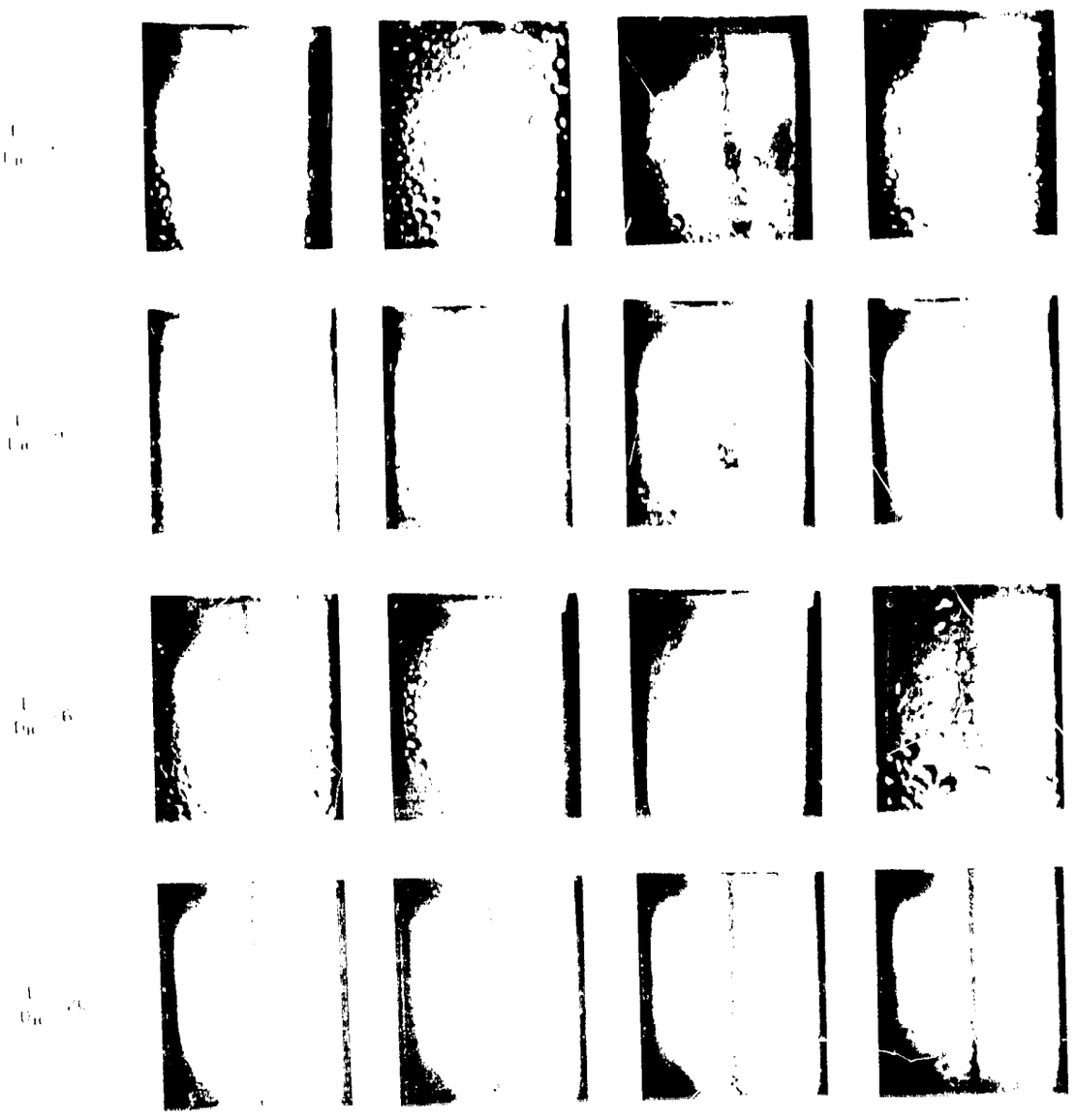

Figure 18. Flow Characteristic of Noncircular Orifices With Variable L/D_H and Cross Velocity--Rectangular Slot

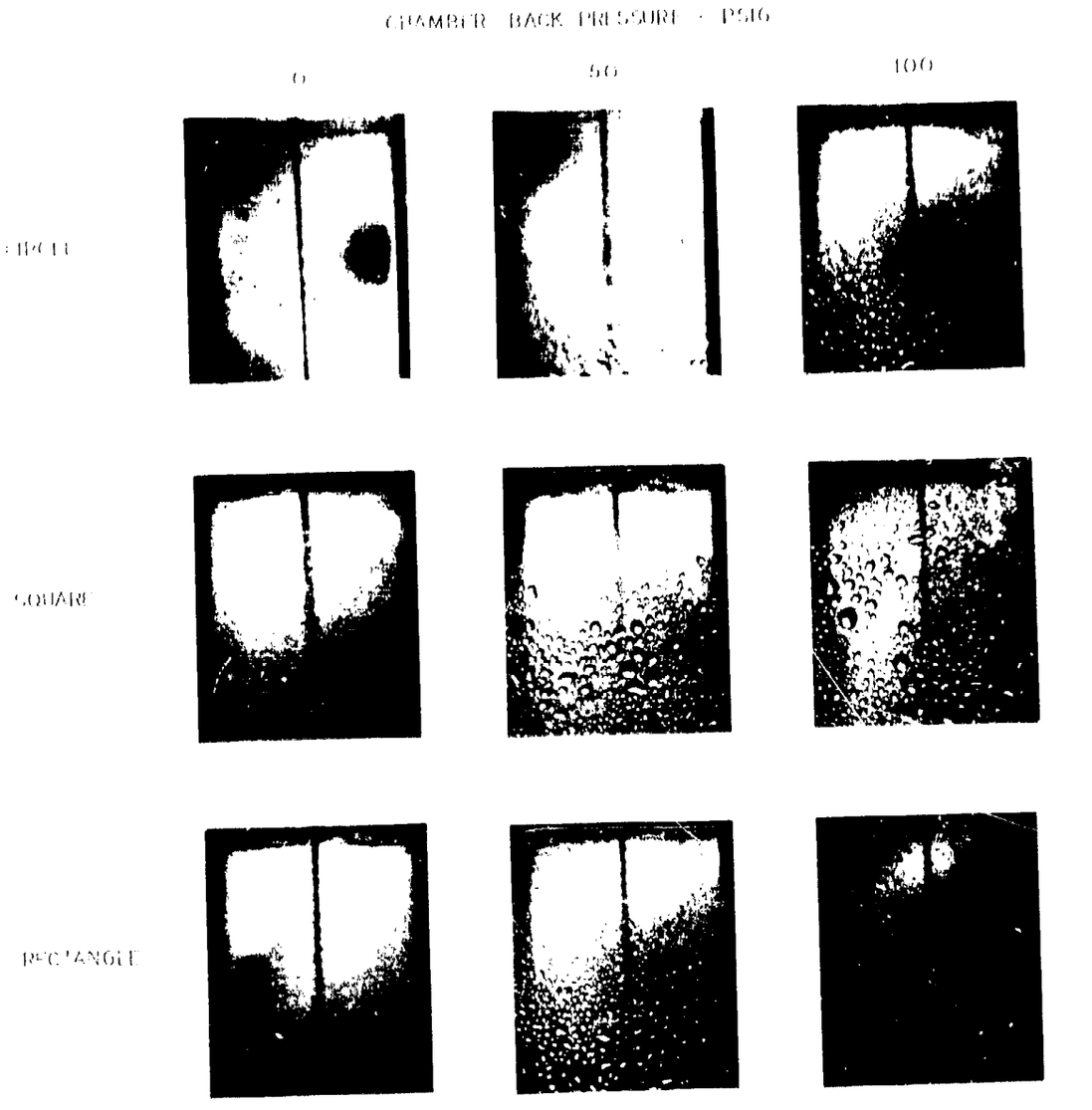

Figure 19. Flow Characteristics of Noncircular Orifices With Variable Backpressure

Figures 16, 17, and 18 show the change in jet appearance produced by changes in orifice L/D and manifold cross velocity for the circle, equilateral triangle, and the rectangular slot (aspect ratio = 8). The backpressure was 100 psig and the orifice ΔP was 20 psid for all tests represented in those figures. All orifices had sharp entrances.

Increased agitation and jet breakup are noted as cross velocity is increased for any fixed value of L/D. However, as L/D is increased, jet stability is restored. Cross velocity has almost no effect on jet appearance at L/D = 20 for any of the three shapes shown.

The "brushy" appearance of the jets emanating from the shorter orifices at all cross velocities indicate that these orifices are flowing "full" (i.e., not separated). This is attributed to the high backpressure (100 psig) and the low ΔP (20 psid).

The effect of backpressure upon jet appearance is shown in Fig. 19 for the circle, square, and rectangle. For the tests represented, the orifice ΔP was 50 psid, the L/D was 6 and cross velocity was set equal to zero. All orifices had sharp entrances. Examination of the various photographs in Fig. 19 shows that all jets are quite similar in appearance, regardless of backpressure, except that from the circular orifice at a backpressure of zero psig. All the other jets are "brushy" indicating that the orifice cross section is flowing full, while the circular jet at $\rho_B = 0$ is very narrow, indicating separated flow or true hydraulic flip. This result is very significant. It points out the fact that orifices can demonstrate large changes of C_D with backpressure, as shown in the orifice result section, and still not exhibit true hydraulic flip. It must not, therefore, be concluded that an abrupt drop in the value of C_D is proof that the orifice has separated.

Comparison of the photograph of the circle with $\rho_B = 0$ psig, $\Delta P = 50$, and L/D = 6 in Fig. 16 with that of the circle with $\rho_B = 100$, $\Delta P = 20$, and L/D = 6 in Fig. 19 shows the difference in jet appearance between a fully separated and a fully attached flow condition.

Discharge Coefficient Data Obtained With Actual Propellants

Discharge coefficient data were obtained with actual propellants. The orifices tested were of circular cross section. One, tested with N_2O_4, had a diameter of 0.0698 and an L/D of 8.81, while the other, tested with UDMH-N_2H_4, had a diameter of 0.0616 and an L/D of 10.0. The tests were conducted with zero cross velocity and ambient backpressure (i.e., 0 psia). Results of these tests are shown in Fig. 20. These lines show that the data obtained with actual propellants are predictable and, therefore, consistant with data obtained with water. It may be concluded that the oxidizer orifice was flowing separated over the entire Reynolds No. range while the fuel orifice was in transition between attached and separated flow. The separation of the oxidizer flow at ambient backpressure is attributable to the high vapor pressure of the NTO (8 to 9 psia). High vapor pressure causes hydraulic flip to occur at relatively low ΔP levels.

However, it may be noted that many of the data points for both sharp and round entrances are of a C_D level not predicted by the theory. These points are found at lower values of Reynolds number. A probable cause for these low C_D values is heat transfer from the combustion chamber through the injector face affecting nucleate boiling in the boundary layer at the wall of the orifices. At the higher Reynolds numbers the cooling is sufficient to prevent boiling and the orifices flow full. At low Reynolds number, boiling is encountered and causes the flow to separate. It must be remembered that low orifice Reynolds numbers are associated with low chamber pressures. This fact amplifies the credibility of the boiling hypothesis. The theories used are discussed in the following material.

4.2.2 CORRELATION OF ORIFICE DATA AND UPGRADING OF SINGLE ORIFICE EVALUATION CRITERIA AND TECHNIQUES

The objective of this section is to integrate the results of the separate effects of various parameters on orifice coefficient into a meaningful relationship and to mold these results into a form suitable for application to injector orifice evaluation and design. The section is subdivided into three parts.

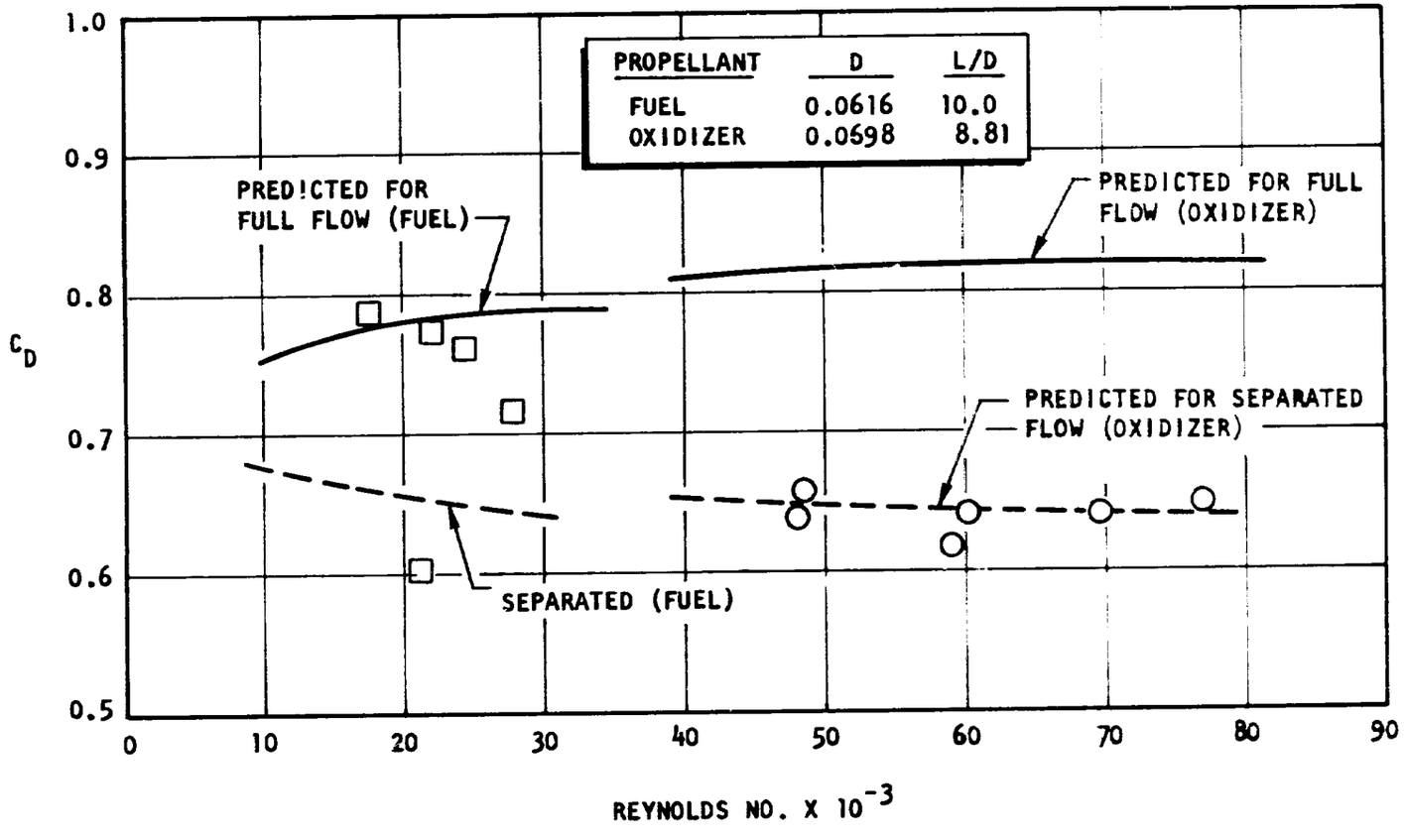

Figure 20. Discharge Coefficient Data Obtained With Actual Propellants

The first part, Orifice Coefficient Model, presents the development of a combination analytical and empirical model for the prediction of effects of orifice shape, L/D, entrance condition, and Reynolds No. on the value of the orifice coefficient. This model is subsequently employed to correlate the data.

In the second part of the discussion, Cross Velocity Model, is a model developed to predict the changes to the value of C_D effected by cross velocity in the feed system.

Finally, in part 3, Application of Results to Injector Orifice Design, Sample Calculation, the results of the models for orifice coefficient are summarized in design charts for direct prediction of discharge coefficient as a function of L/D, Reynolds No., entrance condition, shape, and cross velocity. Predictions are valid only for orifices which are full flowing (i.e., not flipped).

Orifice Coefficient Model

Regardless of the inlet conditions or the manner in which the boundary layer develops at the entrance of an orifice, the discharge coefficient of that orifice should approach, in an asymptotic fashion, the values of C_D predicted using pressure drops obtained from friction factor (pipe flow) calculations as the length of the orifice is increased. Therefore, a simple friction factor model should correlate well with C_D results from long orifices. On the other hand, boundary layer development theories should correlate the data for very short orifices.

One approach to a unified description of the discharge characteristics of an orifice would be to generate the two functional relationships for C_D; one relation for large L/D and one for small L/D. Once these two relationships have been plotted, the solution for the intermediate L/D orifices can be obtained by constructing a smooth curve connecting the two limiting solutions.

In 1956, Rivas and Shapiro (Ref. 7) published the results of a theoretical analysis of the discharge coefficients of rounded-entrance flowmeter orifices. Their work was limited to orifices of circular cross section. The analysis of Rivas and Shapiro considers the development of a laminar boundary layer at the entrance and along the length of well-rounded orifices. Rivas and Shapiro cast their boundary layer results into the form of an effective, entrance friction factor and use this factor to evaluate the orifice coefficient for short orifices:

$$C_{D_f} = \frac{1}{\sqrt{1 + \bar{f}\, L'/D}} \qquad (4)$$

where

$\bar{f}$ = effective friction factor, not the same as standard friction factor for fully developed flow

$\frac{L'}{D}$ = L/D + Leq/D = length to diameter ratio for the orifice, length taken at start of cylindrical section plus an effective Leq/D to account for boundary layer losses in the entrance section

C_{D_f} = orifice coefficient due to friction.

Nomenclature used by Shapiro and Rivas is explained more fully in Fig. 21.

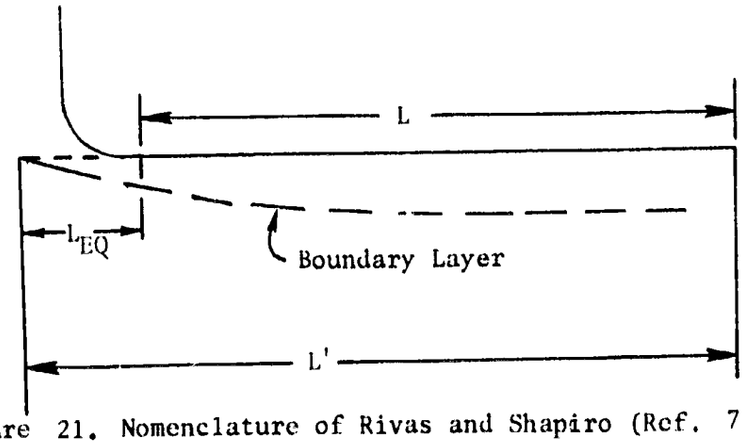

Figure 21. Nomenclature of Rivas and Shapiro (Ref. 7)

If the contour at the entrance of a given orifice is not ideal and an additional entrance loss is incurred, Rivas' formulation may be modified in the following manner to incorporate this loss:

$$C_D = \frac{1}{\sqrt{K_E + \frac{1}{C_{D_f}^2}}} \qquad (5)$$

where

C_D = total orifice coefficient

K_E = entrance loss factor

C_{D_f} = C_D predicted by Ref. 7 for wall frictional effects only.

The effective friction factor, $\bar{f}$, as presented by Rivas and Shapiro, is shown in Fig. 22.

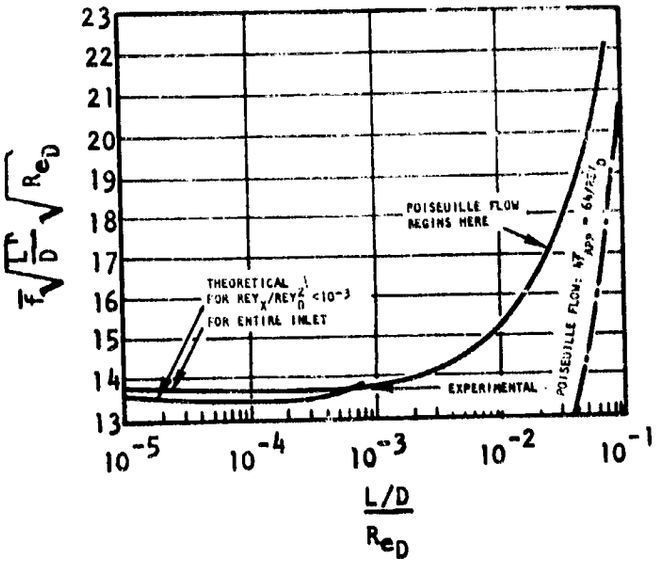

Figure 22. Effective Entrance Friction Factors (After Rivas and Shapiro, Ref. 7)

It is interesting to note that the correlating parameter is $(L/D)/Re_D$. A universal C_D curve is presented in Ref. 7 and is reproduced below in Fig. 23.

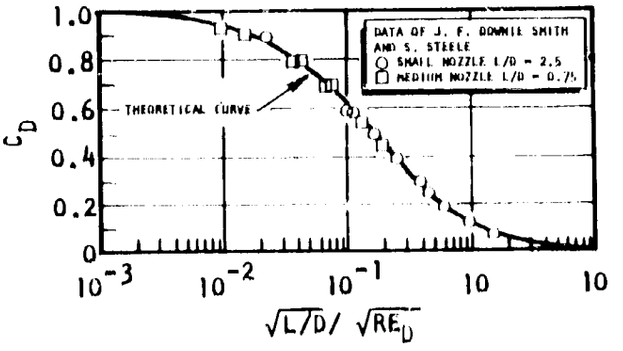

Figure 23. Universal Orifice Coefficient for Well Rounded Entrances (After Ref. 7)

This "universal curve" is only universal if the fully developed flow projected for a very long orifice is laminar. That is, the flow must approach Poiseuille flow, for which $\overline{f} = \frac{64}{Re}$ in long orifices. It is easily shown that this curve will not be applicable to long orifices with projected turbulent flows.

In the high Reynolds number regime, $\sqrt{\frac{L/D}{Re_D}}$ ceases to be a universal parameter because there is no longer a unique relationship between friction factor and Reynolds number. Thus, different results are obtained depending on whether length or Reynolds number is the variable. If both Reynolds number and L/D are varied, a complex relationship would develop.

Results of a sample calculation using this approach appear in Fig. 24. Four curves are presented. One is the "universal" curve, which should be applicable to short orifices or orifices operating at low Reynolds numbers. Another curve is for a fixed Reynolds number of 23,000 with L/D varied and the final curve is for a fixed Reynolds number of 1000 with variable L/D. These latter curves were computed using standard friction factors. For this plot, the characteristics dimension for the noncircular orifices is the hydraulic diameter.

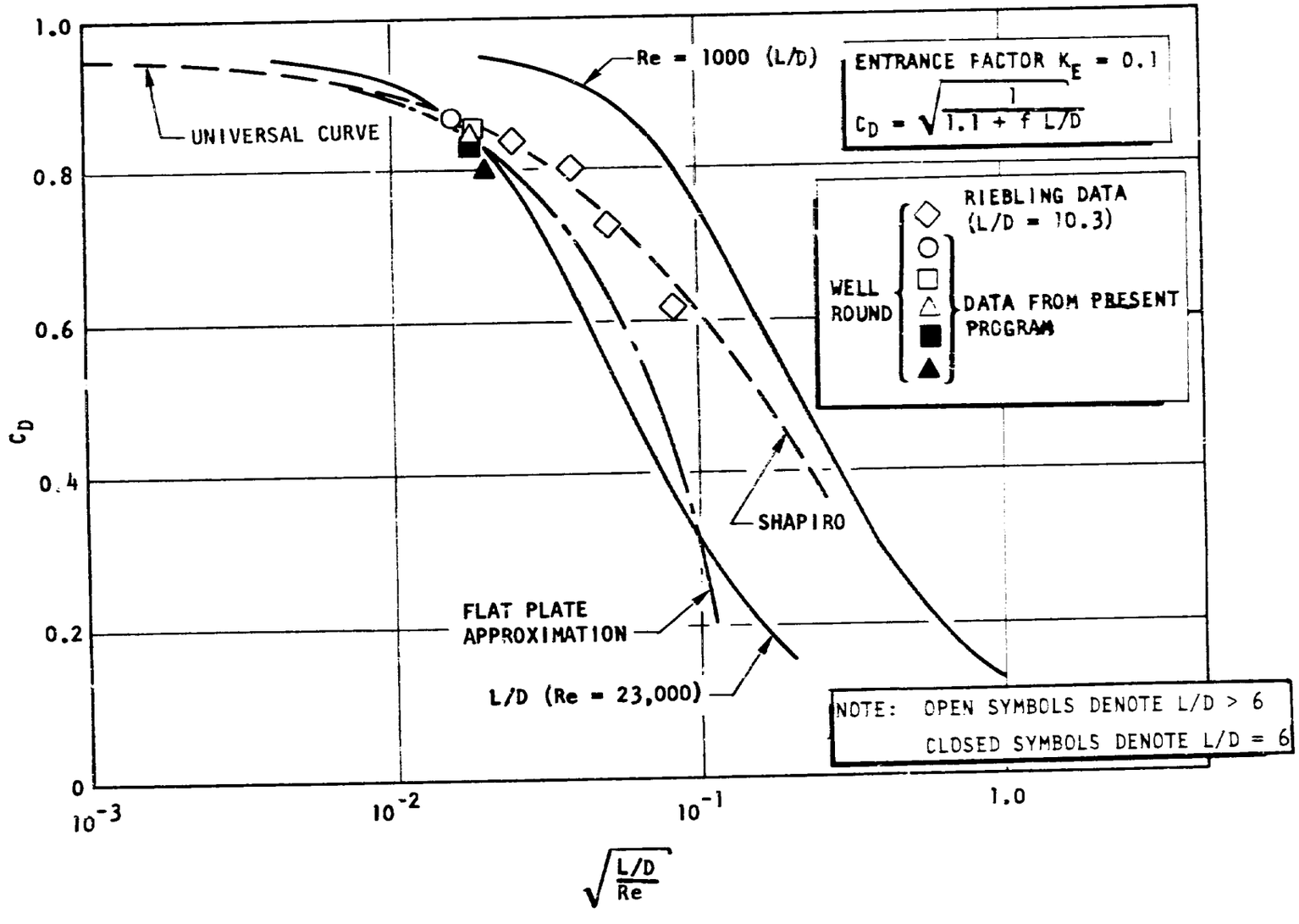

Figure 24. Round Entrance Characteristics

Also plotted in Fig.24 are the data from the well-rounded orifices (L/D = 6) of the five shapes tested at $V_c = 0$, and data taken by Riebling at JPL (Ref. 8) for micro slots (L/D = 10.3, t = 0.003, A = 33). The theory of Shapiro seems to fit all these data quite well except the slot which is not shown. However, the slot was operated at a Reynolds number of 10,000 based on D_H, but 20,000 based on the thickness. It may be that the thickness was more important here than the hydraulic diameter. Riebling's data runs from Reynolds No. 760 to 8500 based on t, or roughly 1520 to 17,000 based on hydraulic diameter. His data correlates quite well based on hydraulic diameter.

It appears that the best procedure for predicting C_D is to first determine the Reynolds number at which a given orifice is to be operated, then compute Shapiro's universal curve as well as a curve based on simple friction for various L/D's. If the L/D of the orifice places its value of $\sqrt{\frac{L/D}{Re}}$ to the right of the intersection of the two curves, then use the simple friction factor value; if the point is to the left, use Shapiro's value.

A simple extension of the model developed for rounded entrances is used to correlate the data from sharp edged orifices. The flow field is broken into two regions: (1) an entrance region in which the flow suffers a standard entrance loss (separated region), and (2) a full flowing region at the start of which the boundary layer begins to grow. The L/D in the frictional calculations must be reduced by the entrance length $(L/D)_e$.

If it is assumed that a standard entrance loss coefficient, K_E, is appropriate, the prelicted values of orifice coefficient would be given by Eq. 6 below.

$$C_D = \sqrt{\frac{1}{1 + K_E + f\left(\frac{L}{D} - \left(\frac{L}{D}\right)_e\right)}} \qquad (6)$$

In the equation used to generate the curves in Fig. 25, $K_E = 0.1$ The same three curves given in Fig. 24 are given in Fig. 25, only with $K_E = 0.5$ and $\frac{L}{D} \sim \frac{L}{D} - \left(\frac{L}{D}\right)_e$. Recall that for the solid curves, Reynolds number is fixed while L/D is the variable.

The data for L/D = 6 and 20 orifices with sharp entrances are also shown in Fig. 25. Only L/D = 6 and 20 data were selected for correlation in Fig. 25, because of the unpredictable nature of the discharge characteristics of orifices with L/D < 6. This uncertainty is evident in the summary of C_D versus L/D presented in Fig. 26. In Fig. 26, the values of C_D are plotted versus L/D (actual) for each of the five shapes. The solid curves on each plot are the predicted functional relationships between C_D and L/D with $K_E = 0.5$ and 0.7. Hydraulic flip problems encountered with orifices with L/D < 6 render their characteristics highly unpredictable. For the noncircular orifice, it appears that a value of $K_E = 0.7$ is appropriate.

As shown in Fig. 26, the discharge coefficients for orifices with L/D > 6 are well approximated by the orifice model. Values of C_D for L/D = 20 fit quite well. The Reynolds numbers of each flow measurement correspond closely to those of the curves nearest the points. For example, the slot was run at Reynolds No. = 10,000. Its C_D is well predicted by the simple friction factor curve for Re = 10,000. The Reynolds numbers for the other shapes lie between 15,000 and 20,000. It appears that they, too, are on simple friction factor curves. From Fig. 26 it appears that the L/D ~ 20 orifices were operated in the transition region between Shapiro's entrance theory and simple friction factor theory. Had these orifices been tested with larger L/D's, it is expected that their data would have followed the simple friction factor curves.

On the graph for the circle in Fig. 26 additional correlations are plotted for both detached and attached flow. Briant's data for short orifices (Ref. 9) and Aerojet's correlation for detached flow in short orifices

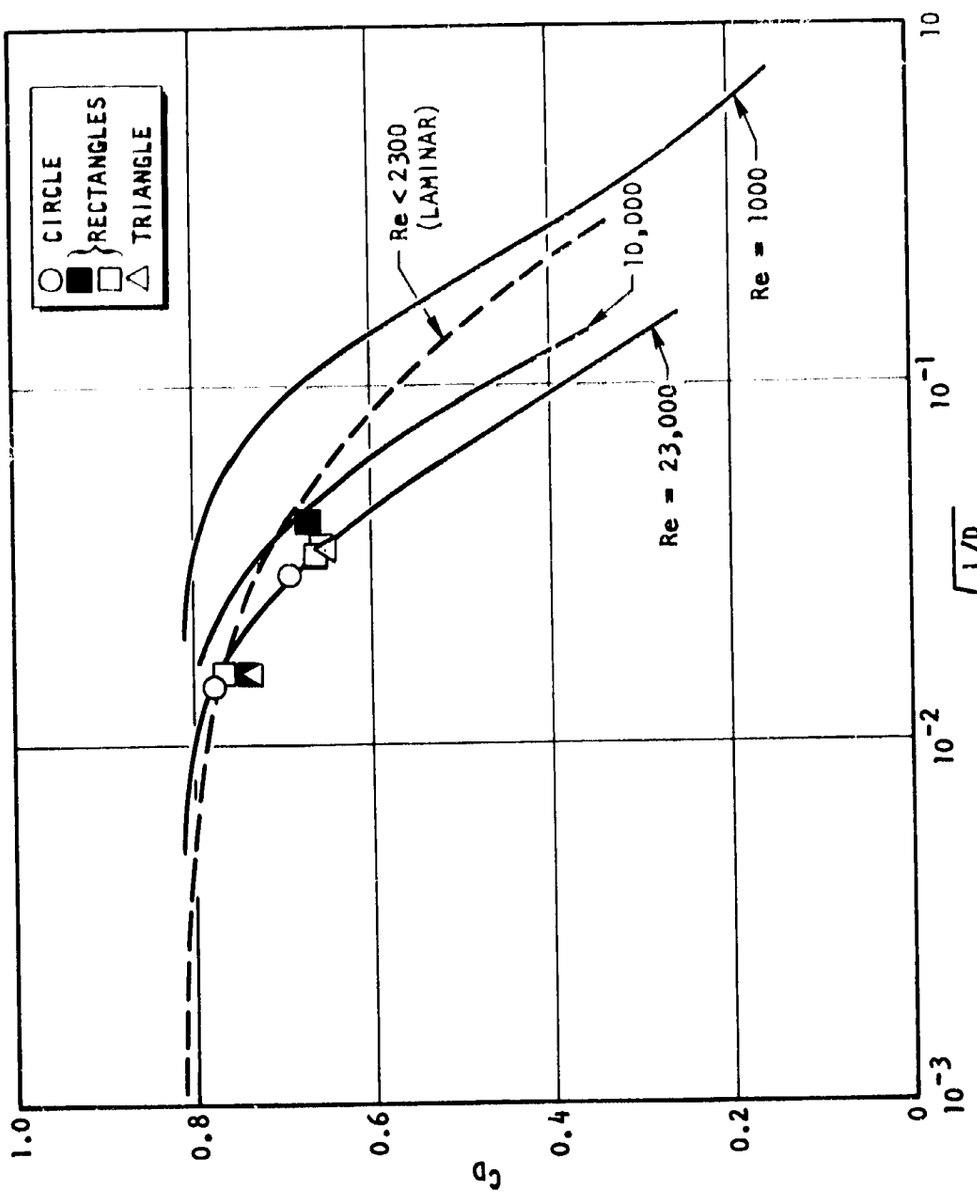

Figure 25. Sharp Entrance Characteristics

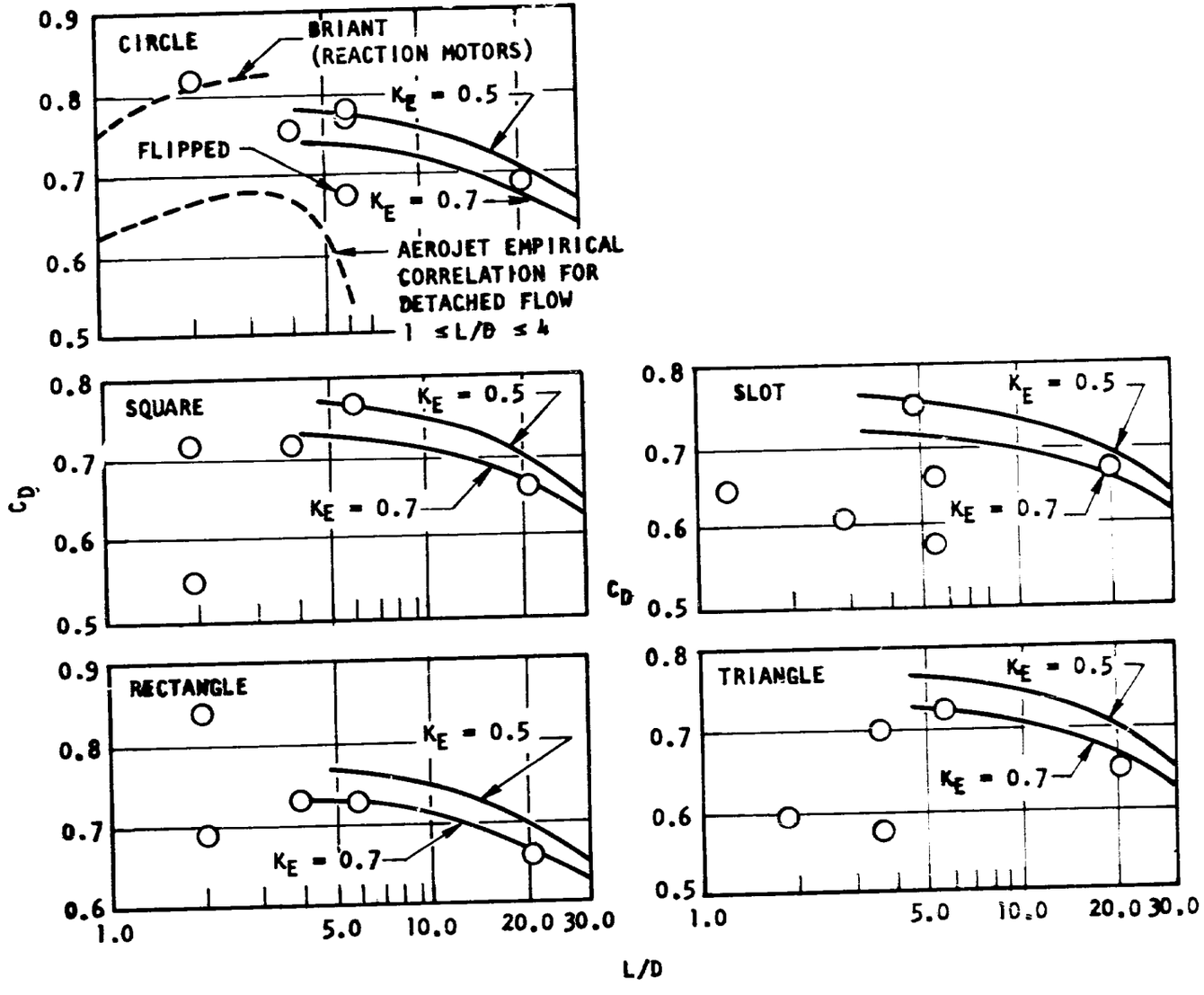

Figure 26. Variation of C_D With L/D

(Ref. 10) are shown. Aerojet's correlation is only valid for orifices with L/D < 3. One "flipped" point at L/D = 6 from this program seems to provide a logical extension of Aerojet's correlation to L/D = 6.

Cross Velocity Model

The most interesting effect of imposition of cross velocity is the reduction of C_D with cross velocity for sharp entrance orifices and the increase of C_D with cross velocity for rounded entrance orifices.

A crude model can be postulated for the effect of cross velocity on orifice coefficient employing qualitative reasoning. Suppose that the "true" value of C_D is really unchanged by the cross velocity, and only the apparent C_D varies with cross velocity because the actual ΔP across the orifice in unknown.

The simplest description of the actual pressure drop would entail the assumption that the upstream pressure is equal to the static pressure in the manifold plus the velocity head for the round orifice (i.e., stagnation pressure) and less the velocity head for the sharp orifice. This can be expressed in equation form as follows:

$$\frac{C_{D_A}}{C_D} = \sqrt{1 \pm \frac{\frac{1}{2}\rho V_c^2}{\Delta P_s}} \qquad (7)$$

where

C_{D_A} = apparent C_D computed directly from test data

C_D = actual C_D at zero cross velocity (a constant)

ΔP_s = measured ΔP computed by subtracting downstream stagnation pressure from upstream static pressure

$\frac{1}{2}\rho V_c^2$ = kinetic pressure in the cross channel upstream of the orifice

The plus sign would be used with rounded entrances and the minus sign with sharp entrances.

To check this model, all cross velocity data (C_D) at L/D = 6 were normalized by dividing each C_D value by the C_D found at 10 ft/sec with an average straight line fit for each shape. The parameter $C_D/C_{D_{10}}$ was computed for both round and sharp data. These parameters are plotted versus cross velocity in Fig. 27. Since $C_D/C_{D_{10}} \neq 1$ at $V_c = 0$, an appropriate multiplier was applied to Eq. 7 to best fit the data. The value of $(C_D/C_{D_{10}})V_c = 0$ was then multiplied by $\sqrt{1 \pm \frac{1}{2}\rho V_c^2/\Delta P_s}$ to produce the solid curve on each graph. For such a crude analysis, it correlates the data very well. For all the points in Fig. 27, ΔP_s was approximately equal to 20 psid. Thus, Eq. 7 may be used to estimate the "apparent" discharge coefficient as a function of both cross velocity and level of ΔP for sharp and well-rounded entrances. However, it must be emphasized that there are additional effects for orifices which are not perpendicular to the manifold channel as well as entrance conditions which are neither well rounded nor sharp. Equation 7 is far from being all encompassing; it does, however, show roughly how the sensitivity to cross velocity would vary with ΔP level. At very high ΔP's, the effects of cross velocity would damp out.

Improved Evaluation Criteria

Summaries of results of the orifice coefficient models which have been discussed appear in Fig. 24, 25, and 26. Predicted values of orifice coefficient are plotted as functions of orifice L/D, Reynolds number and the parameter L/D/Re in Fig. 28 for round entrance orifices and Fig. 29 for sharp entrances. The Reynolds number is based on the hydraulic diameter, making these results applicable to orifices of arbitrary shape. The effect of cross velocity on orifice coefficient is shown in Fig. 30. Orifice coefficient, normalized with respect to its value at zero cross velocity is plotted as a function of manifold kinetic pressure divided by the static pressure drop across the orifice.

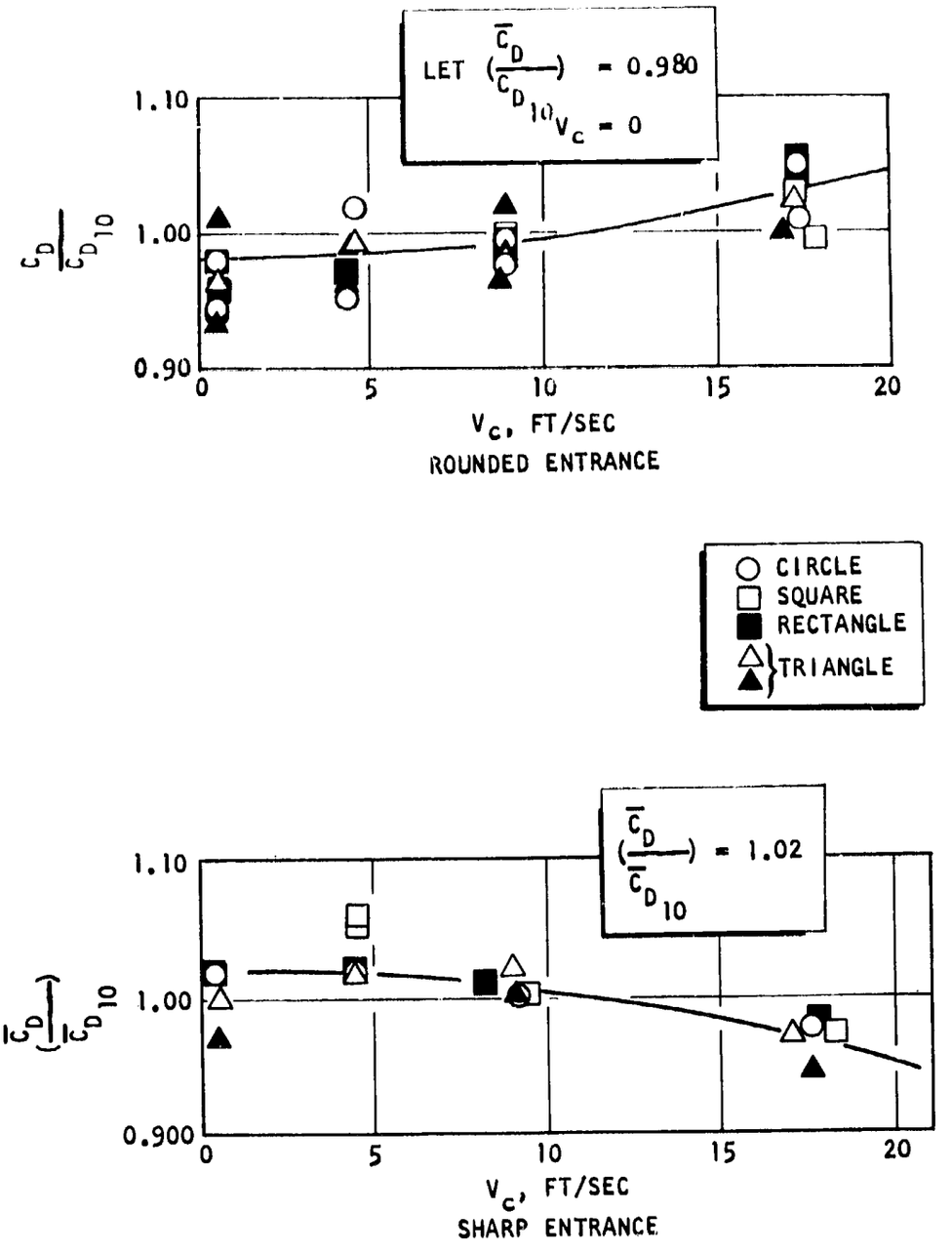

Figure 27. Correlation of Cross-Velocity Data

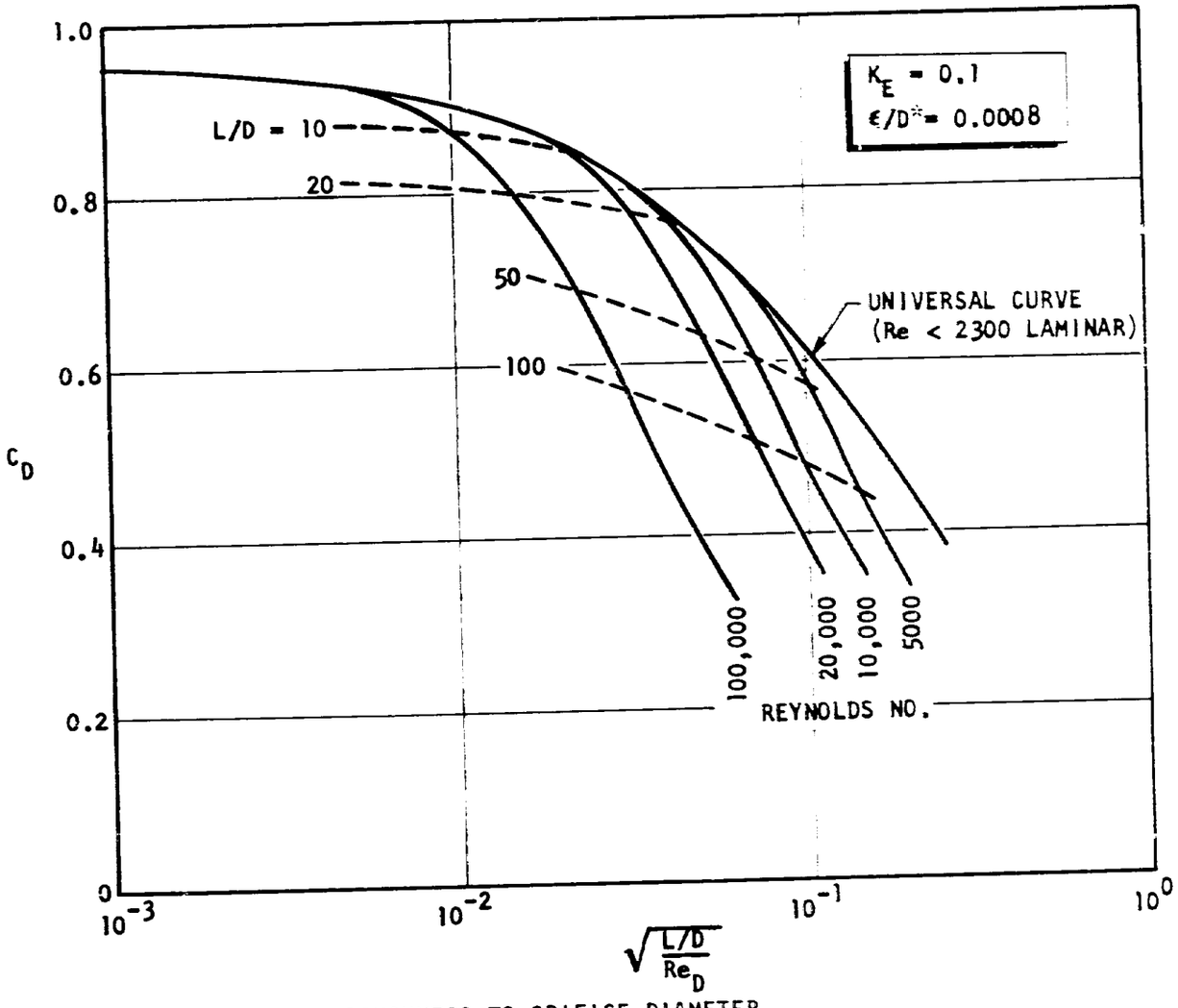

Figure 28. Orifice Coefficient for Round Entrance Orifices

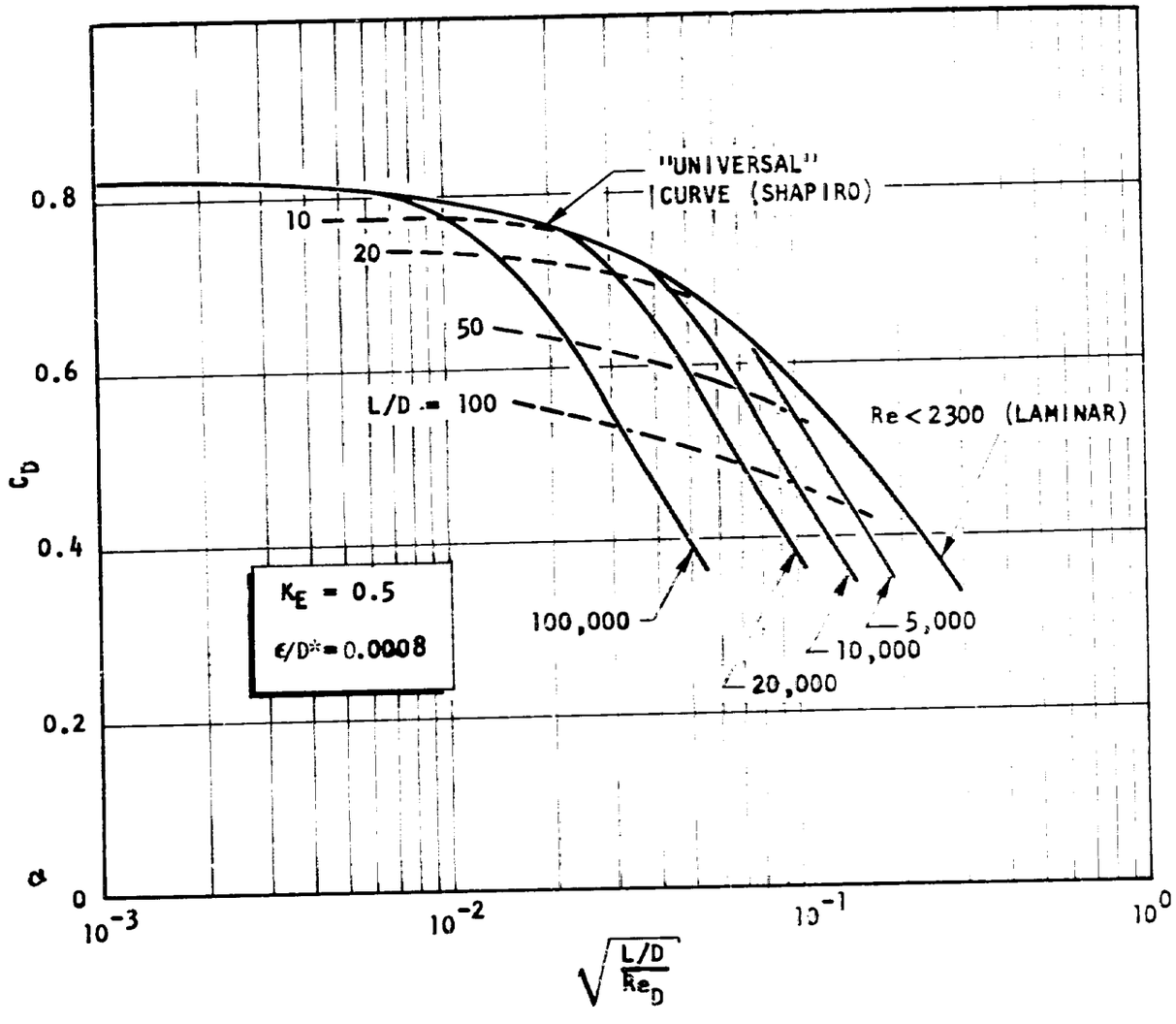

*ϵ/D - SURFACE ROUGHNESS TO ORIFICE DIAMETER

Figure 29. Orifice Coefficient for Sharp Entrance Orifices

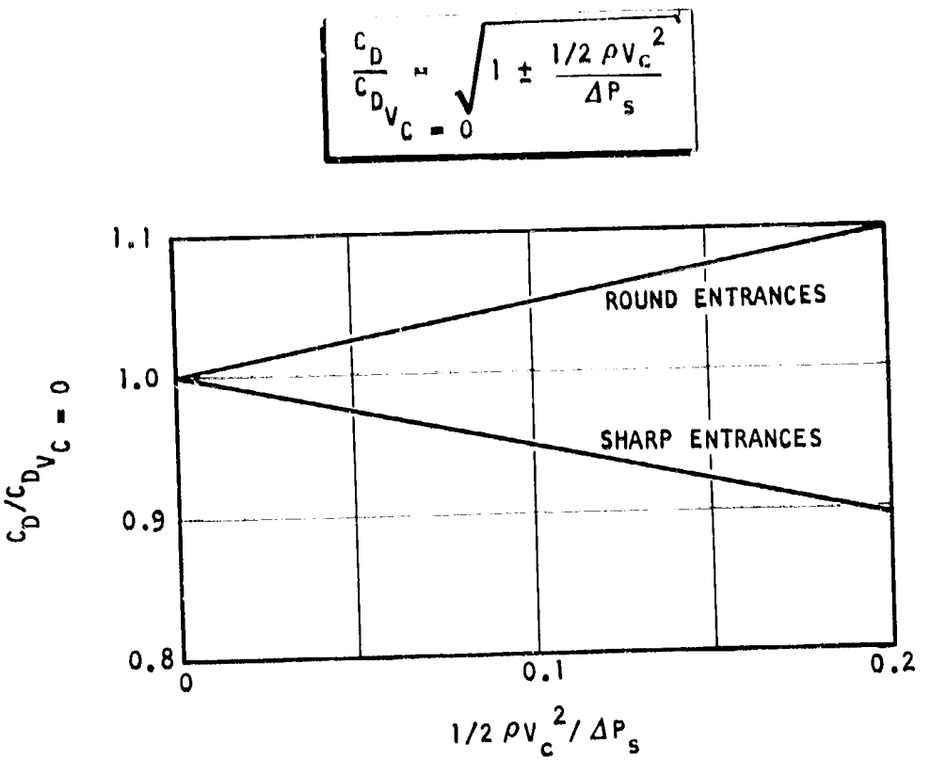

Figure 50. Effect of Cross Velocity on Orifice Coefficient (Normalized) for Orifices Normal to Manifold Only (Attached Flow)

These functional relationships between orifice coefficient and the physical parameters involved provide tools upon which to base a reevaluation of orifice shapes. Using the data in Fig. 28, 29, and 30, a more realistic comparison may be made of circular and noncircular orifices.

A final comparison of the orifices was made with the assumption that the orifices were of the same area, Fig. 31, same L/D, and were being operated at the same flowrate. As a standard, the circle was assigned a Reynolds No. of 20,000. The results of this calculation are presented in Fig. 31. Discharge coefficient is plotted as a function of shape factor, which is the ratio of the diameter of a circle to the hydraulic diameter of an arbitrary shape with the same area as the circle. The results of the comparison show that the circle produces the highest C_D while the slot produces the lowest. However, the important conclusion from Fig. 31 must be that the differences between the various C_D values are quite small.

4.2.3 SINGLE ELEMENT STUDY

Mixing

Cold-flow experiments were conducted employing several noncircular element shapes as well as the standard circular unlike doublet. The objective is to determine optimum design criteria so that optimally designed noncircular element mixing characteristics could be compared to an optimally designed circular unlike-doublet element. An additional objective is to determine the sensitivity of mixing to variations in orifice L/D, cross velocity, total injected momentum, and entrance condition.

In general, the parameters influencing the mixing characteristics for injector elements are:

$$\eta_{mix} = f(D, V, D_1/D_2, \dot{W}_T, V_1/V_2, \theta, \beta, \frac{L}{D}, X, Y, V_c, \text{physical properties}) \quad (8)$$

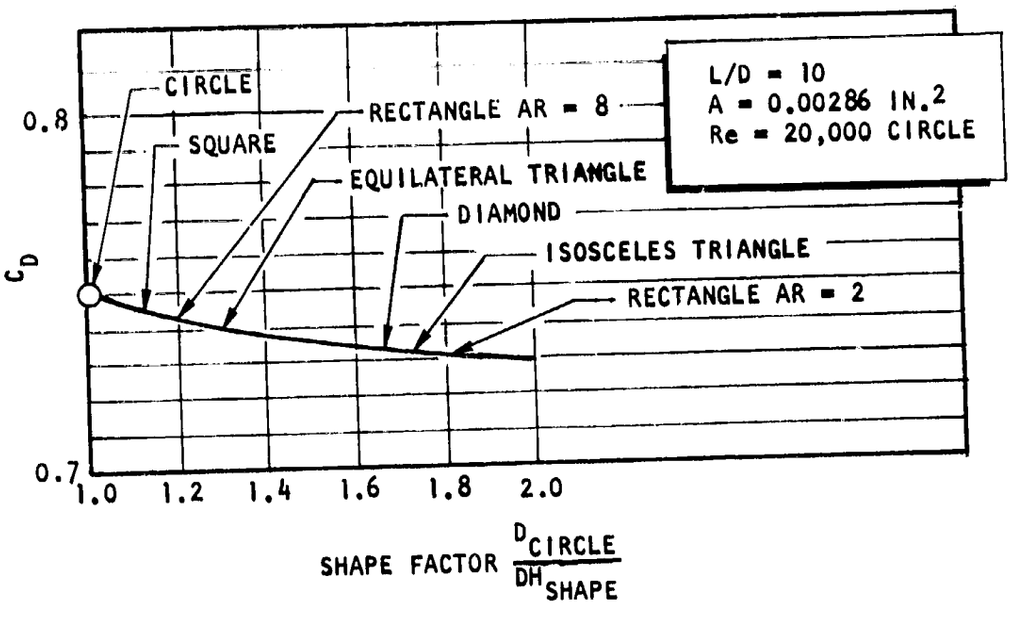

Figure 31. Comparison of C_D for Various Shapes

where

D	=	orifice diameter
V	=	injection velocity
θ	=	impingement angle
β	=	fan cant angle between spray fans
$\frac{L}{D}$	=	orifice length to diameter ratio
X,Y	=	spacing between elements, or spray fans
$\dot{w}_T$	=	total flowrate level
V_c	=	manifold cross velocity
1,2	=	fuel and oxidizer

The particular importance of each of the above parameters on the mixing characteristics depends largely upon the particular element type. Rupe (Ref. 2) evaluated the effect of V and D upon mixing for unlike doublets and found that for optimum mixing the following equality must hold.

$$\rho_1 V_1^2 D_1 = \rho_2 V_2^2 D_2 \tag{9}$$

or

$$N^{DEF} = \frac{1}{1 + \frac{\rho_1 V_1^2 D_1}{\rho_2 V_2^2 D_2}} = 0.5 \tag{10}$$

For Rupe's study, only single elements were utilized with large L/D's producing fully developed turbulent flow at the orifice exits. Consequently, the above equation applies to the local mixing of a pair of uniformly turbulent impinging unlike-doublet jets. Nurick and Clapp (Ref. 11) have shown the importance of β, X, and Y on the mixing characteristics for multielement like-doublet injectors.

Unlike-Doublet Elements. For the unlike impinging jet elements, it was assumed that the equation developed by Rupe of circular unlike doublets would still apply. However, the characteristic dimension instead of being diameter would by hydraulic diameter. Or

$$N = \frac{1}{1 + \phi \left[\frac{D_f}{D_o}\right]_H} \tag{11}$$

where

$$\phi \quad \text{DEF} \quad \frac{\rho_f V_f^2}{\rho_o V_o^2}; \text{ dynamic pressure ratio} \tag{12}$$

ρ = density

V = jet velocity

$\left(\frac{D_f}{D_o}\right)_H$ = hydraulic diameter ratio of the orifices

o,f = oxidizer and fuel, respectively

For circular orifices, in terms of engine operating specifications, Eq.11 is:

$$N = \frac{1}{1 + \left(\frac{1}{MR}\right)^2 \frac{\rho_o}{\rho_f} \left(\frac{D_o}{D_f}\right)^3} \tag{13}$$

where

MR = mixture ratio

D_o/D_f = orifice diameter ratio

Because MR and ρ are fixed for a specific propellant combination, the only remaining variable for circular orifices which can be perturbated to produce an optimum value of N is the diameter ratio.

For noncircular orifices, an additional degree of freedom can be obtained in Eq. 11. This is illustrated by rewriting Eq. 11 in the following form:

$$N = \frac{1}{1 + \left(\frac{1}{MR}\right)^2 \left(\frac{A_o}{A_f}\right)\left(\frac{D_o}{D_f}\right)_H \frac{\rho_o}{\rho_f}} \tag{14}$$

where

A = orifice area

For noncircular orifices, the area ratio of the orifices is not equal to the hydraulic diameter ratio. Consequently, both the area ratio and hydraulic diameter can be varied independently to obtain an optimum value of N. This equation is reformulated in Appendix C in terms of the aspect ratios of the orifices. The resulting equation for equal contact dimension is of the following form:

$$N = f(K, AR_f, AR_o) \tag{15}$$

where

$K = MR^2 \rho_f/\rho_o$

AR* = aspect ratio

The specific objective of the unlike-doublet experimental evaluations is, therefore, to determine, for noncircular orifices, the value of N producing optimum mixing and the corresponding aspect ratio for each element pattern.

*See Appendix C for a definition of Aspect Ratio.

The optimum value of N was determined by conducting tests over a range of mixture ratio for several differing aspect ratios with equal contact dimensions for the noncircular orifice elements. Four basic element configurations were evaluated. These were the following:

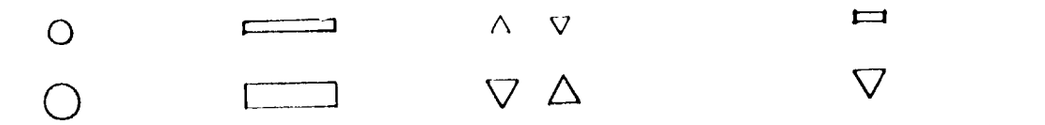

Circular Rectangular Triangular Rectangular/Triangular

and the specific element dimensions were those listed in Table 20.

The mixing results for the various aspect ratio designs over a range of "N" (i.e., MR) are shown in Fig. 32 (see Table 19). The data are presented in terms of E_m and N for each aspect ratio element design. The term E_m is defined as:

$$E_m = 1 - \sum_{1}^{N} \frac{\dot{w}_i}{\dot{w}_T} \frac{(R - r_i)}{R} - \sum_{i}^{N} \frac{\dot{w}_i}{\dot{w}_T} \frac{(R - \bar{r}_i)}{(R - 1)} \qquad (16)$$

where

$\frac{\dot{w}_i}{\dot{w}_T}$ = mass fraction in ith tube

R = ratio of total oxidizer to total flow

r_i = ratio of total oxidizer to total flow in ith tube for $r_i < R$

$\bar{r}_i$ = ratio of total oxidizer to total flow in ith tube for $r_i > R$

This expression was first defined by Rupe (Ref. 2). It represents the sum of the mass weighted deviations of the mixture ratio from the overall injected mixture ratio. In a sense, it is a special type of standard deviation. Both hot-fire and cold-flow evaluations at Rocketdyne (Ref. 12, and 13) have shown that E_m is an excellent measure of the uniformity of the mass and mixture ratio distribution.

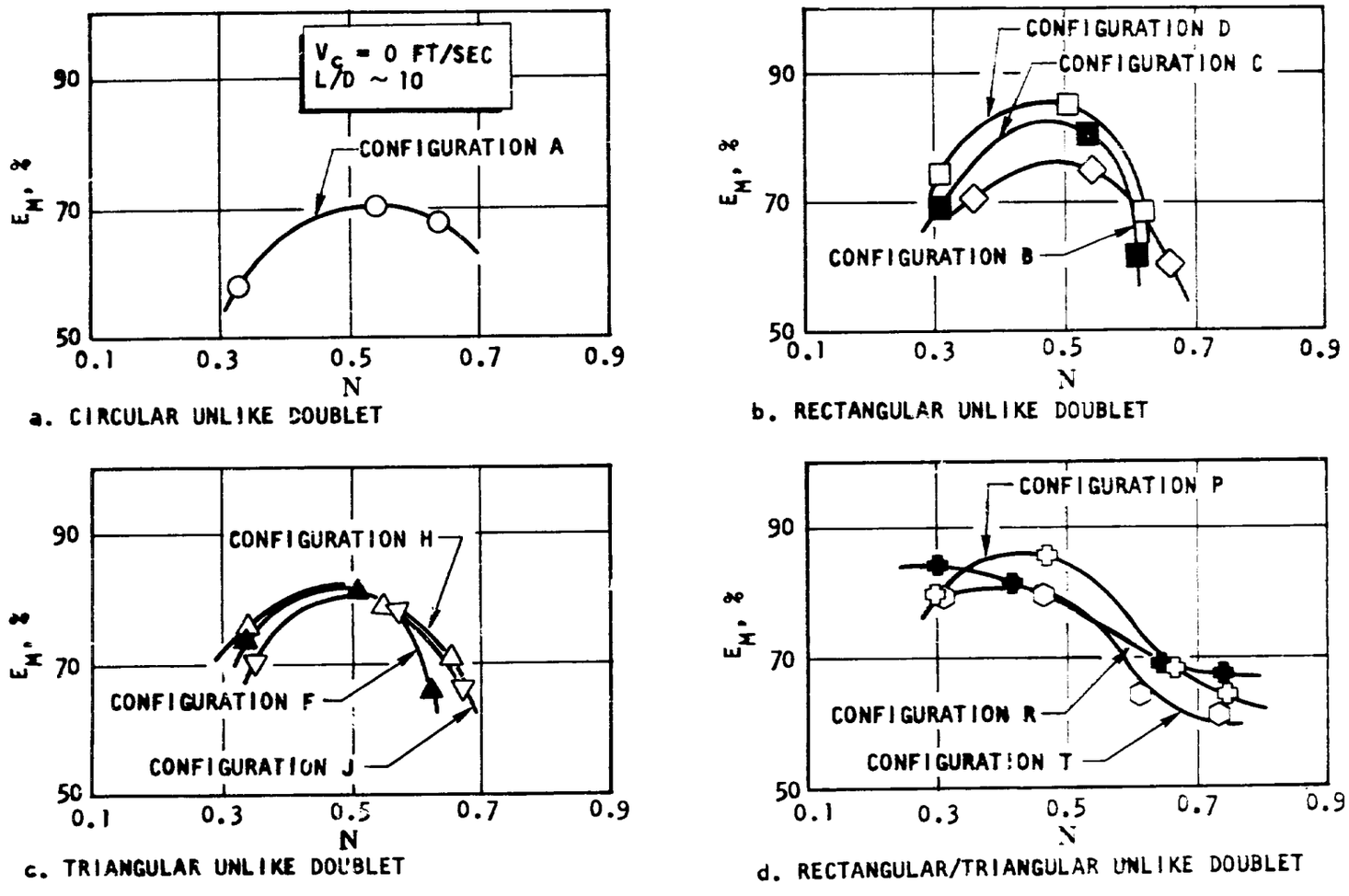

a. CIRCULAR UNLIKE DOUBLET

b. RECTANGULAR UNLIKE DOUBLET

c. TRIANGULAR UNLIKE DOUBLET

d. RECTANGULAR/TRIANGULAR UNLIKE DOUBLET

Figure 32. Mixing Uniformity for Several Aspect Ratio Designed Circular and Noncircular Injector Elements

Note in Fig. 32 that the triangular, rectangular, and circular elements all optimize at a value of N of 0.5, while the combination rectangle/triangle element resulted in a differing optimum for each aspect ratio design. The fact that the rectangular and triangular elements all optimize at a single value considerably simplified the determination of the optimum designs.

As shown in Appendix C for the rectangular and triangular elements, the optimum aspect ratios for NTO/50-50 propellants at a MR = 1.6 are:

Rectangular Element Optimum

$$AR_f = 2.3$$
$$AR_o = 3.2$$

Triangular Element Optimum

$$AR_f = 0.7$$
$$AR_o = 1.0$$

These values are very close to configurations D (rectangle) and F (triangle). The rectangle/triangle configuration was dropped from further evaluation because (1) it did not appear to affect better mixing characteristics than the rectangular pattern, and (2) more configurations would be required to determine the optimum aspect ratio.

Several other variables which can effect mixing (Eq. 8) were also studied. These additional variables are manifold cross velocity (V_c), orifice L/D, entrance condition, and total momentum (i.e., flowrate). Manifold cross velocity and L/D effects were studied utilizing configurations "A" (circle), "D" (rectangle), and "F" (triangle). These configurations represent the designs which most nearly represent optimum aspect ratio configurations. For the cross velocity study, the nominal orifice L/D's were about 5.0 to 6.0. The specific L/D for each, used in all but the variable L/D test, are listed below.

ORIFICE L/D's FOR V_c EXPERIMENTS

Configuration	$(L/D)_{ox}$	$(L/D)_{fuel}$
A	4.43	5.17
D	5.63	6.18
F	5.80	6.87

Manifold cross velocity was varied from 0 to 20 ft/sec utilizing each of the above elements and the overall spray mixing uniformity determined. The results are presented in Fig. 33. These results, obtained over the above range of V_c, show that no substantial effect of cross velocity on mixing was found. For instance, for the triangular element, over the entire range of V_c, mixing uniformity for the rectangular element varied only by about 5 percent, decreasing with increasing cross velocity. The circular element appeared to be most sensitive, varying by 8 percent in E_m. It is important to note that these experiments were conducted at ambient backpressure and at these conditions the orifice C_D at zero cross velocity is on the order of 0.7 for the rectangle and triangle, and 0.6 for the circle (oxidizer orifices). For the rectangular and triangular configurations, these values represent jet flow which is attached, but the jets tend to be somewhat bushy at the orifice exit. For the circular orifices, this condition represents fully separated flow. It was shown in the single orifice study that cross velocity can cause a separated orifice to attach; however, the resulting jet tends to be bushy with considerable breakup occurring near the orifice exit.

In addition, the jet direction at the exit is altered as was shown in both the orifice study of this program and that of Ref. 10. Consequently, it is difficult to intuitively judge whether this type of phenomena will increase or decrease mixing. The results suggest that for the circle and rectangle the overall effect was to decrease mixing uniformity.

a. MANIFOLD CROSS VELOCITY

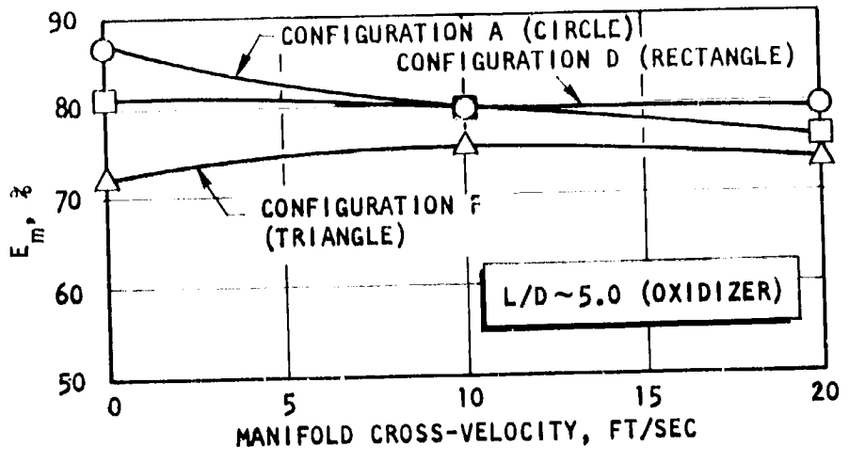

b. ORIFICE L/D

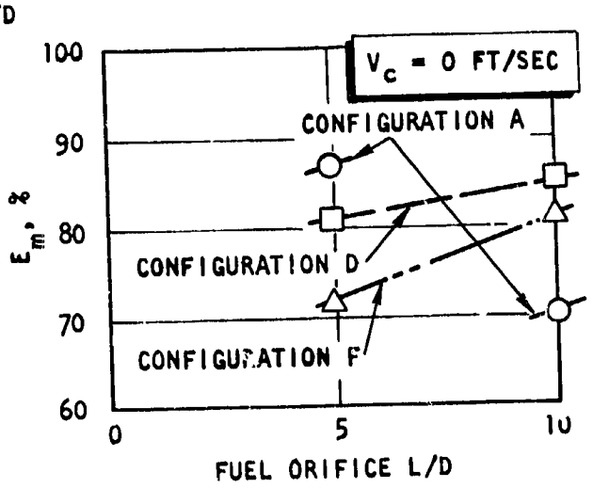

Figure 33. Mixing Uniformity (E_m) as a Function of Injector Design and Operating Variables for Selected Circular and Noncircular Unlike-Doublet Elements (Simulants: Trichlorethylene/Water)

A more surprising result was obtained at zero cross velocity for fuel L/D's of from 5 to 10 and ambient backpressure. The results are shown in Fig. 33. Note that for the circular element, mixing was considerably higher (~17 percent) for the short L/D than for that obtained at an L/D of 10.

The specific measured C_D's for both the fuel and oxidizer orifices are listed below.

C_D's Obtained During L/D Study

Configuration	$(L/D)_{oxidizer}$	$(L/D)_{fuel}$	$(C_D)_{oxidizer}$	$(C_D)_{fuel}$
△	8.6	10.	0.69	0.69
○	4.3	5.2	0.59	0.66
◇	10.9	12.	0.71	0.76
□	5.6	6.2	0.63	0.66
F	11.3	13.3	0.71	0.76
△	5.8	6.9	0.76	0.7

Inspection of the table shows that the circular orifice had the shortest L/D's and produced fully separated flow (C_D = 0.6) at the short L/D condition. Also, the rectangular element at the short L/D condition (C_D = 0.63) appears to be separated. Note that these two patterns showed an effect of cross velocity on mixing uniformity while the triangle did not. For zero cross velocity, both the triangular and rectangular elements produced a decrease in mixing uniformity with decreased L/D. For the circle, however, fully separated flow resulted in about a 17 percent increase in the mixing uniformity over that obtained for "quasi-attached" flow. This significant variation in E_m illustrates that the circular element mixing uniformity is much more sensitive to L/D than that for noncircular orifices.

Cold-flow mixing experiments were also conducted for several manifold and orifice entrance conditions. In addition to the sharp entry design discussed above (configuration A), the entrance was rounded. Also, for the sharp entrance condition the manifold entrance port was enlarged, thereby reducing the manifold velocity entering to the orifice. For easy comparison, these results are presented in Fig. 34 along with the results obtained over the flowrate range of about 0.075 to 0.4 lbm/sec.

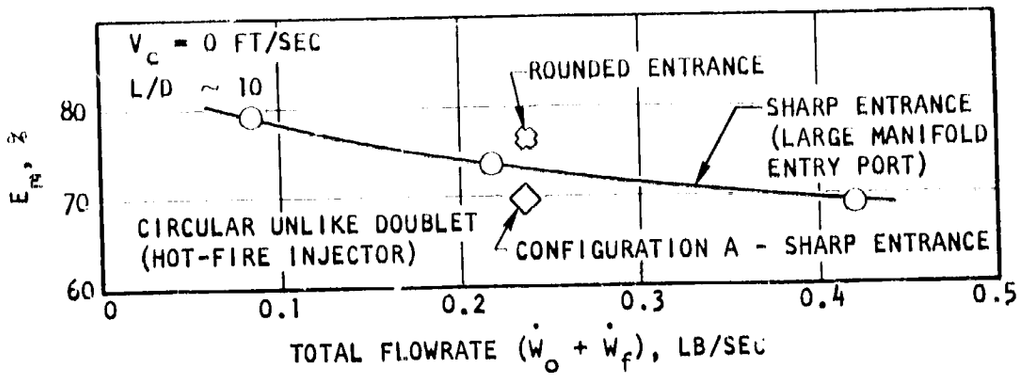

Figure 34. Mixing Characteristics for a Circular Unlike-Doublet Injector Over a Range of Total Flowrate and Comparison With Various Entrance Configurations

These results show that the circular element is extremely sensitive to variations in the manifold configuration. Note that a 6 percent increase in E_m occurred when the entry to the orifice was rounded. Also note that a 3 percent increase in E_m occurred when the manifold entry port was enlarged. These results certainly emphasize that extreme caution must be exercised in the design of the orifice manifold and orifice entry configuration.

Self-Atomizing Nozzle Elements. In addition to the unlike impinging doublet patterns, two types of self-atomizing nozzle elements were evaluated; a hydraulic swirl and a fan nozzle configuration. Both the hydraulic swirl and fan element designs were described in Table 18.

For the self-atomizing nozzle, five parameters were evaluated: (1) fan impingement angle, (2) spacing between fans, (3) relative fan width, (4) total momentum, and (5) momentum ratio. Total momentum was studied by variations in total flowrate, and momentum ratio was investigated by variations in mixture ratio.

The hydraulic swirl element results are shown in Fig. 35. For the hydraulic swirl design, note that the fuel and oxidizer nozzles are separated by 0.5 inch and then the elements canted (β) toward each other from 0 to 70 degrees. As shown in Fig. 35, mixing is exceptionally low (E_m = 45 percent) over the entire range. As a result, this element was eliminated from further study.

The results obtained over a range of cant angle using two configurations of the fan nozzle employing equal orifice size elements are also shown in Fig. 35. The specific orifice dimensions for this design are 0.062 for both orifices. The mixing characteristics, for both a 1-inch and 0.5-inch spacing between the oxidizer and fuel nozzles, were evaluated over a range of cant angle (β) from zero to 75 degrees. For both configurations, mixing improves with increasing β angle until about 50 to 60 degrees and then tends to slowly decrease. The 1.0-inch spacing injector element is about 4 percent higher in mixing uniformity.

In addition to equal sized orifices, the influence of relative fan width on mixing was also studied. Variation in the relative fan width was accomplished by using fan nozzles of differing sizes. The specific design utilized a 0.062-inch fuel and a 0.072-inch oxidizer equivalent diameter self-atomizing spray fan nozzle. For this specific design, experiments were conducted over a range in mixture ratio and total flowrate. The results are shown in Fig. 36. First, comparing the values of mixing uniformity at a mixture ratio of 1.6 for the equal and unequal sized orifices shows that changing the relative fan width from other than 1.0 resulted in a substantial loss in mixing uniformity; about 13 percent in E_m. This result clearly demonstrates that the self-atomizing fan injector is extremely

a. SELF-ATOMIZING NOZZLE
70-DEGREE SWIRL UNLIKE DOUBLET

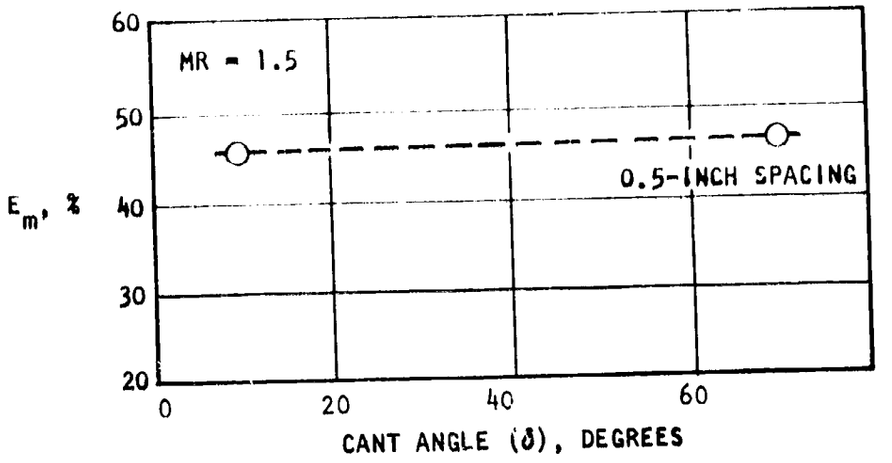

b. SELF-ATOMIZING NOZZLE
80-DEGREE FAN UNLIKE DOUBLET

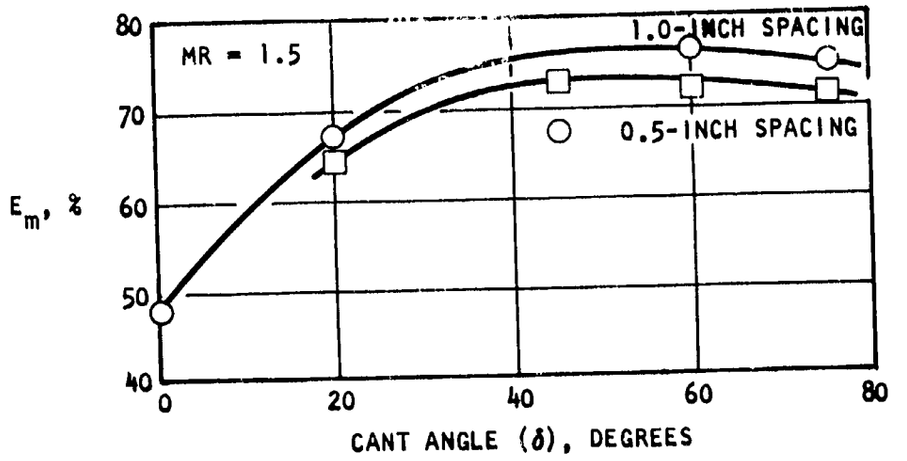

Figure 35. Mixing Uniformity (E_m) as a Function of Injector Design Parameters for Several Self-Atomizing Nozzle Injector Elements Using Equal Nozzle Sizes
(Simulants: trichlorethylene/water)

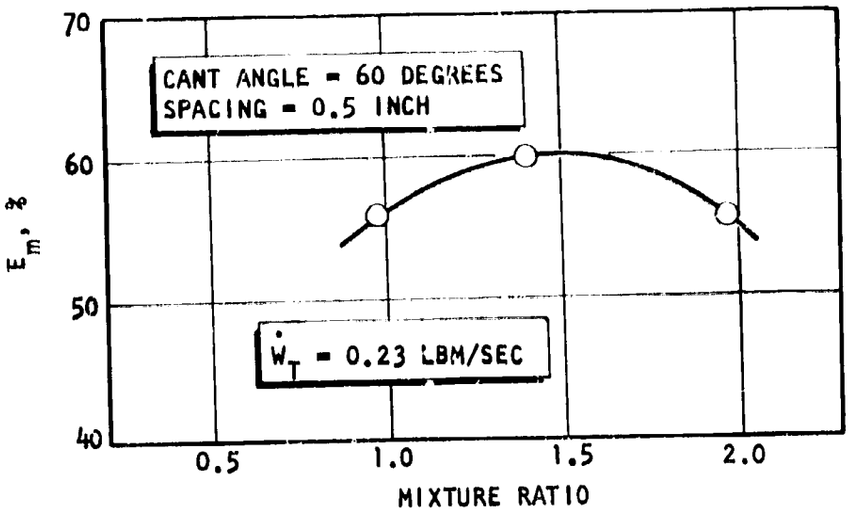

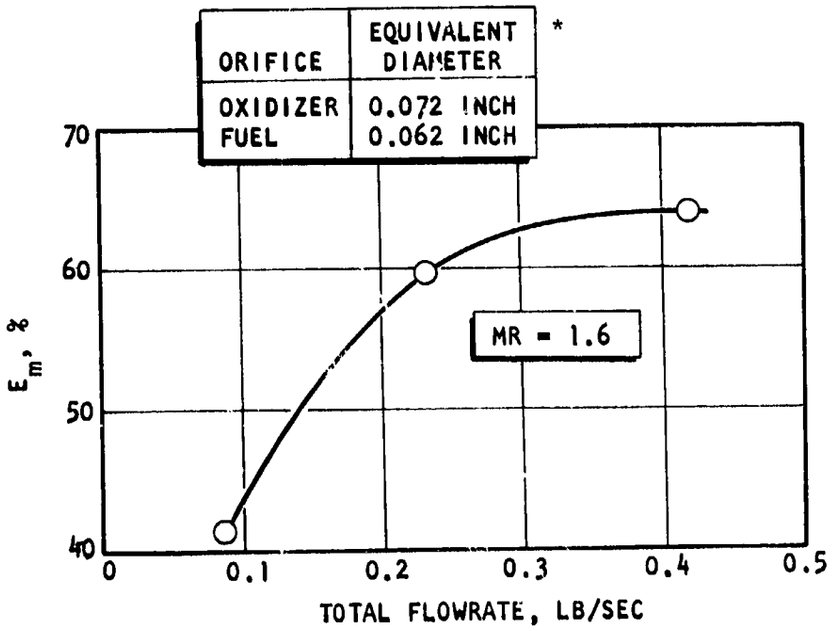

*See Table 18

Figure 36. Mixing Characteristics for Self-Atomizing Fan Injector Utilizing Unequal Fan Nozzle Sizes

sensitive to the relative fan width. In addition, note that the mixture ratio trend shows that E_m increases until a mixture ratio of about 1.6 and then tends to decrease. This variation in mixing uniformity is about equal to that for the circular unlike doublet. However, note from the plot of total flowrate versus E_m that at low values of total flowrate there is insufficient momentum for the sprays to accomplish a high degree of mixing uniformity. In fact, the overall drop in E_m over the range in total flowrate from about 0.4 to 0.075 is 25 percent in E_m. The mixing uniformity for this injector pattern is much more sensitive to total injected momentum than the circular unlike doublet.

Comparison of Mixing Characteristics for Circular and Noncircular Elements. Comparisons of the injectors are made for the optimum configuration for each injector element type. For the unlike doublet elements, the optimum configurations were:

1. Circle--Configuration A
2. Triangle--Configuration F
3. Rectangle--Configuration D

and for the self-atomizing fan injector:

Relative Fan Width = 1.0

Spacing, inch = 1.0

Cant Angle, degrees = 60

The comparisons are made in terms of both the mixing uniformity (E_m) and the mixing limited c* efficiency ($\eta_{c^* \text{ mix}}$). Values of E_m and η_{c^*} can be found for each cold-flow experiment in Appendix A, Table A-3. The mixing limited c* efficiency is obtained from input of the specific spray distribution into a mixing limited combustion model. The model is based on a streamtube analysis and requires knowledge of the mass and mixture ratio distribution throughout the spray field. A complete derivation of the streamtube model can be found in Appendix J of Ref. 13. The general features of the analysis are as follows: consider the rocket engine to be divided into N-imaginary streamtubes; also consider that complete vaporization

is accomplished in the combustion chamber for each streamtube (based on the flow conditions of that tube). The combustion gases of each streamtube then expand isentropically through the nozzle. It is assumed that no intertube mixing, either thermal or chemical, occurs between adjacent streamtubes, and pressure continuity is maintained at each transverse station in the nozzle. Chamber pressure, throat area, contraction ratio, and propellant distribution are specified. The static pressure at the throat and the total propellant flowrate are determined by an iteration process.

The result of this derivation in terms of c* efficiency is:

$$\eta_{c^*,dist} = \frac{100}{c^*_{theo}} \sum_{i}^{N} \left[(MF_i) \ (c^*_i) \left(\frac{A_{ti}}{A^*_i} \right) \right] \tag{17}$$

where

c^*_{theo} = theoretical shifting c*

MF_i = mass fraction in ith streamtube

c^*_i = theoretical shifting c* based on flow conditions in ith tube

A_{ti} = area of ith streamtube at the geometric nozzle throat

A^*_i = area of ith streamtube at the sonic condition

From Eq. 17, the loss in c* efficiency caused by propellant maldistribution is determined by summing the mass weighted c^*_i associated with each streamtube multiplied by an area correction factor. The A_{ti}/A^*_i factor is a correction to account for the shift in the location of the sonic point resulting from changes in the specific heat ratio.

In Fig. 37a, the mixing uniformity (E_m) is plotted as a function of the mixing parameter N. For N = 0.5, these results for the unlike doublets show that the pattern producing the most nonuniform spray pattern will be the circular element (E_m ~70 percent), then the triangular element (E_m ~80 percent). The highest mixing uniformity was produced by the rectangular element (E_m ~86 percent). All unlike doublet patterns seem to

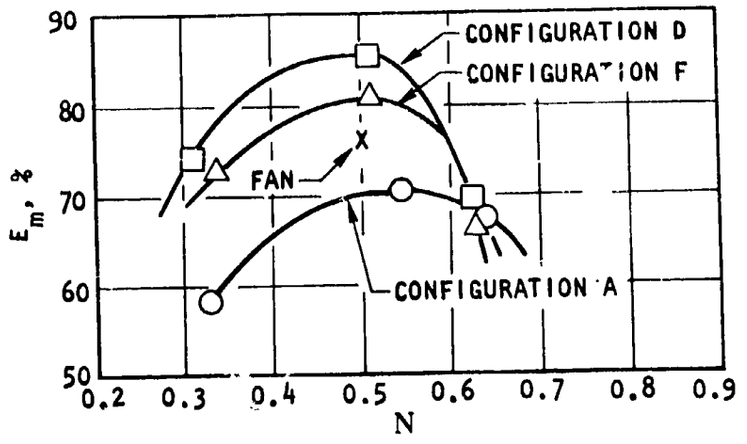

a. MIXING UNIFORMITY

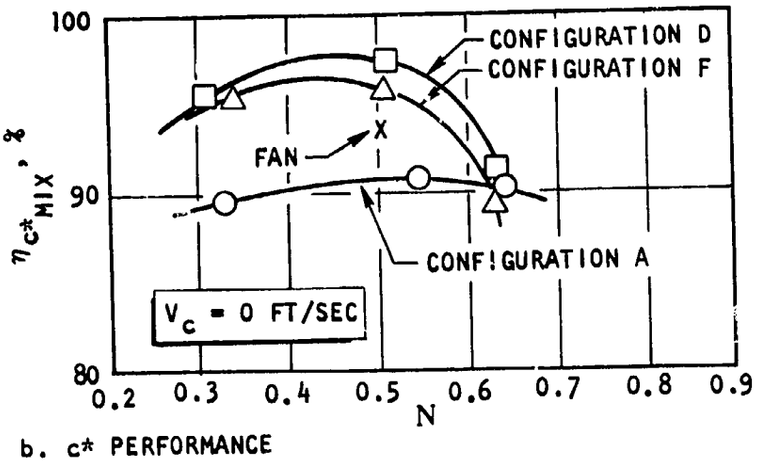

b. c* PERFORMANCE

Figure 37. Comparison of Mixing Characteristics for Optimally Designed Elements

be equally sensitive to N for values less than 0.5 and the noncircular patterns are more sensitive to variations in N for values greater than 0.5. All unlike-doublet patterns produce equally uniform sprays at a value of N equal to 0.63. Because variations in N for each specific design were obtained by varying mixture ratio only and not hydraulic diameter, the fan results can be presented on the same plot (it should be remembered that N may in itself not be a valid parameter for this element). The fan injector result shown in this figure is plotted at a value of N equal to 0.5 which corresponds to the mixture ratio of 1.6 for all designs. Note that the fan design produces mixing uniformity between the circular designs and the noncircular doublet elements.

In Fig. 37b the same results are presented in terms of the predicted overall mixing c* efficiency (η_{mix}). Note that identical trends for the unlike doublet designs are shown for η_{mix} and E_m as a function of N. However, the magnitude of the differences is somewhat less. At a value of N = 0.5, the triangular element should produce an increase of 5-percent c* mixing performance because of improved spray uniformity over that obtained for the circular element, while the rectangular element would result in about a 7-percent increase in c* performance. The fan injector shows that the mixing limited c* performance is about 3-percent greater than the circular design.

For convenience, the results shown in Fig. 38 are summarized in bar chart form below.

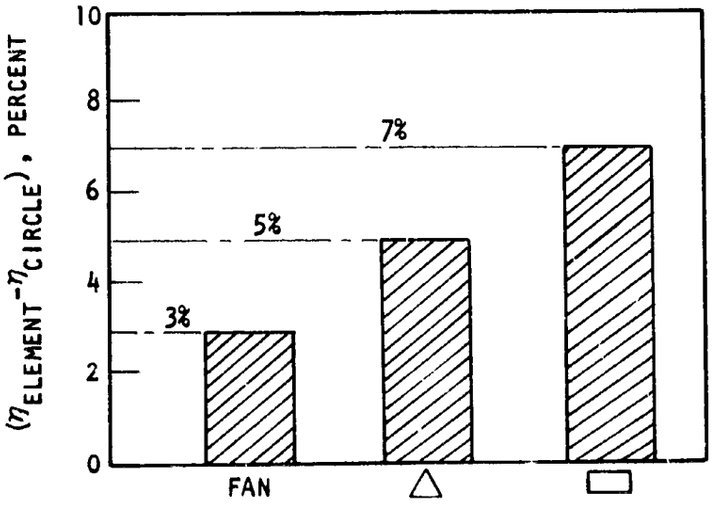

Figure 38. Comparison of Mixing Limited c* Performance Improvement by Noncircular Orifice Elements

Atomization

The objective of the atomization study is to compare the atomization characteristics obtained with circular and noncircular orifice elements designed for optimum mixing. Therefore, atomization experiments were conducted employing only the following unlike doublets:

1. Circle--Configuration A
2. Triangle-Configuration F
3. Rectangle--Configuration D

Because little data were available for the self-atomizing nozzle designs, several such nozzles were evaluated.

Cold-flow tests were conducted utilizing noncircular and circular element injectors to determine atomization characteristics over the range of operating conditions. A total of 89 experiments were conducted. A tabular summary of each experiment is included in Appendix A. Note that the dropsizes are presented as the mass median dropsize ($\overline{D}$) This droplet diameter is the size in a given sample for which half the sample weight is made up of droplets of large diameter and half the same weight is made up of droplets of smaller diameter. The mass median diameter was chosen rather than some other arbitrary statistical dropsize diameter (i.e., volume mean diameter, $\overline{D}_{30}$, etc.) because the data were determined by sieving, which gives $\overline{D}$ directly.

In general, dropsize in the absence of an imposed gas flow field is a function of:

$$\overline{D} = f\ (D,\ V,\ D_o/D_f,\ V_o/V_f,\ \phi,\ \text{physical properties}) \qquad (18)$$

where

D = characteristic orifice dimension
V = injecter velocity
ϕ = dynamic pressure ratio $(\rho_f V_f^2/\rho_o V_o^2)$
ρ = density
o = oxidizer
f = fuel

In a rocket engine, in addition to the above terms, consideration must be given to the relative gas to droplet velocity which can cause secondary atomization.

Unlike-Doublet Elements. For unlike impinging-doublet elements of fixed impingement angle, cold-flow dropsize is proportional to:

$$\bar{D} = f\ (D,\ V,\ D_1/D_2,\ V_1/V_2,\ \text{ratio of physical properties})$$

For fixed orifice sizes this reduces the variables to

$$\bar{D} = f\ (V_1/V_2,\ V,\ \text{ratio of physical properties})$$

A prior study, Ref. 14, has indicated that the parameters should be grouped in the following manner:

$$D_1 = f\ (\phi^*,\ V)$$

To determine the dependence of dropsize on these parameters for the unlike circular doublet, atomization experiments were conducted over a range of injection velocity and ϕ. The atomization results obtained for the unlike-doublet elements are shown in Fig. 39 and 40 in terms of injection velocity, and ϕ. While considerably more data points were obtained than actually shown in these charts (Table A-4 of Appendix A), selected points at near constant ϕ were chosen for presentation. Because data were obtained at various values of ϕ, a plot of the entire data set would tend to be confusing. Note that for ϕ of 0.46 and 1.1, the dependency of dropsize on velocity are similar. However, the level of dropsize is considerably different. The entire set of data was input into a regression analysis program of the form $D = K\phi^n/V^m$ and the values of K, m, and n determined. A plot of the results are shown in the lower plots of Fig. 39 and 40 for the fuel and oxidizer, respectively. The equations best describing the results are:

$$\text{Fuel:}\quad \bar{D}_f = 1.53 \times 10^4\ \frac{(\phi)^{0.41}}{V_f^{0.98}} \tag{19}$$

$$\text{Oxidizer:}\quad \bar{D}_o = 2.1 \times 10^4\ \frac{(\phi)^{-0.32}}{V_o^{1.05}} \tag{20}$$

*$\phi = \rho_f V_f^2/\rho_o V_o^2$

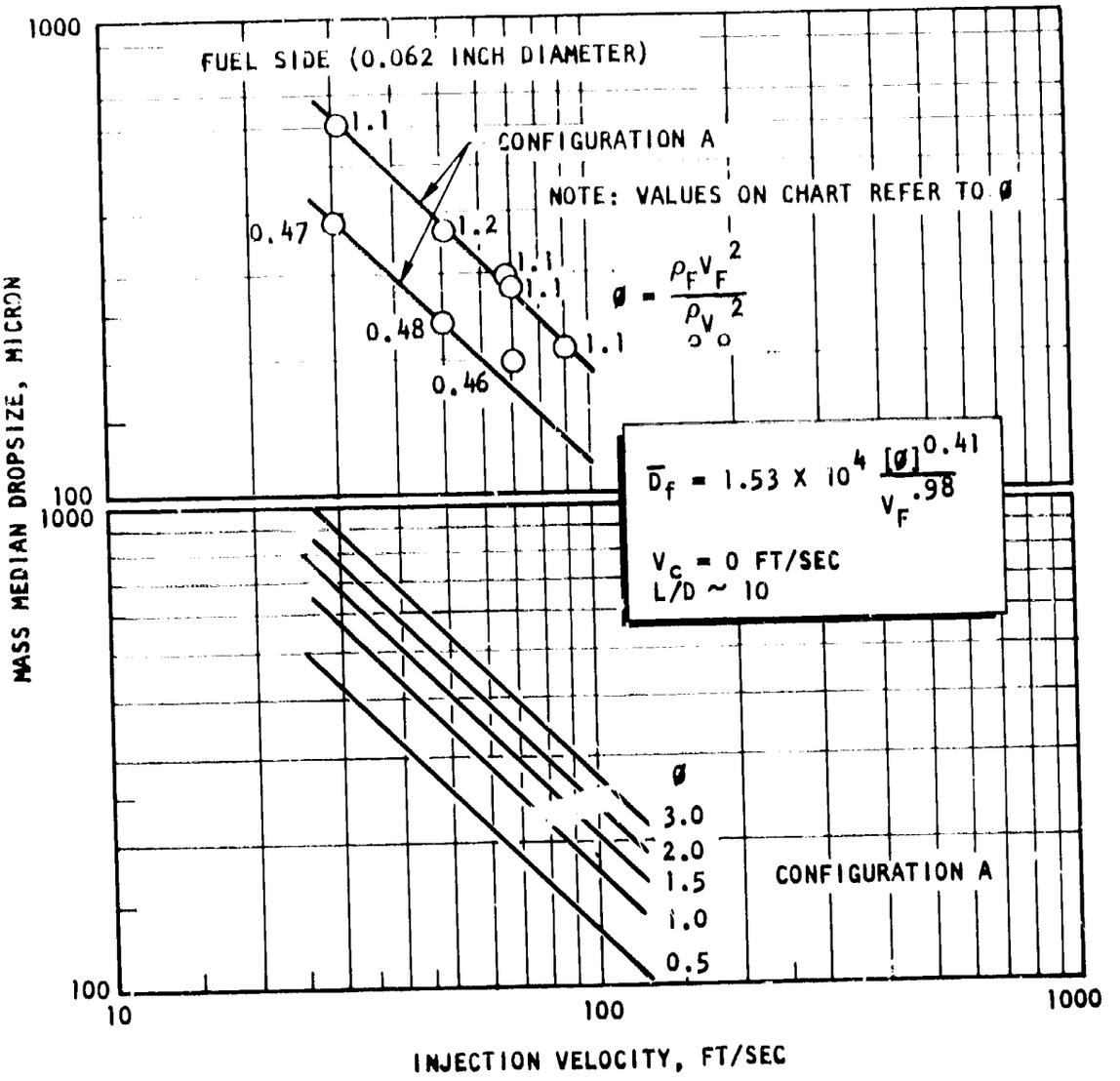

Figure 39. Effect of Injection Velocity and Dynamic Pressure Ratio on Dropsize for a Circular Unlike Doublet (Simulant = Wax/Water)

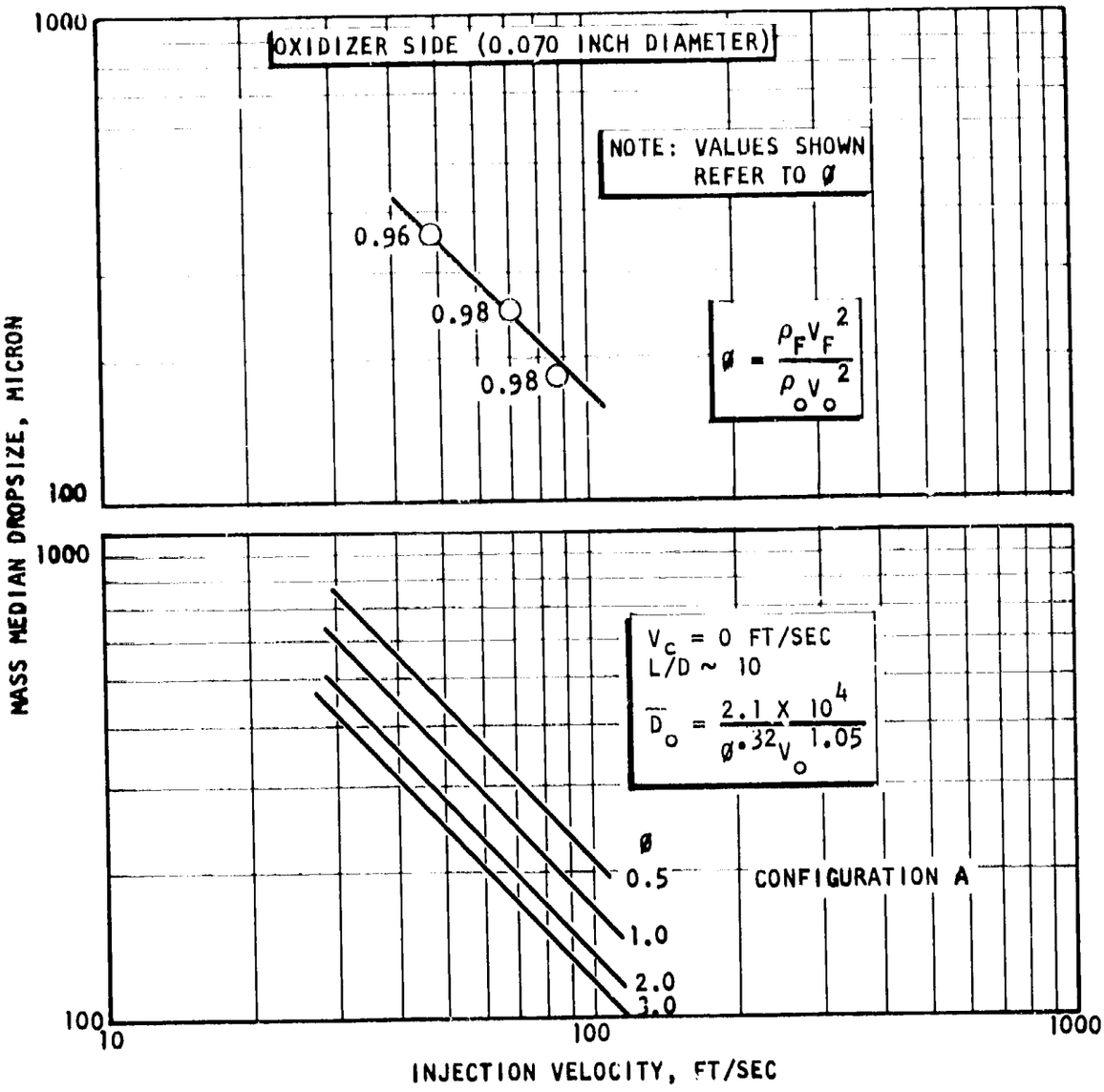

Figure 40. Effect of Injection Velocity and Dynamic Pressure Ratio on Dropsize for a Circular Unlike Doublet

It should be noted that the above equations are not general in terms of diameter ratio or element size, but are specific to the actual elements evaluated. Inspection of the equation illustrates that the fuel dropsize is almost totally dependent upon the oxidizer velocity while the oxidizer dropsize is almost totally dependent upon the fuel. That is, Eq. 19 reduces to

$$D_f = \frac{1.53 \times 10^4 \left(\frac{\rho_f}{\rho_o}\right)^{0.41}}{V_f^{0.16} V_o^{0.82}} \qquad (21)$$

The velocity dependence for the fuel dropsize diameter is somewhat different than that previously assumed in the preliminary evaluation, which was obtained from the Ref. 13 study. However, the Ref. 13 equation was generated with only a minimum of data and could conceivably be in error. The oxidizer dropsize result is in essential agreement with that given in Ref. 13.

The results for the noncircular unlike-doublet elements are presented in Fig. 41. Because of program limitations, data were generated only at a constant value of ϕ for these patterns. Note, however, that the slope of the lines in the high velocity regions are nearly identical to that found for the unlike doublet. In addition, for a value of $\phi \approx 1.0$, the dropsizes for the fuel and oxidizer for a specific element were identical at the same injection velocity. If the circular doublet oxidizer and fuel dropsize diameters for $\phi = 1.0$ are compared, the same trend is found. Because of the similarity of these results, it is assumed that the dependence of dropsize on ϕ for the noncircular elements is identical to that found for the circular elements.

Self-Atomizing Nozzles. The cold-flow atomization results for the self-atomizing nozzles are presented in Fig. 42. Five spray fan types with different orifice sizes were evaluated over a 30- to 345-psi ΔP range, depending upon the element size. The largest size tested (equivalent orifice diameter = 0.072 inch) resulted in mass mean dropsize ($\bar{D}$) from 255 to 435 microns over the ΔP range evaluated. The smallest nozzle produced $\bar{D}$ values of nominally 100 microns. Intermediate dropsizes were measured for the remaining spray fan nozzles.

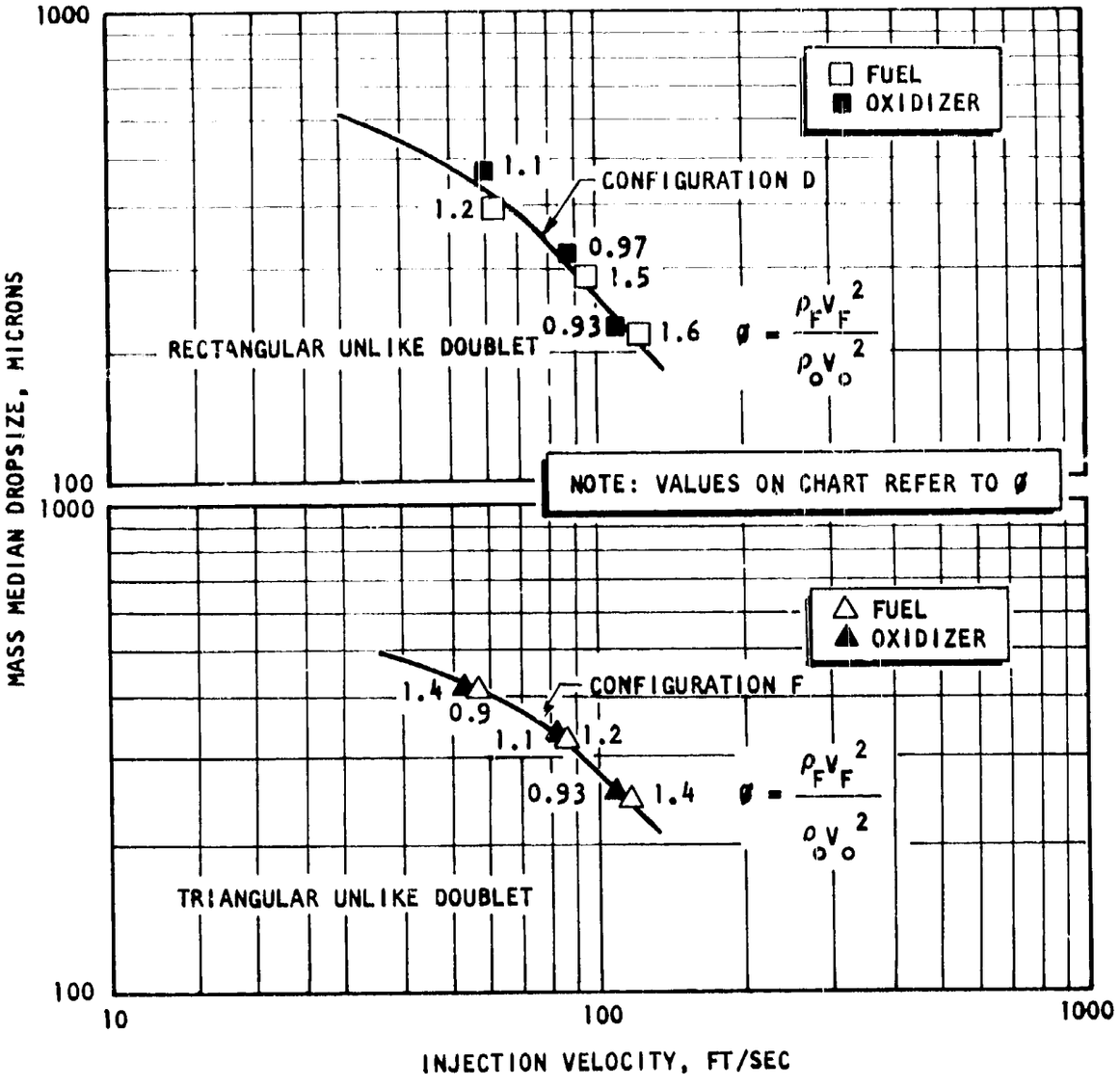

Figure 41. Effect of Injection Velocity on Mass Median Dropsize for Rectangular and Triangular Orifices (Simulant: wax/H_2O)

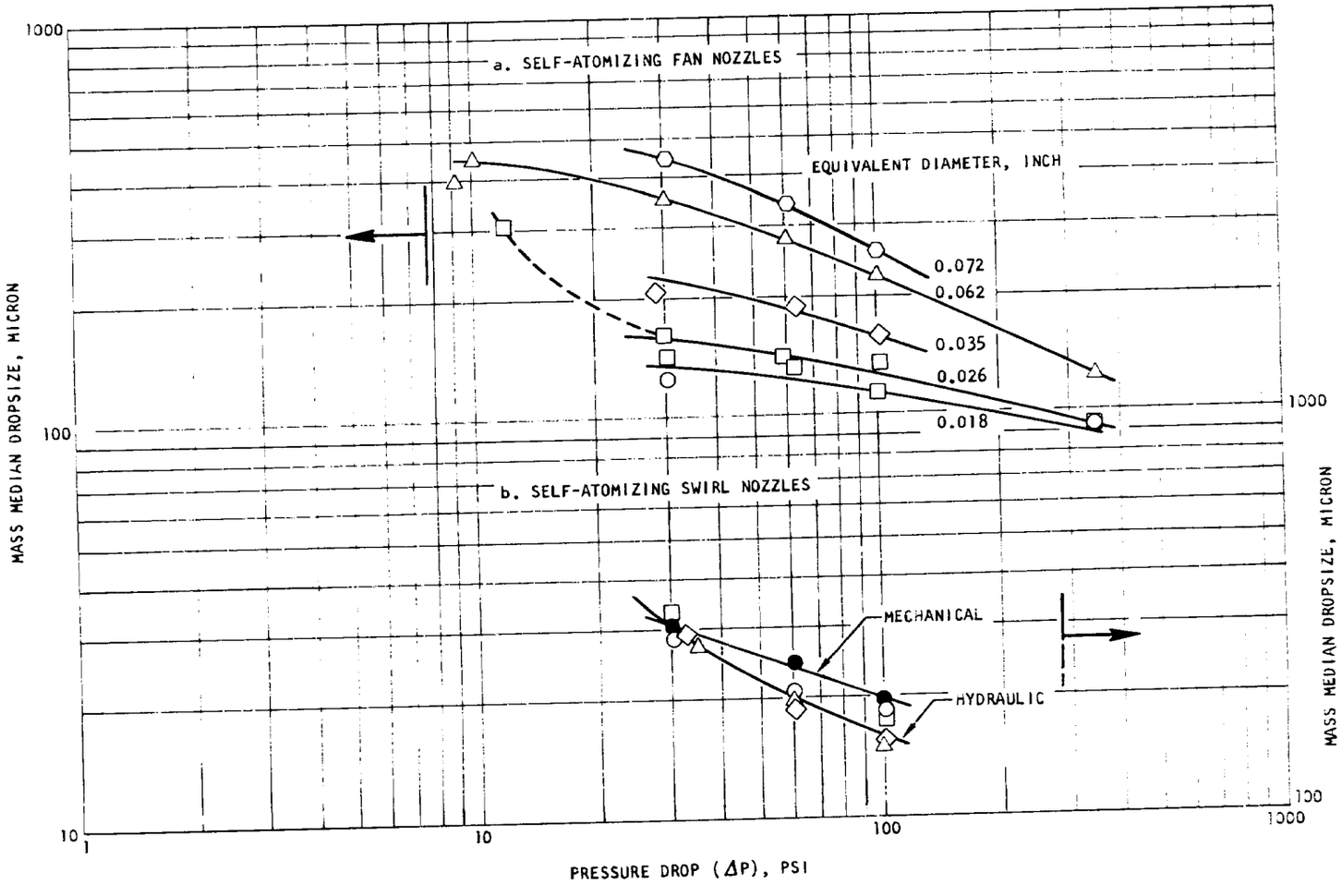

Figure 42. Effect of Injection Pressure Drop on Mass Median Dropsize for Self-Atomizing Nozzles (Simulant: Shell 270 Wax)

The swirl-type nozzle atomization results are also shown in Fig. 42. The dropsizes varied from 150 to 315 microns for all five nozzles over the entire ΔP range. The mechanical-type swirl nozzle produced dropsizes slightly larger than that found for the hydraulic swirl nozzles. Note that the dropsizes produced by the swirl nozzles tested were relatively insensitive to the physical orifice size. The swirl nozzles do not appear to have any significant advantage over that found for the fan-type nozzles, and in addition, the swirl nozzle designs are considerably more complicated in design than the simpler fan type. Consequently, the swirl nozzles were eliminated from further study.

Comparison of Atomization Characteristics for Circular and Noncircular Orifices. Comparison of dropsizes is done on the basis of cold-flow measured wax dropsizes. Because atomization by all of the unlike-doublet elements is dependent upon ϕ, a comparison of these elements must be accomplished at a value of ϕ corresponding to that occurring at a mixture ratio of 1.6. For these designs, ϕ can be determined from rearrangement of Eq. 11.

$$\phi = \left[\frac{1}{N} - 1\right] \left(\frac{d_o}{d_f}\right)_{II} \tag{22}$$

Because all elements were designed for N of 0.5, then

$$\phi = \left(\frac{d_o}{d_f}\right)_{II}, \text{ at optimum design based on mixing uniformity.}$$

For the various elements, this ratio is

Configuration	$(d_o/d_f)_{II}$
Circle	1.14
Triangle	1.17
Rectangle	1.13

Note that the hydraulic diameters are nearly equal and therefore the comparison should be made at near identical values of ϕ.

Qualitative comparisons of wax dropsizes provide a relative comparison of the various elements dropsize characteristics. A comparison of the wax dropsize characteristics for the fuel is shown in Fig. 43 for all elements at equivalent thrust per element sizes. The results are shown in terms of the mass median dropsize as a function of injection velocity.

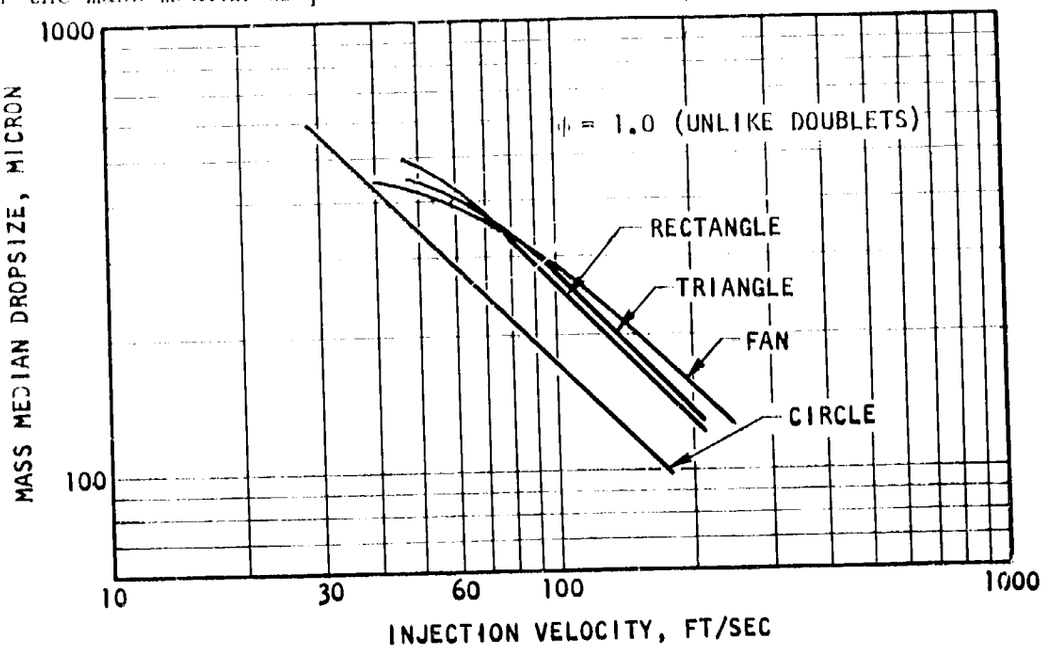

Figure 43. Comparison of Wax Dropsize Characteristics for Noncircular and Circular Orifice Designs

Note that the circular unlike doublet produces dropsizes approximately 1.5 times smaller than noncircular designs. This result is different than that originally expected in that it was postulated that total contact across the entire width of the jets would produce maximum momentum interchange between the jets and thereby produce minimum dropsizes. (The circular design which had a diameter ratio of 1.14 while the noncircular unlike-doublet designs contact width ratios were 1.0.) It is obvious, however, that the sheets produced by the rectangular and triangular designs are considerably thicker than those for the circular design. This is probably due to the fact that the jets thickness (perpendicular to the contact dimension) for the noncircular patterns are greater than that for the circular design. It would be expected therefore that had the rectangular elements been designed such that the minimum side dimension were perpendicular to the contact side, then considerably smaller dropsizes would have been produced.

Compatibility

The propellant distributions along the chamber wall are primarily determined by the specific injector element and geometric design, and these distributions to a large extent control the engine heat flux characteristics. Consequently, analysis of the cold-flow data for all elements was conducted to determine elemental local mass and mixture ratio contours. The results are discussed below.

Unlike Doublet Elements. Contour plots of mass and mixture ratio for the unlike doublets are presented in Fig. 44 through 47. The sensitivity of fan orientation to misimpingement for the circular unlike doublet is shown in Fig. 44 and 45. In Fig. 44 the orifices are aligned such that, at impingement, the orifice center lines misimpinge by 0.006 inch. The contour plot for a misimpingement of 0.002 inch in the other direction is presented in Fig. 45. Note that in both cases the fan is rotated toward the larger orifice and that even for a misimpingement of only 0.002 inch the fan has been rotated about 45 degrees. This could result in significant propellant wall impingement for elements positioned near the chamber wall. In addition, note that the mass is grouped near the central portion of the fan and quickly drops off near the edges. Interesting, however, is the fact that the mixture ratio is high on the side opposite the oxidizer orifice and low on the side opposite the fuel orifice. Rupe, Ref. 2, has observed the same phenomena and suggests that the propellants penetrate through each other.

Contour plots for the rectangular and triangular elements are shown in Fig. 46 and 47. These profiles are quite similar in shape, and in fact are similar to that of equal diameter circular doublets. Note here again that the propellants appear to penetrate through each other creating a mixture ratio profile across the element opposite to that suggested by the element design. As for the circular elements, the mass is concentrated near the central portion of the fan and quickly drops off near the edge.

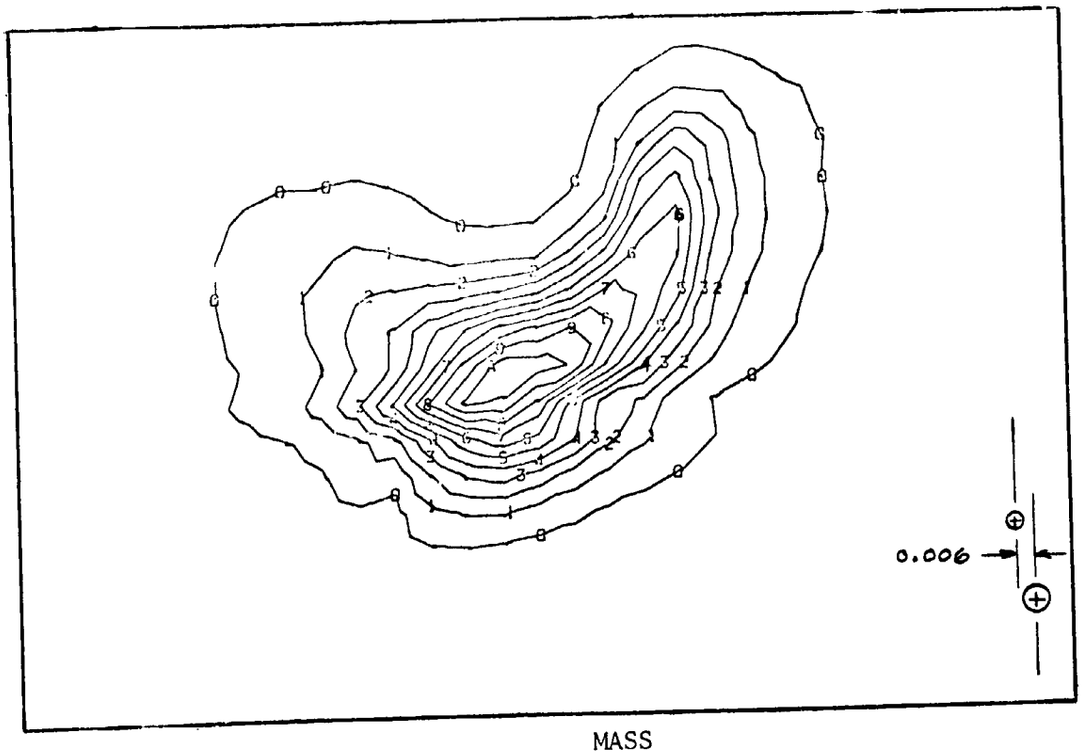

MASS

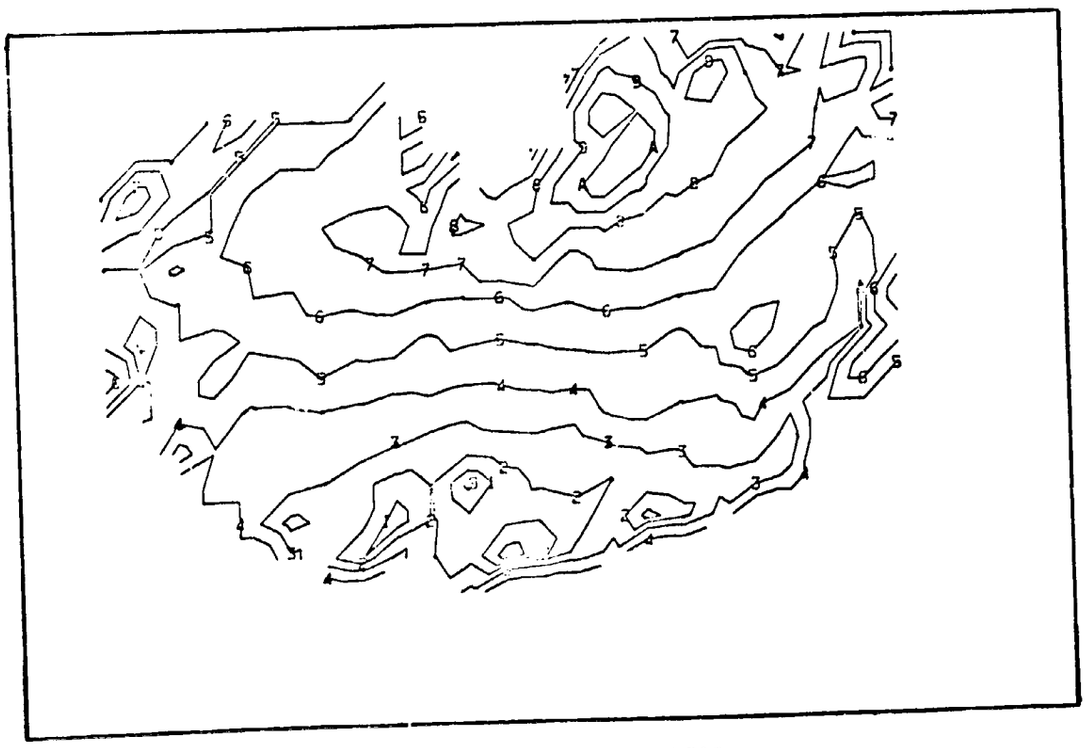

MIXTURE RATIO

Figure 44. Contour Plots for Circular Unlike Doublet, Configuration A

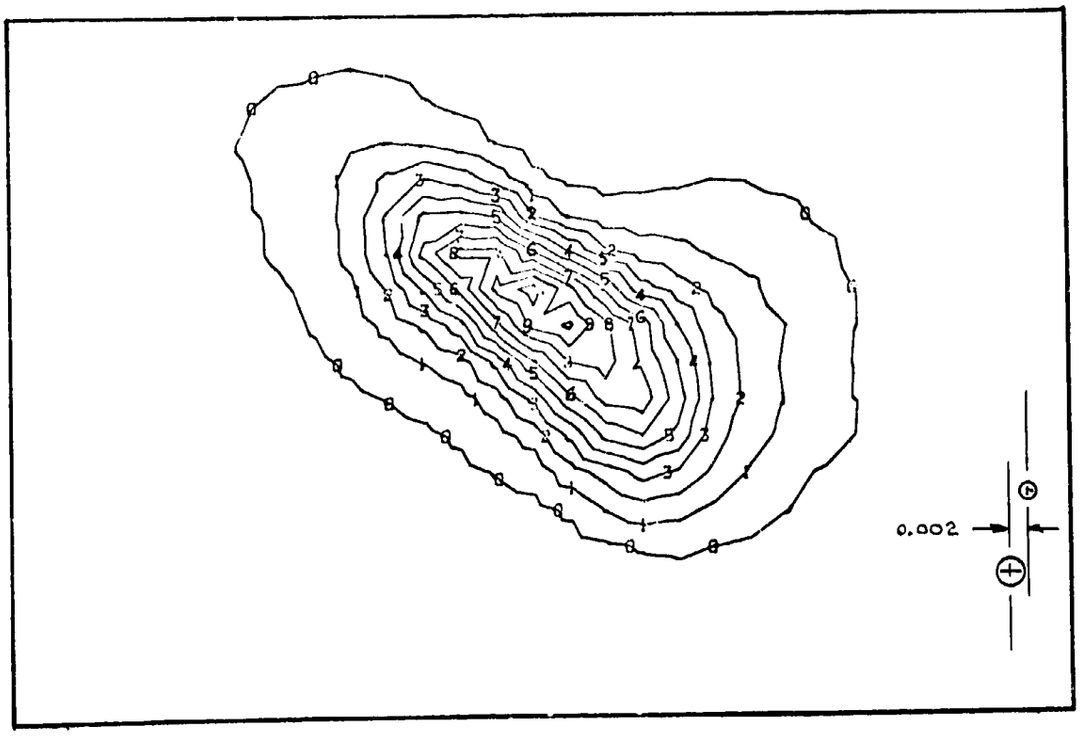

MASS

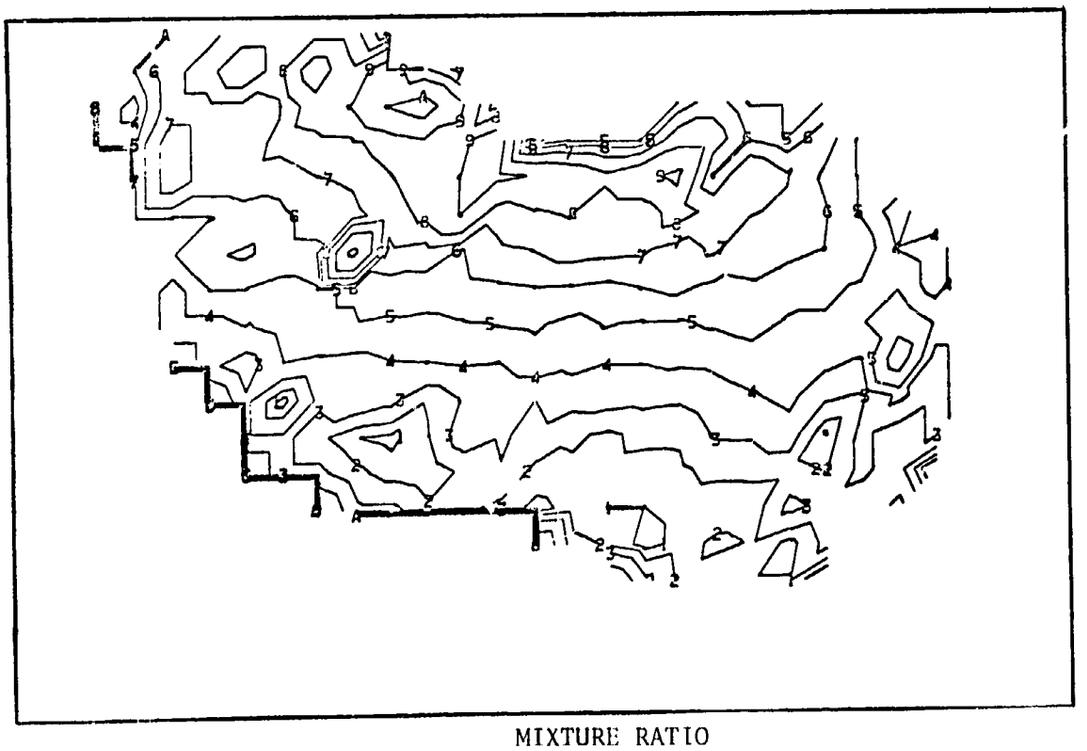

MIXTURE RATIO

Figure 45. Contour Plots for Circular Unlike Doublet, Configuration A

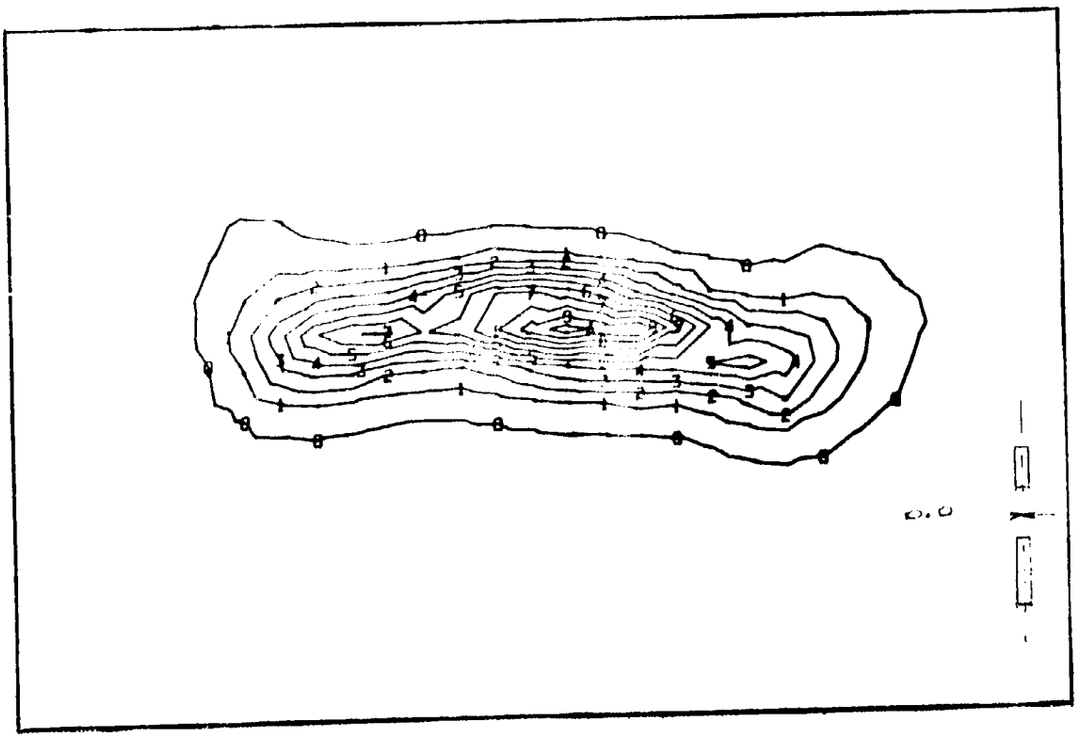

MASS

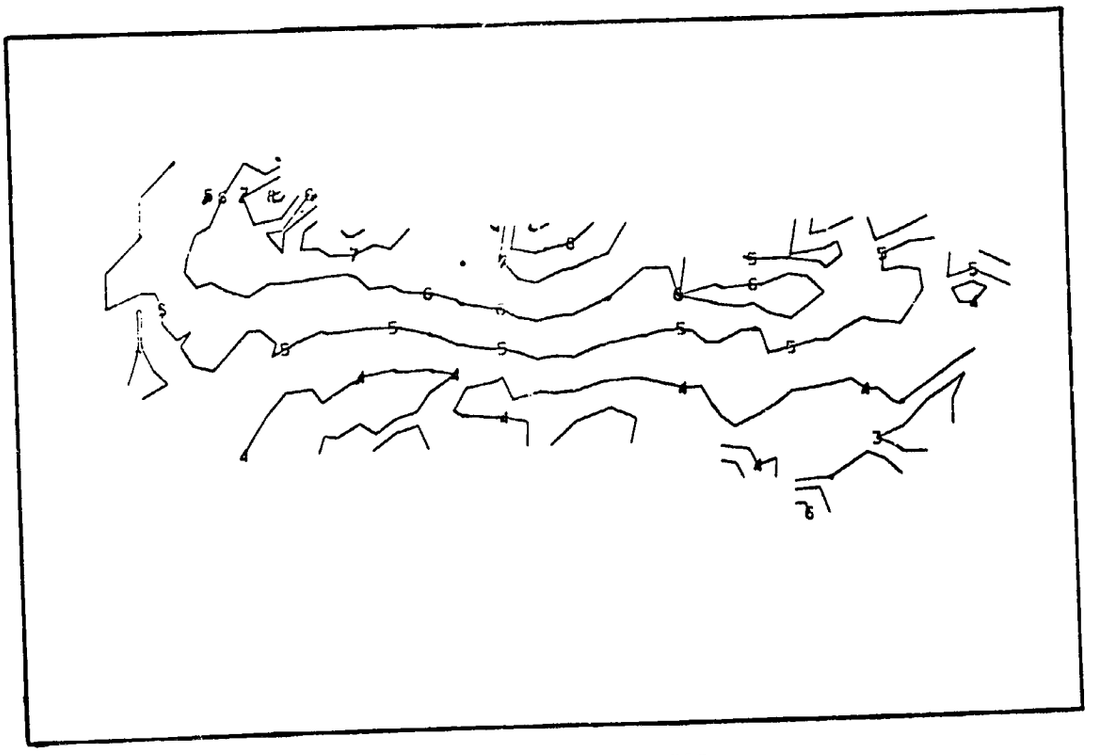

MIXTURE RATIO

Figure 46. Contour Plots for Rectangular Unlike Doublet Element, Configuration D

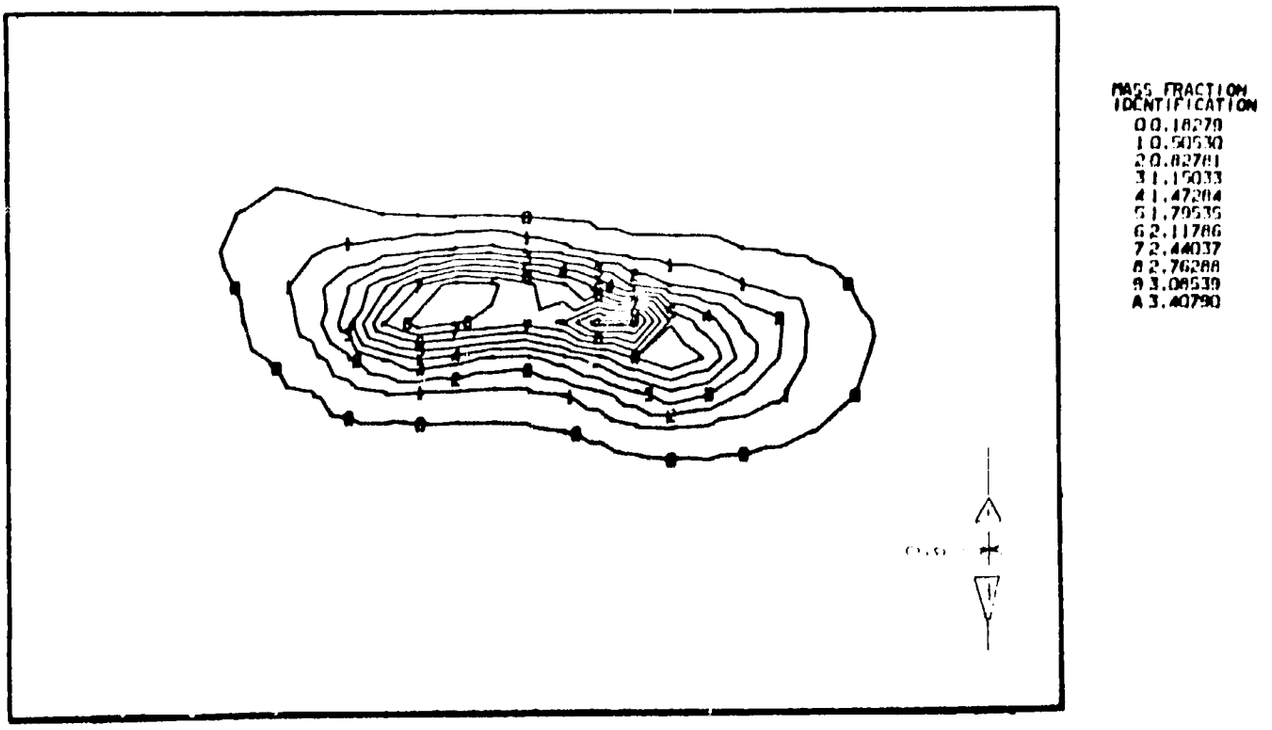

MASS

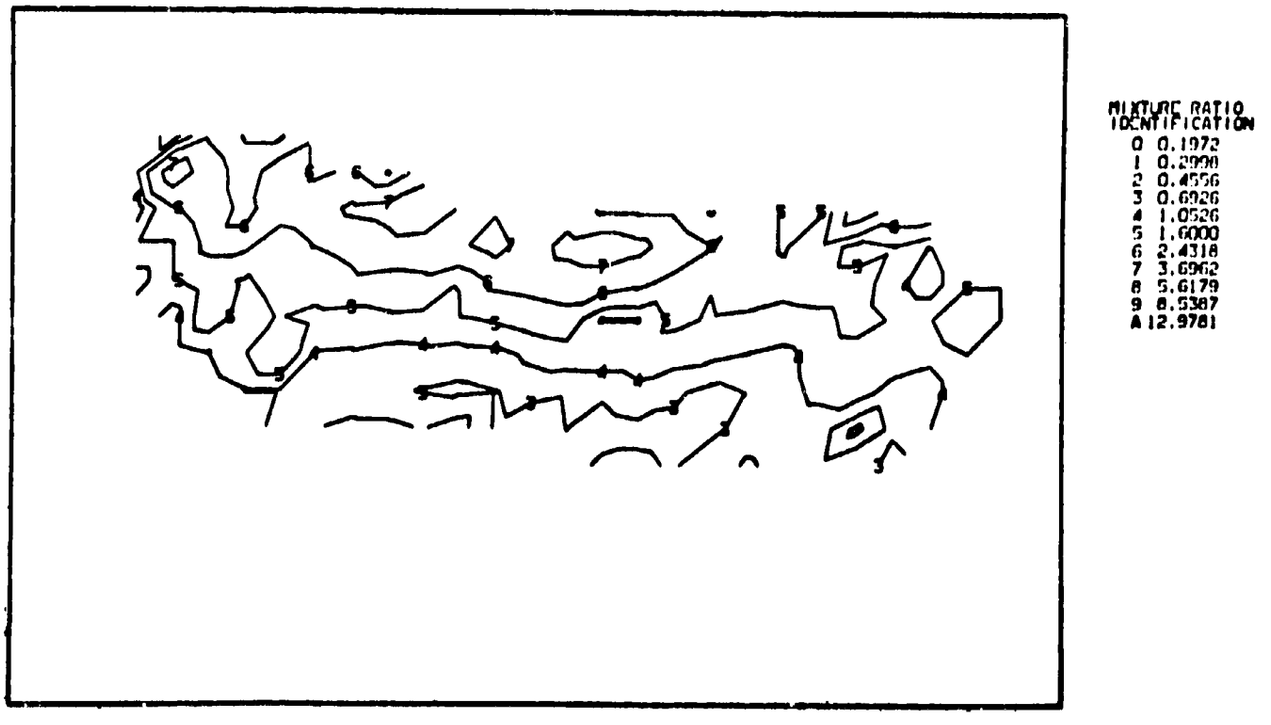

MIXTURE RATIO

Figure 47. Contour Plots for Triangular Unlike Doublet Element, Configuration F

Self-Atomizing Fan. The contour plot for a self-atomizing fan of equal sized nozzles canted 60 degrees toward each other (included angle) is shown in Fig. 48. The mass is again concentrated near the center of the fan and drops off rapidly near the edge. As opposed to the unlike doublet elements, the mixture ratio distribution for the fan injector is not symmetric but has high mixture ratio along the ends and low mixture ratio along the edges. These results compared to the unlike doublet data suggest that all afford about the same degree of uniformity of mixture ratio near at least one edge of the spray fan to provide chamber wall compatibility.

Stability Analysis

A stability analysis was conducted for both the circular and noncircular elements. The objective was to rank the elements in terms of their likli hood to be unstable when compared to the circular element.

The Priem model was utilized for this analysis. The predicted zones of engine operating conditions in which a tangential mode of high-frequency instability could be initiated were found by examining the response of the system to initial pressure disturbances of various amplitudes. The boundaries of the instability regions depend primarily on $\mathcal{L}$, the burning rate parameter, and $\Delta V'$, the axial velocity difference between the combustion gas and the liquid droplets divided by the local speed of sound, i.e., $\Delta V' = (V_Z - V_{LZ})/a$.

The burning rate parameter, $\mathcal{L}$, is defined as

$$\mathcal{L} = \frac{mR}{\epsilon} \qquad (\ )$$

where

m = fraction of total propellant burned per unit length of combustor

R = radius of combustor (or annular element)

ϵ = combustor contraction ratio

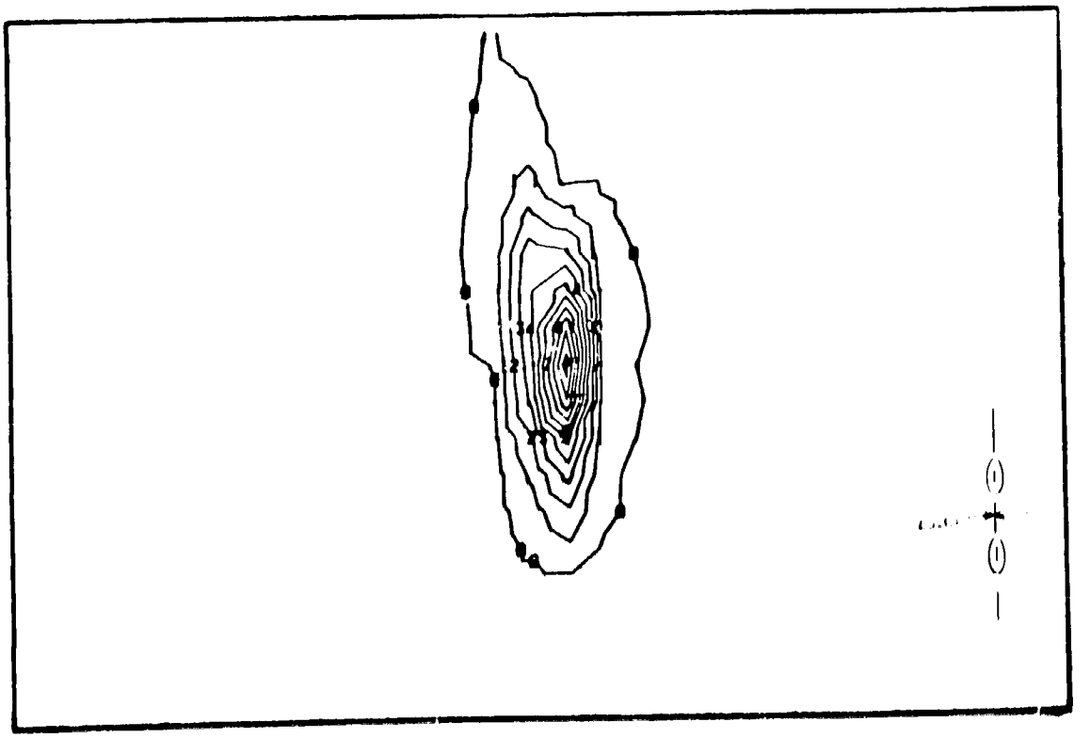

MASS

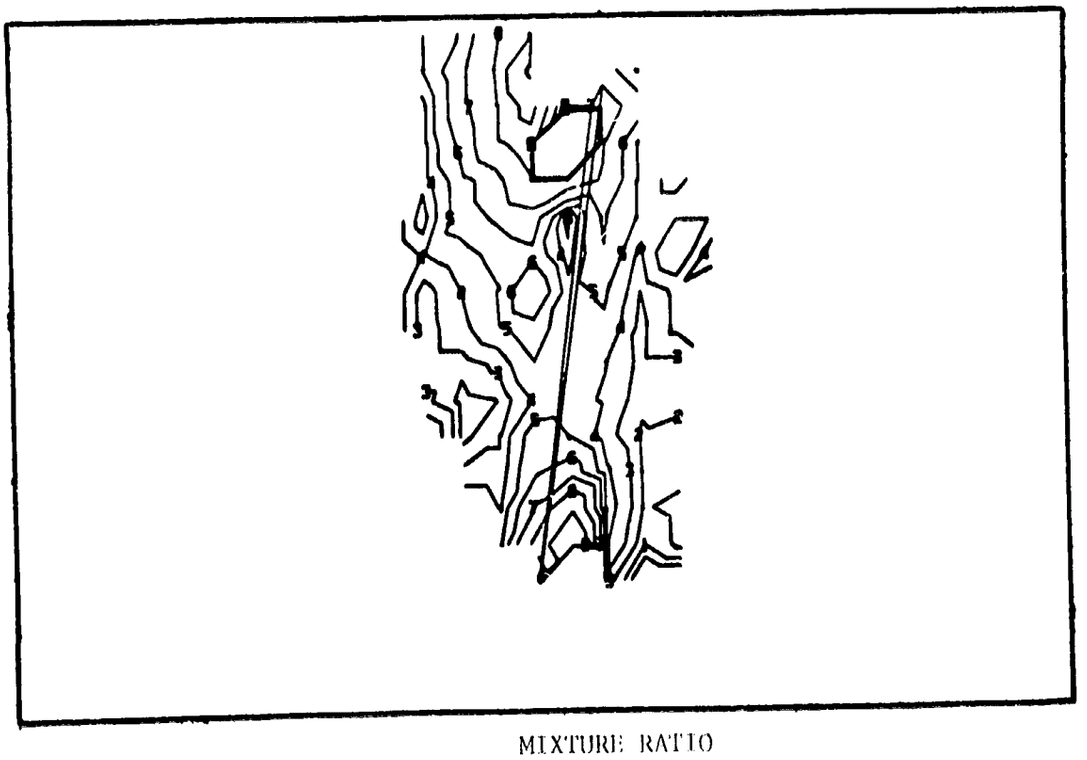

MIXTURE RATIO

Figure 48. Contour Plots for Self-Atomizing Fan Element

A stability map was obtained by first plotting the neutral stability limit, Λ_p (the minimum reduced pressure disturbance amplitude required to initiate sustained instability) for several dropsizes versus the burning rate parameter, $\mathcal{L}$. Then the minimum disturbance for each input dropsize was determined. The minimum values were then plotted as a function of dropsize and the results of this analysis are presented in Fig. 49. Note that the larger the dropsize the higher the pressure amplitudes can be without producing instability. The differences shown in this figure suggest that the circular element which produces the smallest dropsizes will tend to be more unstable than the noncircular elements.

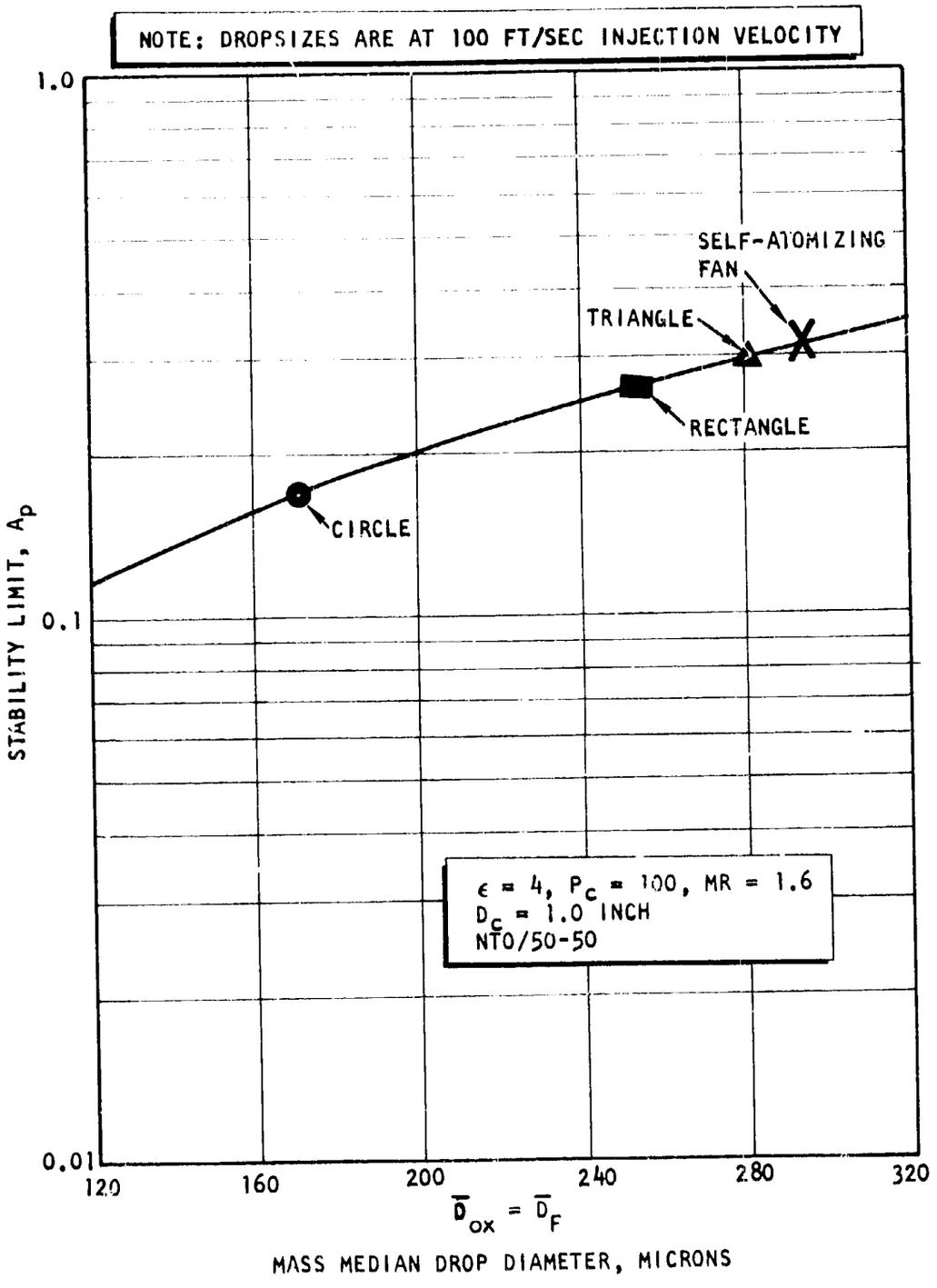

Figure 49. Variation of the Stability Limit With Injected Propellant Spray Droplet Diameter

4.3 HOT-FIRE EVALUATION

Hot firing experiments were conducted to gain information concerning the operational characteristics of single elements using the various orifice types under actual engine conditions.

Based upon the results of cold-flow experimental studies, four injector elements were selected for the hot-fire evaluations. The element types chosen were:

1. Circle (Configuration A)*
2. Rectangle (Configuration D)
3. Triangle (Configuration F)
4. Self-Atomizing Fan Nozzle

All of the above configurations had orifice sizes identical to those previously cold-flow evaluated. For the fan element, the orifice sizes for the oxidizer and fuel were 0.072 and 0.062, respectively (Fig. 36 and Table 18). The injectors were fired in a combustion chamber with contraction ratio, $\varepsilon_c = 4.0$ (Fig. 10).

4.3.1 SELF-ATOMIZING FAN ELEMENT

Hot-firing test results for the self-atomizing fan element are presented in Fig. 50, 51, and 52. (See Appendix A for a complete tabular listing of all hot-fire test results.) Shown in these figures is the influence upon characteristic velocity efficiency of mixture ratio, characteristic chamber length, and chamber pressure.

*See Table 19 for definition of configurations.

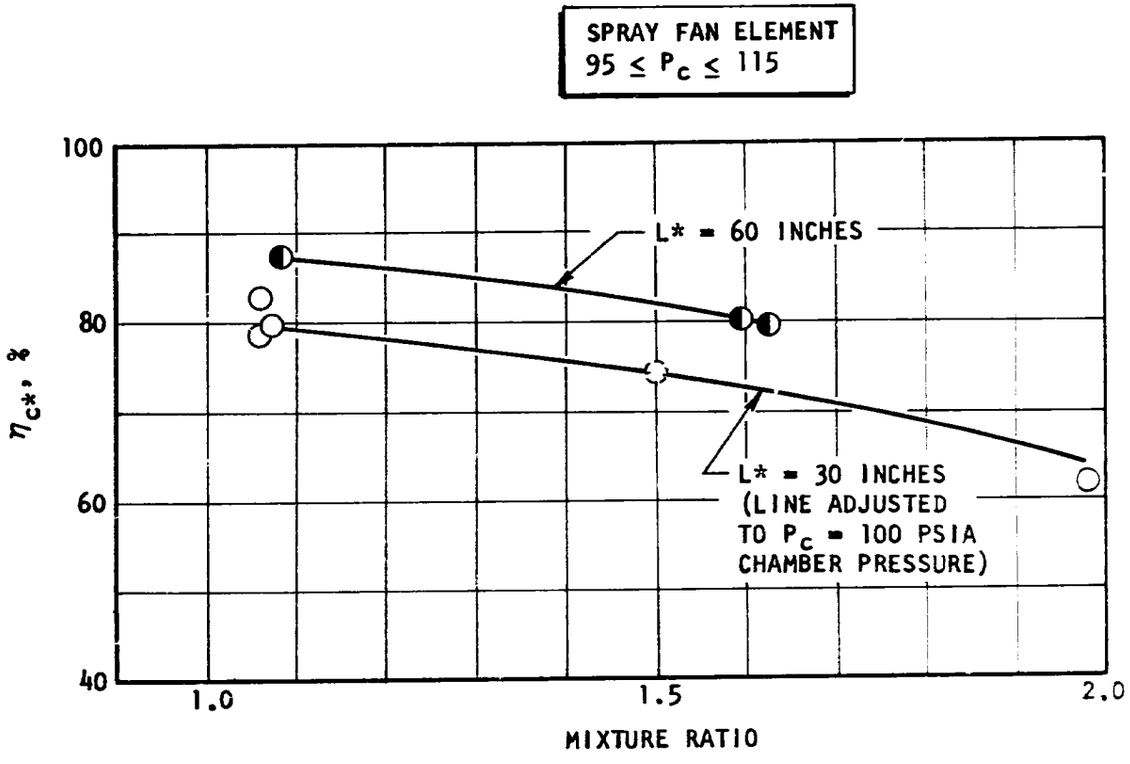

Figure 50. Variation of c* Efficiency With Mixture Ratio for the Spray Fan Element

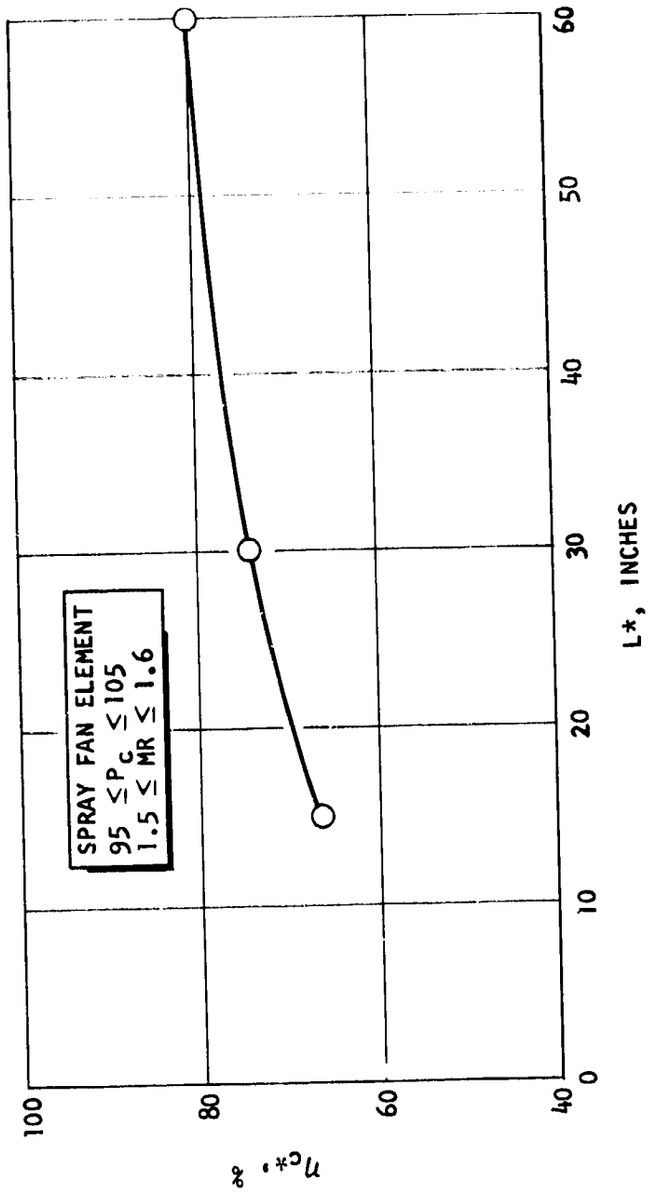

Figure 51. Variation of c* Efficiency With L* For The Spray Fan Injector

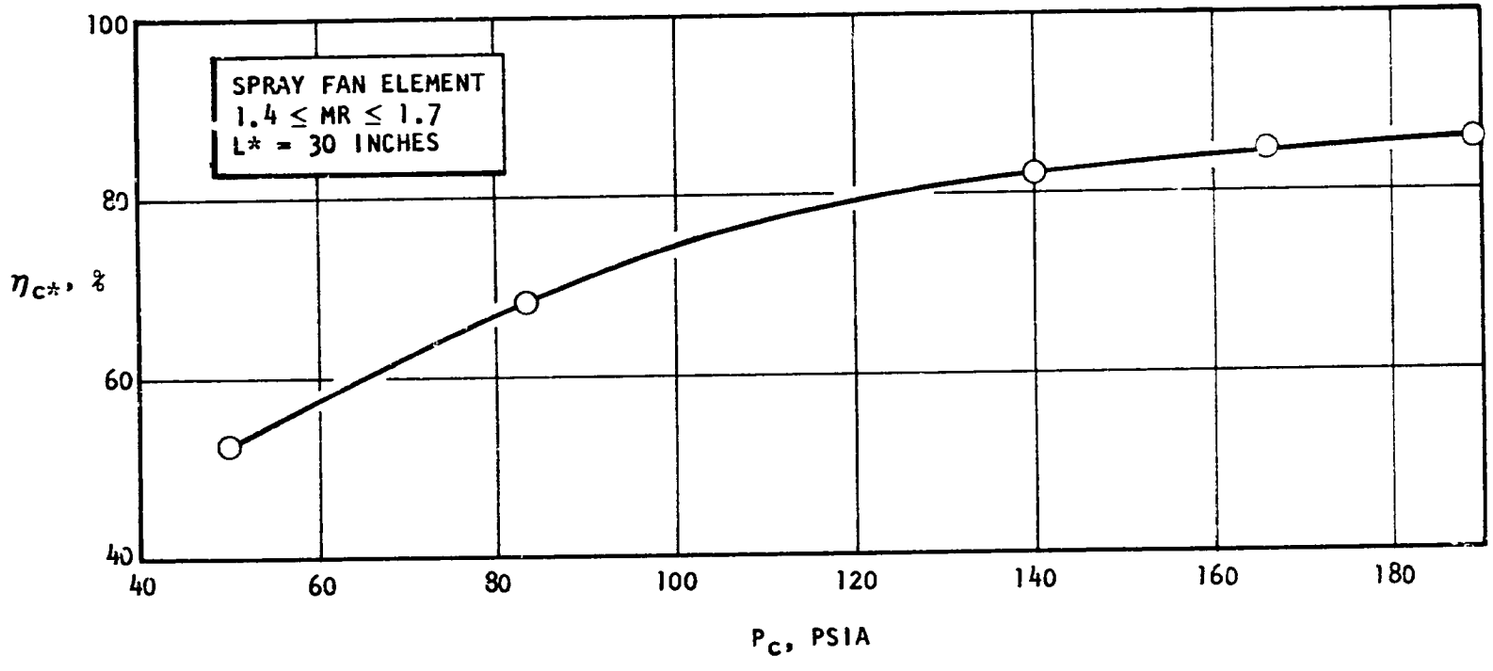

Figure 52. Variation of c* Efficiency With Chamber Pressure for the Spray Fan Element

The first figure, Fig. 50, shows the variation of η_c* with mixture ratio for chamber (characteristic) lengths of 30 and 60 inches. For the tests shown, chamber pressure was approximately 100 psia (adjustments have been made by minor interpolation to 100 psia as noted). Characteristic velocity efficiency (at L* = 30 inches) falls some 16 percentage points as mixture ratio is varied from 1.0 to 2.0. The same trend is suggested by the data for L* = 60 inches.

The improvement in η_c* with L* suggested in Fig. 50 is amplified in Fig. 51 Here, η_c* is shown as a function of L* for chamber pressure of 100 psia and mixture ratio close to 1.5. It may be noted that η_c* increases from about 66 percent to slightly over 80 percent with an increase of L* from 15 to 60 inches. Extrapolation of these data to larger values of L* suggests that the maximum efficiency obtainable for the single element at P_c = 100, MR = 1.6 lies between 83 and 85 percent. This is commensurate with the cold flow mixing limited efficiencies predicted for this injector.

The variation of η_c* with chamber pressure is depicted in Fig. 52 , for L* = 30 inches and mixture ratio about 1.5. A striking improvement of efficiency with increased chamber pressure is noted. This increase is attributed mainly to improved mixing and atomization resulting from higher injection velocities at elevated pressures rather than the absolute level of pressure. In this engine, the chamber throat area remained fixed as well as the injector orifice areas. Thus, increased pressure required increased flowrates, and subsequently, higher injection velocities.

4.3.2 UNLIKE-DOUBLE ELEMENTS

Characteristic velocity efficiency as a function of mixture ratio, L*, and P_c, respectively, for the three types of impinging jet unlike doublets is shown in Fig. 53, 54, and 55. These injectors were similar in design

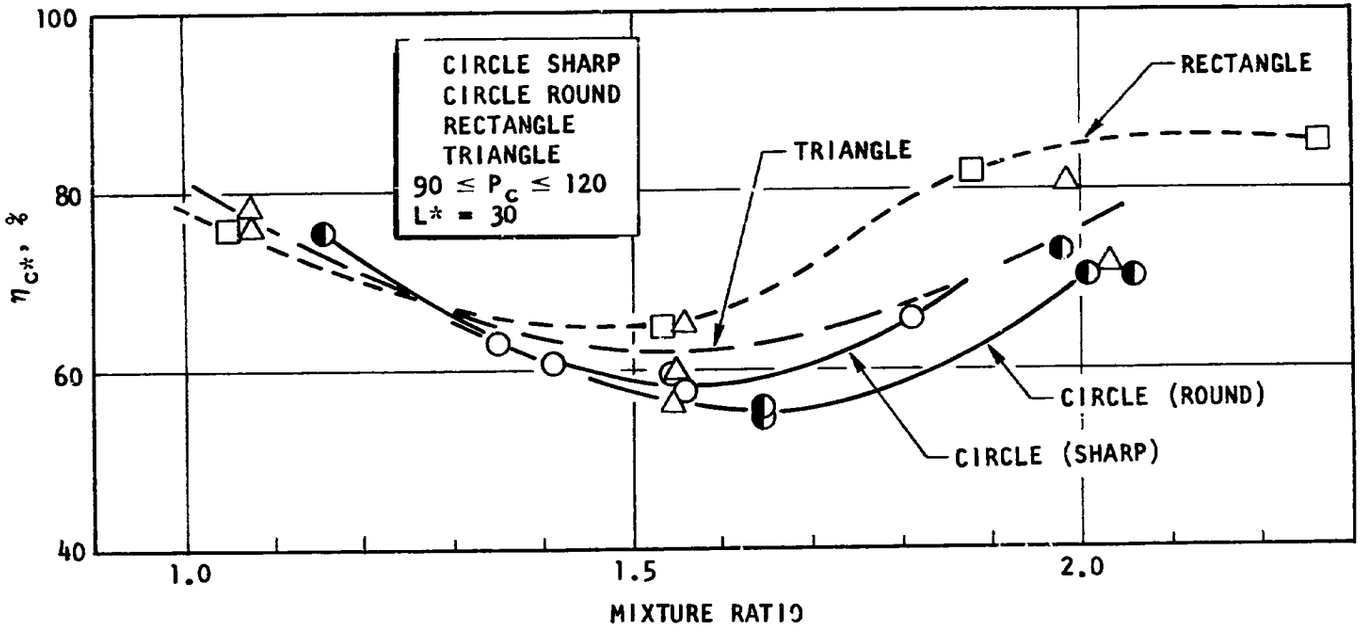

Figure 53. Variation of c* Efficiency With Mixture Ratio for Circular and Noncircular Unlike Doublets

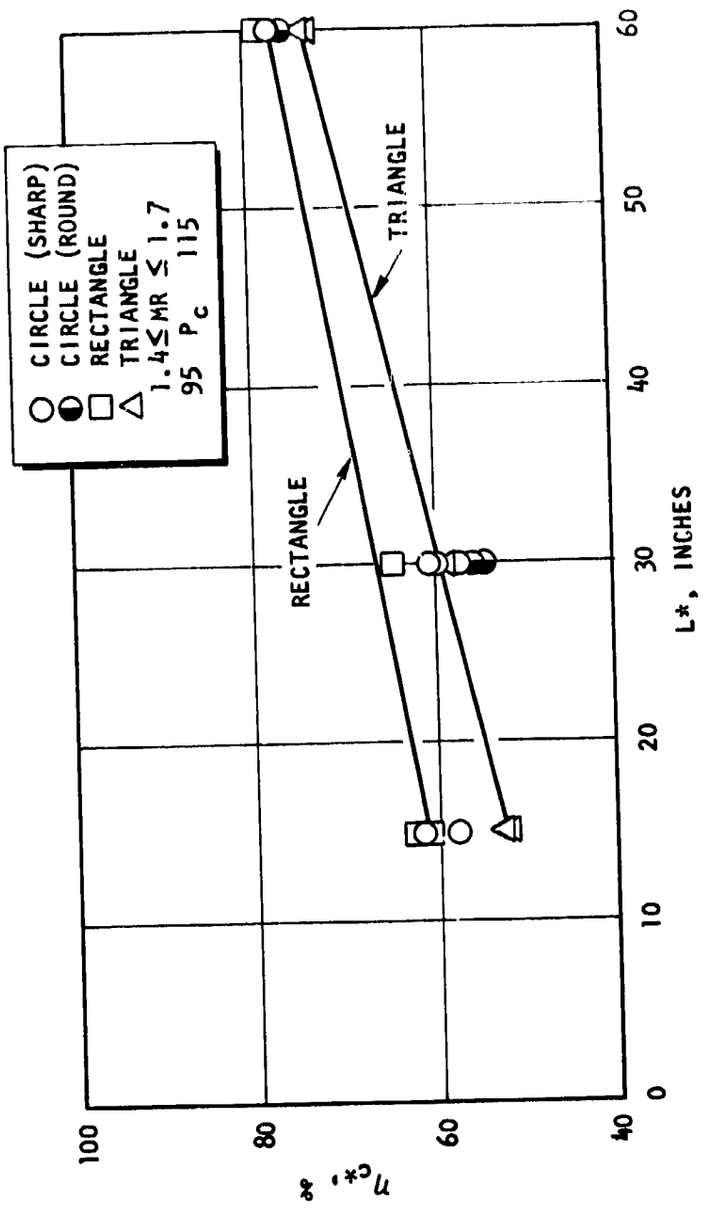

Figure 54. Variation of c* Efficiency With Characteristic Chamber Length for Circular and Noncircular Unlike Doublets

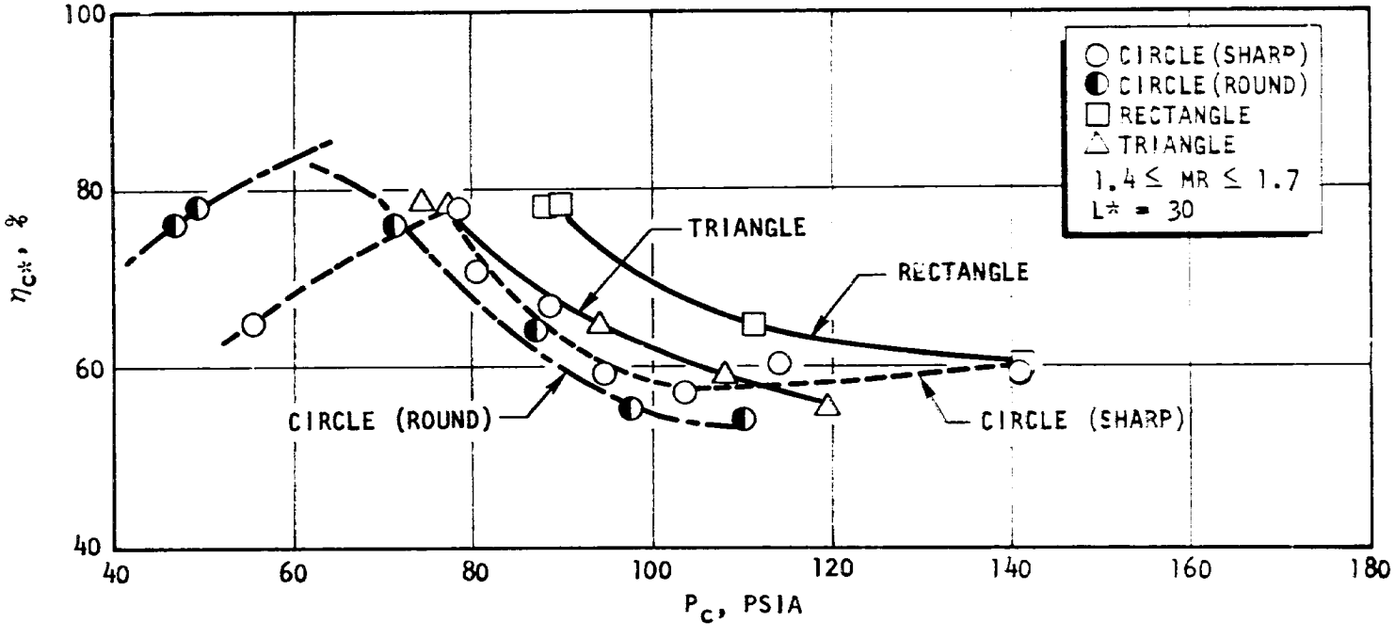

Figure 55. Variation of c* Efficiency With Chamber Pressure for Circular and Noncircular Unlike Doublets

except for orifice shape. Orifice shapes tested were the circle, triangle, and rectangle. (Note that the circle-on-circle injector was tested with both sharp and rounded entrances to the orifices.)

It is evident from the data shown in Fig. 53 and 55 that the impinging jet unlike doublets have produced performance results which are quite different from those of the fan-type element. Rather than maximizing at "optimum" mixture ratio as suggested by cold flow, efficiency is actually lowest at this mixture ratio. Further, as noted in Fig. 55 , performance for the impinging-type elements decreases with increasing chamber pressure, in contrast to the fan elements. These contrary operational characteristics are indicative of reactive stream separation or "blowapart."

Because blowapart can alter the spray characteristics, prior to injector design selection, the injectors and operating conditions were critically examined in terms of the potential for blowapart. Previous data (Ref. 15 and 16) had indicated that blowapart would occur for the element sizes being utilized in this study. Data available at that time suggested that there were two ways to avoid blowapart: (1) by reducing the orifice sizes to about 0.020 inch, or (2) by keeping the oxidizer temperature below its boiling point. Because it was desirable to keep the thrust per element no smaller than 30 lbf/element, the hot-fire facility was equipped with a temperature-conditioning system which would maintain the oxidizer temperature below 40 F. Unfortunately, as the data demonstrate, temperature conditioning of the propellants did not keep blowapart from occurring for the unlike doublet elements.

Because all unlike impinging jet injectors, regardless of orifice shape, were subject to blowapart, evidently, noncircular orifice unlike doublets designed at N = 0.5 offer no significant improvement in operational characteristics for the prevention of blowapart. Although from Fig. 53, it does appear that the rectangular orifices were less affected by blowapart than the other orifice shapes at the higher mixture ratios. It should be noted, however, that experimental evidence suggests a slight variation in

aspect ratio for the noncircular unlike doublets may reduce or even eliminate blowapart. This "off option" design condition may result in a significant improvement in performance because of the large suppression in c* efficiency caused by blowapart.

Variations of c* efficiency with characteristic chamber length is shown in Fig. 54 for P_c = 100 psia and MR = 1.5. As expected, efficiency increases significantly with increased L* from 15 to 60 inches. The efficiency for the rectangles increases some 16 percentage points while the trimngles increase 22 percentage points. However, at each L*, the overall level of performance is depressed by the blowapart phenomenon.

4.4 COMPARISON OF ACTUAL AND PREDICTED c* EFFICIENCY CHARACTERISTICS

The hot-fire results are compared with the cold-flow predicted c* efficiency in two ways. First, the cold-flow mixing results are compared with hot-fire results at conditions where vaporization is nearly complete. Secondly, overall performance predictions for the self-atomizing fan nozzle are compared with those obtained in hot-fire experiments.

4.4.1 MIXING LIMITED c* EFFICIENCY

Self-Atomizing Fan Element

Unless vaporization has been completed, the level of c* efficiency measured in hot-fire testing is not representative of the mixing losses alone. The most straightforward method of comparing the predicted levels of mixing with hot-fire data is to compare the cold-flow predictions with hot-fire results obtained at a chamber length long enough that complete vaporization has occurred. That is, the maximum level of c* efficiency obtained with increasing chamber length is dependent upon the level of mixing attained by the injector.

In Fig. 56, the cold-flow predictions for a mixture ratio of 1.1 and 1.6 at a chamber pressure of 100 psia are compared to those obtained in hot-firing experiments. The results are presented in terms of c* efficiency and chamber characteristic length (L*).

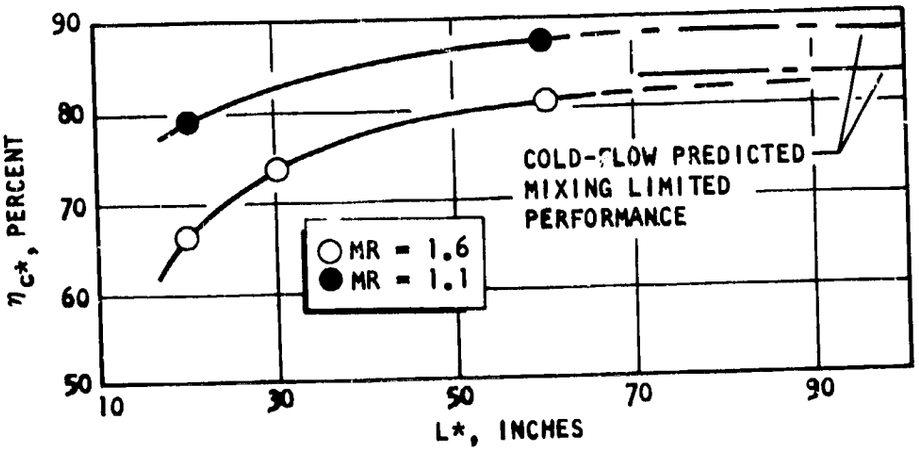

Figure 56. Comparison of Cold-Flow Predicted Mixing Limited c* Efficiency With Actual Hot-Fire Results; Self-Atomizing Fan

As shown in Fig. 56, excellent agreement is found between the cold-flow predicted mixing limited c* efficiency and the extrapolated values of the hot-fire results. The ability to predict the mixing limited c* efficiency under conditions of no reactive stream separation has been previously demonstrated (e.g., Ref. 12 and 13). The above result combined with previous data clearly illustrates the accuracy of the cold-flow mixing technique and analytical model in predicting the level of mixing efficiency attainable in rocket engines.

Unlike Doublets

Presented in Fig. 57 are the results obtained with the unlike doublet elements. It is obvious from the results that the mixing limited performance was not obtained even at an L* (extrapolated) of 90 inches. These results clearly demonstrate that "blowapart" significantly altered the performance characteristics, and consequently, does not allow a comparison of the cold-flow and hot-fire mixing limited performance.

This result affects the ability of directly predicting hot-fire performance characteristics for the unlike doublet patterns. To date, blowapart models have not been developed sufficiently to predict mixing and atomization levels occurring under this condition. If sufficient hot-fire data had been obtained over a wide range of mixture ratios at large L*'s, then at least the cold-flow mixing data combined with hot-fire data could have been used to show the effect of blowapart on mixing. A few isolated data points are available at an L* of 60 inches for off-optimum mixture ratio; however, these data are insufficient to accurately extrapolate to the mixing limited c* value. It seems appropriate to mention that the inability to predict c* efficiency when blowapart occurs has been recognized by NASA and the Air Force and several studies are currently under way to attempt to fill in this gap in technology. These efforts, however, are not sufficiently completed for the results to be utilized in analysis during this program.

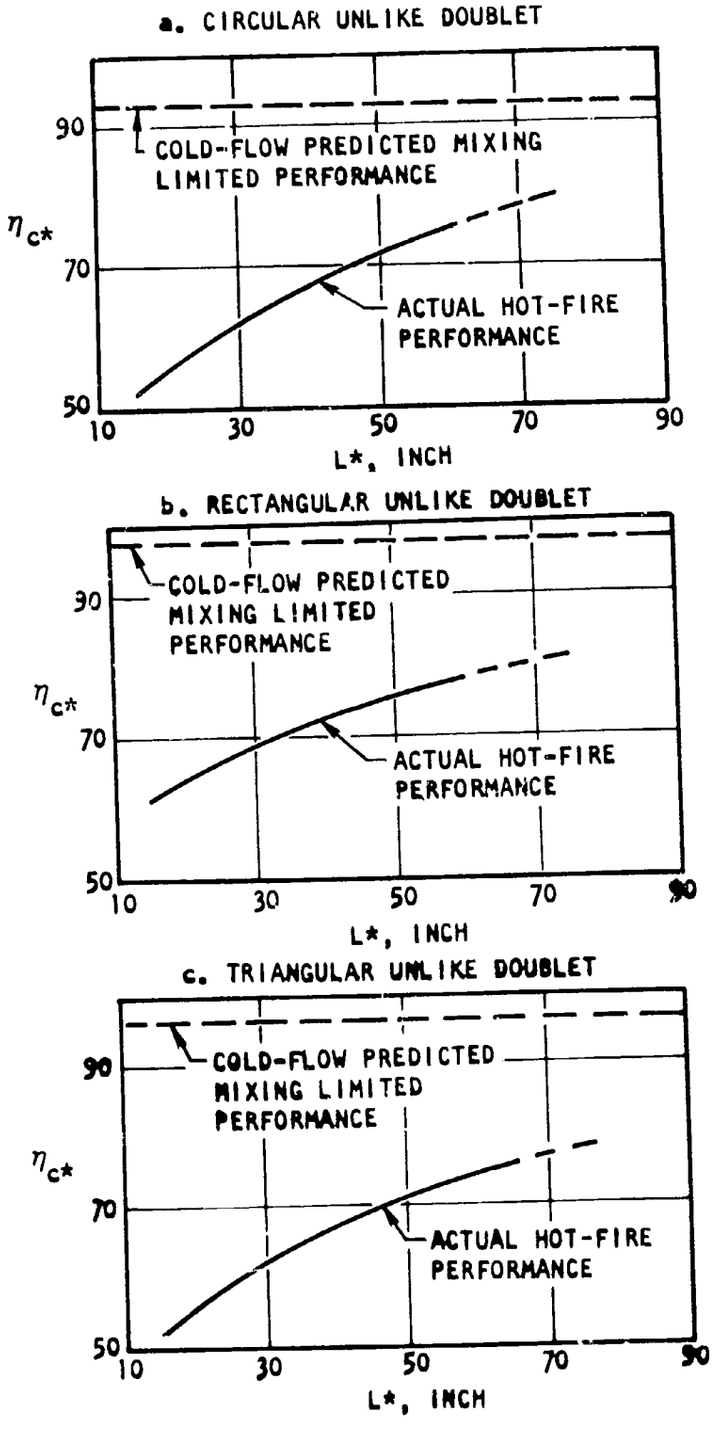

Figure 57. Comparison of Cold-Flow Predicted Mixing Limited Efficiency With Actual Hot-Fire Results--Unlike Doublets

4.4.2 PREDICTION OF OVERALL c* PERFORMANCE CHARACTERISTICS

Self-Atomizing Fan

The overall c* efficiency within a rocket engine depends upon (1) the mixing limited c* efficiency, and (2) the vaporization rate limited c* efficiency. It has been found (Ref. 12 and 13) that these effects can be combined as shown in Eq. 23 to calculate the overall predicted c* efficiency.

$$\eta_{c^*pred} = \eta_{c^*mix} \times \eta_{c^*vap} \tag{23}$$

η_{c^*mix} is determined from the cold-flow mixing data and as verified in the previous section is an excellent measurement of the hot-fire mixing levels. Unfortunately, η_{c^*vap} is not determined in such a straightforward manner and requires some explanation.

Prediction of vaporization rate limited c* efficiency requires the determination of the propellant dropsizes actually occurring within the rocket engine. The actual dropsize will differ from the dropsize obtained with wax in still air because of the influence of physical properties and combustion gas velocity. The latter parameter causes the primary dropsizes to undergo aerodynamic breakup resulting in a reduction in the sprays overall dropsize. Once the dropsize is determined, then the Rocketdyne vaporization-rate-limited combustion model is used to determine η_{c^*vap}.

Data have been obtained utilizing the self-atomizing fan and cone nozzles using wax as well as normal liquids (Ref. 17 and 18). The results of Hasson and Mizrahi (Ref. 17) showed that dropsize is related to injector size, ΔP, and physical properties in the following manner

$$\overline{D} = C' \left(\frac{\sigma_L}{C_q^2} \frac{K}{\Delta P} \right)^{1/3} (\rho_L \mu_L)^{1/6}$$

and $$K = A_j/2 \sin \theta/2$$

where

σ_L = surface tension

μ_L = viscosity

c_q = discharge coefficient

ρ_L = liquid density

ΔP = pressure drop

A_j = area of orifice

θ = impingement angle

Comparison of ΔP dependence on dropsize obtained utilizing Shell 270 wax during this program with Eq. 24 shows excellent agreement. The constant, C', was determined from the data shown in Fig. 42.

Equation 24 was then utilized to determine the primary dropsizes for the actual propellants utilized in the hot-fire study (NTO/50-50). The results are shown in Fig. 58. It is interesting to note that the effect of physical properties was to reduce the oxidizer dropsize by a factor of 1.8 while the fuel dropsize changed only by a factor of 1.1.

At injection velocities encountered during hot firing, the self-atomizing fan produces rays of droplets, rather than the thin sheet of liquid which eventually breaks down into ligaments and droplets and, therefore, the dropsizes obtained from Eq. 24 represent the primary dropsizes occurring within the rocket engine. In support of this, several photographs are shown in Fig. 59 illustrating the various stages of droplet formation characteristics as a function of ΔP (the fluid is water). Note that at a ΔP of 3 psi, a teardrop sheet is formed with rays of droplets being torn tangentially away from the edges of the fan. Then at 25 psi the sheet is spread out over a much wider area than before and sheet breakup is occurring. In the last photograph, ΔP 40 psi, the sheet has been totally

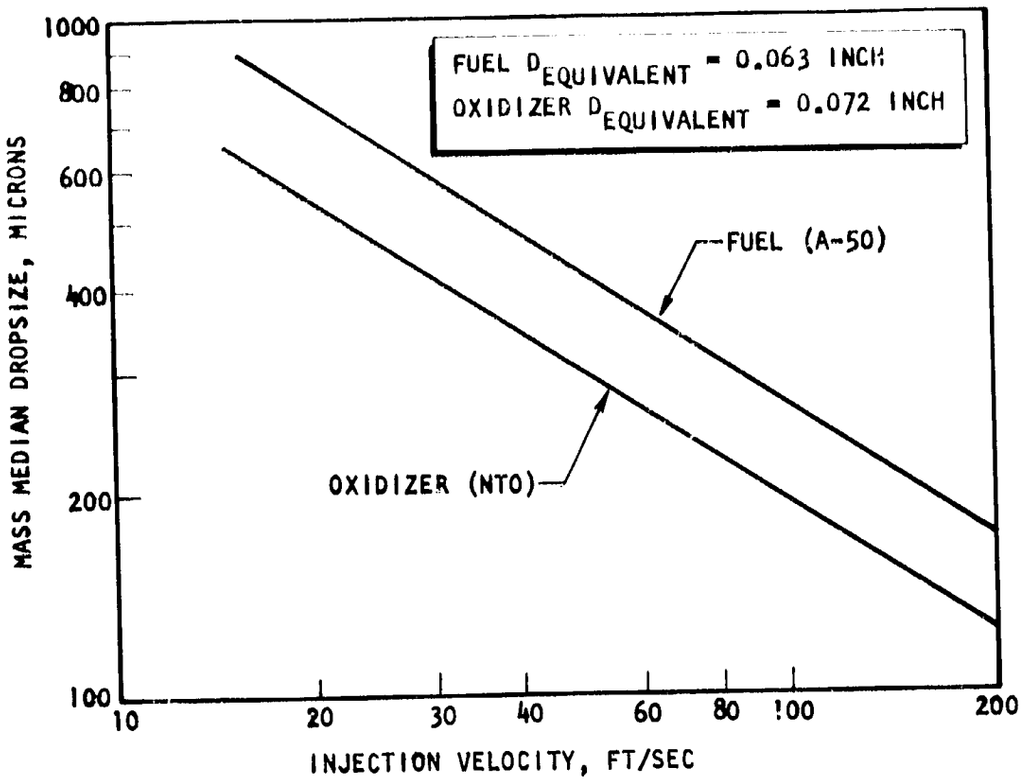

Figure 58. Dropsize Predictions in Still Air for Self-Atomizing Fan Injector as a Function of Injection Velocity

ΔP ≈ 3 psi
Surface Tension Forces Dominating Breakup

ΔP ≈ 25 psi
Sheet Breakup Mode

ΔP ≈ 40 psi
Droplet Formation at Nozzle Exit

Figure 59. Photographs of Spray Field From an 0.063-inch Equivalent Orifice Size Self-Atomizing Fan Nozzle at Various ΔP's (Fluid:Water)

destroyed and rays of droplets emanate from the injector as though they were formed from a point source. Consequently, within the rocket engine, it is reasonable to assume that droplets emanate from the injector, enter into a combustion gas flowfield, are acted upon by the gas, and if sufficient interaction occurs then secondary breakup results.

For the dropsize distributions and injection velocity ranges encountered in the hot-fire study, it is assumed that droplet breakup will occur upon injection for all conditions.

Secondary dropsizes may be calculated from the theoretical equation which was experimentally verified by Wolfe and Andersen (Ref. 19). The equation is

$$\overline{D}_{43} = \left[\frac{k \mu_L \sigma^{3/2} d^{1/2}}{\rho_L^{1/2} \rho_g^{2} \Delta V_g^{4}} \right]^{1/3} \tag{25}$$

where

$\overline{D}_{43}$ = mass mean diameter

μ_L = viscosity

ρ_L = liquid density

ρ_g = gas density

σ = surface tension

d = initial dropsize

k = constant

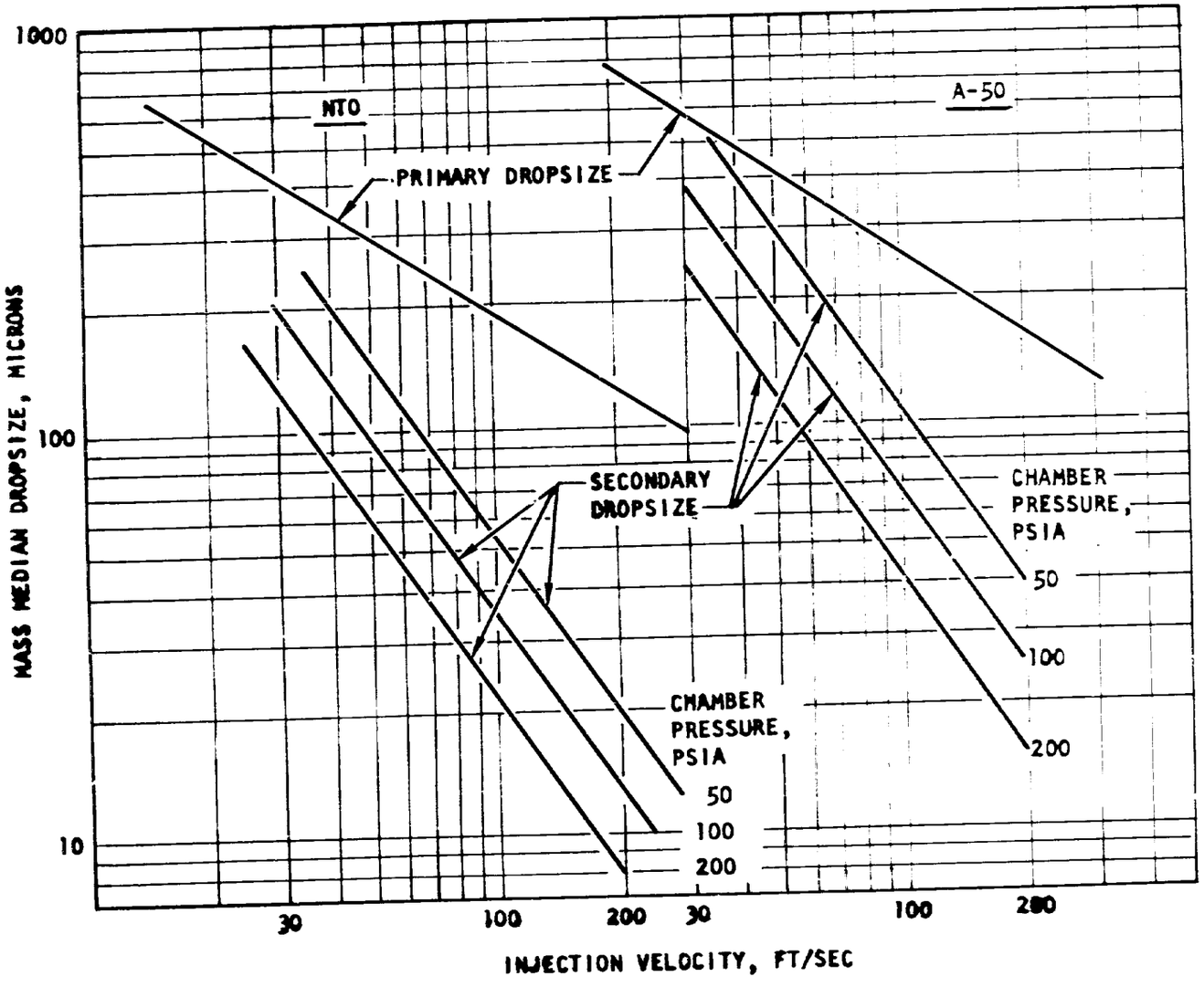

Figure 60. Primary and Secondary Dropsizes for Self-Atomizing Fan Injector ($D_{eq_{ox}}$ = 0.072 inch, D_{eq_f} = 0.062 inch)

$$
\begin{aligned}
\Delta V &= \left|V_L - V_g\right| \\
V_L &= \text{droplet velocity} \\
\bar{D} &= 1.52\ \bar{D}_{43} \text{ (Ref. 4)} \\
\bar{D} &= \text{mass median dropsize}
\end{aligned}
\tag{26}
$$

Because breakup should be initiated near the injection point within the rocket engine and also a relatively large engine contraction ratio was used, it is reasonable for the conditions of this study to assume that

$$\Delta V \sim V_L$$

Calculations were made of the mass median dropsize ($\bar{D}$) of the secondary droplets using Eq. 25 and 26. The value of k found to best fit our data is 1.67. The results are shown in Fig. 60 for various chamber pressures.

The dropsize characteristics shown in Fig. 60 were used to specify the propellant dropsizes under hot-fire conditions. These dropsizes were then input into the vaporization-rate-limited combustion model to determine η_{c^*vap}. The details of the combustion model are described in Ref. 20 The results of application of the model are shown in Fig. 61.

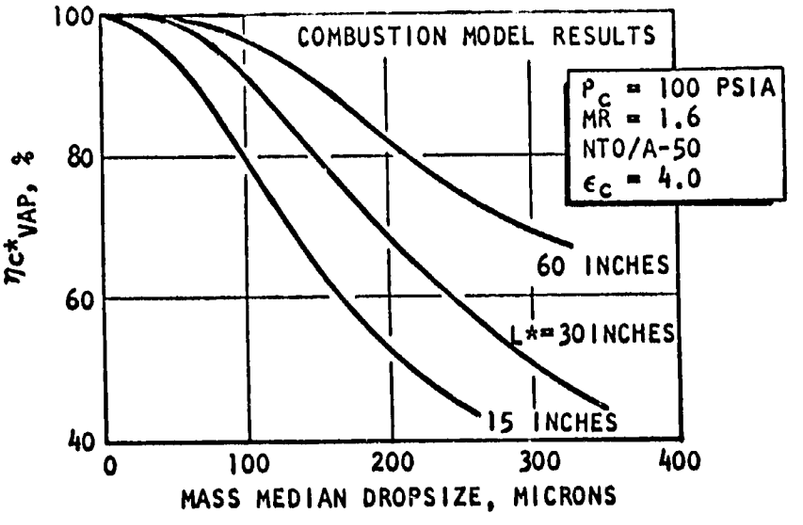

Figure 61. Effect of Dropsize on Vaporization c* Efficiency for Several L*'s

The value of η_{c^*vap} determined from Fig. 61 for given dropsize combined with η_{c^*mix} were then combined as specified in Eq. 23 and the overall predicted c* efficiency determined. The results of this analysis are shown in Table 22. The actual c* efficiencies are specified in Appendix A. The predicted values were then compared to that actually obtained during hot firing. The comparison between predicted and actual c* efficiency is shown in Fig. 62.

Note that excellent comparison is shown between predicted and actual c* efficiency except for the L* of 15-inch data. The most probable reason for this lack of comparison at an L* of 15 inches is that there is not sufficient stay times for the droplets to complete their breakup. No explanation can be given for the lack of correlation for the one point which is grouped near the L* = 15-inch data. (No predictions were attempted for the unlike doublets since the independent effect of blow-apart on mixing or atomization could not be determined.)

It should be noted that the objective of Phase I is to develop injector design criteria so that the various functional and fabrication factors can be evaluated and a comparison between circular and noncircular elements made. This requires performance predictions utilizing cold-flow analysis techniques and verification by hot firing. Consequently the primary task of Phase I is to develop injector criteria and not necessarily to demonstrate high c* performance. As a result of this objective, the hot-fire results shown do not necessarily represent the maximum possible performance for single-element designs. For example, the unlike-doublet elements c* performance levels were suppressed because of blow-apart affects, while the self-atomizing fan injector actually hot fired with not the "optimum" element design. In fact the maximum performance levels that can be obtained with the single element designs, as shown in the Mixing section of this report, is in the low to mid 90's. For the "optimum" design of the self-atomizing nozzle the maximum mixing limited performance attainable is η_{c^*}, about 93 percent.

TABLE 22

PREDICTED OVERALL c* EFFICIENCY FOR SELF-ATOMIZING FAN INJECTOR

Run No.	V_o, ft/sec	V_f, ft/sec	D_o, μ	D_f, μ	η_{vap}, percent	η_{mix}, percent	η_{pred}, percent	η_{act}, percent
28	62	91	58	64	98.4	84.5	83.0	82.4
29	45	66	140	140	82.0	84.5	69.5	68.2
30	35	52	250	270	58.0	80.5	46.8	52.4
31	40	52	205	270	61.8	80.0	49.5	51.4
32	72	105	44	46	99.0	87.0	86.0	84.9
33	43	91	115	73	91.9	88.5	81.4	82.6
34	42	87	120	82	90.7	88.0	79.8	79.8
35	40	83	140	94	88.5	88.0	78.0	78.8
36	52	59	130	200	77.8	80.0	62.0	57.9
37	63	70	73	120	91.5	81.0	74.0	61.7
38	84	107	32	40	99.5	84.5	84.0	84.3
39	84	116	30	35	99.9	84.5	86.4	85.9
40	59	84	74	92	85.0	85.5	72.0	66.2
41	59	82	80	98	85.0	85.5	72.0	62.4
42	45	61	115	140	94.6	83.0	78.5	79.8
43	48	66	115	130	95.4	84.0	80.0	80.2
44	42	85	130	80	96.5	88.0	85.0	87.0

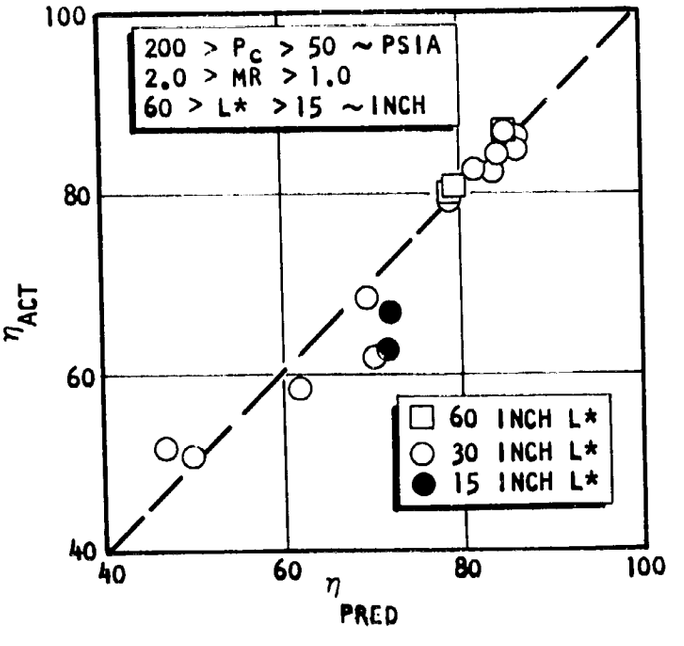

Figure 62. Comparison of Predicted and Actual c* Efficiency for the Self-Atomizing Nozzle

5.0 FINAL EVALUATION

In this section, the experimental data and analytical techniques developed during the program are employed to evaluate the differences between circular and noncircular orifices and elements. The Final Evaluation follows the same format as the Preliminary Evaluation; and in fact, is an upgrading and improvement of the Preliminary Evaluation.

The objective is to determine if noncircular orifices and injector elements offer any advantages over their circular counterparts.

The method employed in determining the numerical values assigned to evaluation criteria is identical to that used for the preliminary evaluation.

5.1 FINAL EVALUATION OF ORIFICE SHAPES

The final evaluation of orifice shapes is divided into two sections, Functional and Fabrication.

5.1.1 FUNCTIONAL EVALUATION

Results obtained during this program indicate that the conclusions reached by the Preliminary Functional Evaluation must be changed. Results of the final functional evaluation appear in Table 23. The evaluation is based upon the results of the single-orifice cold-flow study and the analytical methods developed during the correlation of the data from that study. A brief discussion of the logic used for reevaluation is presented below. (See Preliminary Evaluation for Definition of the considerations for each criterion.)

Orifice Coefficient, C_D

In Table 23 then are two headings listed under the evaluation criterion, C_D. The first is "variation", and the second is "level". Variation refers to the stability or repeatability of the value of C_D for a given range of operating conditions. Level refers to the relative magnitude of the average value of C_D among the various shapes. As shown, the rectangle AR = 8 and the spray nozzle have the least variation of C_D while the circular orifice has the highest level of C_D.

The analytical orifice model, verified by comparison with experimental data, was used to generate the level evaluation of C_D for the various shapes. Evaluation of the spray nozzle is based upon data taken from the single element mixing and atomization tests. The relative position of each of the seven shapes was shown in Fig. 31. It is evident from the figure that only a minor variation of C_D level occurs between the various shapes.

TABLE 23

FINAL FUNCTIONAL EVALUATION OF SINGLE ORIFICES

Orifice Configuration	Functional Rating Parameter								Functional Total
	C_D		Free Stream Stability	Operating Sensitivity				Contamination	
	Var	Level		Temperature	Pressure	Cross Velocity	ΔP Variation		
Circle	10 (10)	10 (10)*	10 (10)	10 (10)	10 (10)	10 (10)	10 (10)	10 (10)	80 (80)
Square	14 (8)	9 (12)	9 (9)	10 (9)	14 (9)	10 (9)	10 (8)	10 (10)	86 (74)
Rectangle AR = 2	19 -	9 -	7 -	10 -	16 -	10 -	10 -	8 -	86 -
Rectangle AR = 8	20 (3)	8 (15)	3 (3)	10 (12)	20 (12)	10 (6)	10 (5)	5 (4)	86 (59)
Equilateral Triangle	11 (7)	9 (13)	8 (8)	10 (8)	11 (8)	10 (8)	10 (7)	9 (9)	78 (68)
Isosceles Triangle	18 (6)	8 (14)	5 (5)	10 (8)	18 (8)	10 (6)	10 (6)	3 (3)	82 (56)
Diamond	18 (4)	8 (13)	5 (4)	10 (8)	18 (8)	10 (6)	10 (7)	4 (4)	83 (54)
Spray Nozzle	20 (8)	5 (8)	14 (11)	10 (13)	20 (12)	15 (12)	10 (8)	10 (8)	104 (80)

*Numbers in ( ) are the values obtained during the preliminary evaluation

Free Stream Stability

Judgement for this criteria was based upon qualitative analysis of photographs taken of the jets under various operating conditions. Photographs of the free stream jets are reproduced in Fig. 16 through 19. Evaluation of the jets free stream stability was based upon qualitative analysis of these photographs as well as observation of the orifices during testing. In the evaluation, the circular orifice is given the highest rating for stability. In general, jets produced by noncircular orifices tended to become circular at low velocities and break up much faster than a circular jet at high velocities. The shapes which deviated most from the circular jet, such as the slot, produced the least stable jets. Jet characteristics of the slot orifice are shown in Fig. 18. These jets become striated close to the injector face. At lower injection velocities the jets often recollect to form a single jet. At higher velocities and shorter L/D values, the jet forms a spray as in the upper left-hand photo in Fig. 18.

Sensitivity to Temperature, Pressure, Cross Velocity, and ΔP Variation

Experimental evaluation showed that all orifices responded in a very similar manner to temperature, cross velocity, and fluctuations of ΔP. The spray nozzle receives a rating which is slightly higher than the other shapes under cross velocity. It was not demonstrated, but it is assumed that the spray nozzle would be relatively insensitive to cross velocity. This is due to the fact that the spray nozzle is a compound orifice consisting of a large, straight orifice at the end of which is a closed spherical dome. A slot is cut in the dome producing an orifice with a "football" shape of less area than the main orifice. The sheet is produced by the geometry of the compound orifice shape and the spray is produced as the result of a thin sheet of liquid breaking up. Because the secondary orifice in the spray fan element is shielded from the propellant manifold (i.e., cross velocity) by the primary orifice, it is expected that the flow field of the fan would not be greatly effected by manifold velocity.

Judgements concerning pressure drop and sensitivity to pressure level are made based on the data presented in Fig. 13, showing the effects of ΔP on C_D for various backpressures. It is evident from these data that the circle and triangle are more sensitive to ΔP level and backpressure than the other shapes. The least affected of the shapes are the thin rectangular orifice and the spray nozzle. No data have been presented for the spray nozzle; however, data recorded during hot-fire studies showed that C_D for the nozzle is constant over a fairly broad range of ΔP. Typical values of orifice coefficient were 0.750 ±0.025 for the oxidizer fan and 0.820 ±0.025 for the fuel fan for chamber pressures ranging from 50 to 190 psia. These evaluations were made at a fixed L/D. At different L/D values, the characteristics of the orifices would be quite different. Although L/D is not one of the specific rating criteria, it is worth mentioning the relative sensitivity of the various shapes to L/D.

The data which were presented in Fig. 14, show the effect of L/D on C_D for the shapes over a cross velocity range. These data suggest that the slot (fine rectang e) is least sensitive to L/D. (It must be remembered that these data were obtained at a backpressure of 100 psig.). The square orifice appears to be the most sensitive, showing tendencies to operate at both flipped conditions, depending on cross velocity.

Contamination

The contamination evaluation is essentially the same as the preliminary evaluation.

5.1.2 FABRICATION EVALUATION

During the course of the program, no particular evidence was discovered which would suggest that the Fabrication results, presented in the Preliminary Evaluation, should be changed. This is due, in part, to the highly qualitative nature of the Fabrication Evaluation.

On the initial stages of the program, it was found that the time required to produce an orifice hole by the EDM process was significantly affected by the shape of the orifice. This result was published and is reproduced in Fig. 63. In Fig. 63 then EDM time is presented for several orifice shapes relative to the time required to EDM a circle.

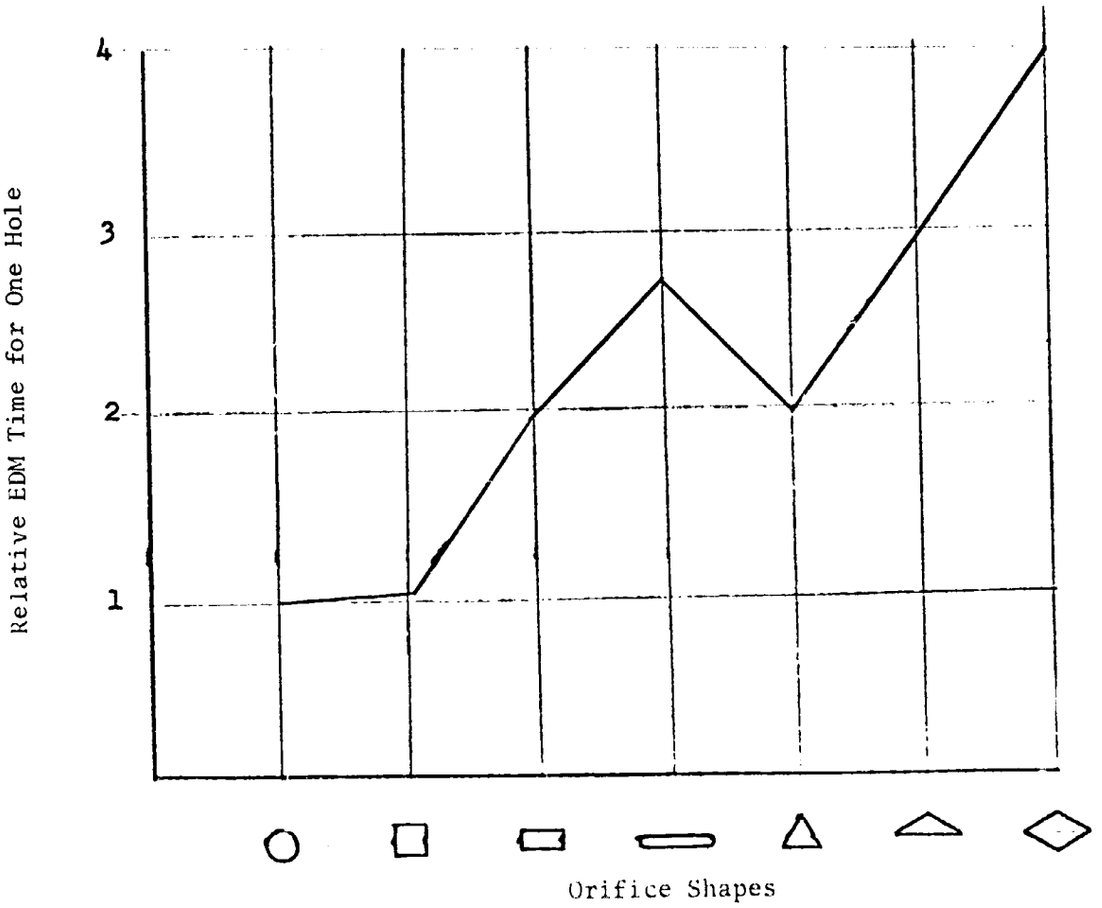

Figure 63. Orifice EDM Machining Time Comparison

As the program progressed and the machinists gained more experience with small noncircular orofices, the time differences between the shapes were decreased until the times were equal.

There were still significant differences in the fabrication of orifice shapes. For example, tool wear was more a problem for shapes with five corners formed by small, acute angles. Also, the electrodes for the finer shaped orifices required more time to fabricate. It must be concluded that the total cost of producing orifice holes is a complex quantity and is not totally reflected in the EDM time required. Such factors as electrode fabrication costs, tool replacement costs, and tolerances required must be considered.

A summary of the Fabrication Evaluation has been presented in Table 14 for the EDM fabrication technique only. The results were given in terms of the average rating number for each shape.

5.1.3 SUMMARY OF ORIFICE EVALUATION

The results of the final evaluation of orifice shapes are presented in Table 24. (For purposes of comparison, reference may be made to the Preliminary Evaluation results which appear in Table 15). In Table 24, the seven orifice shapes investigated during the program are evaluated and rated with respect to a circle (produced by twist drilling) using the same criteria as were used for preliminary evaluation.

From the functional point of view, the spray nozzle received the highest rating with the rectangular shapes rated second. The lowest rating was given to the equilateral triangle.

In contrast to its high rating for function, the spray nozzle received the lowest rating for fabrication considerations. This is attributed to the fact that it is not a simple orifice, but rather a composite of shapes. The highest rating given for fabrication was received by the circle; it is still the least difficult shape to produce.

However, the important result of the evaluation is that the magnitude of the differences between the ratings for all shapes are small, indicating that no particular shape should be excluded from application to injector design merely on the basis of these evaluation criteria.

TABLE 24

SUMMARY OF FINAL EVALUATION OF ORIFICE SHAPES

Configuration	Functional Average	Fabrication Average (EDM Only)
 Circle	10	11.7 (11.7)
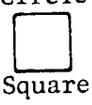 Square	10.7	10.8 (10.8)
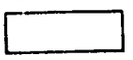 Rectangle $AR^2 = 8$	10.7	9.3 (9.3)
 Equilateral Triangle	9.8	10.2 (10.2)
 Isosceles Triangle	10.3	9.2 (9.2)
 Diamond	10.4	9.3 (9.3)
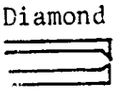 Spray Nozzle	13	7.7 (7.7)

Numbers in ( ) refer to values determined during preliminary evaluation.

5.2 FINAL EVALUATION OF ELEMENT TYPES

Final evaluation of element types is slightly different from the preliminary evaluation in that only unlike-doublet elements (including self-atomizing fan nozzle) are considered. The elements are those unlike doublets incorporating circular orifices, rectangular orifices, triangular orifices, and spray nozzles of equal size. Results of the final evaluation for the elements are presented in Table 25. Two evaluations are shown: one for large L*'s and one for small L*'s. The comparison is made at two L*'s because the relative importance of mixing or atomization to c* performance is dependent upon the completeness of the vaporization process. Consequently, the importance of atomization depends upon chamber length (i.e., L*). If the rocket engine is sufficiently large that complete combustion occurs, then overall c* performance would depend only on the mixing levels attained. Therefore, meaningful comparison should include the influence of L*.

At small L*'s, the resulting c* performance for the circular elements is higher than the noncircular injectors since the unlike doublet with circular orifices yields smaller dropsizes.

At large L*'s, the large chamber volume results in complete vaporization and thus mixing limited performance is realized. The noncircular orifices produce higher efficiencies than the circle here because of their superior mixing characteristics.

These results, along with qualitative judgments of the relative sensitivity to tolerance sensitivity, wall compatibility, and combustion stability were employed to generate the evaluation presented in Table 25.

It must be remembered that the comparisons made in Table 25 are based on the premise that "blowapart" has not taken place for the impinging-type elements. For these conditions, the circular orifices prove to be superior

TABLE 25

ELEMENT CONFIGURATION EVALUATION (UNLIKE DOUBLETS)

Element Configuration \ Ranking Parameter	Tolerance Sensitivity (Fabrication and Operation)	Performance		Compatibility	Combustion Stability	Total		Average	
		Large L*	Small L*			Large L*	Small L*	Large L*	Small L*
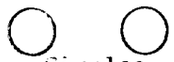 Circles	10	10	10	10	10	40	40	10	10
 Triangles	12	15	5	10	11	48	38	12	9.5
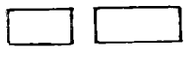 Rectangles	12	17	7	10	11	50	40	12.5	10
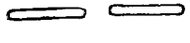 Spray Fans	9	20	15	10	11	60	45	15.0	11.2

to noncircular at small L*'s whereas the reverse is true at large L*'s. The fan element rates low over all L*'s with respect to the noncircular orifices. However, had "blowapart" been included in the evaluation, the fan element would have rated quite high as it was not subject to blowapart.

It should be noted that higher combustion gas velocities produced by lower contraction ratios would decrease the drop sizes for the various elements. Thus, the mixing limited levels of performance would be realized at lower values of L*. The performance of the noncircular elements at small L*'s would be greatly improved. As an example for the self atomizing fan element this effect is shown on a qualitative basis in Fig. 64. Qualitative estimates of the effect of reduced contraction ratio are presented. At lower contraction ratios, the benefits of noncircular orifices are extended to smaller L* values. This is due to the fact that the noncircular elements exhibited mixing limited efficiencies which were higher than those of the elements with circular orifices. It should be noted that similar trends as that shown in Fig. 64 would be obtained for the other elements.

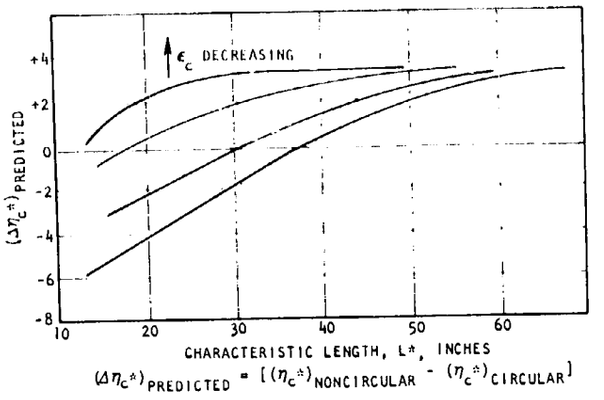

Figure 64. Qualitative Effect of Reduced Contraction Ratio on the Predicted Performance Differences for the Self-Atomizing Fan Element

6.0 CONCLUSIONS

Before generalized conclusions can be made, an assessment of the validity of the overall program approach must be done. There are always possible pitfalls associated with trying to shrink the scope of any program to practical limits. For instance, during the preliminary evaluation it is possible that the best orifice shape or element might be eliminated because of the limited amount of data available. In addition, it is possible that unknown complexities can seriously affect the ability to proceed through the program such that each criterion can be rated and subsequently each element or orifice accordingly ranked. If the program is structured to allow enough feedback and iterations, then these possibilities are minimized. However, there is always the possibility that at the end of the program sufficient data would not be available to know specifically and predictably how to design an injector to operate optimally. Because this particular program was structured to allow significant feedback, the approach used is certainly acceptable.

In the overall view, for liquid/liquid applications the results show that the selection of noncircular or circular orifice designs would be based solely on the specific application. For instance, if mixing were the primary consideration, then noncircular injectors would be selected. In addition, for some propellant combinations such as FLOX/CH_4, noncircular unlike-doublet injector designs can be designed with reasonable orifice dimensions, while circular element designs would be unrealistic. This difficulty for circular orifice designs can be overcome by utilizing a four-on-one pattern rather than the unlike-doublet, however, with a penalty in design complexity and in the ability to pack a larger number of elements into the cross-sectional area of the given injector. Clearly, the availability of noncircular element designs provides the designer with an extended capability and with more flexibility in his selection of element types.

For the specific designs considered, the following conclusions can be made:

1. Orifice flow and spray characteristics are predictable for noncircular orifices using identical techniques as those for circular orifices.
2. Noncircular elements produce significantly better mixing than a circular unlike doublet at equivalent design conditions
3. Circular unlike-doublet elements produce smaller dropsizes than the specific noncircular elements evaluated. This conclusion could be different if the elements were designed to impinge in the following manner.

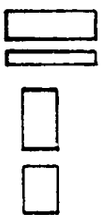

rather than

4. Noncircular element spray characteristics are less sensitive to orifice flow characteristics than circular orifices.
5. Self-atomizing fan elements are not subject to blowapart because they mix in the atomized state rather than from impingement of solid jets.
6. EDM provides an ideal fabrication method for making noncircular elements.

7.0 REFERENCES

1. Elverum, G. W. and T. Morey, Criteria for Optimum Mixture Ratio Distribution Using Several Types of Impinging-Stream Injector Elements, Memorandum No. 30-5, Jet Propulsion Laboratory, Pasadena, California, 25 February 1959.

2. Rupe, J. A., A Correlation Between the Dynamic Properties of a Pair of Impinging Streams and the Uniformity of Mixture-Ratio Distribution in the Resulting Spray, Progress Report No. 20-209, Jet Propulsion Laboratory, Pasadena, California, 28 March 1956.

3. Arbit, H. A., R. Dickerson, S. Clapp, and C. Nagai, Lithium-Fluorine-Hydrogen Propellant Study, NASA CR-72325, R-7257, Final Report, Rocketdyne, a Division of North American Rockwell Corp., Canoga Park, California, 22 February 1968.

4. Dickerson, R., K. Tate, and N. Barsic, Correlation of Spray Injector Parameters with Rocket Engine Performance, AFRPL-TR-68-147, Final Report, Rocketdyne, a Division of North American Rockwell Corp., Canoga Park, California, June 1968.

5. Ingebo, R. D., Dropsize Distributions for Impinging-Jet Breakup in Airstream Simulating the Velocity Conditions in Rocket Combustors, NACA TN 4222, March 1958.

6. Calleghan, E. E., and D. T. Bowden: Investigation of Flow Coefficient of Circular, Square, and Elliptical Orifices at High Pressure Ratios, NACA-TN-1947, Lewis Flight Propulsion Laboratory, Cleveland Ohio, September 1949.

7. Rivas, M. A. and Shapiro, A. H., On the Theory of Discharge Coefficients for Rounded-Entrance Flowmeters and Venturis, Transactions of A.S.M.E.

8. Riebling, R. W., and Powell, W. B., The Hydraulic Characteristics of Flow Through Miniature Slot Orifices, Technical Report (unpublished), Jet Propulsion Laboratory, Pasadena, California, 1969.

9. Briant, D. R., Discharge Coefficients for Common Orifice Forms, Reaction Motors, Inc., Report No. DS-140, Rockway, New Jersey, 15 February 1954.

10. Report No. 6925-F, Injector Orifice Study - Apollo Service Propulsion System - Final Report, Aerojet General Corporation, Sacramento, California, 31 July 1968.

11. Nurick, W. H., and S. D. Clapp, "An Experimental Technique for Measurement of Injector Spray Mixing," J. Spacecraft and Rockets, 6, 11 November 1969, pp 1312-1315.

12. NASA CR-72487, Falk, A. Y., et al, Space Storable Propellant Performance Study, Final Report, Rocketdyne, a Division of North American Rockwell Corp., Canoga Park, California, November 1968.

13. AFRPL-TR-68-147, Correlation of Spray Injector Parameters with Rocket Engine Performance, Final Report, Rocketdyne, a Division of North American Rockwell Corp., Canoga Park, California, June 1968.

14. R-7995, Knight, R. M., and W. H. Nurick, Correlation of Spray Drop-size Distribution and Injector Variables, Interim Report, Rocketdyne, a Division of North American Rockwell Corp., Canoga Park, California, September 1969.

15. Kushida, R. and J. Houseman, Criteria for Separation of Impinging Streams of Hypergolic Propellants, JPL Report WSCI-67-38, 1967.

16. NASA 7-467, Dynamic Sciences Quarterly Report No. SN95-6, October 1967.

17. Hasson, D. and J. Mizrahi, "The Drop Size of Fan Spray Nozzles: Measurement by the Solidifying Wax Method Compared With Those Obtained by Other Sizing Techniques," Trans. Instn. Chem. Engr., Vol 39, 1961.

18. Dombrowski, D., D. Hasson, and D. Word, "Some Aspects of Liquid Flow Through Fan Spray Nozzles," Chem. Engr. Science, 12, No. 35, 1960.

19. Wolfe, H. and W. Andersen, Kinetics, Mechanism and Resultant Droplet Sizes of the Aerodynamic Breakup of Liquid Drops, Report No. 0395-04(18)SP, Aerojet-General Corp., Downey, California, April 1964.

20. Lambiris, S., et al, "Stable Combustion Processes in Liquid Propellant Rocket Engines," Combustion and Propulsion Fifth AGARD Colloquium, High Temperature Phenomena, The MacMillan Co., N.Y., 1962, pp 569-636.

0

8.0 APPENDIX A

TABLES OF EXPERIMENTAL DATA

TABLE A-1

TEST MATRIX AND DATA FOR SINGLE-ORIFICE COLD-FLOW EXPERIMENTS WITH WATER

SYMBOLS

DP = Orifice ΔP, psid

PB = Backpressure, psig

C_D = Discharge Coefficient

WDØT = Orifice Flowrate, lbm/sec

D = Flow Factor $\frac{A}{12}\sqrt{2g\,\rho\Delta p} = \dot{w}/C_D$

V_{C_1} = Upstream Cross Velocity, ft/sec

VC-Ave = Average Cross Velocity, ft/sec

V_{C_2} = Downstream Cross Velocity, ft/sec

TEST NO	DATE	SHAPE								L/D				BACK-PRESSURE			CROSS VELOCITY					TEMP.		REMARKS
		CIRCLE	SQUARE	RECTANGLE	SLOT	EQU. TRIANGLE	ISOS. TRIANGLE	DIAMOND	ENTRANCE ROUND	2	4	6	20	0	50	100	0	5	10	20	PROGRAMMED	SLOT ORIENTATION		COLD	HOT	
001	8/20/69	X										X				X									
002		X										X				X									
003		X										X				X									
004		X										X				X									
005		X										X				X									
006		X										X				X									
007		X										X			X										
008		X										X			X										
009		X										X			X										
010		X										X			X										
011		X										X			X										
012		X										X			X										
013		X										X		X											
014		X										X		X											
015		X										X		X											
016		X										X		X											
017		X										X				X		X							
018		X										X				X			X						
019		X										X				X				X					
020		X										X				X	X								
021			X									X				X	X								
022			X									X				X	X								
023			X									X				X	X								
024			X									X				X	X								
025			X									X			X		X								
026			X									X			X		X								
027			X									X			X		X								
028			X									X			X		X								
029			X									X		X			X								
030			X									X		X			X								
031			X									X		X			X								
032			X									X				X		X							
033			X									X							X						
034			X									X								X					
035			X									X													

TABLE A-1

RUN NO.	DATE	CIRCLE	SQUARE	RECTANGLE	SLOT	EQU. TRIANGLE	ISOS. TRIANGLE	DIAMOND	ENTRANCE ROUND	2	4	6	20	PRESSURE 0	50	100	VELOCITY 0	5	10	20	PRESSURANT Ile	SLOT	ORIENTATION	COLD	HOT
036			X									X				X	X								
037			X									X				X	X								
038			X									X				X	X								
039			X									X				X	X								
040			X									X			X		X								
041			X									X			X		X								
042			X									X			X		X								
043			X									X			X		X								
044			X									X		X			X								
045			X									X		X			X								
046			X									X		X			X								
047			X									X		X			X								
048			X									X		X			X								
049			X									X		X			X								
050			X									X				X		X							
051	178		X									X				X			X						
052	8/20/69		X									X				X				X					
053	8/25/69		X									X				X		X							
054	8/26/69		X									X				X		X							
055			X									X				X			X						
056			X									X				X		X							
057			X									X				X			X						
058			X									X				X				X					
059	8/26/69		X									X				X				X					
060	8/27/69		X									X		X			X								
061	8/27/69		X									X				X	X								
062	8/28/69		X									X			X		X								
063			X									X				X	X								
064			X									X				X				X					
065			X									X			X		X								
066				X								X				X	X								
067				X								X				X	X								
068				X								X			X		X								
069				X								X		X			X								
070			X									X				X	X								
071			X									X				X	X								
072			X									X			X		X								

⊙ — Dot denotes special photo run with purges on which render data unacceptable for numerical interpretation

Bad Sample

		CIRCLE	SQUARE	RECTANGLE	SLOT	EQU. TRIANGLE	ISOS. TRIANGLE	DIAMOND	ENTRANCE ROUND	2	4	6	20	PRESSURE 0	50	100	VELOCITY 0	5	10	20	PRESSURANT He	SLOT	ORIENTATION	COLD SLOT
073	8/28/69	X																						
074	8/29/69							X																
075								X																
076								X																
077								X																
078	8/29/69							X																
079	8/29/69							X																
080								X																
081								X																
082								X																
083								X																
084								X																
085								X																
086								X																
087								X																
088								X																
089								X																
090							X																	
091							X																	
092							X																	
093							X																	
094							X																	
095							X																	
096							X																	
097							X																	
098							X																	
099							X																	
100							X																	
101							X																	
102							X																	
103							X																	
104							X																	
105	8/29/69							X																
106	9/2/69							X																
107								X																
108								X																
109								X																

TEST NO.	DATE	SHAPE								[illegible]				BACK-PRESSURE			CROSS VELOCITY						[illegible]	
		CIRCLE	SQUARE	RECTANGLE	SLOT	EQU. TRIANGLE	ISOS. TRIANGLE	DIAMOND	ENTRANCE ROUND	2	4	6	20	0	50	100	0	5	10	20	PRESSURANT He	SLOT ORIENTATION	COLD	HOT
110							X					X			X		X							
111							X					X			X		X							
112							X					X			X		X							
113							X					X			X		X							
114							X					X				X	X							
115							X					X				X	X							
116							X					X				X	X							
117							X					X				X	X							
118							X					X				X		X						
119							X					X				X			X					
120							X					X				X				X				
121					X							X		X			X					X		
122					X							X		X			X					X		
123					X							X		X			X					X		
124					X							X		X			X					X		
125					X							X		X			X					X		
126					X							X			X		X					X		
127					X							X			X		X					X		
128					X							X			X		X					X		
129					X							X			X		X					X		
130					X							X				X	X					X		
131					X							X				X	X					X		
132					X							X				X	X					X		
133					X							X				X	X					X		
134					X							X				X		X				X		
135					X							X				X			X			X		
136	9/2/69				X							X				X				X		X		
137	9/3/69	X										X			X		X							
138		X										X		X			X							
139		X										X			X		X							
140		X										X			X		X							
141					X							X				X	X					X		
142					X							X				X	X					X		
143					X							X				X					X	X		
144					X							X				X					X	X		
[illegible]					X							X				X					X	X		

CIRCLE
SQUARE
RECTANGLE
SLOT
EQU. TRIANGLE
ISOS. TRIANGLE
DIAMOND
FAMILIARITY
ROUND
2
4
6
20
0
50
100
0
5
10
20
PRESSURANT
ile
SLOT
ORIENTATION
COLD
SLOT
9/3/69
9/4/69
9/4/69
9/4/69
9/4/69
9/10/69
146
147
148
149
150
151
152
153
154
155
156
157
158
159
160
161
162
163
164
165
166
167
168
169
170
171
172
173
174
175
176
177
178
179
180
181
182
183
184

TEST NO.	DATE	SHAPE								L/D				BACK-PRESSURE			CROSS VELOCITY				PROPELLANT	SLOT ORIENTATION	TEMP.	REMARKS
		CIRCLE	SQUARE	RECTANGLE	SLOT	EQU. TRIANGLE	ISOS. TRIANGLE	DIAMOND	ENTRANCE ROUND	2	4	6	20	0	50	100	0	5	10	20			COLD HOT	
185					X						X					X			X			X		Lost sample
186					X						X					X				X		X		
187					X						X					X			X			X		
188			X								X					X		X						
189			X								X					X			X					
190			X								X					X				X				
191			X								X					X	X							Lost sample
192	9/10/69		X								X					X	X							
193	9/11/69	X											X			X	X							
194		X											X			X		X						
195		X											X			X			X					
196		X											X			X				X				
197				X									X			X		X						
198				X									X			X			X					
199				X									X			X				X				
200				X									X			X			X					
201				X									X			X	X							
202			X										X			X	X							
203			X										X			X		X						
204			X										X			X			X					
205			X										X			X			X					
206	9/11/69		X										X			X				X				
207	9/12/69		X								X					X	X							
208			X								X					X		X						
209			X								X					X			X					
210			X								X					X				X				
211			X								X					X	X							
212			X								X					X	X							
213			X								X					X	X							
214						X					X					X	X							
215						X					X					X		X						

		Circle	Square	Rectangle	Slot	Equ. Triangle	Isos. Triangle	Diamond	Entrance Round	2	4	6	20	Pressure 0	Pressure 50	Pressure 100	Velocity 0	Velocity 5	Velocity 10	Velocity 20	Pressurant He	Slot	Orientation	Cold	Hot	
216						X					X					X			X							
217						X					X					X				X						
218						X					X					X	X									
219				X							X					X	X									
220				X							X					X		X								
221				X							X					X			X							
222				X							X					X				X						
223	9/12/69			X							X					X		X								
224					X						X					X	X					X				
225					X						X					X		X				X				
226					X						X					X			X							
227					X						X					X				X						
228					X						X					X		X								
229			X										X			X		X								
230			X										X			X			X							
231			X										X			X				X						
232	9/15/69		X										X			X	X									
233	9/15/69			X						X						X	X									
234				X						X						X		X								
235				X						X						X			X							
236				X						X						X				X						
237		X											X			X		X								
238		X											X			X			X							
239		X											X			X				X						
240	9/15/69	X											X			X	X									
241	9/16/69					X							X			X	X									
242						X							X			X	X									
243						X							X			X	X									
244						X							X			X		X								
245						X							X			X			X							
246						X							X			X			X							
247						X							X			X				X						Water depletion
248						X							X			X				X						
249					X								X			X		X				X				
250					X								X			X			X			X				

TEST NO.	DATE	SHAPE								L/D			BACK-PRESSURE			CROSS VELOCITY				PRESSURANT	SLOT ORIENTATION		TEMP.		REMARKS
		CIRCLE	SQUARE	RECTANGLE	SLOT	EQU. TRIANGLE	ISOS. TRIANGLE	DIAMOND	ENTRANCE ROUND	2	4	20	0	50	100	0	5	10	20				COLD	HOT	
251					X							X			X				X		X				
252					X							X			X	X					X				
253		X									X				X	X									
254		X									X				X		X								
255		X									X				X			X							
256	9/16/69	X									X				X				X						
257	9/18/69				X							X			X	X						X			
258					X							X			X		X					X			
259					X							X			X			X				X			
260					X							X			X				X			X			
261			X							X					X		X								
262			X							X					X			X							
263			X							X					X				X						
264			X							X					X				X						
265			X							X					X	X									
266						X				X					X	X									
267						X				X					X	X									
268						X				X					X		X								
269						X				X					X			X							
270						X				X					X				X						
271				X						X					X		X								
272				X						X					X			X							
273				X						X					X				X						
274				X						X					X		X								
275				X						X					X			X							
276				X						X					X	X									
277	9/18/69				X					X					X	X					X				
278	9/19/69					X						X			X	X							X		Start of new L/D=6 orifices
279						X						X			X	X							X		
280						X						X			X	X							X		

TEST NO.	DATE	SHAPE: CIRCLE	SQUARE	RECTANGLE	SLOT	EQU. TRIANGLE	ISOS. TRIANGLE	DIAMOND	ENTRANCE ROUND	L/D: 2	4	6	20	BACK-PRESSURE: 0	50	100	CROSS VELOCITY: 0	5	10	20	PRESSURANT He	SLOT ORIENTATION	[illegible]: COLD	HOT	[illegible]
281	9/19/69					X						X				X	X						X		
282	9/22/69	X										X		X			X				X				
283		X										X			X		X				X				
284		X										X				X	X				X				
285		X										X		X			X				X				
286			X									X		X			X				X				
287			X									X			X		X				X				
288	9/22/69		X									X				X	X				X		X		
289	9/23/69	X										X				X	X						X		
290		X										X				X	X						X		
291		X										X				X	X						X		
292		X										X				X	X						X		
293		X										X				X	X						X		
294			X									X				X	X						X		
295			X									X				X	X						X		
296			X									X				X	X						X		
297			X									X				X	X						X		
298			X									X				X	X						X		
299						X						X				X	X						X		
300						X						X				X	X						X		
301						X						X				X	X						X		
302						X						X				X	X							X	
303						X						X				X	X							X	
304						X						X				X	X							X	
305						X						X				X	X							X	
306						X						X				X	X							X	
307						X						X				X	X							X	
308			X									X				X	X							X	
309	9/23/69		X									X				X	X							X	
310			X									X				X	X							X	
311			X									X				X	X							X	
31[illegible]			X																						

NO.	DATE	SHAPE								L/D			BACK-PRESSURE			CROSS VELOCITY						TEMP.		REMARKS
		CIRCLE	SQUARE	RECTANGLE	SLOT	EQU. TRIANGLE	ISOS. TRIANGLE	DIAMOND	ENTRANCE ROUND	2	4	6	20	0	50	100	0	5	10	20	PYRESSURANT He	SLOT ORIENTATION	COLD	HOT	
313	9/23/69	X										X				X	X							X	
314		X										X				X	X							X	
315		X										X				X	X							X	
316	9/25/69	X										X				X	X								
317		X										X				X	X								
318		X										X				X	X								
319		X										X				X	X								
320			X									X				X	X								
321			X									X				X	X								
322			X									X				X	X								
323			X									X				X	X								
324						X						X				X	X								
325						X						X				X	X								
326						X						X				X	X								
327	180					X						X				X	X								
328						X						X				X		X							lost sample
329						X						X				X		X							
330						X						X				X			X						
331						X						X				X			X						
332						X						X				X			X						
333						X						X				X	X								
334						X						X				X	X								
335						X						X				X	X								
336						X						X			X		X								
337						X						X		X			X								lost sample
338	9/25/69					X						X		X			X								
339	9/26/69			X								X				X		X							
340				X								X				X		X							
341				X								X				X		X							
342				X								X				X			X						
343				X								X				X				X					
344			X						X			Y				X		X							
345			X						X			X				X			X						
346			X						X			X				X				X					
347			X						X			Y				X		A							

		CIRCLE	SQUARE	RECTANGLE	SLOT	EQU. TRIANGLE	ISOS. TRIANGLE	DIAMOND	RANCE UND	2	4	6	20	RESSURE 0	50	100	VELOCITY 0	5	10	[illegible]0	RESSURANT He	SLOT	ORIENTATION	COLD	HOT	
383					X							X			X		X					X				
384					X							X		X			X					X				
385					X							X				X	X						X			
386	9/30/69				X							X				X		X					X			
387					X							X				X		X					X			
388					X							X				X			X				X			
389					X							X				X				X			X			
390					X							X				X	X						X			
391				X					X			X				X		X								
392				X					X			Y				X			X							
393				X					X			X				X				X						
394				X					X			X				X	X									
395		X							X			X				X	X									
396		X							X			X				X	X									No sample
397		X							X			X				X	X									
398		X							X			X				X		X								
399		X							X			X				X			X							
400		X							X			X				X				X						
401					X				X			X				X		X				X				
402					X				X			X				X			X			X				
403					X				X			X				X				X		X				
404					X				X			X				X	X					X				
405					X				X			X				X	X						X			
406					X				X			X				X		X					X			
407					X				X			X				X			X				X			
408					X				X			X				X				X			X			
409	9/30/69				X				X			X				X		X					X			

TEST DATA

RUN	DP	PB	CD	WD2T	D	VC1	VC-AVE	VC2
1	51.00	102.00	0.72630	0.07644	0.10524	1.529	0.764	0.000
2	18.70	98.00	0.76139	0.04852	0.06373	0.970	0.485	0.000
3	49.80	103.00	0.75116	0.07812	0.10400	1.562	0.781	0.000
4	38.30	101.00	0.73708	0.06722	0.09120	1.344	0.672	0.000
5	45.40	100.00	0.74090	0.07357	0.09930	1.471	0.736	0.000
6	63.50	98.50	0.73616	0.08645	0.11743	1.729	0.864	0.000
7	53.40	51.00	0.68946	0.07425	0.10769	1.485	0.742	0.000
8	41.40	51.00	0.74552	0.07069	0.09482	1.414	0.707	0.000
9	31.10	51.00	0.75162	0.06177	0.08218	1.235	0.618	0.000
10	17.80	50.70	0.75197	0.04675	0.06217	0.935	0.468	0.000
11	65.20	50.10	0.66706	0.07938	0.11899	1.588	0.794	0.000
12	50.30	50.10	0.70505	0.07369	0.10452	1.474	0.737	0.000
13	57.50	0.00	0.51464	0.05751	0.11175	1.150	0.575	0.000
14	46.10	0.00	0.50370	0.05040	0.10006	1.008	0.504	0.000
15	30.00	0.00	0.56558	0.04565	0.08072	0.913	0.457	0.000
16	18.00	0.00	0.66924	0.04184	0.06252	0.837	0.418	0.000
17	22.80	0.00	0.67454	0.04747	0.07037	0.949	0.475	0.000
18	20.00	99.90	0.75838	0.04998	0.06590	5.079	4.579	4.079
19	19.80	98.40	0.74723	0.04900	0.06557	9.514	9.024	8.534
20	19.80	98.00	0.72831	0.04776	0.06557	18.246	17.768	17.291

RUN	DP	PB	CD	WD2T	D	VC1	VC-AVE	VC2
21	53.80	97.80	0.71100	0.07906	0.11120	1.581	0.791	0.000
22	40.50	98.10	0.73034	0.07047	0.09648	1.409	0.705	0.000
23	32.00	98.70	0.71979	0.06173	0.08576	1.235	0.617	0.000
24	22.00	101.10	0.70084	0.04984	0.07111	0.997	0.498	0.000
25	51.50	51.60	0.71507	0.07780	0.10880	1.556	0.778	0.000
26	38.10	51.60	0.73259	0.06856	0.09358	1.371	0.686	0.000
27	28.80	51.60	0.73519	0.05982	0.08136	1.196	0.598	0.000
28	17.30	51.00	0.73938	0.04662	0.06306	0.932	0.466	0.000
29	53.60	0.00	0.69712	0.07738	0.11100	1.548	0.774	0.000
30	37.00	0.00	0.73751	0.06801	0.09222	1.360	0.680	0.000
31	30.40	0.00	0.74630	0.06238	0.08359	1.248	0.624	0.000
32	18.90	0.00	0.74452	0.04907	0.06591	0.981	0.491	0.000
33	20.30	101.10	0.75953	0.05188	0.06831	4.944	4.425	3.906
34	19.60	98.70	0.72462	0.04864	0.06712	9.434	8.947	8.461
35	20.00	98.10	0.71912	0.04876	0.06780	18.033	17.546	17.058

RUN	DP	PB	CD	WDJT	D	VC1	VC-AVE	VC2
36	48.40	101.40	0.74820	0.07506	0.10032	1.501	0.751	0.000
37	38.80	102.00	0.78153	0.07020	0.08982	1.404	0.702	0.000
38	31.80	100.80	0.74816	0.06084	0.08131	1.217	0.608	0.000
39	17.00	98.70	0.80147	0.04765	0.05945	0.953	0.477	0.000
40	49.10	54.00	0.74996	0.07578	0.10104	1.516	0.758	0.000
41	42.40	54.00	0.77266	0.07255	0.09389	1.451	0.725	0.000
42	28.30	53.40	0.78341	0.06009	0.07671	1.202	0.601	0.000
43	17.00	52.80	0.77837	0.04628	0.05945	0.926	0.463	0.000
44	49.60	0.00	0.76377	0.07756	0.10155	1.551	0.776	0.000
45	37.60	0.00	0.70289	0.06215	0.08842	1.243	0.621	0.000
46	25.50	0.00	0.69732	0.05078	0.07282	1.016	0.508	0.000
47	15.00	0.00	0.79831	0.04458	0.05585	0.892	0.446	0.000
48	42.20	0.00	0.68256	0.06394	0.09367	1.279	0.639	0.000
49	21.60	0.00	0.71754	0.04809	0.06702	0.962	0.481	0.000
50	20.30	99.00	0.83387	0.05418	0.06497	5.160	4.618	4.077
51	20.00	96.90	0.78945	0.05091	0.06449	9.918	9.409	8.900
52	19.80	100.20	0.76571	0.04913	0.06416	18.780	18.289	17.797

RUN	DP	PB	CD	WDJT	D	VC1	VC-AVE	VC2
53	20.00	97.00	0.78220	0.05044	0.06449	3.245	2.741	2.236
54	19.90	95.70	0.75766	0.04874	0.06433	3.191	2.704	2.217
55	19.80	97.00	0.75961	0.04874	0.06416	7.340	6.853	6.365
56	20.00	96.00	0.76367	0.04925	0.06449	5.032	4.569	4.067
57	20.00	96.60	0.74979	0.04835	0.06449	9.542	9.159	8.575
58	20.00	96.30	0.73889	0.04765	0.06449	18.328	17.852	17.375
59	19.40	97.00	0.72694	0.04617	0.06351	3.542	3.080	2.619
60	51.10	0.00	0.75477	0.07780	0.10308	1.556	0.778	0.000
61	21.70	101.00	0.74123	0.04979	0.06717	0.996	0.498	0.000
62	51.40	50.00	0.78225	0.08087	0.10338	1.617	0.809	0.000
63	52.00	100.00	0.74156	0.07711	0.10398	1.542	0.771	0.000
64	19.60	97.00	0.73313	0.04680	0.06384	18.567	18.099	17.631
65	51.50	56.00	0.74839	0.07744	0.10348	1.549	0.774	0.000

RUN	DP	PB	CD	WDJT	D	VC1	VC-AVE	VC2
66	20.40	101.00	0.74841	0.05125	0.06848	1.025	0.513	0.000
67	50.60	102.00	0.79056	0.07556	0.10785	1.511	0.756	0.000
~~68~~	~~52.10~~	~~50.00~~	~~0.13663~~	~~0.01714~~	~~0.10944~~	~~0.343~~	~~0.171~~	~~0.000~~
69	49.20	2.00	0.67714	0.07201	0.10635	1.440	0.720	0.000

RUN	DP	PB	CD	WDJT	D	VC1	VC-AVE	VC2
70	20.50	101.50	0.70302	0.04691	0.06673	0.938	0.469	0.000
71	48.20	103.50	0.73312	0.07501	0.10232	1.500	0.750	0.000
72	53.20	50.00	0.75921	0.08161	0.10749	1.632	0.816	0.000
73	49.90	3.00	0.55992	0.05829	0.10411	1.166	0.583	0.000

RUN	DP	PB	CD	WDOT	D	VC1	VC-AVE	VC2
74	21.60	0.00	0.80059	0.06352	0.07934	1.270	0.635	0.000
75	32.20	0.00	0.73283	0.07099	0.09687	1.420	0.710	0.000
76	39.70	0.00	0.78825	0.08478	0.10756	1.696	0.848	0.000
77	51.00	0.00	0.76503	0.09327	0.12191	1.865	0.933	0.000
78	22.00	52.80	0.81212	0.06503	0.08007	1.301	0.650	0.000
79	30.50	54.90	0.79348	0.07481	0.09428	1.496	0.748	0.000
~~80~~	~~40.00~~	~~48.60~~	~~0.55441~~	~~0.05986~~	~~0.10797~~	~~1.197~~	~~0.599~~	~~0.000~~
81	49.50	51.00	0.78722	0.09455	0.12010	1.891	0.945	0.000
82	39.10	51.00	0.79237	0.08458	0.10674	1.692	0.846	0.000
83	22.00	101.40	0.76455	0.06128	0.08007	1.224	0.612	0.000
84	29.30	101.70	0.78826	0.07868	0.09978	1.452	0.726	0.000
85	41.00	101.40	0.74816	0.08178	0.10931	1.636	0.818	0.000
86	50.00	100.50	0.75667	0.09134	0.12071	1.827	0.913	0.000
87	20.20	99.90	0.77879	0.05975	0.07672	5.080	4.482	3.885
88	19.60	99.60	0.78285	0.05916	0.07558	9.623	9.032	8.440
89	19.60	99.90	0.76199	0.05759	0.07558	18.515	17.940	17.364

RUN	DP	PB	CD	WDOT	D	VC1	VC-AVE	VC2
90	20.05	0.00	0.72001	0.05230	0.07263	1.046	0.523	0.000
91	31.00	0.00	0.64718	0.05845	0.09032	1.169	0.585	0.000
92	40.20	0.00	0.65608	0.06748	0.10285	1.350	0.675	0.000
93	49.60	0.00	0.61783	0.07058	0.11424	1.412	0.706	0.000
94	48.60	0.00	0.62894	0.07112	0.11308	1.422	0.711	0.000
95	22.50	51.50	0.59378	0.04569	0.07694	0.914	0.457	0.000
96	32.70	48.50	0.61018	0.05660	0.09276	1.132	0.566	0.000
97	39.60	51.00	0.61296	0.06257	0.10208	1.251	0.626	0.000
98	50.50	51.00	0.68059	0.07845	0.11527	1.569	0.785	0.000
99	22.10	100.00	0.72003	0.05491	0.07626	1.098	0.549	0.000
100	30.50	99.60	0.73058	0.06545	0.08958	1.309	0.654	0.000
101	40.50	99.30	0.71269	0.07357	0.10323	1.471	0.736	0.000
102	50.00	100.00	0.68636	0.07873	0.11470	1.575	0.787	0.000
103	20.50	100.00	0.73239	0.05379	0.07344		5. } NOMINAL NO	
104	19.80	99.30	0.73268	0.05289	0.07218		10. } FLOW METER	
105	20.00	99.30	0.70113	0.05086	0.07254		20. } OUTPUT.	

RUN	DP	PB	CD	WDOT	D	VC1	VC-AVE	VC2
106	19.40	0.00	0.75379	0.05790	0.07682	1.158	0.579	0.000
107	29.10	0.00	0.77907	0.07330	0.09408	1.466	0.733	0.000
108	39.60	0.00	0.77588	0.08515	0.10975	1.703	0.852	0.000
109	51.50	0.00	0.70319	0.08801	0.12516	1.760	0.880	0.000
110	21.80	49.00	0.79856	0.06421	0.08143	1.284	0.642	0.000
111	32.20	48.50	0.72700	0.07195	0.09897	1.439	0.719	0.000
112	37.80	53.00	0.77565	0.08317	0.10722	1.663	0.832	0.000
113	51.40	52.50	0.75457	0.09435	0.12504	1.887	0.944	0.000
114	20.80	102.50	0.76511	0.06086	0.07954	1.217	0.609	0.000

115	31.00	102.50	0.77598	0.07535	0.09711	1.507	0.754	0.000
116	39.40	99.50	0.77432	0.08477	0.10947	1.695	0.848	0.000
117	50.40	99.50	0.71318	0.08830	0.12382	1.766	0.883	0.000
118	20.00	98.50	0.76494	0.05966	0.07800	4.971	4.374	3.778
119	19.95	98.50	0.79482	0.06192	0.07790	9.568	8.949	8.330
120	19.90	98.00	0.76352	0.05940	0.07780	18.327	17.733	17.139

RUN	DP	PB	CD	WD3T	D	VC1	VC-AVE	VC2
~~121~~	~~17.90~~	~~0.00~~	~~0.86487~~	~~0.06474~~	~~0.07469~~	~~1.295~~	~~0.647~~	~~0.000~~
122	29.00	0.00	0.75807	0.07226	0.09533	1.445	0.723	0.000
123	40.90	0.00	0.75758	0.08576	0.11321	1.715	0.858	0.000
124	50.00	0.00	0.68335	0.08554	0.12517	1.711	0.855	0.000
125	50.40	0.00	0.69376	0.08719	0.12567	1.744	0.872	0.000
126	19.80	51.00	0.75877	0.05977	0.07877	1.195	0.598	0.000
127	30.00	50.50	0.74089	0.07183	0.09696	1.437	0.718	0.000
128	41.30	50.00	0.75252	0.08561	0.11376	1.712	0.856	0.000
129	51.50	50.00	0.75845	0.09635	0.12703	1.927	0.963	0.000
130	20.70	100.00	0.73970	0.05957	0.08054	1.191	0.596	0.000
131	32.00	99.00	0.73108	0.07321	0.10014	1.464	0.732	0.000
132	41.20	99.00	0.75434	0.08571	0.11362	1.714	0.857	0.000
133	52.00	99.00	0.73539	0.09387	0.12765	1.877	0.939	0.000
134	20.00	98.00	0.73779	0.05841	0.07917	4.915	4.331	3.747
135	20.00	97.50	0.73095	0.05787	0.07917	9.484	8.905	8.326
136	20.00	102.00	0.71253	0.05641	0.07917	18.319	17.754	17.190

RUN	DP	PB	CD	WD3T	D	VC1	VC-AVE	VC2
137	51.40	52.00	0.70514	0.07450	0.10565	1.490	0.745	0.000
138	50.90	6.00	0.55381	0.05822	0.10513	1.164	0.582	0.000
139	49.20	48.00	0.77290	0.07989	0.10336	1.598	0.799	0.000
140	51.00	48.00	0.73446	0.07729	0.10524	1.546	0.773	0.000

RUN	DP	PB	CD	WD3T	D	VC1	VC-AVE	VC2
141	21.20	102.50	0.74673	0.06087	0.08152	1.217	0.609	0.000
142	22.00	98.50	0.72002	0.05979	0.08304	1.196	0.598	0.000
143	20.00	100.00	0.68944	0.05459	0.07918	18.563	18.018	17.472
144	19.90	101.00	0.67390	0.05322	0.07898	18.537	18.005	17.472
145	21.00	96.00	0.68132	0.05528	0.08113	17.819	17.266	16.714

RUN	DP	PB	CD	WD3T	D	VC1	VC-AVE	VC2
146	21.10	97.50	0.70394	0.05245	0.07451	1.049	0.524	0.000
147	20.00	97.00	0.67441	0.04892	0.07254	18.444	17.955	17.465
148	20.00	96.00	0.67678	0.04909	0.07254	18.431	17.940	17.449
149	20.00	94.00	0.65884	0.04779	0.07254	18.510	18.032	17.555

RUN	DP	PB	CD	WDOT	D	VC1	VC-AVE	VC2
150	23.00	95.00	0.75214	0.06157	0.08186	1.231	0.616	0.000
151	22.00	95.00	0.74676	0.05979	0.08006	1.196	0.598	0.000
152	23.00	94.00	0.75880	0.06212	0.08186	1.242	0.621	0.000
153	21.50	96.50	0.75259	0.05957	0.07915	1.191	0.596	0.000
154	20.00	95.00	0.73904	0.05642	0.07634	18.460	17.896	17.332
155	20.00	101.00	0.74732	0.05705	0.07634	18.433	17.863	17.292

RUN	DP	PB	CD	WDOT	D	VC1	VC-AVE	VC2
156	18.00	102.00	0.73744	0.05457	0.07399	1.091	0.546	0.000
157	20.00	94.00	0.72599	0.05662	0.07800	18.458	17.892	17.326
158	20.00	95.00	0.70139	0.05470	0.07800	18.485	17.938	17.391

RUN	DP	PB	CD	WDOT	D	VC1	VC-AVE	VC2
159	66.00	0.00	0.60475	0.07240	0.11972	1.448	0.724	0.000
160	64.90	102.00	0.65604	0.07788	0.11872	1.558	0.779	0.000
161	20.00	103.00	0.66411	0.04377	0.06590	5.052	4.614	4.176
162	65.00	102.00	0.69107	0.08211	0.11861	4.971	4.150	3.329
163	65.00	102.00	0.64388	0.07643	0.11861	9.514	8.750	7.986
164	63.90	101.00	0.72402	0.08529	0.11780	1.706	0.853	0.000
165	64.40	51.50	0.73865	0.08735	0.11826	1.747	0.874	0.000
166	65.20	0.00	0.58525	0.06964	0.11899	1.393	0.696	0.000
167	65.00	0.00	0.57290	0.06807	0.11881	1.361	0.681	0.000

RUN	DP	PB	CD	WDOT	D	VC1	VC-AVE	VC2
168	19.00	97.50	0.72940	0.04989	0.06840	0.998	0.499	0.000
169	20.00	99.50	0.71349	0.05007	0.07017	5.052	4.551	4.050
170	20.00	99.00	0.68665	0.04818	0.07017	9.648	9.166	8.685
171	20.00	98.50	0.70314	0.04934	0.07017	18.538	18.045	17.551

RUN	DP	PB	CD	WDOT	D	VC1	VC-AVE	VC2
172	21.40	100.50	0.68451	0.04800	0.07012	0.960	0.480	0.000
173	20.50	99.50	0.66611	0.04572	0.06863	0.914	0.457	0.000
174	20.00	100.00	0.66020	0.04475	0.06779	4.915	4.468	4.020
175	20.00	99.50	0.65186	0.04419	0.06779	9.404	8.962	8.520
176	20.00	100.00	0.60673	0.04113	0.06779	18.054	17.642	17.231

RUN	DP	PB	CD	WDOT	D	VC1	VC-AVE	VC2
177	19.30	102.00	0.66768	0.05099	0.07637	1.020	0.510	0.000
178	20.00	101.50	0.65589	0.05099	0.07774	4.915	4.405	3.895
179	20.00	102.00	0.64860	0.05042	0.07774	9.430	8.925	8.421
180	20.00	102.00	0.62337	0.04846	0.07774	18.132	17.647	17.162
181	21.00	102.00	0.66781	0.05320	0.07966	1.064	0.532	0.000

RUN	DP	PB	CD	WD3T	D	VC1	VC-AVE	VC2
182	19.00	100.50	0.66217	0.05691	0.08594	1.138	0.569	0.000
183	20.00	99.00	0.51318	0.04525	0.08817	4.915	4.462	4.010
184	20.00	100.50	0.54566	0.04811	0.08817	4.915	4.434	3.953
~~185~~	~~20.00~~	~~100.00~~	~~0.00000~~	~~0.00000~~	~~0.08817~~	~~9.403~~	~~4.702~~	~~0.000~~
186	20.00	100.50	1.03795	0.09152	0.08817	18.053	17.138	16.222
187	20.00	100.40	0.54420	0.04798	0.08817	9.376	8.897	8.417

RUN	DP	PB	CD	WD3T	D	VC1	VC-AVE	VC2
188	20.00	102.00	0.64610	0.04533	0.07016	4.915	4.461	4.008
189	20.00	101.50	0.63511	0.04456	0.07016	9.323	8.876	8.431
190	20.00	101.50	0.61302	0.04301	0.07016	17.971	17.541	17.111
~~191~~	~~19.80~~	~~100.00~~	~~0.00000~~	~~0.00000~~	~~0.06940~~	~~0.000~~	~~0.000~~	~~0.000~~
192	19.40	102.50	0.68036	0.04701	0.06909	0.940	0.470	0.000

RUN	DP	PB	CD	WD3T	D	VC1	VC-AVE	VC2
193	21.50	101.00	0.66794	0.04449	0.06662	0.890	0.445	0.000
194	19.80	101.50	0.66665	0.04262	0.06393	4.918	4.491	4.065
195	20.00	100.50	0.65601	0.04215	0.06425	9.502	9.081	8.659
196	20.00	100.50	0.63692	0.04092	0.06425	18.248	17.839	17.430

RUN	DP	PB	CD	WD3T	D	VC1	VC-AVE	VC2
197	20.00	99.50	0.65240	0.04470	0.06852	4.944	4.497	4.050
198	20.00	97.50	0.63824	0.04373	0.06852	9.489	9.051	8.614
199	20.00	98.00	0.62991	0.04316	0.06852	18.301	17.870	17.438
200	20.00	98.00	0.64398	0.04412	0.06852	9.515	9.074	8.633
201	20.60	98.50	0.64951	0.04517	0.06954	0.903	0.452	0.000

RUN	DP	PB	CD	WD3T	D	VC1	VC-AVE	VC2
202	18.60	98.00	0.62158	0.03993	0.06424	0.799	0.399	0.000
203	20.00	97.50	0.62306	0.04151	0.06661	5.051	4.636	4.221
204	20.00	98.00	0.61317	0.04085	0.06661	9.514	9.105	8.697
205	20.00	98.00	0.61608	0.04104	0.06661	9.514	9.103	8.693
206	20.00	99.00	0.62163	0.04141	0.06661	18.431	18.017	17.603

RUN	DP	PB	CD	WD3T	D	VC1	VC-AVE	VC2
207	19.90	102.00	0.71946	0.05036	0.06999	1.007	0.504	0.000
208	20.00	102.00	0.69747	0.04894	0.07017	5.078	4.589	4.099
209	20.00	102.00	0.69473	0.04875	0.07017	9.540	9.053	8.565
210	20.00	101.50	0.68738	0.04823	0.07017	18.510	18.028	17.546
211	19.10	99.50	0.72096	0.04944	0.06857	0.989	0.494	0.000
212	21.60	102.00	0.68332	0.04983	0.07292	0.997	0.498	0.000
213	21.90	102.00	0.70332	0.05164	0.07343	1.033	0.516	0.000

RUN	DP	PB	CD	WDOT	D	VC1	VC-AVE	VC2
214	20.50	100.00	0.57649	0.04538	0.07872	0.905	0.454	0.000
215	20.00	101.00	0.68501	0.05396	0.07776	4.997	4.465	3.932
216	20.00	101.50	0.66578	0.05177	0.07776	9.534	9.016	8.496
217	20.00	101.00	0.64174	0.04990	0.07776	13.454	12.935	12.416
218	20.50	102.00	0.57781	0.04549	0.07872	0.910	0.455	0.000

RUN	DP	PB	CD	WDOT	D	VC1	VC-AVE	VC2
219	20.40	99.00	0.71621	0.04904	0.06847	0.904	0.452	0.000
220	20.00	100.00	0.69527	0.04714	0.06780	4.970	4.499	4.027
221	20.00	100.00	0.70408	0.04774	0.06780	9.621	9.143	8.666
222	20.00	100.00	0.66623	0.04521	0.06780	13.510	13.038	12.566
223	20.00	101.00	0.73960	0.05014	0.06780	4.970	4.469	3.968

RUN	DP	PB	CD	WDOT	D	VC1	VC-AVE	VC2
224	20.50	99.50	0.61821	0.05467	0.08930	1.093	0.547	0.000
225	20.00	95.50	0.60296	0.05318	0.08820	4.891	4.359	3.827
226	20.00	101.00	0.60915	0.05373	0.08820	9.194	8.657	8.120
227	20.00	102.00	0.58342	0.05146	0.08820	17.745	17.230	16.716
228	20.00	102.00	0.60408	0.05328	0.08820	4.338	3.806	3.273

RUN	DP	PB	CD	WDOT	D	VC1	VC-AVE	VC2
229	20.00	102.50	0.64021	0.04265	0.06662	4.864	4.437	4.011
230	20.00	101.00	0.65730	0.04379	0.06662	9.408	8.970	8.532
231	20.00	100.00	0.64707	0.04311	0.06662	17.956	17.525	17.094
232	22.00	98.00	0.66479	0.04645	0.06987	0.929	0.465	0.000

RUN	DP	PB	CD	WDOT	D	VC1	VC-AVE	VC2
233	20.10	100.50	0.68382	0.04648	0.06797	0.930	0.465	0.000
234	20.00	101.50	0.68238	0.04627	0.06781	4.837	4.374	3.911
235	20.00	101.00	0.67553	0.04580	0.06781	9.247	8.789	8.331
236	20.00	101.50	0.67166	0.04554	0.06781	17.902	17.447	16.991

RUN	DP	PB	CD	WDOT	D	VC1	VC-AVE	VC2
237	20.00	101.50	0.68926	0.04428	0.06425	4.836	4.393	3.951
238	20.00	101.50	0.66918	0.04299	0.06425	9.354	8.924	8.494
239	20.00	102.00	0.65818	0.04229	0.06425	18.034	17.611	17.188
240	21.50	102.50	0.67899	0.04523	0.06661	0.905	0.452	0.000

RUN	DP	PB	CD	WD3T	D	VC1	VC-AVE	VC2
241	19.60	102.00	0.65304	0.04660	0.07135	0.932	0.466	0.000
242	19.80	102.00	0.61802	0.04432	0.07172	0.886	0.443	0.000
243	19.60	102.00	0.64922	0.04632	0.07135	0.926	0.463	0.000
244	20.00	101.50	0.64340	0.04637	0.07208	4.945	4.461	4.018
245	20.00	101.50	0.64902	0.04678	0.07208	9.463	8.995	8.527
246	20.00	101.50	0.64116	0.04621	0.07208	9.490	9.028	8.565
247	20.00	101.50	0.63779	0.04597	0.07208	18.250	17.791	17.331
~~248~~	~~20.00~~	~~101.00~~	~~0.00000~~	~~0.00000~~	~~0.07208~~	~~18.197~~	~~9.099~~	~~0.000~~

RUN	DP	PB	CD	WD3T	D	VC1	VC-AVE	VC2
249	20.00	101.50	0.66598	0.04942	0.07421	4.918	4.424	3.929
250	20.00	101.50	0.65650	0.04872	0.07421	9.489	9.002	8.515
251	20.00	101.00	0.64853	0.04770	0.07421	16.919	16.442	15.965
252	19.30	102.20	0.67000	0.04864	0.07290	0.977	0.488	0.000

RUN	DP	PB	CD	WD3T	D	VC1	VC-AVE	VC2
253	20.10	101.50	0.75410	0.05108	0.06774	1.022	0.511	0.000
254	20.00	101.50	0.74609	0.05041	0.06757	4.999	4.494	3.990
255	20.00	101.50	0.73981	0.04999	0.06757	9.469	8.989	8.489
256	20.00	102.00	0.72784	0.04918	0.06757	18.036	17.545	17.053

RUN	DP	PB	CD	WD3T	D	VC1	VC-AVE	VC2
257	18.80	100.00	0.65840	0.04737	0.07195	0.947	0.474	0.000
258	20.00	99.50	0.64842	0.04812	0.07421	4.810	4.329	3.848
259	20.00	99.00	0.65096	0.04831	0.07421	9.194	8.711	8.228
260	20.00	100.00	0.65216	0.04840	0.07421	17.639	17.155	16.671

RUN	DP	PB	CD	WD3T	D	VC1	VC-AVE	VC2
261	20.00	101.50	0.72301	0.05297	0.07326	4.945	4.415	3.886
262	20.00	100.50	0.68654	0.05030	0.07326	9.677	9.174	8.671
263	20.00	101.00	0.56878	0.04167	0.07326	18.649	18.232	17.815
264	20.30	100.00	0.52858	0.03873	0.07326	18.675	18.288	17.901
265	21.10	100.50	0.55312	0.04162	0.07525	0.832	0.416	0.000

RUN	DP	PB	CD	WD3T	D	VC1	VC-AVE	VC2
266	18.60	101.50	0.59542	0.04547	0.07636	0.909	0.455	0.000
267	19.90	101.00	0.58369	0.04610	0.07898	0.922	0.461	0.000
268	20.00	101.50	0.57543	0.04556	0.07918	5.051	4.596	4.140
269	20.00	101.50	0.57146	0.04525	0.07918	9.648	9.195	8.743
270	20.00	102.00	0.53238	0.04215	0.07918	18.538	18.116	17.694

RUN	DP	PB	CD	WD ØT	D	VC1	VC-AVE	VC2
271	17.00	102.50	0.83270	0.05205	0.06251	5.078	4.558	4.037
272	17.00	102.50	0.67389	0.04212	0.06251	9.702	9.280	8.859
273	17.00	102.50	0.66330	0.04146	0.06251	18.697	18.282	17.868
274	17.00	102.50	0.83200	0.05201	0.06251	5.078	4.558	4.038
275	17.00	102.00	0.67141	0.04197	0.06251	9.702	9.282	8.862
276	15.60	102.50	0.69287	0.04149	0.05988	0.830	0.415	0.000

RUN	DP	PB	CD	WD ØT	D	VC1	VC-AVE	VC2
277	17.60	102.50	0.62638	0.05321	0.08495	1.064	0.532	0.000

RUN	DP	PB	CD	WD ØT	D	VC1	VC-AVE	VC2
278	16.10	102.50	0.80459	0.05649	0.07020	1.130	0.565	0.000
279	24.70	102.50	0.74618	0.06488	0.08696	1.298	0.649	0.000
280	35.10	99.50	0.74869	0.07761	0.10366	1.552	0.776	0.000
281	42.30	98.00	0.71265	0.08109	0.11379	1.622	0.811	0.000

RUN	DP	PB	CD	WD ØT	D	VC1	VC-AVE	VC2
282	53.50	1.00	0.61664	0.07580	0.12293	1.516	0.758	0.000
283	53.40	52.00	0.74449	0.09143	0.12281	1.829	0.914	0.000
284	52.00	103.00	0.75430	0.09141	0.12119	1.828	0.914	0.000
285	54.30	1.00	0.58524	0.07248	0.12384	1.450	0.725	0.000

RUN	DP	PB	CD	WD ØT	D	VC1	VC-AVE	VC2
286	54.30	3.00	0.60448	0.07320	0.12109	1.464	0.732	0.000
287	55.70	49.00	0.75347	0.09241	0.12265	1.848	0.924	0.000
288	56.90	103.00	0.73695	0.09135	0.12396	1.827	0.914	0.000

RUN	DP	PB	CD	WD ØT	D	VC1	VC-AVE	VC2
289	12.00	103.00	0.72336	0.04211	0.05822	0.842	0.421	0.000
290	24.30	102.50	0.75550	0.06259	0.08285	1.252	0.626	0.000
291	35.90	102.50	0.73341	0.07385	0.10070	1.477	0.739	0.000
292	44.30	102.50	0.71266	0.07972	0.11186	1.594	0.797	0.000
293	13.40	102.50	0.73765	0.04538	0.06152	0.908	0.454	0.000

RUN	DP	PB	CD	WD ØT	D	VC1	VC-AVE	VC2
294	15.60	99.00	0.73350	0.04761	0.06491	0.952	0.476	0.000
295	25.50	98.00	0.74659	0.06196	0.08299	1.239	0.620	0.000
296	35.80	103.00	0.67852	0.06672	0.09834	1.334	0.667	0.000
297	43.20	102.00	0.72768	0.07861	0.10802	1.572	0.786	0.000
298	35.40	100.00	0.71520	0.06994	0.09779	1.399	0.699	0.000

RUN	DP	PB	CD	WD3T	D	VC1	VC-AVE	VC2
299	33.10	100.00	0.72631	0.07311	0.10066	1.462	0.731	0.000
300	43.20	100.00	0.71307	0.08200	0.11499	1.640	0.820	0.000
301	24.60	100.00	0.72710	0.06309	0.08678	1.262	0.631	0.000
302	12.50	101.00	0.84754	0.05224	0.06186	1.045	0.522	0.000

RUN	DP	PB	CD	WD3T	D	VC1	VC-AVE	VC2
303	16.60	101.00	0.83031	0.05909	0.07116	1.182	0.591	0.000
304	23.30	102.00	0.70756	0.05966	0.08431	1.193	0.597	0.000
305	35.30	102.50	0.73430	0.07620	0.10377	1.524	0.762	0.000
306	44.00	105.00	0.73412	0.08506	0.11586	1.701	0.851	0.000
307	25.30	101.00	0.73509	0.06458	0.08785	1.292	0.646	0.000

RUN	DP	PB	CD	WD3T	D	VC1	VC-AVE	VC2
308	26.40	102.00	0.71533	0.06030	0.08429	1.206	0.603	0.000
309	32.80	104.00	0.72714	0.06832	0.09396	1.366	0.683	0.000
310	45.10	103.00	0.69991	0.07711	0.11017	1.542	0.771	0.000
311	14.20	100.00	0.75592	0.04673	0.06182	0.935	0.467	0.000

RUN	DP	PB	CD	WD3T	D	VC1	VC-AVE	VC2
312	13.30	97.50	0.72256	0.04421	0.06119	0.884	0.442	0.000
313	23.30	99.00	0.72969	0.05910	0.08099	1.182	0.591	0.000
314	32.80	99.50	0.71168	0.06839	0.09609	1.368	0.684	0.000
315	46.50	100.00	0.74013	0.08468	0.11441	1.694	0.847	0.000

RUN	DP	PB	CD	WD3T	D	VC1	VC-AVE	VC2
316	13.20	100.00	0.71616	0.04373	0.06106	0.875	0.437	0.000
317	23.10	99.00	0.67933	0.05487	0.08077	1.097	0.549	0.000
318	34.90	100.00	0.73519	0.07299	0.09928	1.460	0.730	0.000
319	46.20	100.00	0.74080	0.08462	0.11423	1.692	0.846	0.000

RUN	DP	PB	CD	WD3T	D	VC1	VC-AVE	VC2
320	45.30	101.50	0.72013	0.07965	0.11061	1.593	0.797	0.000
321	35.80	100.50	0.73192	0.07197	0.09833	1.439	0.720	0.000
322	24.80	100.00	0.73385	0.06006	0.08184	1.201	0.601	0.000
323	13.40	99.00	0.70360	0.04233	0.06016	0.847	0.423	0.000

RUN	DP	PB	CD	WD3T	D	VC1	VC-AVE	VC2
324	14.70	100.00	0.69380	0.04654	0.06708	0.931	0.465	0.000
325	25.40	100.00	0.71613	0.06314	0.08817	1.263	0.631	0.000
326	33.30	102.00	0.73546	0.07425	0.10095	1.485	0.742	0.000
327	46.40	102.00	0.73474	0.08756	0.11917	1.751	0.876	0.000

RUN	DP	PB	CD	WD0T	D	VC1	VC-AVE	VC2
~~0PH~~	~~14.40~~	~~100.00~~	~~0.00000~~	~~0.00000~~	~~0.06636~~	~~4.917~~	~~2.458~~	~~0.000~~
329	14.50	100.00	0.70386	0.04688	0.06661	4.890	4.421	3.952
330	14.50	100.50	0.68683	0.04588	0.06661	9.272	8.813	8.354
331	14.50	100.50	0.69897	0.04656	0.06661	9.272	8.807	8.341
332	14.50	101.00	0.69679	0.04641	0.06661	9.192	8.727	8.263
333	41.90	100.00	0.72396	0.08197	0.11323	1.639	0.820	0.000
334	44.10	100.50	0.70188	0.08153	0.11616	1.631	0.815	0.000
335	44.40	101.00	0.72215	0.08417	0.11656	1.683	0.842	0.000
336	45.30	50.00	0.70170	0.08261	0.11773	1.652	0.826	0.000
~~337~~	~~46.40~~	~~0.00~~	~~0.00000~~	~~0.00000~~	~~0.11916~~	~~0.000~~	~~0.000~~	~~0.000~~
338	43.80	0.00	0.61070	0.07070	0.11577	1.414	0.707	0.000

RUN	DP	PB	CD	WD0T	D	VC1	VC-AVE	VC2
339	14.50	99.50	0.80509	0.05721	0.07106	4.945	4.373	3.801
340	14.50	99.00	0.73157	0.05199	0.07106	4.945	4.425	3.905
341	14.50	99.00	0.74127	0.05268	0.07106	4.945	4.418	3.892
342	14.50	98.50	0.72053	0.05120	0.07106	9.329	8.817	8.305
343	14.50	98.00	0.69528	0.04941	0.07106	18.251	17.757	17.263

RUN	DP	PB	CD	WD0T	D	VC1	VC-AVE	VC2
344	14.50	99.00	0.88354	0.05530	0.06258	18.384	17.831	17.278
345	14.50	98.50	0.86883	0.05437	0.06258	9.383	8.839	8.295
346	14.50	98.50	0.90213	0.05646	0.06258	17.745	17.181	16.616
347	14.50	98.00	0.86969	0.05443	0.06258	9.409	8.865	8.321

RUN	DP	PB	CD	WD0T	D	VC1	VC-AVE	VC2
348	14.50	97.50	0.76957	0.04925	0.06400	5.080	4.587	4.095
349	14.50	96.00	0.76313	0.04884	0.06400	9.436	8.948	8.459
350	14.50	101.00	0.77188	0.04940	0.06400	9.436	8.942	8.448
351	14.50	101.00	0.75031	0.04802	0.06400	17.665	17.185	16.705

RUN	DP	PB	CD	WD0T	D	VC1	VC-AVE	VC2
352	14.50	101.00	0.63264	0.04879	0.07712	5.080	4.592	4.104
353	14.50	100.50	0.62776	0.04841	0.07712	9.436	8.952	8.468
354	14.50	101.50	0.63858	0.04925	0.07712	17.479	16.986	16.494
355	15.50	100.50	0.65057	0.05187	0.07973	1.037	0.519	0.000

RUN	DP	PB	CD	WD0T	D	VC1	VC-AVE	VC2
356	16.60	100.00	0.86075	0.05763	0.06696	1.153	0.576	0.000

RUN	DP	PB	CD	WDOT	D	VC1	VC-AVE	VC2
357	14.50	100.00	0.60844	0.04692	0.07711	5.106	4.637	4.167
358	14.50	100.00	0.60000	0.04627	0.07711	9.461	8.998	8.536
359	14.50	100.00	0.57761	0.04454	0.07711	18.114	17.669	17.223
360	14.50	100.00	0.62984	0.04857	0.07711	5.106	4.620	4.134
361	16.10	100.00	0.60873	0.04946	0.08125	0.989	0.495	0.000

RUN	DP	PB	CD	WDOT	D	VC1	VC-AVE	VC2
362	14.00	100.50	0.84353	0.05581	0.06546	1.104	0.552	0.000
363	14.50	100.50	0.86571	0.05767	0.06661	5.106	4.529	3.952
364	14.50	100.00	0.86318	0.05750	0.06661	9.542	8.967	8.392
365	14.50	100.00	0.89508	0.05963	0.06661	17.795	17.199	16.602

RUN	DP	PB	CD	WDOT	D	VC1	VC-AVE	VC2
366	14.50	100.50	0.79723	0.04651	0.05834	5.133	4.668	4.203
367	14.50	100.00	0.76021	0.04435	0.05834	9.595	9.152	8.708
368	14.50	100.00	0.68337	0.03987	0.05834	17.981	17.582	17.184
369	14.50	100.50	0.76370	0.04455	0.05834	18.008	17.562	17.117
370	15.20	100.00	0.83892	0.05011	0.05973	1.002	0.501	0.000

RUN	DP	PB	CD	WDOT	D	VC1	VC-AVE	VC2
371	15.10	100.50	0.87981	0.05745	0.06530	1.149	0.575	0.000
372	14.50	101.00	0.91776	0.05873	0.06399	5.133	4.545	3.958
373	14.50	100.50	0.89325	0.05716	0.06399	9.568	8.997	8.425
374	14.50	101.00	0.94364	0.06038	0.06399	18.008	17.404	16.800

RUN	DP	PB	CD	WDOT	D	VC1	VC-AVE	VC2
375	14.50	100.50	0.85722	0.06091	0.07106	5.133	4.524	3.914
376	14.50	102.00	0.88153	0.06264	0.07106	9.595	8.969	8.342
377	14.50	102.00	0.91237	0.06483	0.07106	18.008	17.359	16.711
378	14.10	103.00	0.87550	0.06134	0.07007	1.227	0.613	0.000

RUN	DP	PB	CD	WDOT	D	VC1	VC-AVE	VC2
379	14.50	100.00	0.67183	0.06035	0.08982	4.755	4.151	3.548
380	14.50	99.50	0.66653	0.05987	0.08982	9.084	8.486	7.887
381	14.50	99.50	0.57984	0.05208	0.08982	9.044	8.523	8.002
382	45.80	105.00	0.66151	0.10560	0.15964	2.112	1.056	0.000
383	43.90	53.00	0.52411	0.08191	0.15629	1.638	0.819	0.000
384	45.60	0.00	0.55511	0.08842	0.15929	1.768	0.884	0.000

RUN	DP	PB	CD	WDØT	D	VC1	VC-AVE	VC2
385	14.20	99.00	0.71741	0.06377	0.08889	1.275	0.638	0.000
386	14.50	98.00	0.70255	0.06310	0.08982	4.890	4.259	3.627
387	14.50	99.00	0.70035	0.06291	0.08982	4.863	4.234	3.604
388	14.50	97.50	0.70216	0.06307	0.08982	9.353	8.722	8.091
389	14.50	98.50	0.68416	0.06145	0.08982	17.713	17.098	16.484
390	14.50	98.00	0.70129	0.06299	0.08982	4.917	4.287	3.657

RUN	DP	PB	CD	WDØT	D	VC1	VC-AVE	VC2
391	14.50	99.00	0.83697	0.05947	0.07105	4.943	4.349	3.754
392	14.50	99.00	0.83751	0.05951	0.07105	9.379	8.784	8.189
393	14.50	98.50	0.86535	0.06148	0.07105	17.553	16.938	16.324
394	14.30	99.00	0.80830	0.05703	0.07056	1.141	0.570	0.000

RUN	DP	PB	CD	WDØT	D	VC1	VC-AVE	VC2
395	13.60	102.00	0.85065	0.05271	0.06197	1.054	0.527	0.000
~~396~~	~~13.50~~	~~102.00~~	~~0.00000~~	~~0.00000~~	~~0.06174~~	~~0.000~~	~~0.000~~	~~0.000~~
397	12.90	98.50	0.84757	0.05115	0.06035	1.023	0.512	0.000
398	14.50	98.00	0.86412	0.05529	0.06398	4.943	4.390	3.837
399	14.50	97.50	0.88501	0.05663	0.06398	9.378	8.812	8.246
400	14.50	98.50	0.90599	0.05797	0.06398	18.003	17.424	16.844

RUN	DP	PB	CD	WDØT	D	VC1	VC-AVE	VC2
401	14.50	98.50	0.81429	0.07314	0.08981	5.050	4.319	3.588
402	14.50	98.50	0.82642	0.07422	0.08981	9.485	8.743	8.000
403	14.30	99.00	0.86862	0.07747	0.08919	18.029	17.254	16.479
404	15.20	100.00	0.79938	0.07351	0.09196	1.470	0.735	0.000

RUN	DP	PB	CD	WDØT	D	VC1	VC-AVE	VC2
405	16.20	100.00	0.80273	0.07621	0.09494	1.524	0.762	0.000
406	14.50	99.00	0.81253	0.07298	0.08982	5.158	4.428	3.699
407	14.50	100.00	0.83233	0.07476	0.08982	9.619	8.872	8.124
408	14.50	99.00	0.85801	0.07706	0.08982	18.242	17.471	16.701
409	14.50	99.00	0.81321	0.07304	0.08982	5.131	4.401	3.671

TABLE A-2

TABLE OF DATA FOR ORIFICE FLOW TESTS

WITH ACTUAL PROPELLANTS

	Test No.	ΔP, psid	$\dot{W}$, lb/sec	C_D	Reynolds No.
NTO (Oxidizer)	Oxidizer-1	17.3	0.0648	0.640	48,000
	Oxidizer-2	16.2	0.0641	0.656	48,400
	Oxidizer-3	26.1	0.0797	0.641	60,000
	Oxidizer-4	35.0	0.0923	0.641	69,500
	Oxidizer-5	41.7	0.1021	0.650	77,000
	Oxidizer-6	27.0	0.0784	0.620	59,000
UDMH/N_2H_4 (Fuel)	Fuel-1	13.8	0.0436	0.785	17,400
	Fuel-2	34.5	0.0529	0.602	21,100
	Fuel-3	28.3	0.0606	0.762	24,200
	Fuel-4	41.6	0.0691	0.717	27,600
	Fuel-5	22.2	0.0545	0.774	21,800

NOTE: $A_{ox} = 0.00382$ in.^{2}

$A_{fuel} = 0.00298$ in.^{2}

TABLE A-3

TABLE OF DATA FOR MIXING DISTRIBUTION TESTS

SYMBOLS

MR = mixture ratio, $\dot{w}_{ox}/\dot{w}_f$

$$N = \frac{1}{1 + \left(\frac{D_{ox}}{D_{fuel}}\right)_{II} \left(\frac{1}{MR^2}\right) \left(\frac{\rho_o}{\rho_f}\right) \left(\frac{A_o}{A_f}\right)}$$

$\eta_{c^*_{mix}}$ = predicted mixing limited c* efficiency

V_c = cross velocity, ft/sec

X = spray nozzle spacing, inches

θ = spray nozzle impingement angle, degrees

$$E_m = 100 \left[1 - \sum_i^n \frac{\dot{w}_i}{\dot{w}_T} \frac{(R-r_i)}{R} - \sum_i^n \frac{\dot{w}_i}{\dot{w}_T} \frac{(R-\bar{r}_i)}{(R-1)} \right]$$

where

E_m = mixing index

$\dot{w}_i/\dot{w}_T$ = mass fraction in the i^{th} tube

R = ratio of oxidizer mass to total oxidizer and fuel mass to total oxidizer plus fuel mass

r_i = ratio of oxidizer mass to total oxidizer and fuel mass in an individual stream tube for $r_i < R$

$\bar{r}_i$ = ratio of oxidizer mass to total oxidizer and fuel mass in an individual stream tube for $r_i > R$

Run	Element Type	$\dot{W}_T$	MR	N	E_m	η_{c^*mix}	V_c	X	0
1	A	0.1820	1.65	0.530	70.24	90.75			
2	A	0.1780	1.09	0.325	57.15	89.55			
3	A	0.1815	2.08	0.639	67.40	90.16			
4	B	0.1813	1.60	0.534	74.21	93.06			
5	B	0.1782	1.09	0.345	70.24	93.31			
6	B	0.1815	2.15	0.670	59.88	84.20			
7	C	0.1816	1.71	0.525	80.01	95.35			
8	C	0.1765	1.08	0.306	69.69	93.48			
9	C	0.1784	2.10	0.626	62.21	86.98			
10	D	0.1763	1.59	0.491	84.76	97.48			
11	D	0.1758	1.09	0.315	74.48	95.37			
12	D	0.1784	2.07	0.619	69.61	91.45			
13	E	0.1788	1.61	0.493	84.82	96.56			
14	F	0.1785	1.62	0.495	81.32	95.83			
15	H	0.1789	1.66	0.565	78.69	95.26			
16	H	0.1748	1.09	0.357	76.18	96.37			
17	H	0.1828	2.11	0.654	70.45	92.30			
18	F	0.1776	1.13	0.323	73.15	95.51			
19	F	0.1802	2.09	0.624	65.84	89.49			
20	J	0.1787	1.67	0.589	73.34	94.74			
21	J	0.1760	1.06	0.364	70.78	95.33			
22	J	0.1828	2.09	0.712	65.75	89.78			
23	P	0.1818	1.65	0.680	68.01	90.64			
24	P	0.1786	1.10	0.487	84.98	98.19			
25	P	0.1838	2.07	0.770	64.38	89.15			
26	R	0.1793	1.65	0.654	68.44	90.89			
27	R	0.1750	1.09	0.448	80.09	96.90			
28	R	0.1810	2.16	0.763	66.41	89.95			
29	T	0.1853	1.51	0.619	64.16	88.82			
30	T	0.1759	1.11	0.468	79.39	97.01			
31	T	0.1828	2.09	0.737	61.20	88.13			

Run	Element Type	$\dot{W}_T$	MR	N	E_m	η_{c^*mix}	V_c	X	0
32	A	0.1795	1.65	0.525	69.14	90.55			
33	A	0.1753	1.09	0.324	Not Reduced				
34	A	0.1769	2.14						
35	Fan	0.1710	1.64					1.0	60
36	Fan 2*	0.1681	1.57		76.35	93.41		1.0	60
37	Fan 2	0.1712	1.59		67.06	90.67		1.0	45
38	Fan 2	0.1713	1.57		74.62	92.22		1.0	75
39	Fan 2	0.1718	1.61		71.31	89.80		0.5	75
40	Fan 2	0.1719	1.60		71.45	90.50		0.5	60
41	Fan 2	0.1715	1.61		72.47	90.14		0.5	45
42	Swirl	0.1539	1.56		45.89	74.66		0.5	0
43	Swirl	0.1548	1.60		46.16	80.41		0.5	60
44	P	0.1704	0.78	0.240	74.61	99.61			
45	R	0.1768	0.86	0.294	84.20	98.73			
46	T	0.1765	0.85	0.290	79.42	98.93			
47	A	0.1792	1.46	0.462	87.00	95.57	0		
48	Fan 2	0.1796	1.49		66.07	85.64		1.0	20
49	Fan 2	0.1804	1.53		47.21	71.44		1.0	0
50	Fan 2	0.1773	1.56		64.68	88.70		0.5	20
51	A	0.1761	1.68	0.532	79.88	95.39	10		
52	D	0.1795	1.53	0.461	81.21	96.35	0		
53	F	0.1773	1.60	0.489	71.82	91.62	0		
54	F	0.1761	1.68	0.513	75.40	93.98	10		
55	D	0.1761	1.69	0.510	79.55	95.72	10		
56	D	0.1761	1.69	0.510	76.21	93.62	20		
57	F	0.1761	1.69	0.516	73.84	93.61	20		
58	A	0.1761	1.69	0.535	79.65	95.79	20		
59	Fan 2	0.1780	1.67		33.25	69.03		0.5	20
60	A	0.2127	1.62	0.514	73.71	93.42			
61	A	0.4090	1.59	0.505	69.02	91.76			

*Element 8006/8006

Run	Element Type	$\dot{w}_T$	MR	N	E_m	η_{c^*mix}	V_c	X	θ
62	A	0.0812	1.65	0.523	78.92	94.89			
63	A	0.2307	1.66	0.526	69.84	91.88			
64	A-Round*	0.2278	1.59	0.505	76.78	94.13			
65	Fan 4**	0.0862	1.58		41.17	71.10		0.5	60
66	Fan 4	0.2241	1.57		59.85	84.68		0.5	60
67	Fan 4	0.4097	1.60		63.63	86.48		0.5	60
68	Fan 4	0.2256	1.02		55.93	89.05		0.5	60
69	Fan 4	0.2266	2.07		55.72	80.22		0.5	60

*Rounded orifice entrance
**Element 8006/8008

TABLE A-4

TABLE OF ATOMIZATION DATA FOR SELF-ATOMIZING NOZZLES

Run	Nozzle No.	Equivalent* Diameter, inch	ΔP, psi	ẇ, lb/sec	V, ft/sec	$\overline{D}$, μ	Remarks
28	800050	0.018	30	--	75	122	All self-atomizing nozzles are flowing separated; therefore, the velocity was determined using the equation shown below. The velocity coefficient C_v was assumed equal to 0.98
29	↓	↓	66	--	111	105	
30			100	--	136	92	
7	8001	0.026	100	--	133	134	
8			62	--	104	131	$V = 0.98\sqrt{2gLP/\rho}$
9			30	--	73	141	
1A			12	0.00748	46	306	All fan self-atomizing nozzles canted 60 degrees toward each other--spacing between fans, 0.5 inch.
2A			345	0.020	246	92	
5A			29	0.0113	71	164	
6A			59	0.0151	102	140	
7A	↓	↓	99	0.01665	132	111	
10	8002	0.036	100	--	136	159	
11			62	--	107	187	
12			28	--	72	207	
13	8006	0.062	100	--	136	221	
14			60	--	107	280	
15			30	--	75	355	
34			10	--	44	445	
3A			9	--	40	395	
4A	↓	↓	345	0.2019	256	111	
25	8008	0.072	30	--	75	455	

*See Table 18 for orifice sizes

TABLE A-4 (concluded)

Run	Nozzle No.	Equivalent Diameter, inch	ΔP, psi	$\dot{w}$, lb/sec	V, ft/sec	$\overline{D}$, μ	Remarks
26	8008	0.072	60	0.107	107	338	
27	↓	↓	100	--	136	256	
1	1/4 M-26	0.086	100	0.0581		192	Mechanical swirl
2	↓	↓	60	0.0457		247	↓
3	↓	↓	30	0.0303		305	
4	1/8 B-2	0.0785	100	0.0651		180	Hydraulic swirl
5	↓	↓	60	0.0507		208	↓
6	↓	↓	30	0.0396		280	
16	1/8 B-3	0.004	30	--		320	
17	↓	↓	100	0.8527		177	
19	1/8 B-1	0.062	33	--		285	
20	↓	↓	61	0.0267		186	
21	↓	↓	101	0.0340		151	
22	1/8 B-05	0.124	35	--		270	
23	↓	↓	60	--		195	
24	↓	↓	98	0.0195		142	↓

Symbols:

ΔP = pressure drop across nozzle, psid

$\dot{w}$ = flowrate, lb/sec

V = injection velocity, ft/sec

$\overline{D}$ = mass median dropsize, microns

TABLE A-5

SUMMARY OF DROPSIZE RESULTS FOR UNLIKE-DOUBLET ORIFICE INJECTOR

Circle/Circle

Run	Wax System			H_2O System				$\rho_f V_f^2/\rho_o V_o^2$	Wax
	D_f	W_f	V_f	D_o	W_o	V_o	N	ϕ	$\bar{D}$
39	0.060	0.088	94.0	0.070	0.120	72.0	0.472	1.33	182
40	0.060	0.062	66.2	0.070	0.090	54.0	0.504	1.13	291
41	0.060	0.047	50.2	0.070	0.055	33.0	0.397	1.71	424
42	0.060	0.029	31.0	0.070	0.052	31.2	0.607	.727	405
43	0.060	0.039	39.5	0.070	0.047	28.2	0.437	1.45	500
68	0.062	0.042	42.5	0.070	0.043	25.8	0.335	2.23	589
69	0.062	0.089	90.0	0.070	0.102	61.2	0.387	1.78	229
70	0.062	0.066	66.8	0.070	0.151	90.5	0.716	.451	175
71	0.062	0.046	46.4	0.070	0.076	45.6	0.568	.857	302
72	0.062	0.037	37.4	0.070	0.081	48.6	0.698	.485	284
73	0.062	0.111	112.0	0.070	0.223	133.7	0.660	.575	113
74	0.062	0.150	152.0	0.070	0.155	92.9	0.340	1.96	133
1A	0.062	0.0306	31	0.070	0.0427	25.6	0.504	1.12	614
2A	0.062	0.0298	30	0.070	0.0625	37.4	0.70	.468	374
3A	0.062	0.0498	50.5	0.070	0.0445	26.6	0.294	2.68	495
4A	0.062	0.0507	51.4	0.070	0.0680	40.7	0.485	1.19	366
5A	0.062	0.0496	50.7	0.070	0.1052	63.2	0.702	.475	237
6A	0.062	0.0684	69.2	0.070	0.0621	37.3	0.302	2.59	368
7A	0.062	0.069	70	0.070	0.0951	56.0	0.500	1.12	279
8A	0.062	0.0684	69.2	0.070	0.1473	88.5	0.707	.462	195
9A	0.062	0.0883	89.4	0.070	0.0805	48.4	0.304	2.58	289
10A	0.062	0.0883	89.4	0.070	0.1250	75	0.513	1.07	209
11A	0.062	0.0788	80	0.070	0.164	98.5	0.695	.495	202
12A	0.062	0.1061	108	0.070	0.1000	60	0.316	2.42	215
13A	0.062	0.0283	28.6	0.070	0.0417	25.1	0.532	.985	559
	H_2O System			Wax System					
35	0.060	0.051	41.6	0.070	0.062	48.6	0.549	.96	356
36	0.060	0.073	59.6	0.070	0.088	69.0	0.545	.978	255
37	0.060	0.093	75.9	0.070	0.112	87.9	0.544	.978	185
38	0.060	0.037	30.2	0.070	0.048	37.7	0.581	.84	527
75	0.062	0.190	155.1	0.070	0.138	108.3	0.303	2.64	118
76	0.062	0.139	113.4	0.070	0.206	161.6	0.614	.641	121
77	0.062	0.111	90.6	0.070	0.084	65.9	0.320	2.45	207
82	0.062	0.054	44.1	0.070	0.046	36.1	0.374	1.95	353

TABLE A-5 (concluded)

Circle/Circle (Continued)

Run	H_2O System			Wax System				$\rho_f V_f^2/\rho_o V_o^2$	Wax
	D_f*	W_f	V_f	D_o	W_o	V_o	N	ø	$\bar{D}$
83	0.062	0.035	28.6	0.070	0.058	45.5	0.693	.519	554
84	0.062	0.069	56.3	0.070	0.110	86.3	0.677	.556	207
85	0.062	0.105	85.7	0.070	0.106	83.2	0.454	1.39	204
Triangle		Wax System			H_2O System				
53	0.0465	0.096	115	0.0543	0.130	84.5	0.44	1.42	245
54	0.0465	0.073	86.5	0.0543	0.104	67.8	0.475	1.25	328
55	0.0465	0.047	55.5	0.0543	0.079	51.6	0.56	.89	418
		H_2O System			Wax System				
50	0.0465	0.099	90.5	0.0543	0.126	107	0.544	.935	250
51	0.0465	0.080	73.5	0.0543	0.094	80.2	0.510	1.09	336
52	0.0465	0.059	54	0.0543	0.063	53.7	0.459	1.33	416
Rectangle		Wax System			H_2O System				
44	0.0512	0.091	121	0.0579	0.122	83	0.41	1.63	221
45	0.0512	0.071	94.5	0.0579	0.099	67.5	0.429	1.50	287
46	0.0512	0.046	61.3	0.0579	0.075	51.2	0.51	1.09	396
		H_2O System			Wax System				
47	0.0512	0.056	57	0.0579	0.066	58.6	0.481	1.22	478
48	0.0512	0.073	74.5	0.0579	0.097	86.4	0.537	.972	326
49	0.0512	0.091	92.4	0.0579	0.123	109	0.548	.935	230

*D = Hydraulic Diameter for noncircular elements and orifice diameter for circular elements

Symbols:

D_f = fuel orifice hydraulic diameter, inches

$\dot{w}_f$ = fuel simulant flowrate, lb/sec

V_f = fuel simulant injection velocity, ft/sec

D_o = oxidizer orifice hydraulic diameter, inches

$\dot{w}_o$ = oxidizer simulant flowrate, lb/sec

V_o = oxidizer simulant injection velocity, ft/sec

N = Rupe factor $\dfrac{1}{1+\left(\dfrac{D_o}{D_f}\right)\left(\dfrac{1}{MR^2}\right)\left(\dfrac{\rho_o}{\rho_f}\right)}$

ø = dynamic pressure ratio $\dfrac{\rho_f V_f^2}{\rho_{ox} V_{ox}^2}$

$\bar{D}$ = wax droplet mass median diameter, microns

TABLE A-6

TABLE OF HOT-FIRE DATA

SYMBOLS

L* = characteristic chamber length, inches

P_c = chamber pressure, psia

MR = mixture ratio, $\dot{w}_o/\dot{w}_f$

$\dot{w}$-TOT = total flowrate, lb/sec

N = Rupe factor $= \left[1 + \left(\frac{D_{ox}}{D_{fuel}}\right)_{II}\left(\frac{1}{MR^2}\right)\left(\frac{\rho_o}{\rho_f}\right)\left(\frac{A_o}{A_f}\right)\right]^{-1}$

N-c* = c* efficiency, percent

CIRCULAR ORIFICES

RUN	L#	PC	M.N.	N-1.5T	N	N-C*
2	30.0	102.31	1.349	0.150	0.433	69.63
3	30.0	80.34	1.491	0.173	0.482	71.54
4	30.0	114.89	1.410	0.091	0.454	60.59
5	30.0	140.79	1.597	0.354	0.549	64.50
6	30.0	154.33	0.994	0.170	0.273	41.59
7	30.0	119.91	1.408	0.379	0.577	65.60
8	60.0	120.57	1.585	0.255	0.499	75.69
9	60.0	101.91	1.593	0.295	0.515	74.92
10	15.0	98.62	1.487	0.231	0.466	61.96
11	15.0	100.99	1.587	0.273	0.497	57.64
12	30.0	55.76	1.490	0.154	0.482	69.83
13	30.0	55.45	1.285	0.124	0.409	70.39

RECTANGULAR ORIFICES

RUN	L#	PC	M.N.	N-1.5T	N	N-C*
15	30.0	111.96	1.536	0.271	0.476	64.92
16	30.0	89.91	1.510	0.181	0.468	73.55
17	30.0	141.60	1.511	0.369	0.463	60.84
18	30.0	88.56	1.670	0.179	0.513	77.54
19	60.0	114.21	1.047	0.245	0.293	73.58
20	30.0	88.16	1.039	0.192	0.295	73.91
21	60.0	113.35	2.266	0.218	0.660	85.15
22	30.0	102.98	1.576	0.202	0.571	71.53
23	60.0	98.50	1.560	0.230	0.476	73.54
24	60.0	98.36	1.575	0.232	0.484	77.95
25	15.0	101.28	1.519	0.249	0.485	63.59
26	15.0	103.92	1.561	0.256	0.479	60.45

SPRAY NOZZLES

RUN	L*	PC	M.R.	M-TOT	N	N-C*
28	30.0	140.28	1.510	0.2[illegible]	0.470	82.42
29	30.0	83.53	1.520	0.196	0.473	68.16
30	30.0	50.03	1.480	0.153	0.460	52.38
31	30.0	53.22	1.713	0.167	0.533	51.40
32	30.0	166.23	1.525	0.314	0.474	84.92
33	30.0	110.66	1.559	0.221	0.305	82.56
34	30.0	103.13	1.072	0.213	0.308	79.75
35	30.0	96.92	1.059	0.204	0.303	78.77
36	30.0	72.64	1.958	0.207	0.598	57.86
37	30.0	92.98	1.978	0.249	0.603	61.71
38	30.0	181.13	1.741	0.349	0.541	84.35
39	30.0	189.14	1.613	0.358	0.502	85.91
40	15.0	102.99	1.559	0.255	0.485	66.22
41	15.0	95.80	1.604	0.253	0.499	62.44
42	60.0	91.50	1.625	0.190	0.506	79.77
43	60.0	98.31	1.594	0.204	0.496	80.16
44	60.0	107.54	1.065	0.210	0.313	87.05

TRIANGULAR ORIFICES

RUN	L*	PC	M.R.	M-TOT	N	N-C*
45	30.0	94.45	1.559	0.243	0.504	64.99
46	30.0	108.05	1.544	0.304	0.499	59.40
47	30.0	77.18	1.568	0.165	0.507	78.68
48	30.0	74.34	1.463	0.159	0.472	79.09
49	30.0	121.89	1.075	0.270	0.325	78.02
50	30.0	84.27	1.056	0.193	0.317	76.18
51	30.0	95.39	1.079	0.220	0.327	75.68
52	30.0	119.30	2.032	0.29[illegible]	0.633	71.26
53	30.0	75.36	2.077	0.183	0.643	72.55
54	30.0	80.72	1.954	0.186	0.614	75.91
55	30.0	92.62	1.984	0.201	0.622	80.82
56	30.0	119.96	1.547	0.371	0.502	56.06
57	15.0	93.77	1.531	0.310	0.496	52.66
58	15.0	96.61	1.564	0.322	0.507	52.46
59	60.0	104.04	1.546	0.248	0.501	73.52
60	60.0	102.34	1.549	0.243	0.502	73.84

CIRCULAR ORIFICES

RUN	L*	PC	M.N.	M-TOT	N	N-C*
61	30.0	94.94	1.541	0.291	0.499	59.49
62	30.0	104.06	1.555	0.322	0.504	57.20
63	30.0	78.70	1.605	0.179	0.519	78.15
64	30.0	88.99	1.551	0.237	0.503	67.21
65	30.0	133.49	1.087	0.288	0.332	85.02
61	30.0	94.94	1.541	0.291	0.499	59.49
62	30.0	104.06	1.555	0.322	0.504	57.20
63	30.0	78.70	1.605	0.179	0.519	78.15
64	30.0	88.99	1.551	0.237	0.503	67.21
65	30.0	133.49	1.087	0.288	0.332	85.02

CIRCULAR ORIFICES (ROUNDED ENTRANCES)

RUN	L*	PC	M.N.	M-TOT	N	N-C*
71	30.0	97.76	1.646	0.317	0.532	55.81
72	30.0	87.13	1.697	0.246	0.548	64.29
73	30.0	49.18	1.308	0.120	0.419	74.56
74	30.0	47.01	1.403	0.120	0.453	71.30
75	30.0	71.37	1.588	0.172	0.515	75.58
76	30.0	60.93	1.612	0.148	0.522	75.39
77	30.0	99.80	1.155	0.249	0.360	74.44
78	30.0	94.17	1.978	0.240	0.622	73.07
79	30.0	120.06	2.058	0.319	0.642	70.34
80	30.0	102.54	2.006	0.273	0.629	70.26
81	30.0	110.43	1.645	0.373	0.535	54.70
82	60.0	118.90	1.663	0.295	0.538	74.61
83	60.0	128.78	1.678	0.317	0.543	75.27
84	60.0	42.83	1.618	0.153	0.524	58.17
86	60.0	61.33	1.693	0.149	0.547	77.25
87	60.0	81.07	1.774	0.185	0.570	68.35
88	60.0	98.26	1.874	0.229	0.597	81.10
89	60.0	105.58	1.667	0.260	0.540	76.02

11.0 APPENDIX B

ANALYSIS OF EXPERIMENTAL ERROR

When several measured variables are combined algebraically to yield an experimental result, the standard deviation of the result, which takes into account the propagation of the individual errors, is given by the following equation (Ref. B-1):

$$S_R \simeq \sqrt{\sum_{i=1}^{n} \left(\frac{\partial R}{\partial X_i} \right)^2 S_i^2} \qquad \text{(B-1)}$$

where

S_R = estimate of standard deviation of the calculated result

X_i = the ith variable required to compute the result

R = R (X_i's)

S_i = estimate of the standard deviation of the ith variable

If the individual measurements are combined by addition, and are independent, the standard deviation is given by:

$$S_R = \sqrt{\sum_{i=1}^{n} S_i^2} \qquad \text{(B-2)}$$

Equation (B-1) is rather difficult to apply. An easier form can be obtained by normalizing with respect to the dependent variable, R:

$$\frac{S_R}{R} = \sqrt{\sum_{i=1}^{n} a_i^2 \left(\frac{S_i}{X_i} \right)^2} \qquad \text{(B-1a)}$$

where

a_i = exponent of X_i in the equation $R = R(X_i)$

Reference B-1: Arkin, H. and Colton, R. R., Statistical Methods, Barnes & Noble, Inc., New York.

In Eq. B-1a, the standard deviation of the dependent variable, expressed as a percentage of the variable, is given as a function of the percentage deviations of each independent variable.

THE ORIFICE COEFFICIENT

The equation required to compute an orifice coefficient from a set of data is:

$$C_D = \frac{\dot{w}}{A\sqrt{2\rho\ \Delta P}} \tag{B-3}$$

where

$\dot{w}$ = flowrate, lb/sec

A = orifice area, $in.^2$

ρ = pressure drop, lb/ft^3

ΔP = pressure drop, lbm/ft^2-delta

To estimate the standard deviation of a given orifice coefficient, Eq. B-3 is used to generate a specific equation of the form of Eq. B-1a for (S_{C_D}/C_D):

$$S_{C_D} = \sqrt{\left(\frac{S_A}{A}\right)^2 + \left(\frac{S_{\dot{w}}}{\dot{w}}\right)^2 + \frac{1}{4}\left(\frac{S_\rho}{\rho}\right)^2 + \frac{1}{4}\left(\frac{S_{\Delta P}}{\Delta P}\right)^2} \tag{B-4}$$

A list of the estimated, normalized standard deviations of each independent variable is given in Table B-1.

TABLE B-1

ESTIMATED STANDARD DEVIATIONS FOR THE DEPENDENT VARIABLES REQUIRED TO COMPUTE C_D

Variable X_i	$(S_{X_i}/X_i) \times 100$, percent
A	2.0
$\dot{w}$	2.0
ρ	0.5
ΔP	2.0

The estimated deviations presented in Table B-1 for $\dot{w}$ and ΔP include considerations of repeatability under dynamic test conditions as well as static calibration of instrumentation. Substitution of the numbers in Table B-1 into Eq. B-4 yields an estimated deviation for C_D:

$$\frac{S_{C_D}}{C_D} \times 100 = 3.01 \text{ percent}$$

For an orifice coefficient value of 0.75, this would produce the following limits:

$$C_D = 0.75 \pm 0.0226$$

or

$$0.7274 < C_D < 0.7726$$

CHARACTERISTIC VELOCITY

The equation used to compute the characteristic velocity for a given test from the measured independent variables is:

$$c^* = \frac{P_c A_t g}{\dot{w}_t} \tag{B-5}$$

where

P_c = chamber pressure, psia

A_t = throat area, $in.^2$

$\dot{w}_t$ = flowrate, lb/sec

It must be remembered that the total flowrate is composed of two separate flowrates; i.e.,

$$\dot{w}_t = \dot{w}_o + \dot{w}_f \tag{B-6}$$

or, in terms of mixture ratio

$$\dot{w}_t = \dot{w}_o \left(\frac{MR+1}{MR}\right) \tag{B-7}$$

Equation B-5 may be written:

$$c^* = \frac{P_c A_t g}{\dot{w}_o + \dot{w}_f} \tag{B-8}$$

Analysis of standard deviation for Eq. B-8 is extremely complex because of such factors as: (1) during a test, the throat area may change in either a predictable or unpredictable manner, (2) each flowrate is a composite measurement in itself, requiring a reading of cycles per second, a flowmeter calibration, and a fluid density, and (3) chamber pressure must be determined from a static pressure by assumption of isentropic flow in the convergent section of the nozzle. Therefore, what follows is an extremely crude estimate of the standard deviation of c* based only on known error sources. First, an equation of the form of Eq. B-1a must be generated:

$$\frac{S_{c^*}}{c^*} = \sqrt{\left(\frac{S_{P_c}}{P_c}\right)^2 + \left(\frac{S_{A_t}}{A_t}\right)^2 + \left(\frac{S_{\dot{w}_t}}{\dot{w}_t}\right)^2} \tag{B-9}$$

Equation B-2 is used to estimate $S_{\dot{w}_t}$. This is dictated by knowledge of Eq. B-6.

$$S_{\dot{w}_t} = \sqrt{S^2_{\dot{w}_{ox}} + S^2_{\dot{w}_t}} \tag{B-10}$$

Equation B-10 is then divided by $\dot{w}_t$:

$$\frac{S_{\dot{w}_t}}{\dot{w}_t} = \sqrt{\left(\frac{S_{\dot{w}_{ox}}}{\dot{w}_t}\right)^2 + \left(\frac{S_{\dot{w}_f}}{\dot{w}_t}\right)^2}$$

or

$$\frac{S_{\dot{w}_t}}{\dot{w}_t} = \sqrt{\left(\frac{S_{\dot{w}_{ox}}}{\dot{w}_{ox}}\,\frac{\dot{w}_{ox}}{\dot{w}_t}\right)^2 + \left(\frac{S_{\dot{w}_f}}{\dot{w}_f}\,\frac{\dot{w}_f}{\dot{w}_t}\right)^2} \qquad \text{(B-11)}$$

If it assumed that

$$\frac{S_{\dot{w}_{ox}}}{\dot{w}_{ox}} = \frac{S_{\dot{w}_f}}{\dot{w}_f} \qquad \text{(B-12)}$$

then

$$\frac{S_{\dot{w}_t}}{\dot{w}_t} = \frac{S_{\dot{w}_{ox}}}{\dot{w}_{ox}}\sqrt{\left(\frac{\dot{w}_{ox}}{\dot{w}_t}\right)^2 + \left(\frac{\dot{w}_f}{\dot{w}_t}\right)^2} = \frac{S_{\dot{w}_{ox}}}{\dot{w}_{ox}}\sqrt{\frac{1+MR^2}{(1+MR)^2}} \qquad \text{(B-13)}$$

Substituting this expression in Eq. B-9, the deviation of c* becomes:

$$\frac{S_{c^*}}{c^*} = \sqrt{\left(\frac{S_{p_c}}{p_c}\right)^2 + \left(\frac{S_{A_t}}{A_t}\right)^2 + \left(\frac{S_{\dot{w}_{ox}}}{\dot{w}_{ox}}\right)^2\left(\frac{1+MR^2}{(1+MR)^2}\right)} \qquad \text{(B-14)}$$

The estimated, normalized standard deviations for each variable are listed in Table B-2.

TABLE B-2

ESTIMATED STANDARD DEVIATIONS FOR THE DEPENDENT VARIABLES REQUIRED TO COMPUTE c*

Variable, X_i	S_{X_i}/X_i, percent
p_c	1
A_t	1
$\dot{w}_{ox}$	1.5
$\dot{w}_{fuel}$	1.5

A sample calculation is presented with the assumption that MR = 1.6. Under these conditions, from Eq. B-14 and Table B-2:

$$\frac{S_{c^*}}{c^*} = 1.786 \text{ percent}_{\text{minimum}}$$

10.0 APPENDIX C

DETERMINATION OF DESIGN CRITERIA FOR OPTIMUM MIXING FOR SEVERAL NONCIRCULAR ELEMENTS

The objective of this appendix is to develop the approach to determination of the element design criteria for optimum spray mixing. The results of the cold-flow mixing studies were presented in the text of this report. The results presented in Fig. 32 for the unlike doublets of the impinging type showed that mixture ratio uniformity optimizes around N = 0.5 for noncircular and circular orifices, and that the level of mixing varies with orifice aspect ratio as well as with momentum ratio. N as defined by Rupe is

$$N = \frac{1}{1 + \frac{M_f}{M_o}\left(\frac{D_o}{D_f}\right)_{II}} \qquad \text{(C-1)}$$

where

N = momentum ratio parameter

M_f/M_o = fuel to oxidizer momentum ratio

$(D_o/D_f)_{II}$ = oxidizer to fuel orifice hydraulic diameter ratio

$D_{o,f}$ = 4 x area/perimeter = hydraulic diameter

Because all of the injectors of a given geometry optimize at a value of N of 0.5, Eq. C-1 can be written as

$$\left(\frac{M_f}{M_o}\right) x \left(\frac{D_o}{D_f}\right)_{II} = 1.0 \qquad \text{(C-2)}$$

For Optimum Mixing

or

$$\left(\frac{\rho_f A_f V_f^2}{\rho_o A_o V_o^2}\right)\left(\frac{D_o}{D_f}\right) = 1 \qquad \text{(C-3)}$$

where

ρ = density

A = orifice area

V = injection velocity

D = hydraulic diameter

Introducing the concept of mixture ratio and the continuity equation, the geometric variables can be separated from propellant physical variables. Equation C-3 becomes

$$\left(\frac{A_o}{A_f}\right)\left(\frac{D_o}{D_f}\right) = (MR)^2 \left(\frac{\rho_f}{\rho_o}\right) = K \qquad \text{(C-4)}$$

This equation defines a propellant combination parameter K. The factor K may be computed from the propellant density ratio and optimum mixture ratio. For N_2O_4/N_2H_4-UDMH (50-50), K = 1.62. Thus, the area and hydraulic diameter ratio product for an element which will yield high mixing uniformity is defined.

The orifices are designed such that the orifices in a given element have the same width. The orifice dimensions are defined as:

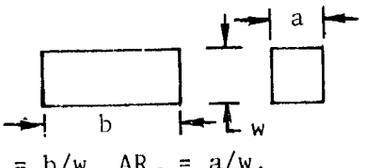

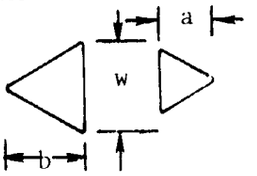

and $AR_o = b/w$, $AR_f = a/w$.

where

AR = aspect ratio

o,f = refers to oxidizer and fuel, respectively.

Because the width (W) of the fuel and oxidizer orifice for a particular element are equal, then from simple geometric considerations of area,

aspect ratio, and hydraulic diameter, expressions may be derived which relate oxidizer and fuel orifice aspect ratio to the given propellant combination. These expressions are presented below for rectangular and triangular orifices.

Rectangles:

$$K \frac{(AR_f)^2}{(AR_f + 1)} = \frac{(AR_o)^2}{(AR_o + 1)} \qquad \text{(C-5)}$$

Triangles:

$$K \frac{(AR_f)^2}{(1 + \sqrt{4\ AR_f^2 + 1})} = \frac{(AR_o)^2}{(1 + \sqrt{4\ AR_o^2 + 1})} \qquad \text{(C-6)}$$

These functions are plotted for values of K of 1.0, 1.62, and 2.0 in Fig. . In addition, the aspect ratios for the three elements tested for each shape are also plotted in Fig.C-1. It may be seen that the design points fall on the curve K = 1.62. Thus, each injector is optimum for mixing for its own particular aspect ratio.

The mixing uniformity levels at N = 0.5 (from Fig. 32) for each element design are plotted in the right-hand plots of Fig. C-1 as functions of the aspect ratio of the fuel orifice. It can be seen that there is an optimum fuel orifice aspect ratio for each shape, and due to the relationships of Eq. C-5 and C-6, there is also an optimum oxidizer orifice aspect ratio. Note that the optimum values are shown in the left-hand plots of Fig. C-1.

Overall, the cold flow mixing study has supplied design criteria for unlike doublet elements for N_2O_4/N_2H_4-UDMH (50-50) incorporating noncircular orifices. These criteria describe requisite area ratios and aspect ratios for optimum propellant mixing.

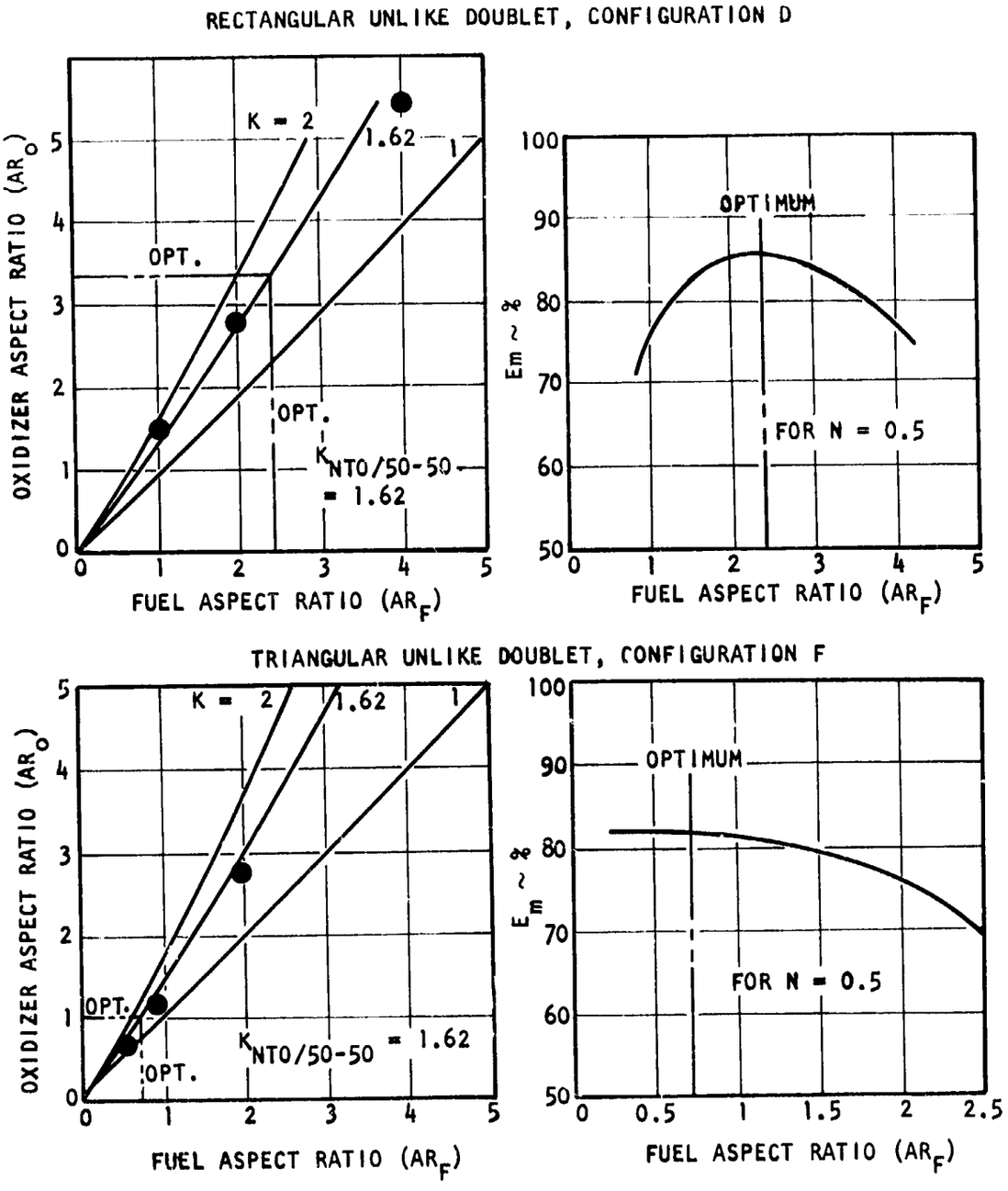

Figure C-1. Determination of Optimum Design Aspect Ratios for Rectangular and Triangular Unlike-Doublet Injector Elements (Simulants: Trichlorethylene/Water)

11.0 APPENDIX D

EXPERIMENTAL APPRATUS AND PROCEDURES

Experimental apparatus and test procedures for single-orifice cold-flow, single-element mixing, single-element atomization, and element hot firings are described in the following pages.

SINGLE ORIFICE, COLD-FLOW TEST FACILITY

The operational objectives of the single-orifice cold-flow test program, as outlined prior to program initiation, were:

1. Measure small flowrates (less than 0.1 lbm/sec) through orifices of various shape flowing into a pressurized atmosphere (pressures up to 100 psig).
2. Establish cross velocities in the feed manifold behind the orifices and maintain them for sustained periods of time (cross velocities up to 20 ft/sec).
3. Allow for photographic documentation of the free jets emanating from the orifices.
4. Measure the pressure drop from the feed manifold to the chamber into which the orifices were exhausting.

A diagram showing the experimental setup is presented in Fig. D-1.

A schematic diagram of the experimental apparatus designed to fulfill the test objectives is shown in Fig.D-2. Major components of the apparatus as noted are (1) main water supply tank (25 gallon capacity), pressurizing and fill equipment, (2) control venturis, for producing 5 ft/sec, 10 ft/sec, and 20 ft/sec cross velocity in the orifice feed manifold, (3) orifice and manifold block (photographs of these components are shown in Fig.D-3), (4) main pressurant chamber with transparent section

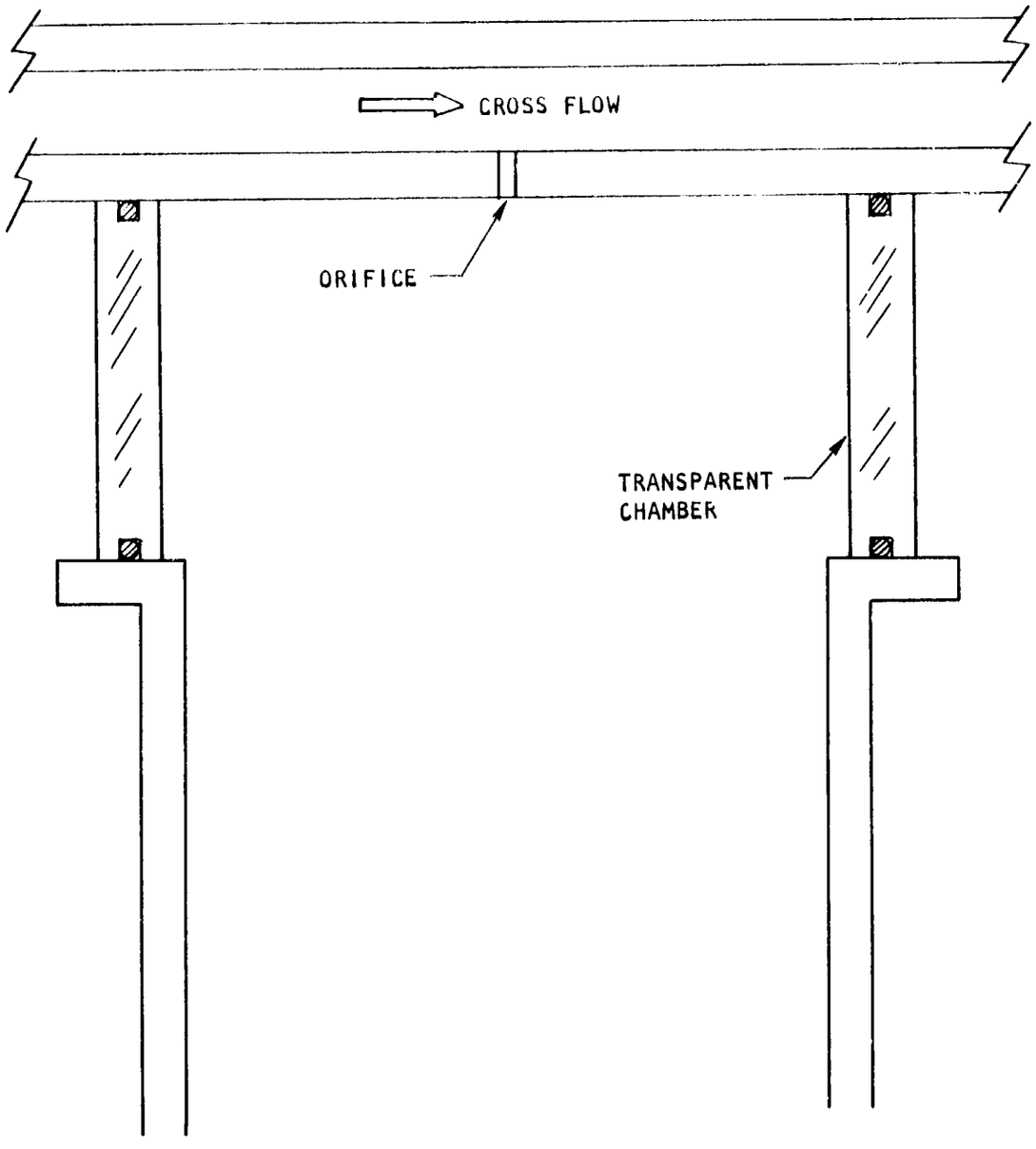

Figure D-1. Diagram of Single Orifice Test Hardware

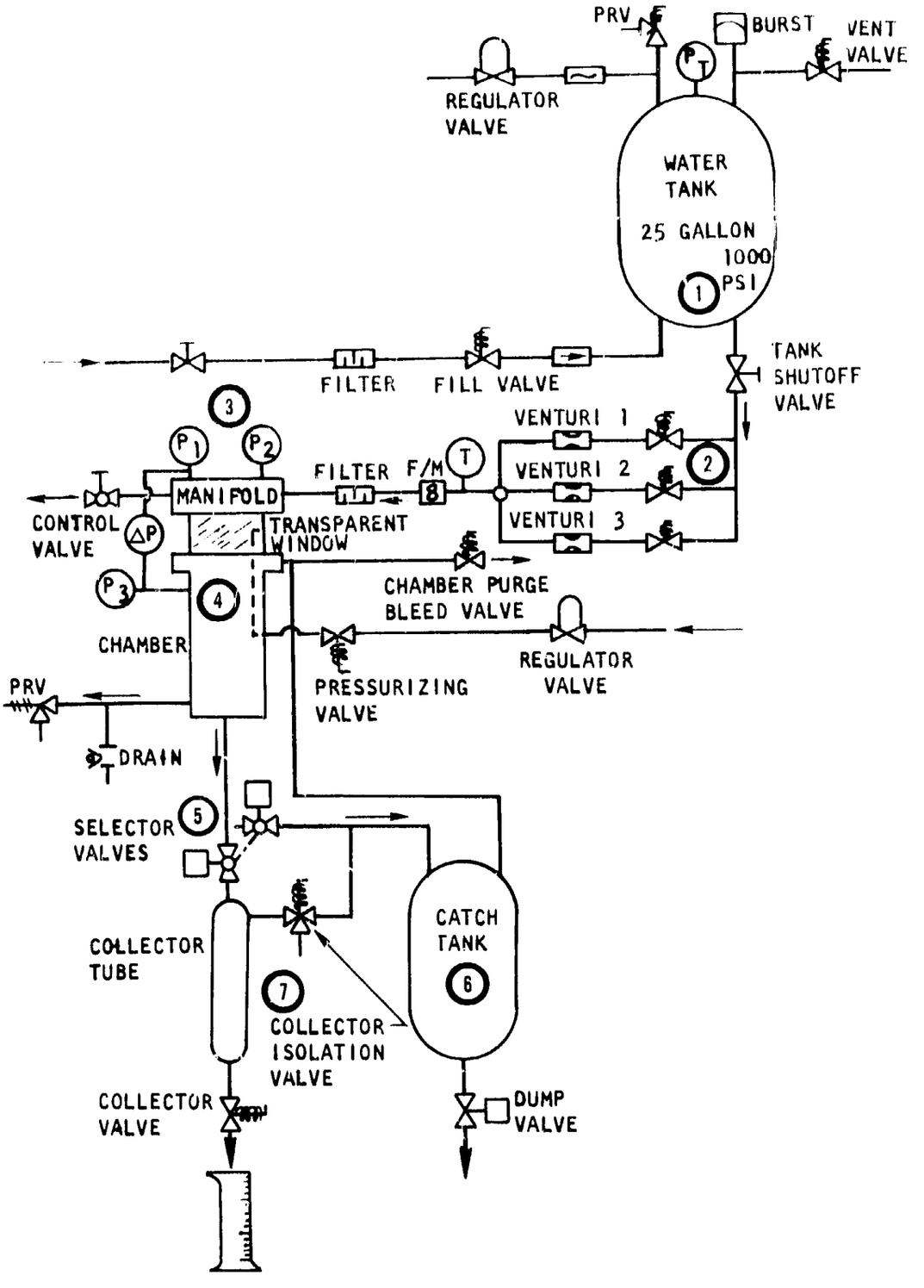

Figure D-2. Single Orifice Cold-Flow Test Facility

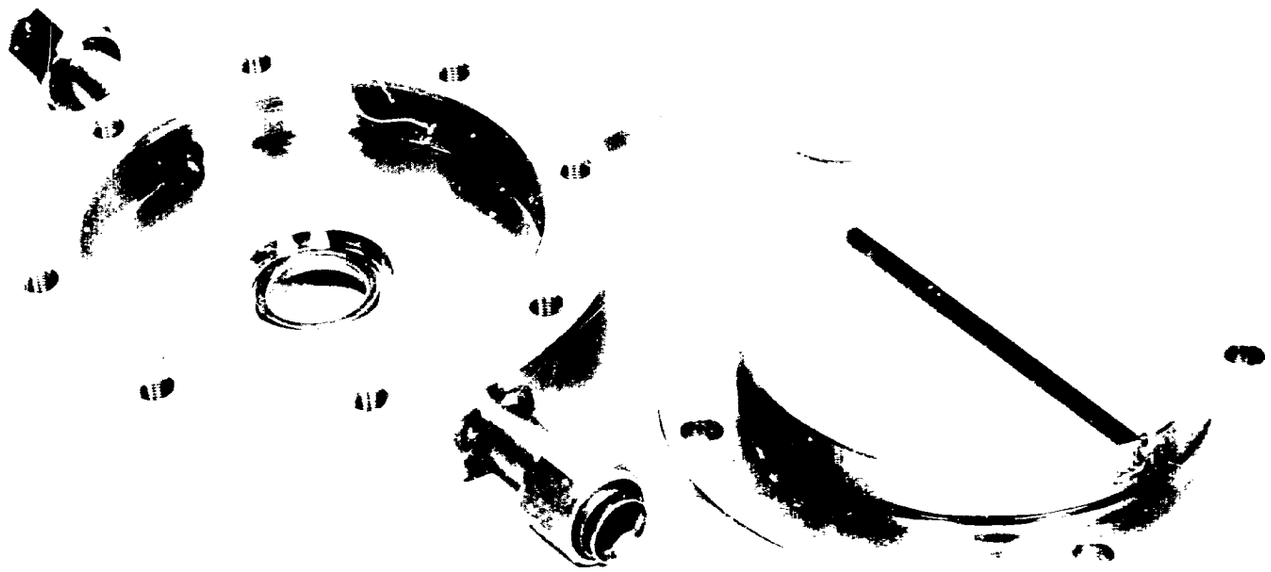

Figure D-3. Orifice and Manifold Block for Single Orifice Study

(shown in Fig.D-4), pressurization and pressure measurement equipment, (5) selector valves slaved together, (6) catch tank, and (7) collector tank and valve.

EXPERIMENTAL PROCEDURE

For each test, the objective was to determine the discharge coefficient of a particular orifice under specific operating conditions. Those parameters which are required to determine discharge coefficient are:

1. Orifice area (A)
2. Flowrate through the orifice ($\dot{W}$)
3. Pressure drop across the orifice (ΔP)
4. Density of the fluid flowing (ρ)

Knowing these parameters, the orifice coefficient is computed using Eq. D-1

$$C_D = \frac{\dot{W}}{A\sqrt{2g\rho\ \Delta P}} \qquad \text{(D-1)}$$

The procedure employed to set desired operating conditions and to measure requisite parameters is outlined in Table D-1.

Pressures, flowrate, and flow time were recorded on direct-inking graphic recorders.

High-speed motion pictures and still microflash photographs were taken during selected test runs. These photographs show the character of the free jet from the orifice exit to a distance of about 3 inches downstream.

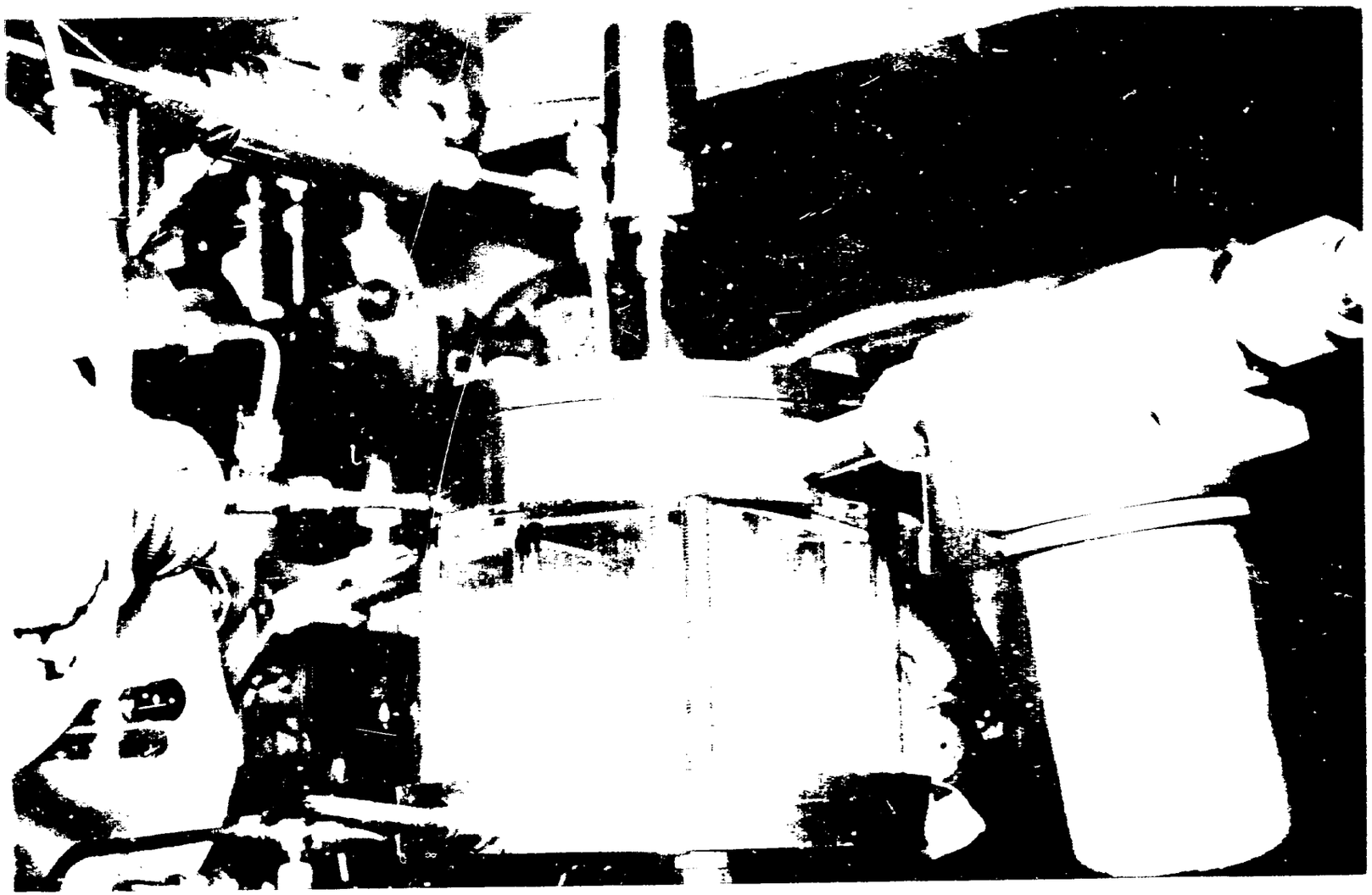

Figure D-4. Pressirized System for [illegible]

TABLE D-1

SINGLE-ORIFICE COLD-FLOW TEST PROCEDURE

Step No.	Item
1	Open pressurizing valve and set regulator to desired backpressure
2	Pressurize water tank
3	Open one of three cavitating venturi valves (each yields a different cross velocity)
4	Set desired orifice ΔP by opening control valve
5	Switch selector valves to collector tubes (starts timer)
6	Switch selector valves back to catch tank after desired time interval (stops timer)
7	Close venturi valve
8	Open collector isolation valve (vents collector tube to atmosphere)
9	Open collector valve (sample flows into a graduated cylinder, the volume was recorded in cc's)

ATOMIZATION

Cold Flow Facility

The wax flow facility used for the dropsize measurements is shown in Fig. D-5 and D-6. The overall system consists of wax and water supply tanks immersed in hot oil bath container and a particle collector which catches the frozen wax particles. Instrumentation requirements of pressure, flow-rate, and temperature are provided by strain gauge transducers, turbine flowmeters and iron constantan thermocouples, respectively. Each wax and water tank has an independent pressurizing and vent system. Also, each

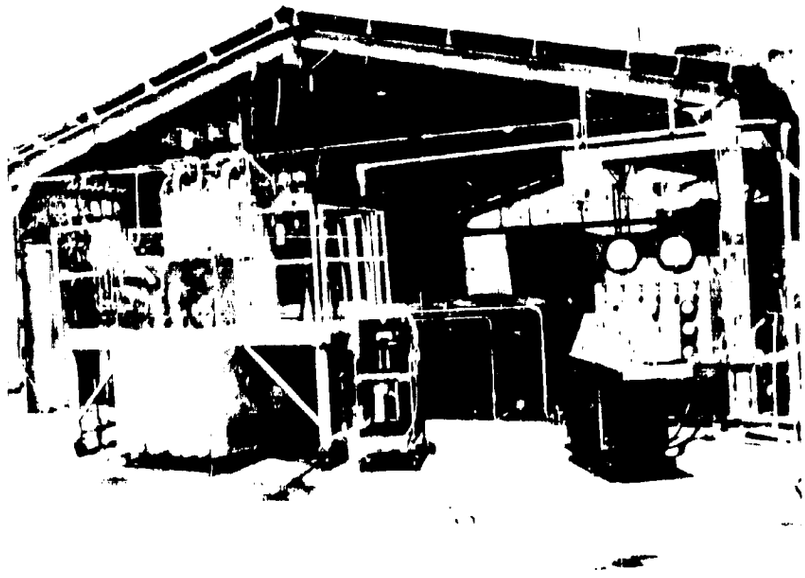

a. Wax Flow System

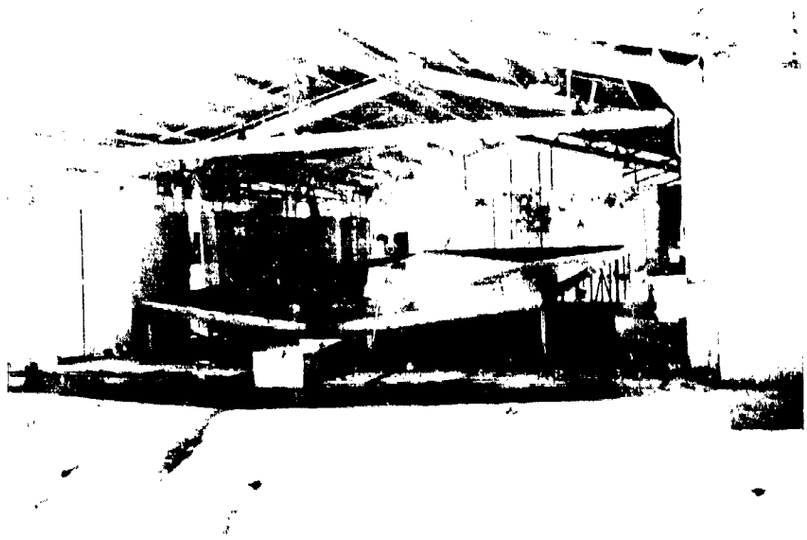

b. Particle Collector

Figure D-5. Wax Flow Facility

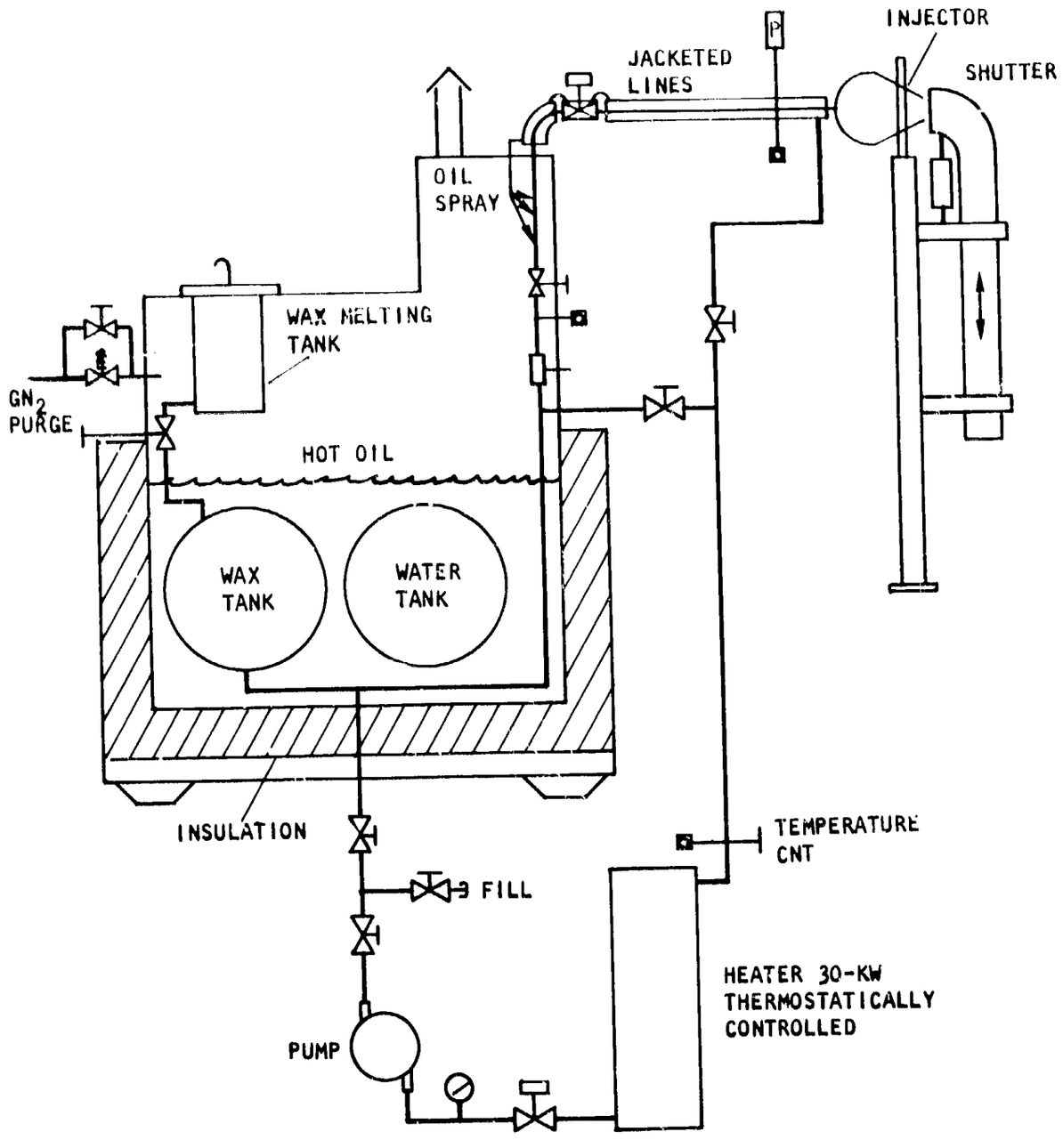

Figure D-6. Schematic of Hot Wax Flow Facility

product outline has three flowmeters, thermocouples, and hand shutoff valves arranged in parallel so a wide range of flowrates can be obtained. The hot oil bath, shown schematically in Fig.D-6, is heated by means of a 30-kw thermostatically controlled heater. An electrically operated pump circulates the oil from the oil bath container through the heater and back again to ensure uniform temperature. Also, hot oil is forced through jacketed run lines and valves to ensure that the wax does not freeze in the feed lines.

The particle collector (Fig.D-5) is an 18 by 50 foot epoxy-coated wooden platform which is located under a roofed structure. This shields the collection area from wind currents which might cause the smaller particles to be blown away. When the impact surface is washed down, the slope of the collector causes the wash water to be directed into a particle catch basin. The catch basin has several baffles to ensure that none of the wax particles are washed overboard.

Experimental Procedure

The experimental procedure for droplet size measurement is as follows:

1. The proper injector configuration is installed on the wax facility in such an orientation that the wax spray created by the orifices after freezing during its ballistic trajectory strikes the particle collector.
2. The electrical oil heater and pump are turned on to bring the propellant simulant tanks and run lines up to 210 F.
3. After all parts of the system are thoroughly heated and instrumentation requirements checked, the run tanks are pressurized.
4. With the piston operated shutter in the up position, the test is initiated by actuating the main pneumatic shutoff valves. When the flowrates and injection pressures reach a steady

condition, the shutter is actuated and the wax particles are allowed to spray onto the particle collector. The use of the shutter minimizes the influence of start and stop transients on the size distribution of the collected particles.

5. The injector flow is continued for approximately 10 seconds. The shutter is then actuated to the up position and main shutoff valves closed.

6. The tanks are then vented and systems secured.

7. The particles are then washed from the collector into the catch basin, where they are scooped from the surface of the water and placed in a plastic bag for temporary storage.

Particle Sample Analysis

The following procedure is used for the analysis of the particles:

1. A 100-gram sample of wax particles is placed in a Buchner funnel and subjected to suction for removal of water.

2. After the particles have been partly dried by suction, they are placed on a large tray in a vacuum chamber for a period of at least 48 hours to ensure that the particles are completely dry.

3. After drying, a random 10-gram sample is selected to be sieved. A series of 23 standard testing sieves ranging in size from 5[illegible] to 2380 microns is available. For any particular sample, only 13 of the sieves are used; the particular sieve sizes used depend on the anticipated size range of the particle sample. The sieves are vibrated on a Ro-TAP automatic sieve shaker for 30 minutes, during which time the shaking is stopped every 6 minutes and each sieve is struck sharply several times to help release any particles which become wedged in the sieve screens.

4. After the sieving operation is completed, the mass of particles retained on each sieve is weighed on an electric balance. It has been found that with considerable care in transferring the wax from the sieves into the weighing pan, a total recovery of 97 to 99 percent of the mass originally introduced into the sieves is possible. The photos shown in Fig. D-7 are typical of the uniformity of sizes of the solid wax particles obtained by the sieving operation.

5. These data are then converted into the total fraction of mass having a particle size smaller than each of the sieve sizes.

MIXING

Cold Flow Facility

The description of the cold-flow mixing facility is divided into two distinct parts: (1) the flow system, and (2) the collection system.

Flow System. The basic components of the flow system are shown in Fig. D-8. The system contains two high-pressure (1000-psia maximum rated pressure) supply tanks. Each are remotely pressurized. The propellant lines are stainless-steel tubing. Pneumatic (Annin) valves are used for tank shut-off and main valves.

Flow system instrumentation consists of four Taber "Teledyne" series-bonded strain gage pressure transducers, and two Fischer-Porter turbine-type volumetric flowmeters. Measurements of both propellant tank pressures and propellant injection pressures are made. These measurements are recorded on Dynalog direct-inking graphical recorders. The volumetric flowmeter signals are recorded on a CEC multichannel oscillograph.

Cold-flow propellant simulants are trichloroethylene and water, which simulate, the oxidizer (NTO) and fuel (Aerozene 50), respectively. These

500 Microns

420 Microns

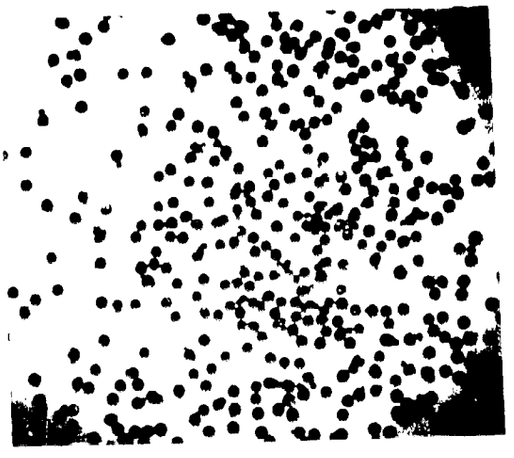

354 Microns

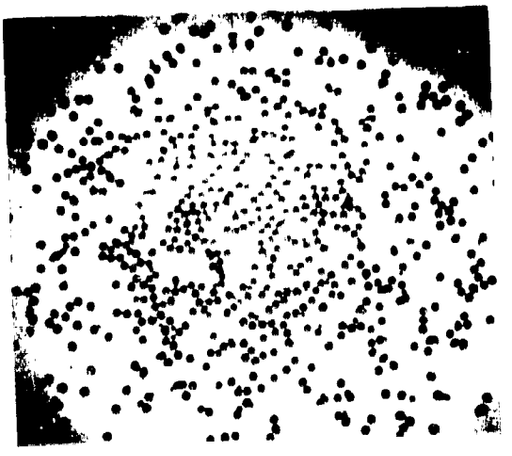

250 Microns

177 Microns

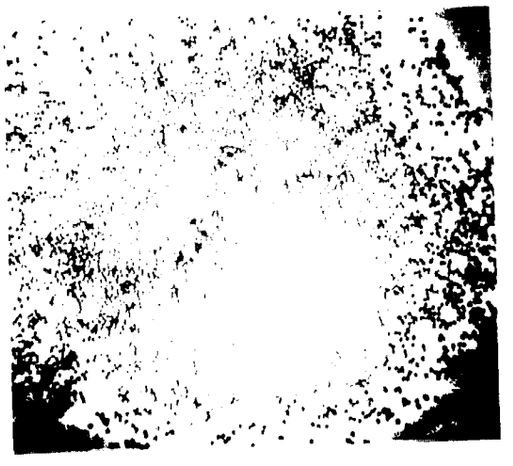

125 Microns

Figure D-7. Photographs of Solidified Wax Droplets Using a 0.063-Inch-Diameter Like-Doublet Element

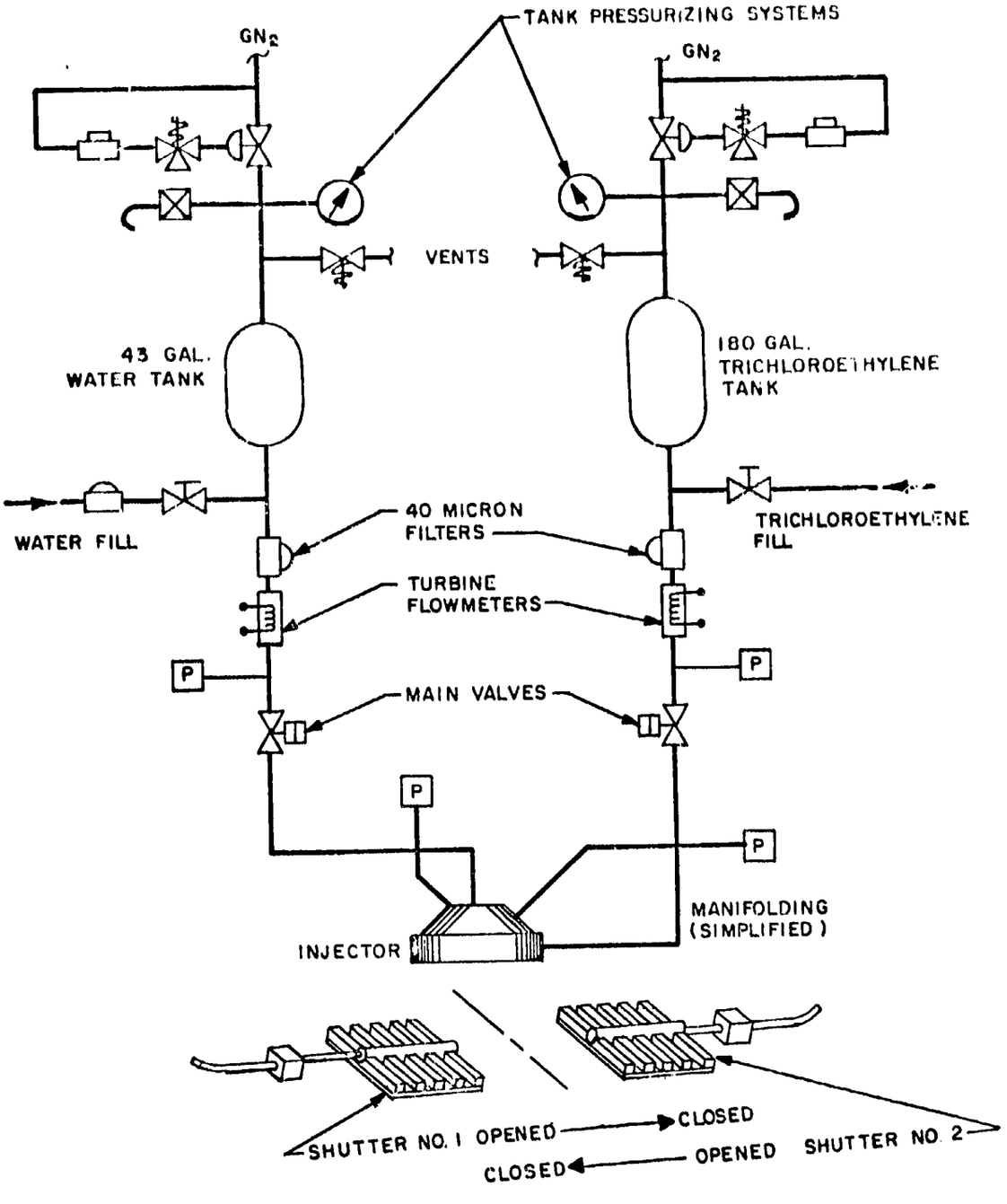

Figure D-8. Schematic Drawing of the Flow System for the Cold-Flow Mass and Mixture Ratio Distribution Study

simulants were chosen on the basis of: (1) availability, being employed on related programs at Rocketdyne using the same facility, (2) ease of handling, and (3) maintainance the oxidizer/fuel immiscibility.

Collection System. The specific details of the collector are illustrated in Fig. D-9. As can be noted, the tubing slants outward from the collection plane to a 7 by 7 foot base. The base is 1/2-inch aluminum plate and separates the upper portion of the assembly from the Pyrex tube racks. Beneath the aluminum plate is a cart which houses the tube racks. The cart is mounted on wheels so that the entire tube matrix is easily removed from under the collector and rolled to the measurement station.

Experimental Test Procedures

The procedure for each of the cold-flow tests are as follows: The fuel and oxidizer simulant tanks are pressurized to give the desired flowrates. The main valves are opened and after the injection pressures become steady, the shutter is opened for a selected time interval and then closed. The main valves are then closed to conclude the test run. All tests are conducted with the elements centered above the collector at a distance of approximately 3 inches. This distance was chosen since prior analytical and experimental data indicate that it represents a good approximation of the primary propellant mixing region during combustion.

The data recorded for each test included oxidizer and fuel simulant flowrates, injection pressures, flow duration, and the volume of oxidizer and fuel simulants in each of the collection tubes.

The individual volumes are determined by a volumetrically calibrated metal strip or graduated cylinders. The metal strip resembled a thin metal scale with a scribe mark at 10-milliliter increments. This strip is inserted into the test tube and the volume of oxidizer simulant and the volume of fuel simulant read directly. For tubes containing insufficient liquid quantities for accurate measurement, the volumetric measurements are obtained by use of graduated cylinders.

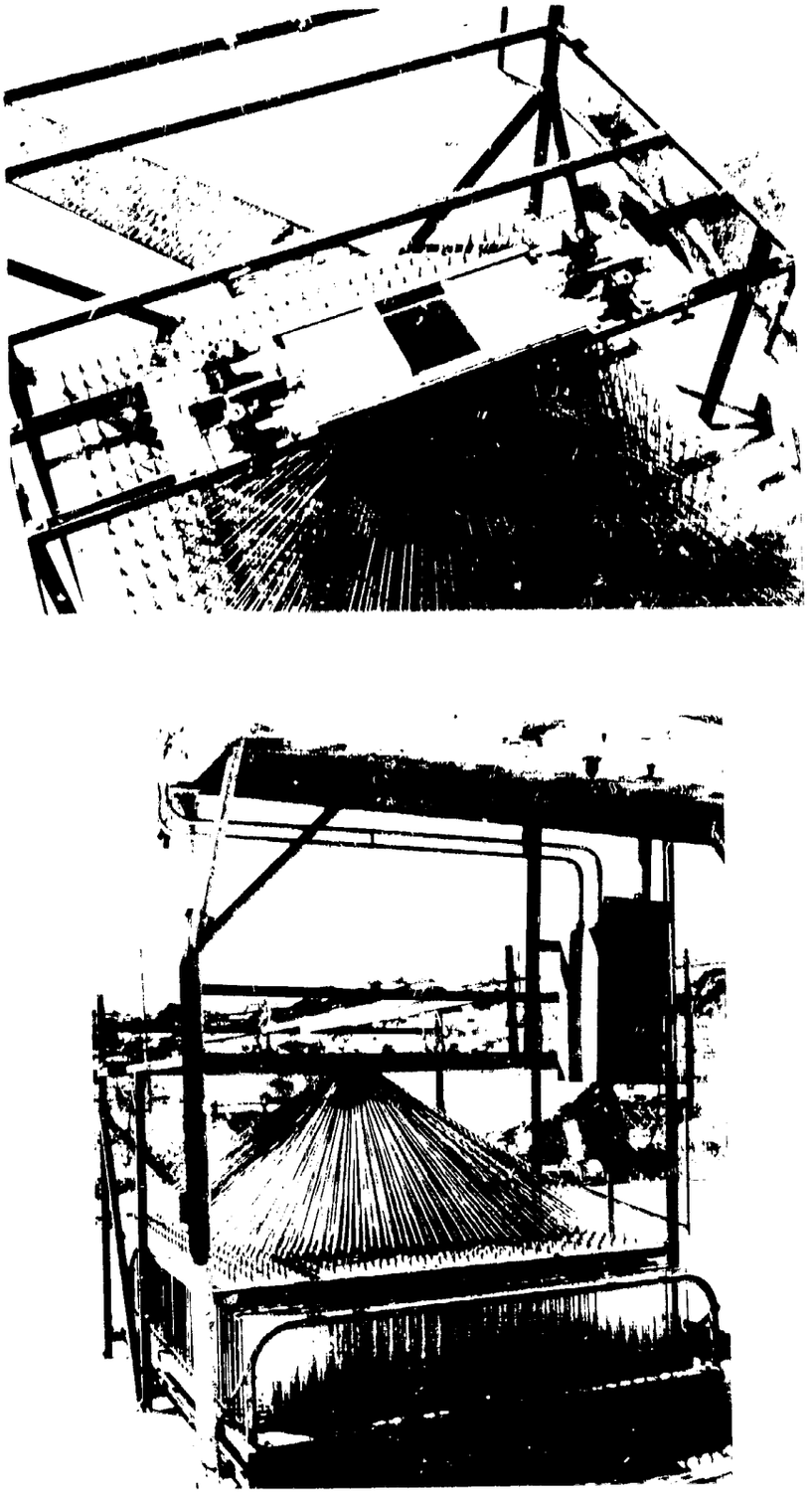

Figure D-9. Injector Spray Collection System

Data Analysis

The collector matrix data and the other recorded data are processed by computer to produce the following output: mass of oxidizer simulant, mass of fuel simulant, mixture ratio, and mass fraction for each tube. The mixing factor (E_m), predicted c* efficiency ($\eta_{c^*,dist}$), center of collected mass (row and column), and percentage of the injected mass collected are computed.

Hot-Fire Test Facility

The single-element hot firings were conducted at the Propulsion Research Area (PRA). A schematic representation of the propellant feed system is shown in Fig. D-10.

Both the N_2O_4 and N_2H_4-UDMH (50-50) propellant tanks are rated for 3 gallons capacity at 2000 psia. Each tank is pressurized with regulated gaseous nitrogen. The oxidizer is temperature conditioned by flow through specially designed heat exchangers. Propellant flowrates are controlled by cavitating venturi meters. Both propellant feed systems can be purged with gaseous nitrogen. All tests were conducted remotely from the blockhouse which allows a direct veiw of the test hardware.

Instrumentation requirements are also shown in Fig.D-10. Redundant chamber pressure measurements were taken at the beginning of nozzle convergence. All measurements were recorded by the Beckman Data Acquision System.

Data Analysis. The index of injector performance used in this program is corrected c* efficiency. This c* efficiency was computed from chamber pressure only, as no thrust measurements were made. Performance losses attributed to the presence of the thrust chamber are computed and corrections for these losses are applied to the measured values of c*.

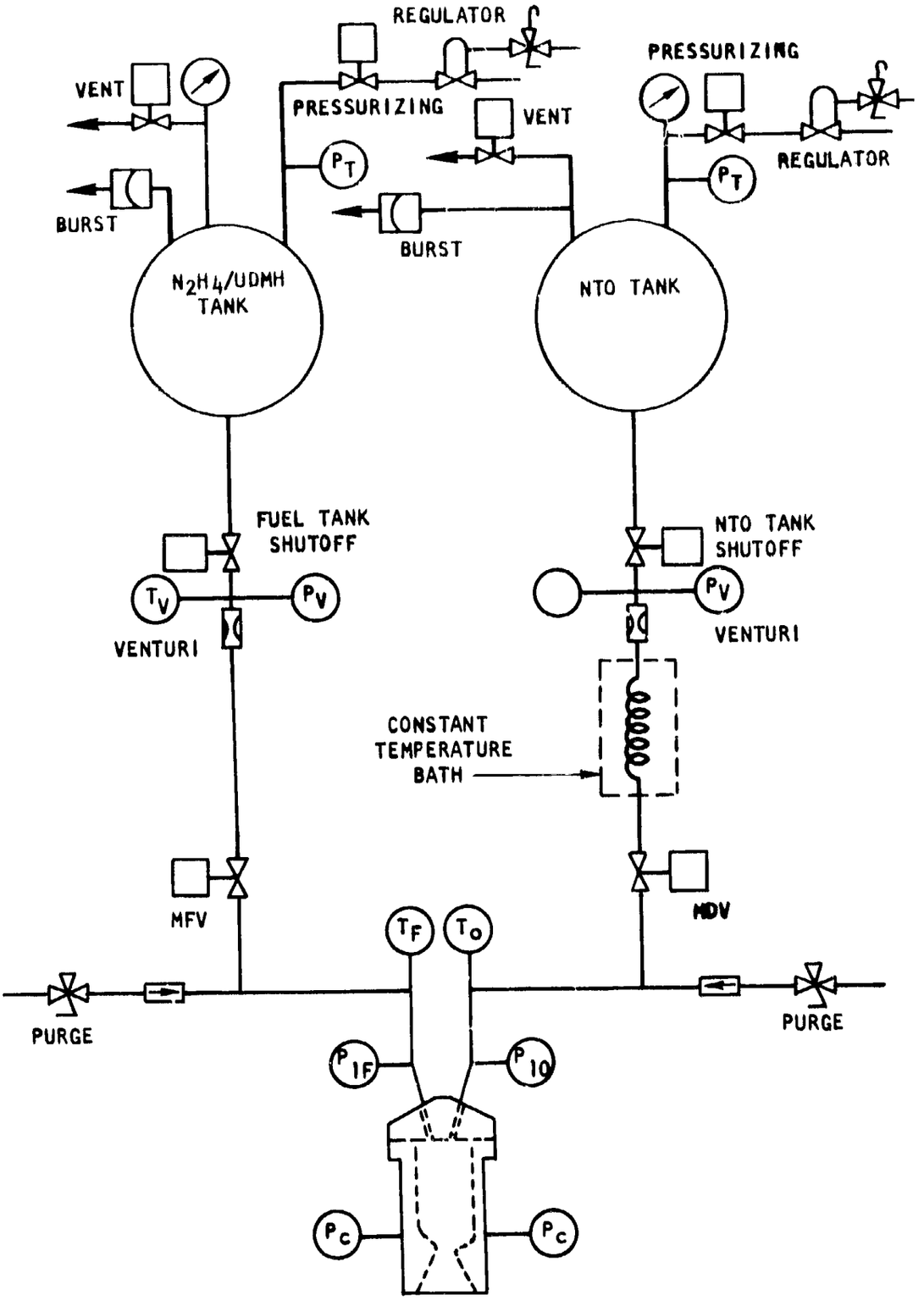

Figure D-10. Single Element Hot-Fire Test Facility

Basic, corrected c* was computed from Eq.

$$c^* = \frac{(P_0)_{ns} \; A_{t_{eff}} \; g_c}{w_t}$$

where

$(P_0)_{ns}$ = nozzle stagnation pressure, lbf/in.^{2}

$A_{t_{eff}}$ = effective throat area, in.^{2}

g_c = conversion factor, 32.174 lbm-ft/lbf-sec^2

$\dot{w}_t$ = total weight flowrate, lbm/sec

c^* = characteristic velocity, ft/sec

Nozzle stagnation pressure was computed from the static pressure measured at the start of nozzle contraction. The assumption is made that the expansion from the point of measurement to the throat takes place both isentropically and quasi-one dimensionally. The stagnation and static pressures are then related through the isentropic relationships based on effective contraction ratio.

Effective throat area is computed by correcting the pretest geometric throat area for boundary layer effects, deviations from one-dimensional flow.

The effect of chamber heat loss and viscous drag on c* is incorporated in the proper determination of the displacement thickness of the boundary layer at the throat. Rocketdyne uses an integral momentum, turbulent boundary layer computation which includes heat transfer from the boundary layer to the chamber wall. The thickness of the displacement boundary is a function of the heat transfer due to the distribution of gas density through the boundary layer caused by temperature gradients. Thus, corrections for both heat loss and drag are included in the determination of an effective throat area.

UNCLASSIFIED

Security Classification

DOCUMENT CONTROL DATA - R & D

(Security classification of title, body of abstract and indexing annotation must be entered when the overall report is classified)

1. ORIGINATING ACTIVITY (Corporate author)
Rocketdyne, a Division of North American Rockwell Corporation, 6633 Canoga Avenue, Canoga Park, California 91304

2a. REPORT SECURITY CLASSIFICATION
Unclassified

2b. GROUP

3. REPORT TITLE
FINAL REPORT--NONCIRCULAR ORIFICE HOLES AND ADVANCED FABRICATION TECHNIQUES FOR LIQUID ROCKET INJECTORS (PHASE I: ANALYTICAL AND EXPERIMENTAL STUDY OF NON-CIRCULAR INJECTOR ORIFICES, AND ELEMENTS FOR LIQUID/LIQUID INJECTORS)

4. DESCRIPTIVE NOTES (Type of report and inclusive dates)
Final Report

5. AUTHOR(S) (First name, middle initial, last name)
W. H. Nurick and R. M. McHale

6. REPORT DATE
15 September 1970

7a. TOTAL NO. OF PAGES
244 (+ xii)

7b. NO. OF REFS
20

8a. CONTRACT OR GRANT NO.
NAS9-9528

b. PROJECT NO.

c.

d.

9a. ORIGINATOR'S REPORT NUMBER(S)
R-8224

9b. OTHER REPORT NO(S) (Any other numbers that may be assigned this report)
NASA CR-108570

10. DISTRIBUTION STATEMENT

11. SUPPLEMENTARY NOTES

12. SPONSORING MILITARY ACTIVITY
NASA Manned Spacecraft Center

13. ABSTRACT

The Phase I results to investigate the use of advanced fabrication techniques for liquid rocket injectors which allow for fabrication of noncircular orifices, and to determine if noncircular orifices can provide greater flexibility and/or a significant improvement in injector element designs are presented. The study consists of an analytical study of various injector patterns and elements that utilize noncircular orifices, and experimental evaluations of promising element configurations. Cold-flow characterization and theoretical combustion modeling combined with single element hot-firing experiments are employed to predict the relative merits of liquid rocket engine injector elements incorporating orifices of noncircular shape as compared to circular shapes. The frozen wax technique is used to determine dropsize; water/trichloroethylene spray collection through a tube matrix is used to determine mixing efficiency. Unlike-doublet elements incorporating circular, triangular, rectangular, and self-atomizing orifices are compared on the basis of overall c* efficiency. Results indicate that at optimum design conditions for equal thrust per element designs, mixing levels are higher for noncircular shapes while circular orifices produce small dropsizes.

DD FORM 1 NOV 68 1473

UNCLASSIFIED

Security Classification

14 KEY WORDS	LINK A		LINK B		LINK C	
	ROLE	WT	ROLE	WT	ROLE	WT
Injectors						
Drop Size						
Mixing						
Noncircular Orifices						